Dublin City University

Ollscoil Chathair Bhaile Átha Cliath

The investigation of the stability of ruthenium based photocatalysts using HPLC, NMR and UV visible techniques

By

Ahmed M A Rashed

A Thesis presented to Dublin City University for the Degree of Doctor of Philosophy

Supervised by Dr. Mary Pryce

And Prof. Johannes G Vos

School of Chemical Sciences

Dublin City University

September 2020

Declaration

I hereby certify that this material, which I now submit for assessment on the programme of study leading to the award of Doctor of Philosophy by research is entirely my own work, that I have exercised reasonable care to ensure that the work is original, and does not to the best of my knowledge breach any law of copyright, and has not been taken from the work of others save and to the extent that such work has been cited and acknowledged within the text of my work.

Signed:----------

(Ahmed. M. A. Rashed)

(Student) ID No: 14210953

Date: **14.9.2020**

Acknowledgements

First of all, I would like to express my gratitude to Mary Pryce and Prof. Han Vos, my supervisors, for the opportunity they gave me their guide and experience during these last almost 5 years to do my Phd at Dublin City University, as well as for the interesting research theme. Especially, I want to thank Prof. Han Vos for his help, guidance and advice throughout my thesis.

Special thanks to all my family for their patience during my study, also to my special "DCU" friends, both past and present.

To Dr. mohammad elshahawy, islam osman, I really appreciate all the help you gave me in preparing this thesis. I always believe you're my real best friends.

Moreover, I want to thank my friends and colleagues in DCU for making the past five years such an enjoyable experience.

I am thankful to all the members of the research groups of Dr Mary Pryce and Prof Han Vos I had met them in lab, Yvonne Halpin, Nivedita Das, jen zersorama, Finn Connaughton Suzanne Mc Mahon, Aoibhin Cullen, Laura O Reilly, Tony ohara, Martin Kaufmann, Michael Brandon, Tasha Donnelly, Liam Bernard Frayne, Diana Hidalgo for the help, and for the friendly atmosphere in the laboratory.

I would also like to thank the technical staff Veronica Dobbyn, John McLaughlin, Mary Ross, Vincent Hooper, Ambrose May, Damien Mcuirk, and our school secretary Julie McArthur.

There are so many people to thank I'm so sorry I cannot remember all of them.

Abstract

In this thesis, the use of high performance liquid chromatography (HPLC) for the analysis, assessment and characterisation of photocatalytic behaviour. The Ru(II) compounds are coordinated at peripheral ligands to create at Ru(II) centre, while bridging ligands are used to connect the ruthenium centre to the Pt catalytic centres in order to create intramolecular systems. The properties of these platinum-containing compounds were compared with the mononuclear ruthenium precursor, without a platinum centre, in terms of photostability and catalytic activity. These intramolecular platinum containing compounds are aimed at create photocatalysts in combination with terminal halogen atoms (iodide or chloride). UV-vis absorption and ^{1}H-NMR analysis were carried out to provide further detailed qualitative and structural information as a result of the photocatalytic experiments terminal, halogen atoms (iodide or chloride) and range of techniques where discussed, to provide further detailed and structural information. UV-vis absorption and ^{1}H-NMR analysis were carried out to provide further detailed information about the possible chemical changes taking place after irradiation as a result of the photocatalytic experiments.

In Chapter 1, a number of relevant topics are discussed and the studies presented in this thesis in order to explain our research targets and experimental techniques.

In Chapter 2, the introduction to HPLC, analytical HPLC, HPLC setup, mobile phases and UV-Vis Spectroscopy used and ^{1}H NMR spectroscopy are discussed and sample preparation for photoanalysis with TEA and without TEA were explained.

In Chapter 3 stability towards visible light by the complexes $[(bpy)_2Ru(2,3dpp)]^{2+}$ (**A-I**), $[(bpy)_2Ru(2,3dpp)PtCl_2]^{2+}$ (**A-II**), and $[(bpy)_2Ru(2,3dpp)PtI_2]^{2+}$ (**A-III**) were carried out. Without TEA all three compounds the compounds are mostly photostable, but in the presence of TEA decomposition of the compounds is observed. In Chapter 4, for the compounds $[(phen)_2Ru(2,3dpp)]^{2+}$ (**B-I**), $[(phen)_2Ru(2,3dpp)PtCl_2]^{2+}$ (**B-II**), and $[(phen)_2Ru(2,3dpp)PtI_2]^{2+}$ (**B-III**), compounds **B-I** and **B-II** are photostable and B-III is partially photostable. In the presence of TEA, changes in the coordination of the bridging ligands are observed. In Chapter 5 compounds $[(dceb)_2Ru(2,3dpp)]^{2+}$ (**C-I**), $[(dceb)_2Ru(2,3dpp)PtCl_2]^{2+}$ (**C-II**), and $[(dceb)_2Ru(2,3dpp)PtI_2]^{2+}$ (**C-III**) are discussed. In the presence of irradiation, compounds **C-I** and **C-III** are photoreactive while that compound **C-II** is photostable. The stability of irradiation in the presence of TEA compounds **C-I**, **C-II** and **C-III** are degrading fast. In Chapter 6 a general overview of the work carried out is discussed.

Table of Content

List of Abbreviations

bpy	2,2'-bipyridyl
MJ/kg	megajoules per kilogram
MC	metal centred
LC	ligand centred
LMCT	ligand-to-metal charge transfer
MLCT	metal-to-ligand charge transfer
^{3}MLCT	triplet metal-to-ligand charge transfer
ILCT	intra-ligand-charge-transfer
HOMO	highest occupied molecular orbital
LUMO	lowest unoccupied molecular orbital
Λ	wavelength
UV	ultraviolet
Vis	visible
nm	nanometre
ISC	Intersystem crossing
k_r	radiative
k_{nr}	non-radiative
HPLC	high performance liquid chromatography
NMR	nuclear magnetic resonance
DMA	N,N-dimethylaniline
EDTA	ethylenediaminetetraacetic acid
TEA	triethylamine
TEOA	triethanolamine

PS	Photosensitiser
Cat	Catalytic center
TON	turn over number
TOF	turn over frequency
hv	light energy
DFT	density functional theory

Figure Credits

Chapter-1

Introduction- The Chemistry of Ruthenium (II) Complexes for the Study of Photochemical Devices.

Chapter one serves as an introduction to the work carried out in the thesis. The area of supramolecular chemistry and a brief overview of excited states are discussed. The photochemical behaviour of a number of ruthenium polypyridyl compounds and the chemistry of ruthenium complexes is reviewed. An assessment of the theoretical background of the mechanism of photocatalytic hydrogen production is discussed using some examples of dinuclear Ru/Pd photocatalysts.

1 Introduction

In the late fifties, the interest in the ruthenium(II) co-ordination compounds research started, especially when $[Ru(bpy)_3]Cl_2$ (bpy is 2,2'-bipyridyl) was discovered as a (photo)stable and strongly luminescent molecule with an emission that is based on triplet metal-to-ligand charge transfer (^{3}MLCT) transitions [1]. During the further development of studies of the photophysical and photochemical properties of these compounds it was quickly realised that these properties could be utilised for the development of solar driven devices such as photovoltaic cells, photocatalysts for water splitting [2], and reduction of CO_2 [3]. Starting from that time, this interest has ramped up and successively led to the development of solar energy conversion devices that are based on the enhanced electron transfer properties of excited ruthenium polypyridyl sensitisers attached to semiconductor surfaces such as Graetzel cells [4,5,6,7].

Investigations on ruthenium-polypyridyl compounds are not only restricted to the fields of photo-catalysis and solar energy conversion [8][9][10], but also incorporated in other fields such as bio [11,12,13], and chemical sensors [14,15], molecular electronics [16,17,18], nonlinear optics [19,20] and optical storage [21]. Moreover, they have also a relevant role in development of supramolecular chemistry[22,23,24,25,26,27,28,29].

One of the greatest concerns for humanity in the modern age is the problem of obtaining clean and affordable energy sources. Fossil fuel started with using the coal in the previous centuries and developed to the petroleum in the industrial revolution in later centuries. This can be considered as the actual commence of

the modern advancing and development for humans. However, they are being depleted around the world in an ever increasing pace. In addition, the combustion of fossil fuels leads to increased CO_2 concentration in the atmosphere and is one of the main contributors to climate change [30]. Ideally, such alternative energy sources should have no impact on the world climate or - at least - less impact than fossil fuels. Sunlight is the main source of energy on earth [31,32]. It provides sufficient energy in the form of light and heat to sustain life on earth and for plants to carry out the photosynthetic processes which leads to the production of all other forms of energy [33,34]. The direct usage of solar energy has been the subject of interest of scientists for many decades and extensive studies in a number of different fields have been carried out. Electric solar panels based on photovoltaic cell technology have been used for decades now in many applications, however, their efficiency has not been improved greatly since their advent in the nineties of the previous century. Also although the cost of production is going down competition with fossil fuel is still a problem [35]. Importantly, the cost for storing electricity is very high, and commercially available batteries have many shortcomings including poor mobility and low capacity. Also the production process is not environmentally friendly. Many industries and applications can not directly use electricity and still require chemical fuel to operate [36].

Photocatalysis on the other hand can provide a more efficient source of energy through the production of hydrogen directly using photocatalytic compounds together with solar energy. Hydrogen is seen as a game changer for our future renewable energy consumption. It has been regarded as a strong alternative form of clean and storable energy [37]. With its very high energy-density/mass ratio

(120 MJ/kg), hydrogen has a huge potential to replace fossil fuels directly especially in the transport. Important is also that the only by-product of hydrogen combustion is water vapour which is extremely environmentally friendly [38,39]. Over the last few decades the development of photocatalytic systems for hydrogen generation and CO_2 reduction have been investigated in great detail and it should be possible to design efficient and stable photocatalysts capable of carrying these processes. Several different approaches have been taken, including the use of photocatalysts immobilised on semiconductors and solution based intermolecular and intramolecular approaches (Fig1-1) [40,41,35]. Note that the solution based systems require sacrificial agents to regenerate the photosensitiser.

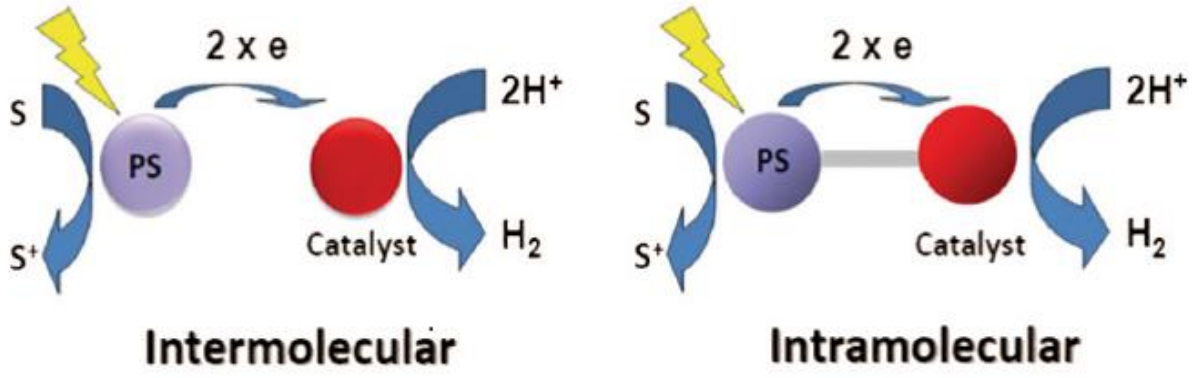

Figure 0.1: Inter vs intramolecular photocatalysis. PS = photosensitiser. S = sacrificial agent [35].

If solar energy is to be used in these studies, photosensitisers need to be developed that can absorb visible light. Therefore, the use of metal based light absorbers has taken a central stage. Over the last number of years the DCU group has been investigating the design and optimisation of intramolecular photocatalytic assemblies for the generation of hydrogen from water [42].

In these, studies ruthenium polypyridyl compounds are used as light absorbers while Pd and Pt centres, connected to the light absorber via a bridging ligand see Fig (1.1) are used [35]. The photo- and catalytic stability of such compounds are investigated using high performance liquid chromatography and nuclear magnetic resonance, together with UV/vis absorption and emission techniques. It is realised that ruthenium is an expensive metal but the wide range of synthetic techniques available allows for the generation of a range of different compounds to develop the design principles that will ultimately control efficient photocatalyst which will be based for example on cheap first row transition metals.

In the following sections a brief overview of the excited state and photochemical behaviour of a number of ruthenium polypyridyl compounds will be given. This will be followed by an overview of the compounds to be studied in this thesis.

1.1 Excited state properties of ruthenium polypyridyl compounds

The unique combination of physical and chemical properties of ruthenium polypyridyl compounds, such as high chemical stability, selective excited state reactivity, long-lived excited states, and well defined redox properties has caught the attention of many research workers [43,44,45]. The importance of electron

transfer can be assessed by considering the different molecular orbital arrangements shown in Figure (1.2) for different types of metal compounds.

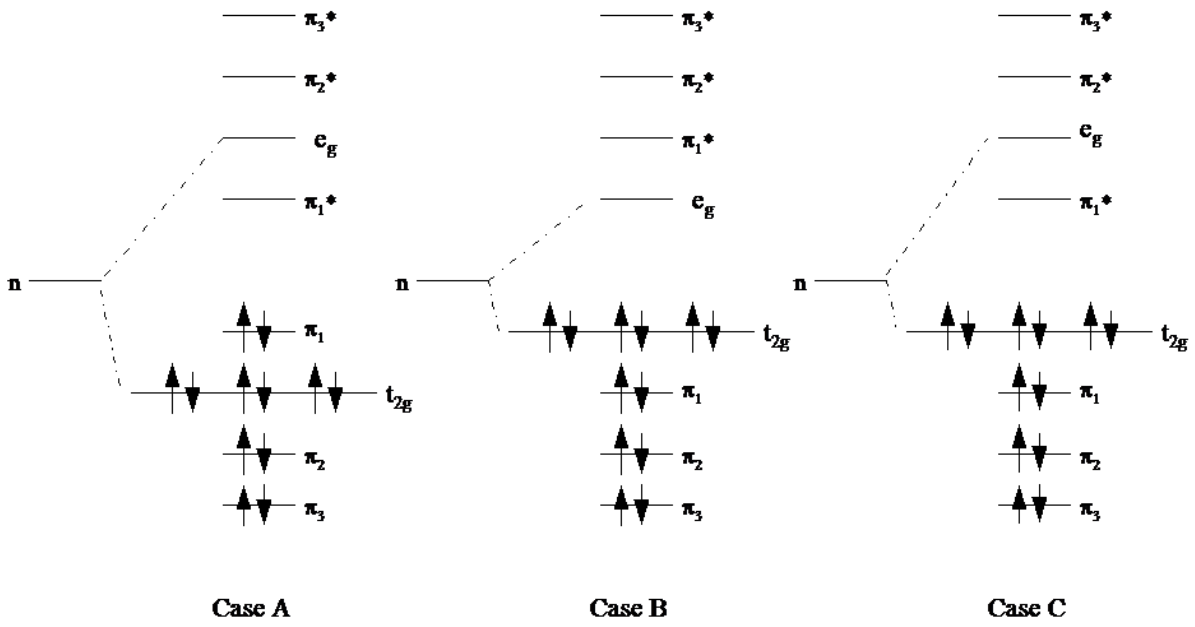

Figure 0.2: Different possible arrangements of the molecular orbitals in d^6 metal compounds[46].

In brief the three types can be considered as;

Ligand based molecular orbitals: in this type, the highest occupied molecular orbital (HOMO) and the lowest unoccupied orbital (LUMO) are ligand based orbitals and both are of the π-type. A complex with this arrangement acts as an organic compound. Energy and electron transfer processes are difficult to assess because both of these orbitals are strongly localized on the same part of the molecule and the difference in energy level is not significant.

Metal based orbitals in this type, both HOMO and LUMO are based on the metal atoms. The properties of these two orbitals are explained by the ligand field theory, and since the e_g (LUMO) has an anti-bonding character, its population will

lead to the breaking of the metal-ligand bond and may lead to loss or rearrangement of the ligands.

Mixed metal/ligand based orbitals. This is the most interesting arrangement among the three different types, in this type, the HOMO is metal based while the LUMO in ligand based. As a consequence, upon excitation the electron can transport from the metal to the ligand (MLCT process) relatively easily and adds to the electron and energy transfer processes [46].

In Figure (1-2), three different orbital arrangements are shown, involving different arrangements of metal and ligand based orbitals. In Case A, the highest occupied molecular orbital (HOMO) and the lowest unoccupied orbital (LUMO) are ligand based orbitals and both are π-type. Therefore, a complex with this arrangement would act as an organic compound since energy and intramolecular electron transfer processes would be localized on the organic part of the molecule.

In Case B, both HOMO and LUMO orbitals are metal based. As the LUMO has an anti-bonding character, its population will lead to decomposition of the metal-ligand bond and potential loss or rearrangement of ligands.

The most interesting arrangement is described in Case C. In this arrangement the HOMO is metal based while the LUMO in ligand based. Consequently, upon excitation the electron can transfer from the metal to the ligand (MLCT process) and expand to further electron and energy transfer processes.

The important electronic processes occur through excitation of these compounds which are illustrated by the prototype $[Ru(bpy)_3]^{2+}$ that is mainly based on the

arrangement shown in Case C. As an example the absorption and emission spectra of the prototype are shown in Figure 1.3 [47].

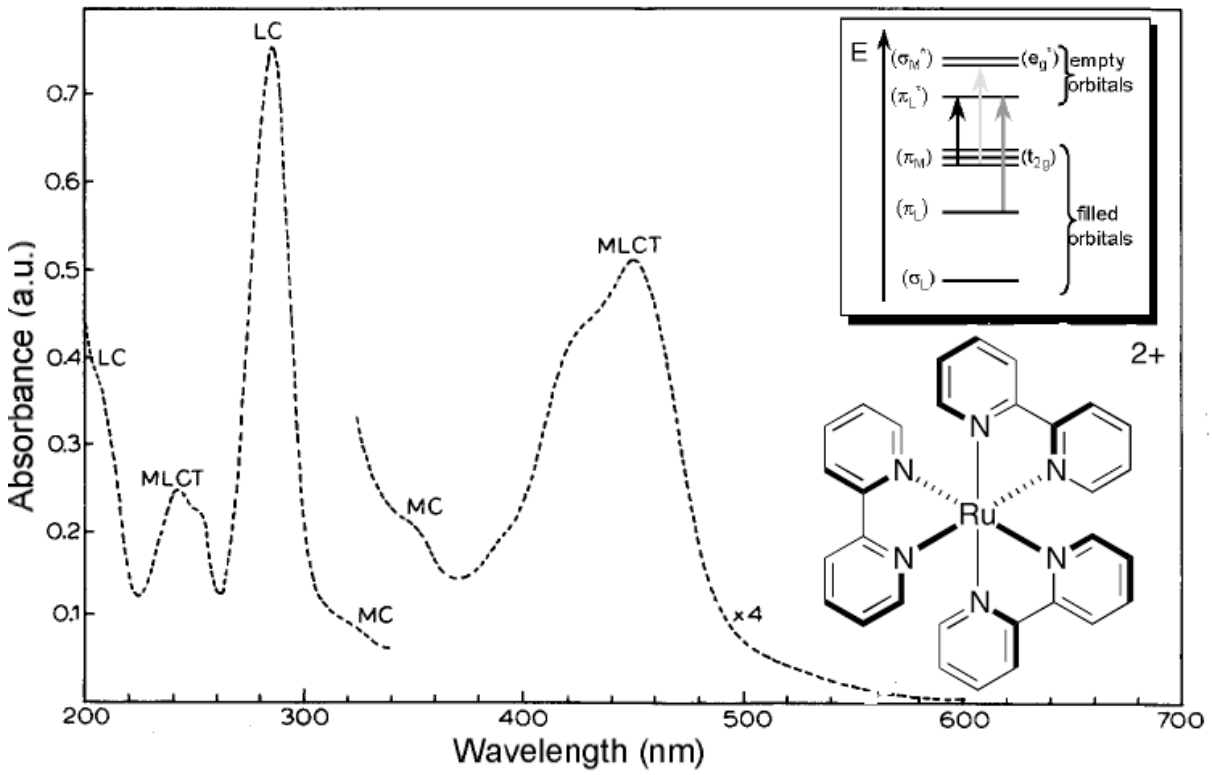

Figure 0.3: Absorption spectrum of $[Ru(bpy)_3](PF_6)_2$ in acetonitrile showing MLCT, ligand centred (LC) and metal centred (MC) transitions Inset: molecular orbital diagram, where the notation (L or M) indicate where the orbital is mostly localized. The d-orbitals, which are mostly localized on the metal, are split into three lower (t_{2g}) and two higher (e_g) orbital energy levels for the presence of the field generated by the bpy-ligands[48].

The strong field complex $[Ru(bpy)_3]^{2+}$ with three bidentate bipyridine ligands consists of an octahedral structure with its electrons in the low-spin t_{2g} configuration. In contrast to other octahedral compounds, the unoccupied π*-orbitals of the ligands are lower in energy than the unoccupied e_g-orbitals of the Ru centre as shown in Figure 1.4.

Therefore, the energy that is required for a MLCT transition, which is critical for the electron transfer from the Ru(II) photocentre to the catalytic centre during the catalytic process, is lower than for the MC transition. Hence, the MLCT transition occurs at higher wavelength (visible light), which is a characteristic aspect with a view to its application in a photocatalytic system and is also responsible for its intense colour[45].

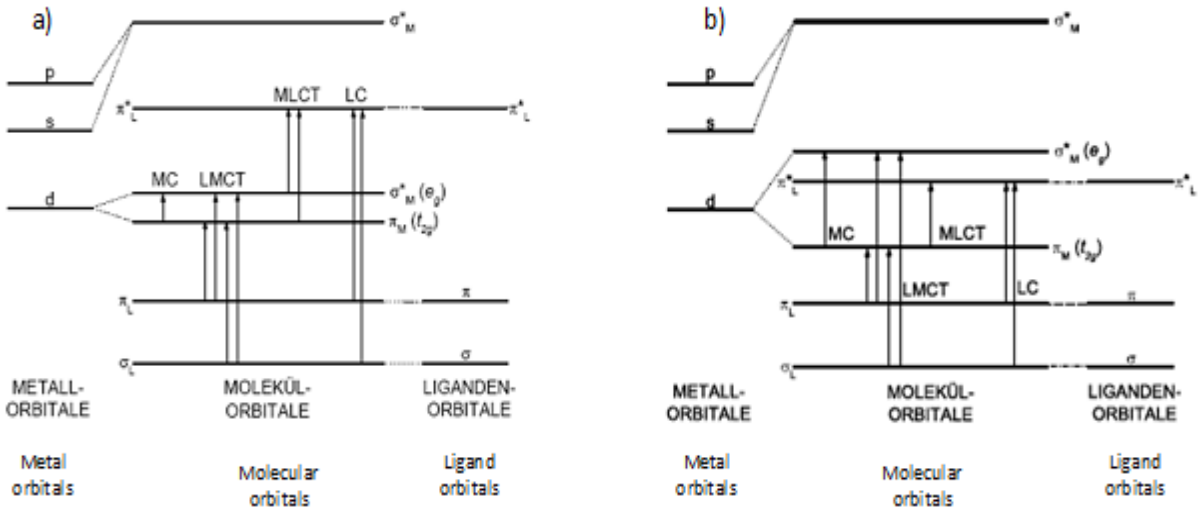

Figure 0.4: Schematic energy level diagram of (a) a typical octahedral transition metal complex and (b) $[Ru(bpy)_3]^{2+}$[45]

$[Ru(bpy)_3]^{2+}$ is a d^6 complex with octahedral geometry. Its absorption spectrum is as shown in Figure 1-3 dominated by the two bands at 240 nm and 450 nm (most intense) due to promotion of an electron from a π metal orbital to π^* ligand orbitals (MLCT processes). Ligand centred (LC) bands at 185 nm and 285 nm arise from promotion of an electron from π to π^* ligand based orbital. This is a typical **C** type compound as shown in Figure (1-2). The weak shoulders observed at 320 and 350 nm are a sign of the presence of the metal centred transitions (MC) from πM

to πM^* [49], the flexibility of the synthetic chemistry of ruthenium polypyridyl compounds allows the facile variation of the chelating ligands [50,51,52,53]. This mainly produces a change of the energy level of the ligand centred LUMO in the complex, with consequent modulation of absorption/emission energies, redox potentials and excited state lifetimes [8,9,10,54,55].

The excitation with light at wavelength 450 nm (as in Figure 1-3) stimulates one electron from a metal d-orbital to the ligand antibonding π*-orbital. For a ruthenium complex the singlet excited state (^{1}MLCT), formed immediately upon excitation, expands rapidly into emissive metal to ligand charge transfer triplet excited state (^{3}MLCT) of a lower energy level through intersystem crossing [56]. This ^{3}MLCT state is described as a Ru(III) centre coordinated to a reduced di-imine radical anion ligand [57], owed to the strong spin-orbit coupling effect of ruthenium.

The quantum yields of the formation of the lowest lying excited state are almost unity, showing that intersystem crossing (ISC) from the upper singlet excited states (obtained by excitation) to the lowest triplet state is very fast and efficient. The radiative (k_r) and non-radiative (k_{nr}) decay pathways of the ^{3}MLCT excited state are also shown in the Jablonski diagram in Figure (1-5) [56].

Basically, photochemical processes are generally initiated by photo-induced ligand exchange. For transition metals compounds ligand exchange is related to the breaking of metal-ligand bonds. Consequently, the photolability of compounds is generally associated with the presence of antibonding metal centred (MC) orbitals.

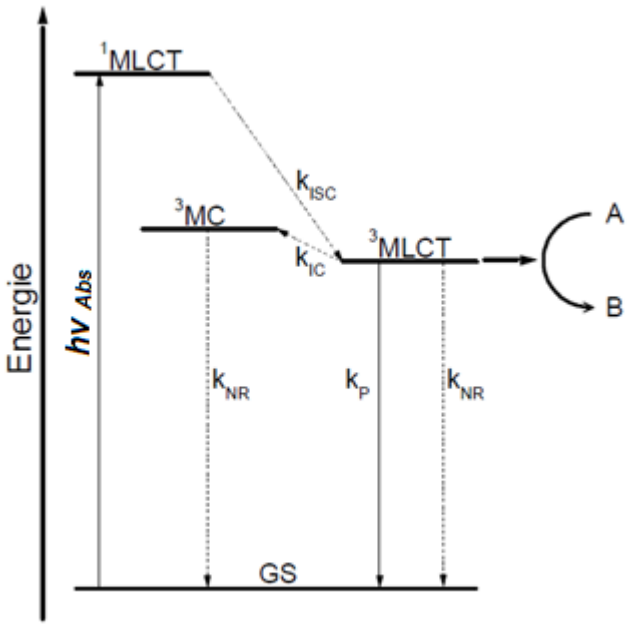

Figure 0.5: Jablonski diagram of $[Ru(bpy)_3]^{2+}$ [58].

Ruthenium polypyridyl compounds energy diagram is outlining the energy levels involved in photochemical processes as in Figure (1.6) shown below.

In this category, the excitation from the metal based ground state to a singlet metal-to-ligand charge-transfer state (^{1}MLCT) and rapid intersystem crossing (takes picoseconds) leads to population of a relatively long lived ^{3}MLCT state.

The detailed work on ruthenium polypyridyl compounds has identified the ^{3}MC (metal centred) orbital to be responsible for the photocomposition [59,60,61]. For photoactive compounds, the population of the antibonding ^{3}MC state from the ^{3}MLCT state takes place at room temperature.

The photolability of the compounds is generally related to the energy difference between the deactivating ^{3}MC state and the emitting ^{3}MLCT level, (See Figure 1.6).

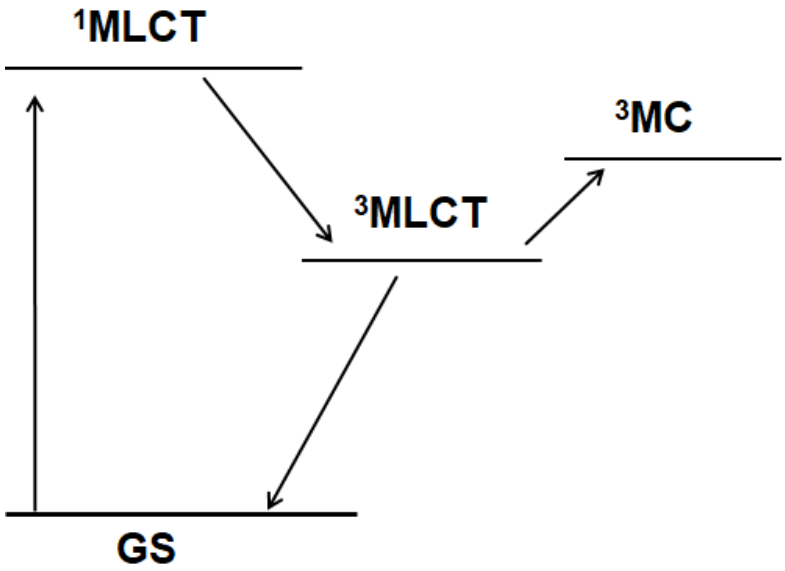

Figure 0.6: Electronic levels in $[Ru(bpy)_3]^{2+}$[46].

It was observed by Meyer and co-worker that such photo processes are influenced by used solvent strong ligands such as acetonitrile and coordinating counter ions increase the quantum yield for ligand loss. Therefore, $[Ru(bpy)_3](PF_6)_2$ exhibits little or no decomposition in CH_2Cl_2. But in the presence of Cl^- or NCS^- ions, formation of species such as $[Ru(bpy)_2Cl_2]$ is observed [46].

The photostability of $[Ru(bpy)_3](PF_6)_2$ is much decreased in coordinating solvents such as acetonitrile and bpy (2,2'-bipyridyl) loss may develop [59,60,61]. The formation of intermediates containing monodentate coordinated bpy ligands has been detected using ^1H NMR coupled with electronic spectroscopy [62].

These studies show that the energy difference between the ^3MLCT and the ^3MC energy levels is an important factor, that extend the control of the photochemical processes.

It can be noted that the photophysical and photochemical properties of these compounds are dependent on the nature of their low–lying excited states. The

presence of an electron-accepting α-diimine ligand in the coordination sphere permits for charge transfer, through electronic transitions directed to the diimine ligand.

Ruthenium compounds are one of the most studies family of compounds in the inorganic metal compounds and belongs to the second row transition metals. The unique combination of physical and chemical properties of ruthenium polypyridyl compounds, such as high chemical stability, selective excited state reactivity, long-lived excited states, and well defined redox properties caught the attention of many research workers [63,64]. The popularity of ruthenium polypyridyl compounds is based on the special arrangement of the energy levels of the outer orbitals (Figure 1.2)

1.2 Photocatalysis

Photocatalytic compounds are considered a trial to mimic photosynthetic processes in living organisms that is why it has the term “artificial photocatalysis”. The basic concept is to design molecular systems that are capable of absorbing light in the region of solar emission and initiating an electron-transfer process that delivers the energy to a catalytic centre, that in turn uses this energy to carry out photocatalytic processes produce hydrogen gas from water.

The basic design of any hydrogen producing photocatalytic molecular system should include the following four main components:

- A photoredox-active centre, which is considered a photosensitizer that is able of absorbing electromagnetic radiation of the sun.

- A catalytic centre, where protons (H^+) are reduced to hydrogen gas.
- A linker that is able to carry out electron transfer process from the photo-centre to the catalytic centre and
- A sacrificial electron donor needed to be present in excess in order to supply electrons for the re-reduction of the photosensitiser.

  Examples for those sacrificial donors include triethylamine **TEA**, triethanolamine **TEOA**, ethylenediaminetetraacetic acid **EDTA** or N,N-dimethylaniline **DMA** those compounds decompose after the initial electron transfer which is naturally irreversible. The by-products of their decomposition may affect the efficiency of the photocatalytic system and eventually inactivate it, that is why they are considered to be one of the major drawbacks of the concept of electrocatalysis. Two typical examples of the photocatalytic systems are depicted in Figure (1.7) highlighting the different functional components of the molecular system. These compounds will be further discussed in other chapters.

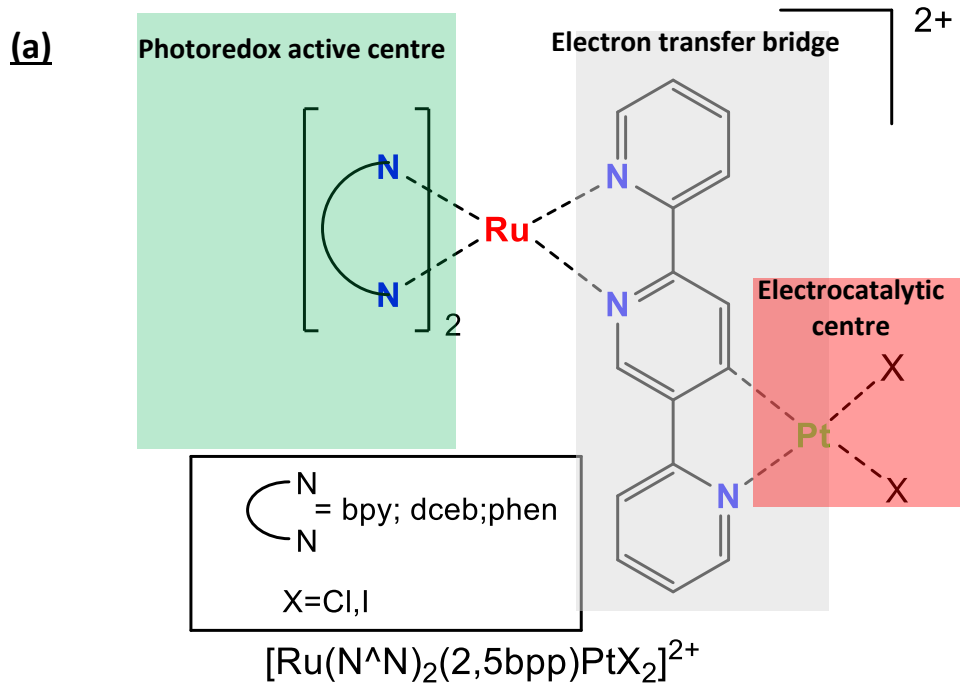

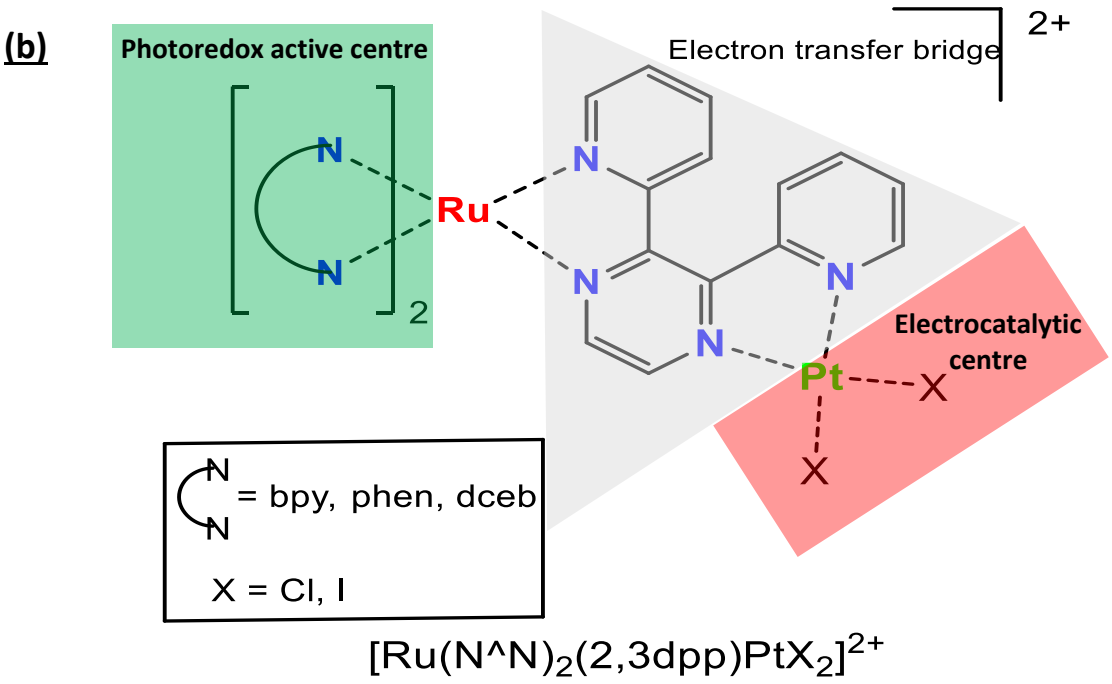

Figures 0.7a and 1-7b: (Example) the three components of photocatalyst Ru/Pt are highlighted: By excitation of the photocentre charge is transferred via the bridging-ligand to the catalytic centre.

1.3 Mechanism of photocatalytic hydrogen production using the example of a dinuclear Ru/Pd complex

Dinuclear Ru/Pd complexes are one example of dinuclear photocatalytic molecular devices that involve intramolecular charge transfer. As pointed out earlier, the term intramolecular charge transfer denotes that the photon-induced electron transfer movement happens inside a molecular assembly[65]. This assembly is composed of three main parts or centres with different photochemical properties and functions as shown in Figure 1.8. The Photosensitiser (PS), the

Catalytic center (Cat) and a linker moiety that connects the two functional centres called the bridging ligand (B) [66]. We will discuss the important properties of each functional component of the molecular assembly in the following parts.

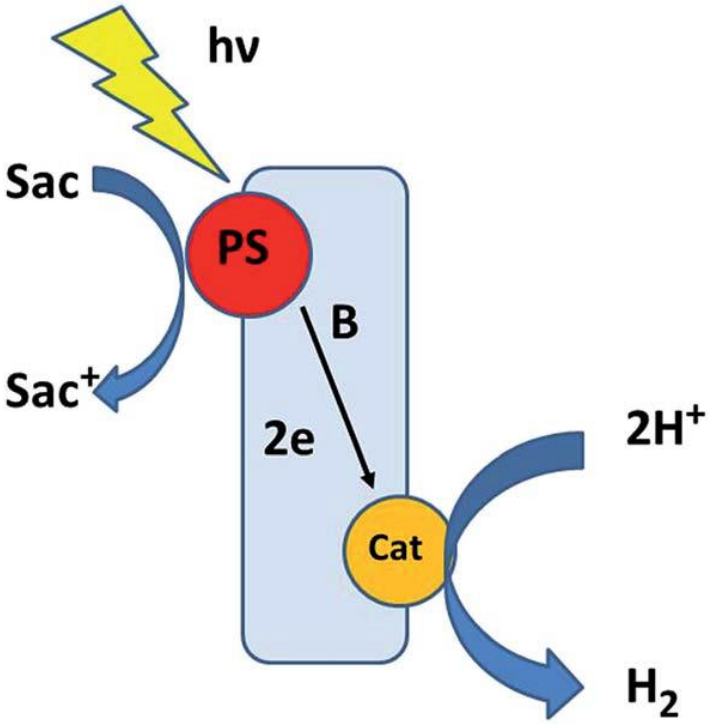

Figure 1.8: Intramolecular approach. Sac = sacrificial reductant, PS = photosensitiser, Cat = catalytic centre, B = bridging ligand [66].

As apparent from their names, the photosensitizer is the centre that is responsible for interaction with the incident photon. This interaction induces an electronic transition to an excited state. This electron is then transferred to the bridging ligand, which should have a π orbital of lower energy to create energy gradient and allow spontaneous movement of electrons in the right direction from the

photosensitizer to the catalytic centre. One of the earliest examples of molecular binuclear photocatalytic assemblies is Compound **1**, $[(tbbipy)_2Ru(tpphz)PdCl_2](PF_6)_2$ where the peripheral ligands are tbbipy = 4,4′-di-tert-butyl-2,2′-bipyridine and bridging ligand is tpphz = tetrapyrido[3,2-a:2′,3′-c:3″,2″-h:2‴,3‴-j]phenazine [67]. The Ru atom is located in the photosensitizer while Pd is in the catalytic centre (See Figure 1-9).

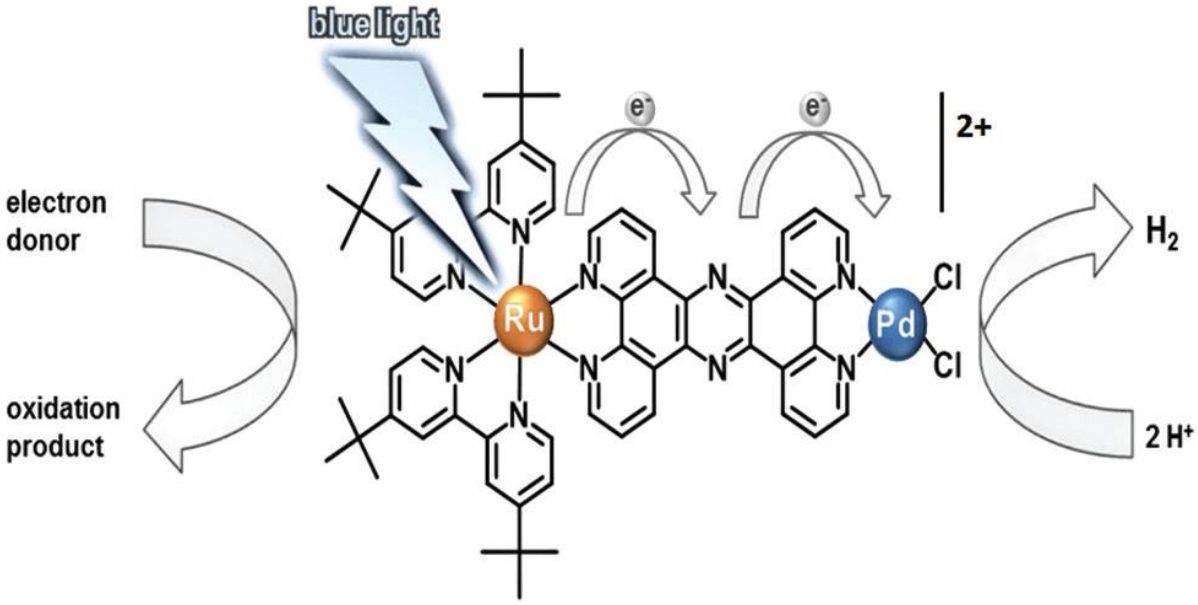

Figure 1.9: The basic mechanism of photocatalytic hydrogen production with Compound 1 as photocatalyst. Light is absorbed by the Ru(II) moiety with subsequent electron transfer to the catalytic metal centre (Pd/Pt) mediated by bridging ligand (tpphz) in acetonitrile[67] .

The vectorial electron transfer process that occurs in this compound upon irradiation can be summarised in the following scheme [65]:

Scheme 1.1 (a): Reaction of the Photocatalytic assembly and hydrogen production

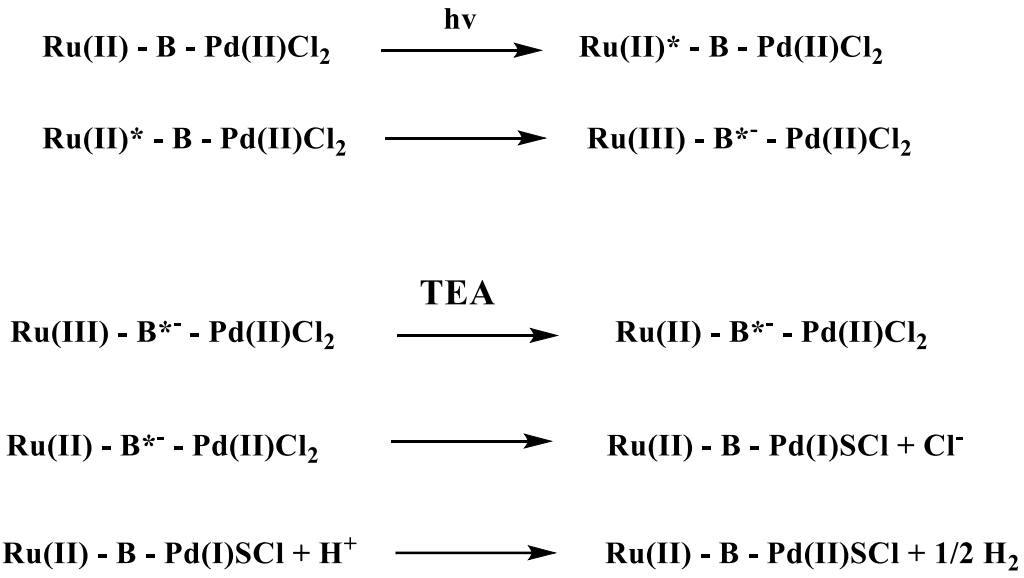

Scheme 1.1 (b): Decomposition of TEA.

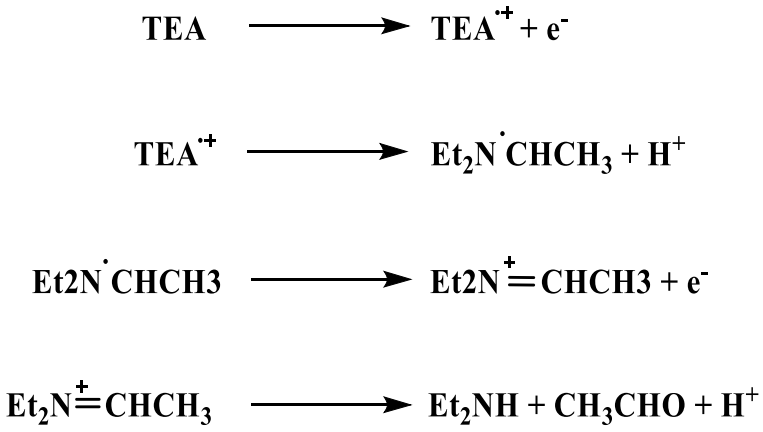

In the scheme shown, for the molecular assembly to produce hydrogen, an efficient vectorial electron transfer must happen, starting from the light absorbing ruthenium centre, through the bridging ligand and the palladium moiety that

serves as the catalytic centre and so bring the oxydised Ru (III) centre back to the ground state after the electron migration to the bridging moiety. TEA (which is the sacrificial agent) is necessarily for the reduction of the reduced Ru (III) atom in the light absorbing centre allows for the making the next photo excitation process. The use of sacrificial agents such as TEA can be problematic since it can be involved in the photocatalytic process. As shown in Scheme 1b above, TEA decomposes after the first electron transfer and produces both protons and electrons in dark reactions. During the decomposition process, two protons and one electron are produced. As noted before these compounds are quite reactive species and they may contribute in the decomposition of the photocatalytic molecule itself [65].

1.3.1 Role of the catalytic centre in the photocatalytic assembly

Tschierlei et al carried out detailed investigations on the photophysical properties of the molecule to acquire more information about its electronic properties. These investigations included time resolved resonance Raman and picosecond (ps) transient absorption. Those experiments were conducted in acetonitrile as a solvent and in the absence of the sacrificial agent so that the photophysical properties of the assembly is evaluated under non-catalytic conditions. Scheme 2 is a comparative study of the photophysical properties of the mononuclear precursor Complex **1a** and the dinuclear photocatalyst Compound **1** as shown in Figure 1.9.[68].

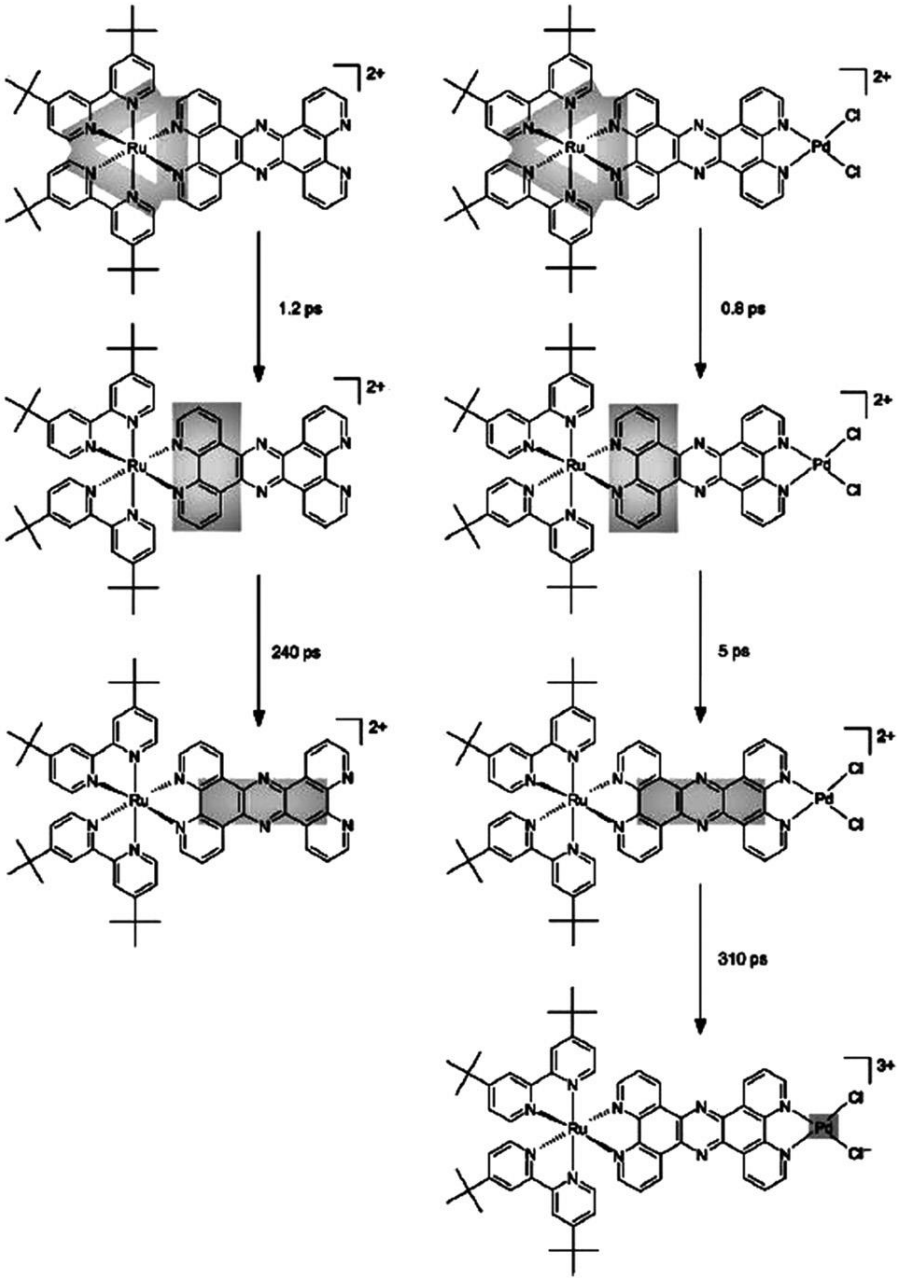

Scheme 1.2: Electron transfer dynamics of compound **1** and its precursor complex **1a**. Localisation of the electron in the photoexcited state is illustrated by shaded areas [68].

As appears in Scheme **1.2** initially, the first singlet metal-to-ligand charge-transfer excited states (^{1}MLCT) are formed in the light absorbing centre on the tbbipy (peripheral) /phenanthroline (bridging) moieties. This initial excited state

undergoes relaxation to a triplet ^{3}MLCT state and it is localised solely on the phenanthroline moiety of the bridging ligand tpphz. This transition from the singlet to triplet (from the photosensitizer to the bridging ligand)[68] occurs in 0.8 ps for the complete photocatalytic compound **1**, and 1.2 ps for the precursor **1a**. This difference is not very significant, which can be attributed to the fact that the transfer occurs away from the catalytic centre and it has small effect on it. It is worth nothing also is that this transition from the peripheral ligand to the phenanthroline unit of the bridging ligand occurs quickly upon the light absorption, which can be attributed to the structural design features of the compound. The bridging ligand was chosen to exhibit an excited state that has lower energy compared to the excited state populated on the peripheral ligands. The difference in decay times between the two compounds starts to be significant in case of the decay of the triplet excited state that is formed on the bridging ligand. The decay of the phenanthroline triplet excited state involves the intra-ligand-charge-transfer (ILCT) to the phenazine unit of the bridging ligand. The decay time is measured for compound **1**a was 240 ps, while for compound **1** it was 5 ps. These results prove that the Pd(II) centre has a major effect on the electronic properties of the bridging ligand. It applies a strong driving force on the bridging ligand to form the phenazine localised ILCT state from the phenanthroline-centred triplet excited state. This ICLT state decays further over 310 ps in the case of compound **1** to produce the long-lived ligand to metal charge transfer (LMCT) state on the Pd(II) catalytic centre. The electron paramagnetic resonance spectroscopy confirmed the presence of an excited electron on the phenazine part of the bridging ligand. The last step in the process is the reduction of the Pd(II) centre which is proven by observing the inhibition of the catalytic activity of 1 upon addition of Cl^- ions.

Because the reduction of the Pd centre involves the production of Cl^- , the addition of Cl^- ions is expected to inhibit the catalytic activity [67].

1.3.2 The effect of wavelength

In the previous section, it was apparent that during the photoexcitation of Compound **1**, the peripheral ligands are populated with the first photo-induced excited state. Also, it is essential for the catalytic activity is that the population of the bridging ligand occurs so that the photoinduced electron transfer to the catalytic centre happens. The differences in the excited states energies between the peripheral and the bridging ligands are important to create an energy gradient that allows a fast electron transfer in the right direction, but the strength of their electronic coupling is also important. NH_4PF_6 is the only material that is suitable for these studies.

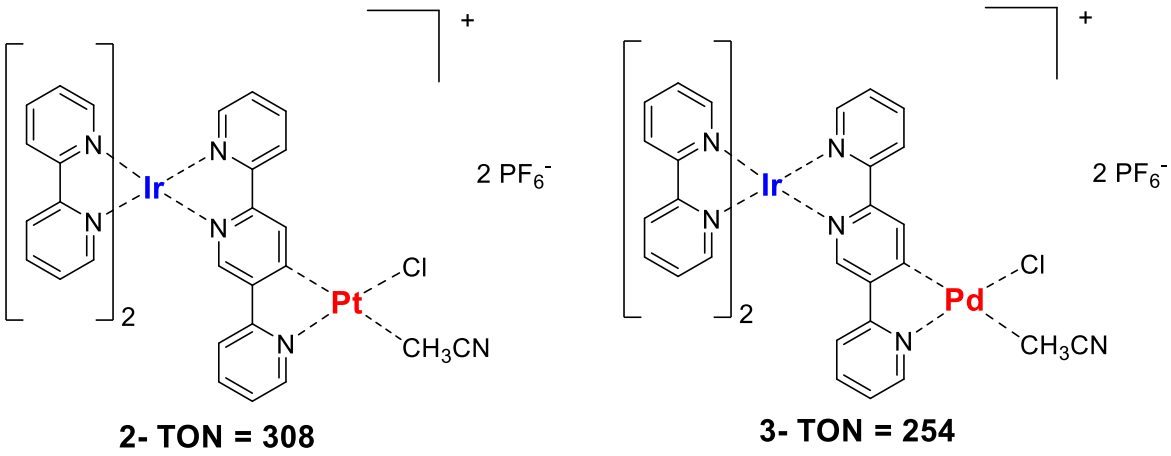

Figure 1.10: Structures of photocatalysts (2, 3) [35,69].

One example is that of Compounds **2** and **3** shown in Figure (1-10). The absorption properties of the two Compounds are very similar. The bridge contains in both cases, a pyrazine unit, that has the lowest MLCT state based most

probably on the bridging ligand [70], However, when the compounds are irradiated at 470 nm , turn over number (TON) numbers of 308 and 254 are obtained, indicating that the photocatalytic process is different. When both compounds are irradiated at 350 nm TON numbers of 65 and 16 are obtained for compounds 2 and 3 respectively. This observation clearly shows that the nature of the irradiation can have a strong influence on the photocatalytic behaviour of the compounds.

Bernhard and coworkers have carried out a large range of detailed studies about intermolecular mechanism of excitation transfer in Ir(III) complexes in which they found that com pounds **(2** and **3)** have high stability as photosensitisers. This increased photostability[71,72] is observed for different iridium complexes acting as photocatalysts for the photogeneration of hydrogen through an intermolecular mechanism of excitation transfer. This stability is a product of the greater ligand-field stabilisation energy of the third row elements imparts an important advantage to Ir(III) complexes over Ru(III) as observed in the comparison between compounds **2** and **3**. For these studies Ru(II) is the mostly used standard material available. For a second row element, direct population of the triplet metal centred (^{3}MC) excited state can result in ligand expulsion followed by decomposition, which is not the case for the Ir(III) based analogues [73]

1.3.3 Role of the peripheral ligands in the photocatalytic assembly

The peripheral ligands are an important part of the photosensitizer centre in the photocatalytic assembly, they coordinate the metal centre, so that, the electronic properties of the ligands alongside the nature of the metal determine the energy of the excited state and the absorption wavelength. These ligands should be

designed to be at the higher end of the energy gradient so that they can promote the vectorial electron transfer from the light harvesting unit to the catalytic centre by the bridging ligand, which is chosen to exhibit a lower energy excited state so as to be the lower end of the energy gradient. Also, the electronic coupling between the peripheral ligands and the bridging ligands should be favourable for populating the bridge orbitals and should drive the electron transfer from the peripheral ligands to the bridging ligand instead of decaying the excite state of the peripheral ligand to the ground state without carrying out the electron transfer. That is why, compounds in which the direct population of ^{3}MLCT states on the bridging ligand occurs have more photocatalytic activity.

One example for that is Compounds **4** and **5** shown Figure (1.11). The absorption properties of the two peripheral ligands are similar, For Compound **4** bpy is used as usual, but for Compound **5** two ester groups are bound to the peripheral ligand as shown in Figure 1.11. Although the two ligands seem very similar they have a very different photocatalytic behaviour. The bridge contains in both cases, a pyrazine unit, that has the lowest MLCT state based most probably on the bridging ligand at about 530 nm[74].

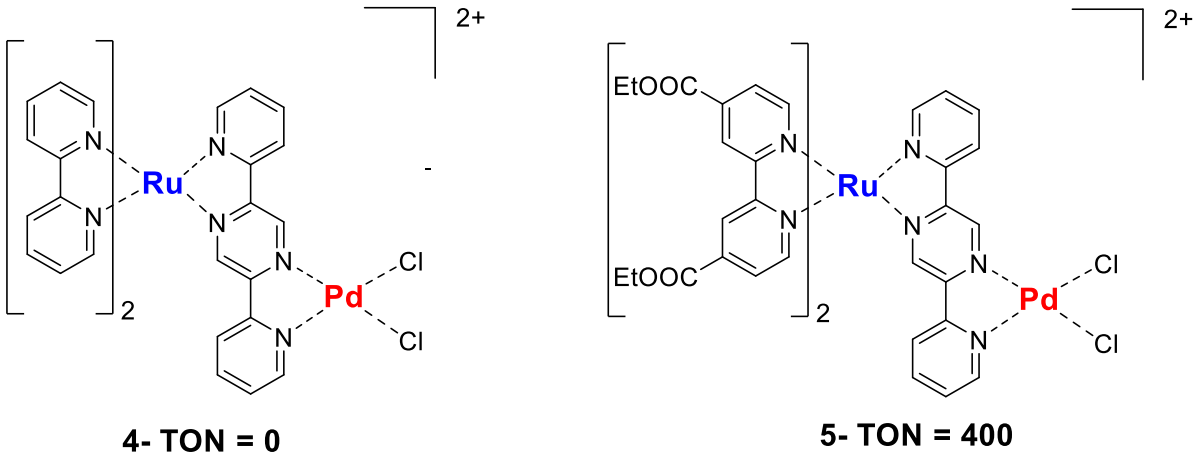

Figure 1.11: Structure of the photocatalyst (**4**, **5**) [35].

For Compound **4**, there is no photocatalytic activity and no hydrogen evolution was observed. But in case of Compound **5**, upon the addition of an ester group to the peripheral ligands the TON value was determined to be 400 in 18 h irradiation. That suggests that esterification causes the formation of peripheral ligands with improved π-acceptor properties. This leads to lower π*-energy levels for the peripheral ligands and improving electronic coupling with the bridging ligand.

1.3.4 The Role of the bridging ligand for photocatalytic assembly

The bridging ligand is the connecting bridge between the photosensitizer centre and the supramolecular catalytic moiety both covalently and also electronically via the conjugated π-electron system. The bridging ligand is coordinating with the metal in the centre of the photosensitizer and the metal of the catalytic centre. Therefore, it should contain two bidentate coordination sites at both ends. The interaction between the units of the photocatalytic supramolecular assembly depend heavily on the size, shape, and electronic nature of the bridge. The bridging ligand is designed bearing several considerations in mind. It should be of a suitable length to allow single direction photoinduced electron transfer, and also limiting the reverse electron transfer. As mentioned before, it is optimum that the design of the molecule ensures that the ^{3}MLCT state is populated on bridging ligand rather than on the peripheral ligands.

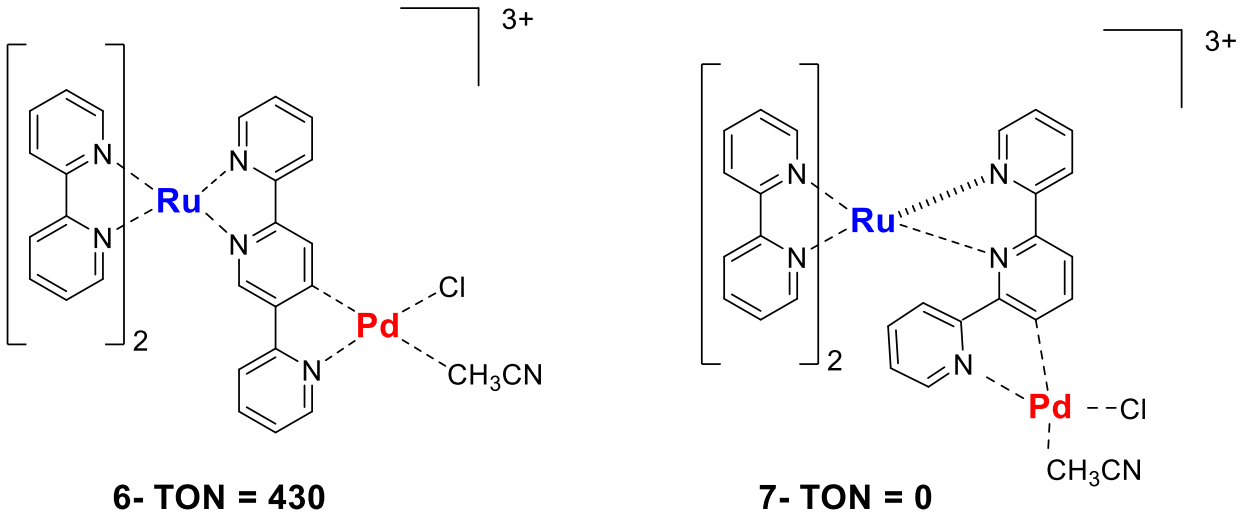

Figure 1.12: Structure of the photocatalyst (6, 7) [35].

Figure 1.12 is a good example of the experiments that shows the effect of the bridging ligand is Compound **6** and **7** are the most interested compounds, they are identical in every aspect except the bridging ligand. For Compound **6** the amount of hydrogen produced, TON value, was determined to be 430 after 18 hours irradiation, while Compound **7** is completely inactive [75]. This difference is attributed to the location of the lowest unoccupied molecular orbital LUMO. As shown by Resonance Raman and density functional theory DFT calculations, Compound **6** orbital is based on the bridging ligand, whereas for Compound **7** it is localised mainly on the bipy ligands and the Ru centre. This arrangement does not encourage the electron transfer from the light harvesting unit to the catalytic centre.

In addition to that, Rau *et al*. [76,77] have carried out small chemical modifications to the bridging ligand and assessed the resulting catalytic activity of Ru/Pd compounds. They added bromide to the tpphz bridging moiety of compound **1** to produce compound **8** which caused large decrease in catalytic activity (TON = 69 after 18 h) compared to 210 after 18 hours for compound **1**.

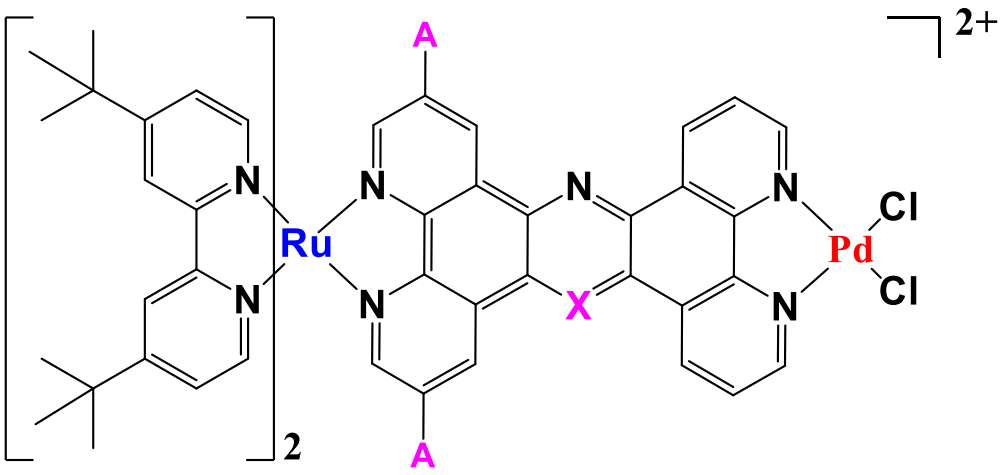

1-	X = N,	A = H	TON = 210
8-	X = N,	A = Br	TON = 69
9-	X = CH,	A = H	TON = 139

Figure 1.13: Structure of the photocatalyst (1, 8 and 9).

Also, for Compound **9** the pyrazine ring of tpphz was replaced by an acridine moiety and the photocatalytic activity was measured to be 139 which is different from the 210 value of the parent Compound **1**. All that shows how important the bridging ligand is to the design of a photo catalytic assembly.

1.4 Aim of the Thesis

To develop highly efficient photocatalytic cells for the production of hydrogen from water the compounds used should have high photosensitivity and photostability. In order to assess those two properties, it was decided that High-Performance Liquid Chromatography (HPLC) would be employed to carry out a qualitative analysis of the developed compounds after exposing them to light for variable

durations of time. HPLC is a powerful analytical tool as it provides qualitative information about the compounds when retention time is known and elution order is expected. Also using a photodiode array can identify substances by their characteristic UV/Vis spectrum. The area under the curve for the eluted peaks provides accurate quantitative information about the concentrations of different molecules. Moreover, HPLC can separate different compounds, even closely related ones, it is also valuable in detecting any degradation products for the compounds hence evaluating their stability. Combining this powerful separation ability with a fraction collector for semipreparative HPLC settings allowed us to obtain highly pure substances which made further analysis possible using other techniques.

In this study we aim to develop a number of techniques such as high performance liquid chromatography (HPLC) as an effective tool for the analysis, characterisation and the determination of the stability of a range of photocatalytic compounds before or after irradiation. The compounds studied are based on a number of intermolecular Ru/Pt compounds with three different bidentate (N^N) chelating ligands. First of all, the variation of the compounds is investigated by the effect that the peripheral ligands at the Ru(II) centre; 4,4'-bipyridine (bpy), 4,4'-diethoxycarbonyl-2,2'-bipyridine (dceb) and 1,10-phenanthroline (phen) have on the general behaviour of the compounds. For the peripheral ligands three distinct sorts of fringe ligands were utilized as a part of the photo-hydrogen-evolving process (PHE), action of the synthesised Ru/Pt compounds and to increase additional data about their impact on the properties of the catalysts. The structures of the three types peripheral ligands see Figure (1.14).

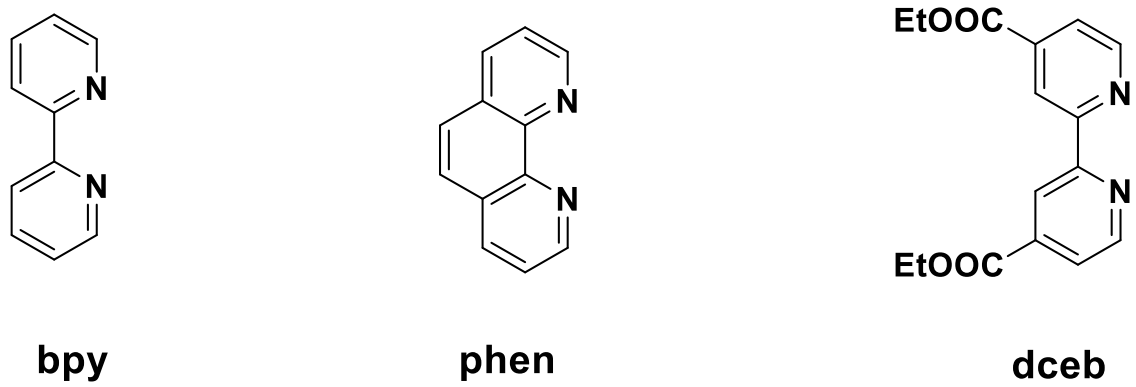

Figure 0.14: Structures of the peripheral ligands bpy, phen and dceb

The effect of the bridging ligands used include 2,2′:5′,2″-terpyridine (**2,5bpp**), 2,3-bis(2'-pyridyl)pyrazine (**2,3dpp**)], 2,2':5',3'':6'',2''-quaterpyridine **(bisbpy)** and 2,2′:6′,2″-terpyridine **(2,6bpp).** The structures of the all bridges ligand are displayed in Figure **1-15**.

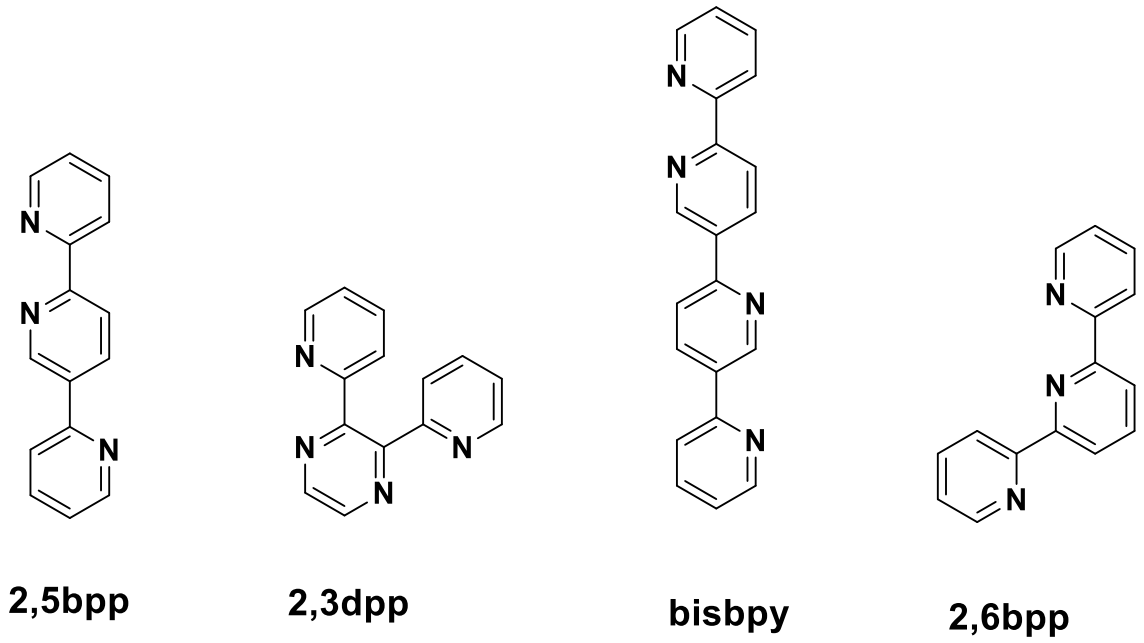

Figure 0.15: Structures of the bridging ligands 2,5bpp, 2,3dpp, bisbpy and 2,6bpp.

These photocatalysts are based on platinum centres as catalytic agents and the stability of these moieties, both mononuclear and intramolecular compounds are compared to those without a platinum centre corresponding to Ru(II) monomers as shown in Figure (**1.16**). It should be noted that the platinum catalytic centres contain halogen terminal ligands. Iodide and chloride were used to assess the effect of the type of the terminal ligand on the catalytic activity of the compound as well.

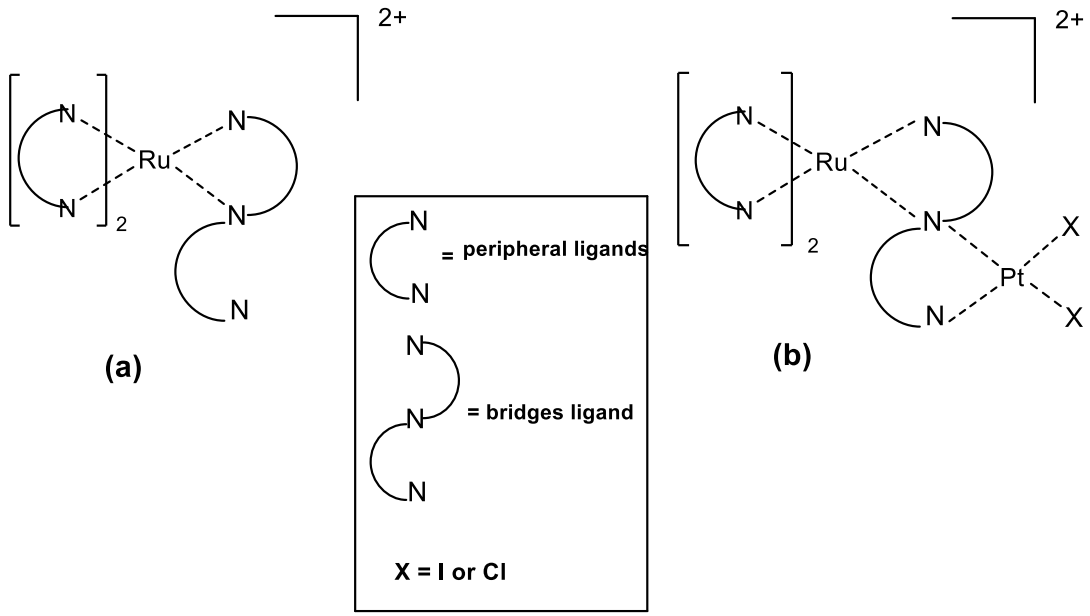

Figure 0.16: Structures of the compounds without platinum centre (corresponding Ru(II) monomers) (a), the compounds with platinum centre (b)

UV-vis absorption and ^{1}H-NMR analysis was carried out also to provides more detailed qualitative and structural information about the possible chemical changes following photocatalytic experiments.

References:

[1] J. P. Paris and W. W. Brandt, “Charge Transfer Luminescence of A Ruthenium(Ii) Chelate,” *J. Am. Chem. Soc.*, vol. 81, no. 18, pp. 5001–5002, 1959.

[2] A. V Balzani *et al.*, “Solar Energy Conversion by Water Photodissociation Published by : American Association for the Advancement of Science Stable URL : http://www.jstor.org/stable/1740342 REFERENCES Linked references are available on JSTOR for this article : You may need to l,” vol. 189, no. 4206, pp. 852–856, 2016.

[3] R. Ziessel, J. Hawecker, and J. -M Lehn, “Photogeneration of Carbon Monoxide and of Hydrogen via Simultaneous Photochemical Reduction of Carbon Dioxide and Water by Visible-Light Irradiation of Organic Solutions Containing Tris(2,2′-bipyridine)ruthenium(II) and Cobalt(II) Species as Homogeneous C,” *Helv. Chim. Acta*, vol. 69, no. 5, pp. 1065–1084, 1986.

[4] B. O’Regan and M. Gratzel, “© 19 9 1 Nature Publishing Group,” *Lett. to Nat.*, vol. 353, pp. 737–740, 1991.

[5] M. M.K. Nazeeruddin, S.M. Zakeeruddin, J.J. Lagref, P. Liska, P. Comte, C. Barolo, G. Viscardi, K. Schenk, “Graetzel Coord,” *Chem. Rev*, vol. 248, p. 1317, 2004.

[6] Z. S. Wang, Y. Cui, K. Hara, Y. Dan-Oh, C. Kasada, and A. Shinpo, “A high-light-harvesting-efficiency coumarin dye for stable dye-sensitized solar cells,” *Adv. Mater.*, vol. 19, no. 8, pp. 1138–1141, 2007.

[7] F. Gao *et al.*, “Enhance the Optical Absorptivity of Nanocrystalline TiO Film with High Molar Extinction Coefficient Ruthenium Sensitizers for High Performance Dye-Sensitized Solar Cells Enhance the Optical Absorptivity of Nanocrystalline TiO 2 Film with High Molar Extinc,” pp. 10720–10728, 2008.

[8] J. G. Vos and M. T. Pryce, “Photoinduced rearrangements in transition metal compounds,” *Coord. Chem. Rev.*, vol. 254, no. 21–22, pp. 2519–2532, 2010.

[9] J. G. Vos and J. M. Kelly, “Ruthenium polypyridyl chemistry; from basic research to applications and back again,” *Dalt. Trans.*, no. 41, p. 4869, 2006.

[10] S. Fanni, T. E. Keyes, C. M. O. Connor, H. Hughes, R. Wang, and J. G. Vos, “Excited-state properties of ruthenium (II) polypyridyl complexes containing asymmetric triazole ligands,” vol. 208, pp. 77–86, 2000.

[11] A. F. Martin and T. A. Nieman, “Chemiluminescence biosensors using tris(2,2’-bipyridyl)ruthenium(II) and dehydrogenases immobilized in cation exchange polymers,” *Biosens. Bioelectron.*, vol. 12, no. 6, pp. 479–489, 1997.

[12] J. G. Lee, K. Yun, G. S. Lim, S. E. Lee, S. Kim, and J. K. Park, “DNA biosensor based on the electrochemiluminescence of Ru(bpy)32+ with DNA-binding intercalators,” *Bioelectrochemistry*, vol. 70, no. 2, pp. 228–234, 2007.

[13] N. C. Han, H. Y. Sook, Y. K. Lyu, and W. Y. Lee, “Electrogenerated chemiluminescence ethanol biosensor based on carbon nanotube-titania-Nafion composite film,” *Electroanalysis*, vol. 19, no. 4, pp. 459–465, 2007.

[14] T. a Ruda-eberenz, A. Nagy, W. J. Waldman, and P. K. Dutta, “Entrapment of Ionic Tris (2 , 2 ′ -Bipyridyl) Ruthenium (II) in Hydrophobic Siliceous Zeolite : O 2 Sensing in Biological Environments,” *Environments*, vol. 29, no. Ii, pp. 9140–9147, 2008.

[15] B. Sun, H. Qi, F. Ma, Q. Gao, C. Zhang, and W. Miao, “Double Covalent Coupling Method for the Electrogenerated Chemiluminescence Sensors,” *Anal. Chem.*, vol. 82, no. 12, pp. 5046–5052, 2010.

[16] S. Welter, F. Lafolet, E. Cecchetto, F. Vergeer, and L. De Cola, “Energy transfer by a hopping mechanism in dinuclear IrIII/ RuII complexes: A molecular wire?,” *ChemPhysChem*, vol. 6, no. 11, pp. 2417–2427, 2005.

[17] K. Seo, A. V. Konchenko, J. Lee, S. B. Gyeong, and H. Lee, “Molecular conductance switch-on of single ruthenium complex molecules,” *J. Am. Chem. Soc.*, vol. 130, no. 8, pp. 2553–2559, 2008.

[18] L. Mercs, A. Neels, and M. Albrecht, “Probing the potential of N-heterocyclic carbenes in molecular electronics: redox-active metal centers interlinked by a rigid ditopic carbene ligand.,” *Dalton Trans.*, vol. 3, no. 41, pp. 5570–5576, 2008.

[19] B. J. Coe *et al.*, “Tuning of charge-transfer absorption and molecular quadratic non-linear optical properties in ruthenium(II) ammine complexes [dagger],” *J. Chem. Soc.{,} Dalt. Trans.*, no. 20, pp. 3617–3625, 1999.

[20] B. J. Coe *et al.*, “Pentacyanoiron(II) as an electron donor group for nonlinear optics: Medium-responsive properties and comparisons with related pentaammineruthenium(II) complexes,” *J. Am. Chem. Soc.*, vol. 128, no. 37, pp. 12192–12204, 2006.

[21] G. Will, G. Boschloo, R. Hoyle, S. N. Rao, and D. Fitzmaurice, “Potentiostatic Modulation of the Direction of Light-Induced Electron Transfer in a Heterosupermolecule,” *J. Phys. Chem. B*, vol. 102, no. 50, pp. 10272–10278, 1998.

[22] J. -M Lehn, “Supramolecular Chemistry—Scope and Perspectives Molecules, Supermolecules, and Molecular Devices (Nobel Lecture),” *Angew. Chemie Int. Ed. English*, vol. 27, no. 1, pp. 89–112, 1988.

[23] S. Campagna *et al.*, “Aggregation in Fluid Solution of Dendritic Supermolecules made of Ruthenium(II)- and Osmium(II)-Polypyridine Building Blocks,” *J. Am. Chem. Soc.*, vol. 117, no. 6, pp. 1754–1758, 1995.

[24] E. C. Constable, “Metallodendrimers: Metal ions as supramolecular glue,” *Chem. Commun.*, vol. E. C. Cons, pp. 1073–1080, 1997.

[25] M. Ruben, J. Rojo, F. J. Romero-Salguero, L. H. Uppadine, and J. M. Lehn, “Grid-type metal ion architectures: Functional metallosupramolecular arrays,”

Angew. Chemie - Int. Ed., vol. 43, no. 28, pp. 3644–3662, 2004.

[26] J.-M. Lehn, *Supramolecular Chemistry*. Germany: Wiley-VCH, Weinheim, 1995.

[27] S. Faulkner, L. S. Natrajan, W. S. Perry, and D. Sykes, “Sensitised luminescence in lanthanide containing arrays and d–f hybrids,” *Dalt. Trans.*, no. 20, p. 3890, 2009.

[28] P. R. Ashton *et al.*, “Simple Mechanical Molecular and Supramolecular Machines: Photochemical and Electrochemical Control of Switching Processes,” *Chem. - A Eur. J.*, vol. 3, no. 1, pp. 152–170, 1997.

[29] A. Kirsch-De Mesmaeker, J.-P. Lecomte, and J. Kelly, “Photoreactions of metal complexes with DNA, especially those involving a primary photo-electron transfer,” *Top. Curr. Chem.*, vol. 177, pp. 25–76, 1996.

[30] IPCC, *Mitigation of climate change: Contribution of working group III to the fourth assessment report of the Intergovernmental Panel on Climate Change*. 2007.

[31] N. S. Lewis and D. G. Nocera, “For the ‘“In This Issue”’ summary,” *J. Qual. Particip.*, vol. 104, no. 42, pp. 20142–20142, 2007.

[32] D. G. Nocera, “Living healthy on a dying planet,” *Chem. Soc. Rev.*, vol. 38, no. 1, pp. 13–15, 2009.

[33] V. Fernández-Moreira, F. L. Thorp-Greenwood, and M. P. Coogan, “Application of d6 transition metal complexes in fluorescence cell imaging,” *Chem. Commun.*, vol. 46, no. 2, pp. 186–202, 2010.

[34] J. Barber, “Revealing the blueprint of photosynthesis,” *Nat.*, vol. 370, p. 31, 1994.

[35] Y. Halpin, M. T. Pryce, S. Rau, D. Dini, and J. G. Vos, “Recent progress in the development of bimetallic photocatalysts for hydrogen generation,” *Dalt. Trans.*, vol. 42, no. 46, p. 16243, 2013.

[36] N. S. Lewis and D. G. Nocera, “Powering the planet: Chemical challenges in solar energy utilization,” *Proc. Natl. Acad. Sci.*, vol. 103, no. 43, pp. 15729–15735, 2006.

[37] K. Bennaceur, B. Clark, F. M. Orr, T. S. Ramakrishnan, C. Roulet, and E. Stout, “Hydrogen : A Future Energy Carrier?,” *Oilf. Rev.*, pp. 30–41, 2005.

[38] G. Singh Bindra *et al.*, “The effect of peripheral bipyridine ligands on the photocatalytic hydrogen production activity of Ru/Pd catalysts,” *Dalt. Trans.*, vol. 40, no. 41, p. 10812, 2011.

[39] P. V. Kamat and J. Bisquert, “Solar fuels. Photocatalytic hydrogen generation,” *J. Phys. Chem. C*, vol. 117, no. 29, pp. 14873–14875, 2013.

[40] S. Berardi *et al.*, “Molecular artificial photosynthesis,” *Chem. Soc. Rev.*, vol. 43, no. 22, pp. 7501–7519, 2014.

[41] J. Hong, W. Zhang, J. Ren, and R. Xu, “Photocatalytic reduction of CO2: a brief review on product analysis and systematic methods,” *Anal. Methods*, vol. 5, no. 5, p. 1086, 2013.

[42] A. FUJISHIMA, “Electrochemical Photolysis of Water at a Semiconductor,” *Nat.*, vol. 238, no. 5358, pp. 37–38.

[43] “Photophysics, photochemistry and solar energy conversion with tris(bipyridyl)ruthenium(II) and its analogues,” *Coord. Chem. Rev.*, vol. 46, pp. 159–244, Oct. 1982.

[44] A. Juris, V. Balzani, F. Barigelletti, S. Campagna, P. Belser, and A. von Zelewsky, “Ru(II) polypyridine complexes: photophysics, photochemistry, eletrochemistry, and chemiluminescence,” *Coord. Chem. Rev.*, vol. 84, no. C, pp. 85–277, 1988.

[45] V. Balzani, A. Juris, M. Venturi, S. Campagna, and S. Serroni, “Luminescent and Redox-Active Polynuclear Transition Metal Complexes †,” *Chem. Rev.*, vol. 96, no. 2, pp. 759–834, 1996.

[46] H. M. Y. Ahmed and S. J. G. Vos, “Investigation of the Photochemical Properties of Ruthenium Polypyridyl Complexes using High Performance Liquid Chromatography (HPLC) By Ollscoil Chathair Bhaile Átha Cliath A Thesis presented to Dublin City University for the Degree of Doctor of Philoso,” 2010.

[47] M. Schwalbe, “Ph.D. Thesis,” Friedrich-Schiller-University of Jena, 2007.

[48] M. L. A. Abrahamsson, *Electron Transfer in Ruthenium-Manganese Complexes for Artificial Photosynthesis*. 2001.

[49] G. A. Crosby, “Spectroscopic Investigations of Excited States of Transition-Metal Complexes,” *Acc. Chem. Res.*, vol. 8, no. 7, pp. 231–238, 1975.

[50] C. J.P. Sauvage, J.P. Collin, J.C. Chambron, S. Guillerez, “No Title,” *Coudret Chem. Rev*, vol. 94, p. 993, 1994.

[51] R. Hage *et al.*, “Ruthenium Compounds Containing Pyridyltriazines with Low-Lying π* Orbitals,” *Inorg. Chem.*, vol. 29, no. 5, pp. 988–993, 1990.

[52] B. E. Buchanan, R. Wang, J. G. Vos, R. Hage, J. G. Haasnoot, and J. Reedijk, “Chromatographic Separation and Characterization of Linkage Isomers of the 3-(Pyridin-2-yl)-1H-1,2,4-triazole Complex of Ruthenium(II) Bis(2,2′-bipyridyl),” *Inorg. Chem.*, vol. 29, no. 17, pp. 3263–3265, 1990.

[53] R. Wang, J. G. Vos, R. H. Schmehl, and R. Hage, “pH Control of Photoreactivity of Ru(II) Pyridyltriazole Complexes: Photoinduced Linkage Isomerism and Photoanation,” *J. Am. Chem. Soc.*, vol. 114, no. 6, pp. 1964–1970, 1992.

[54] M. Maestri, N. Armaroli, V. Balzani, E. C. Constable, and A. M. W. C. Thompson, “Complexes of the Ruthenium(II)-2,2′:6′,2″ -Terpyridine Family. Effect of Electron-Accepting and -Donating Substituents on the Photophysical and Electrochemical Properties,” *Inorg. Chem.*, vol. 34, no. 10, pp. 2759–2767,

1995.

[55] T. F. George, “Laser-Stimulated Molecular Dynamics and Rate Processes,” *Advances*, vol. 100, no. 10, pp. 10–21, 1982.

[56] N. H. Damrauer, “Femtosecond Dynamics of Excited-State Evolution in [Ru(bpy)3]2+,” *Science (80-.).*, vol. 275, no. 5296, pp. 54–57, 1997.

[57] E. S. Andreiadis, M. Chavarot-Kerlidou, M. Fontecave, and V. Artero, “Artificial photosynthesis: From molecular catalysts for light-driven water splitting to photoelectrochemical cells,” *Photochem. Photobiol.*, vol. 87, no. 5, pp. 946–964, 2011.

[58] M. Schwalbe, “Ph.D. Thesis,” Friedrich-Schiller-University of Jena, Institute of inorganic and analytical chemistry, 2007.

[59] B. P. Sullivan and T. J. Meyer, “Comparisons of the Physical and Chemical Properties of Isomeric Pairs. 2. Photochemical, Thermal, and Electrochemical Cis-Trans Isomerizations of M(Ph2PCH2PPh2)2Cl2 (M = RuII, OsII),” *Inorg. Chem.*, vol. 21, no. 3, pp. 1037–1040, 1982.

[60] B. Durham, J. V. Caspar, J. K. Nagle, and T. J. Meyer, “Photochemistry of tris(2,2’-bipyridine)ruthenium(2+) ion,” *J. Am. Chem. Soc.*, vol. 104, no. 18, pp. 4803–4810, 1982.

[61] B. Durham, J. L. Walsh, C. L. Carter, and T. J. Meyer, “Synthetic Applications of Photosubstitution Reactions of Poly(Pyridyl) Complexes of Ruthenium(II),” *Inorg. Chem.*, vol. 19, no. 4, pp. 860–865, 1980.

[62] S. Tachiyashiki, H. Ikezawa, and K. Mizumachi, “Identification of an Intermediate of the Photosubstitution of a Ruthenium(II) Diimine Complex with a Monodentate Chelating Ligand: 1H NMR and HPLC Evidence,” *Inorg. Chem.*, vol. 33, no. 4, pp. 623–625, 1994.

[63] and S. C. F. Puntoriero, F. Nastasi, M. Galletta, *Comprehensive Inorganic Chemistry II*. Oxford, 2013.

[64] C. Balzani, S. Campagna, N. Armaroli, G. Accorsi, F. Cardinali, and A. Listorti, “Photochemistry and Photophysics of Coordination Compounds,” no. June, pp. 69–115, 2007.

[65] Y. Halpin, M. T. Pryce, S. Rau, D. Dini, and J. G. Vos, “Recent progress in the development of bimetallic photocatalysts for hydrogen generation,” *Dalt. Trans.*, vol. 42, no. 46, pp. 16243–16254, 2013.

[66] T. Kowacs *et al.*, “Supramolecular bimetallic assemblies for photocatalytic hydrogen generation from water,” *Faraday Discuss.*, vol. 185, no. November 2017, pp. 143–170, 2015.

[67] S. Rau *et al.*, “A supramolecular photocatalyst for the production of hydrogen and the selective hydrogenation of tolane,” *Angew. Chemie - Int. Ed.*, vol. 45, no. 37, pp. 6215–6218, 2006.

[68] S. Tschierlei *et al.*, “Photophysics of an intramolecular hydrogen-evolving Ru-

Pd photocatalyst," *Chem. - A Eur. J.*, vol. 15, no. 31, pp. 7678–7688, 2009.

[69] S. Soman *et al.*, "Wavelength dependent photocatalytic H 2 generation using iridium-Pt/Pd complexes," *Dalt. Trans.*, vol. 41, no. 41, pp. 12678–12680, 2012.

[70] N. R. Champness, "The future of metal-organic frameworks," *Dalt. Trans.*, vol. 40, no. 40, pp. 10311–10315, 2011.

[71] J. I. Goldsmith, W. R. Hudson, M. S. Lowry, T. H. Anderson, and S. Bernhard, "Discovery and high-throughput screening of heteroleptic iridium complexes for photoinduced hydrogen production," *J. Am. Chem. Soc.*, vol. 127, no. 20, pp. 7502–7510, 2005.

[72] M. S. Lowry and S. Bernhard, "Synthetically Tailored Excited States: Phosphorescent, Cyclometalated Iridium(III) Complexes and Their Applications," *Chem. - A Eur. J.*, vol. 12, no. 31, pp. 7970–7977, 2006.

[73] R. J. Watts and J. Van Houten, "Effect of Ligand Substituents of the 'd-d' Luminescence of Iridium(III) and Rhodium(III) Complexes of 1,10-Phenanthroline," *J. Am. Chem. Soc.*, vol. 96, no. 13, pp. 4334–4335, 1974.

[74] M. Schulz *et al.*, "Reinvestigating 2,5-di(pyridin-2-yl)pyrazine ruthenium complexes: Selective deuteration and Raman spectroscopy as tools to probe ground and excited-state electronic structure in homo- and heterobimetallic complexes," *Dalt. Trans.*, vol. 40, no. 40, pp. 10545–10552, 2011.

[75] G. Singh Bindra *et al.*, "The role of bridging ligand in hydrogen generation by photocatalytic Ru/Pd assemblies," *Dalt. Trans.*, vol. 41, no. 42, pp. 13050–13059, 2012.

[76] M. Karnahl *et al.*, "Tuning of photocatalytic hydrogen production and photoinduced intramolecular electron transfer rates by regioselective bridging ligand substitution," *ChemPhysChem*, vol. 12, no. 11, pp. 2101–2109, 2011.

[77] M. Karnahl *et al.*, "Synthesis and photophysics of a novel photocatalyst for hydrogen production based on a tetrapyridoacridine bridging ligand," *Chem. Phys.*, vol. 393, no. 1, pp. 65–73, 2012.

CHAPTER 2

Methodology, Experimental, Classification and Characterisation of High-Performance Liquid Chromatography.

2.1 Introduction

High performance liquid chromatography (HPLC) is a technique that is often used in the separation and characterisation of inorganic and organic chemistry. However, the DCU group has applied this technique with considerable success [1]. HPLC was used to monitor the tris(2,2'-bipyridyl) ruthenium $[Ru(bpy)_3]^{2+}$ reactions for the first time by Valently and Behnken in the late seventies [2], using UV absorption detectors at wavelength of 280 nm. The ability to developed novel HPLC methods to separate species with very similar structures (either isomers or not), along with the high sensitivity of the technique allows for the identification of products obtained from the photochemical reaction of complexes of the type $[Ru(bpy)_2(X)]^{n+}$ [1]. thanks to the development of an HPLC method based on a cation exchange column [3,4].

An example is the investigation of the potential of HPLC for the study and purification of a range of triazole based compounds such as $[Ru(bpy)_2(Hptr)](PF_6)_2$ where Hptr is 3-(pyridine-2-yl)-1H-1,2,4-triazole, $[Ru(bpy)_2(H_3M_5ptr)](PF_6)_2$ where H3M5ptr is 5-methyl-3-(pyridine-2-yl)-1H-1,2,4-triazole and $[Ru(bpy)_2(Hbpt)](PF_6)_2$ where Hbpt is 3,5-bis(pyridin-2-yl)-1,2,4-triazole. (See Figure 2.1)

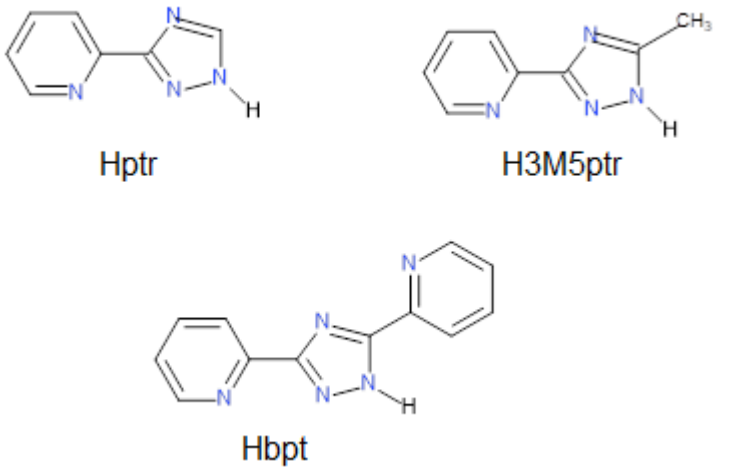

Figure 2.1: Structures of pyridyl triazole ligands 3-(pyridine-2-yl)-1H-1,2,4-triazole (Hptr), 5-methyl-3-(pyridine-2-yl)-1H-1,2,4-triazole (H3M5ptr) and 3,5-bis(pyridin-2-yl)-1,2,4-triazole (Hbpt))

The HPLC traces of two ruthenium compounds and ^{1}H-NMR spectra are outlined in Figure 2.2 and Figure 2.3 below.

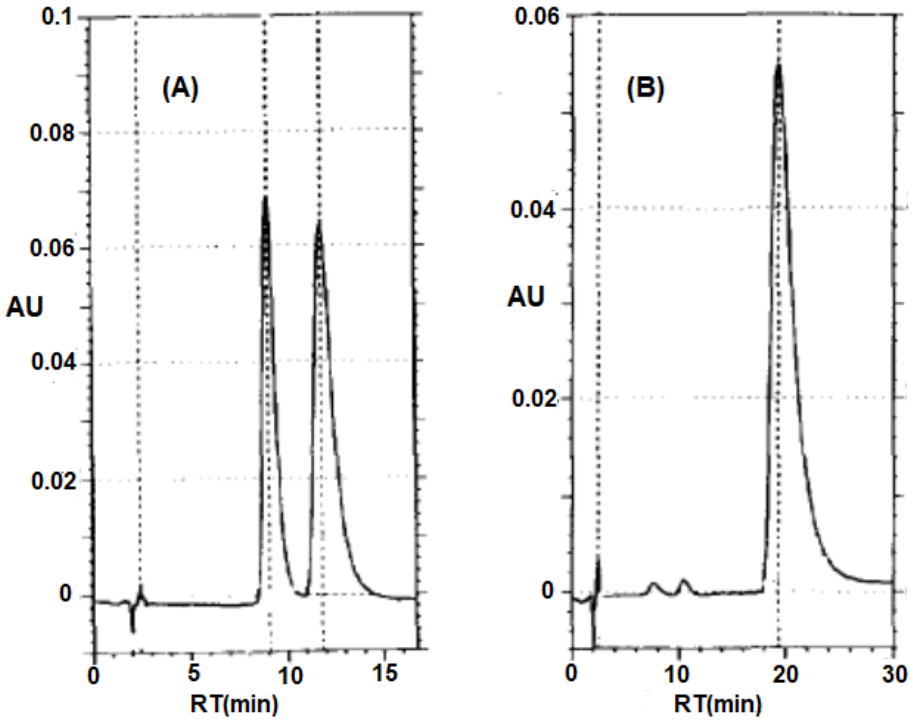

Figure 2. 2: Chromatograms of compounds $[Ru(bpy)_2(Hbpt)](PF_6)_2$ (A) and the $[Ru(bpy)_2(H_3M_5ptr)](PF_6)_2$ (B), Columns SCX, mobile phase acetonitrile / water (80/20) containing 0.08 M LiClO4, detection wavelength 280 mn, Flow rate 2.0 ml /min [2].

The chromatograms shown above suggest that for both complexes the pyridyl triazole ligands deprotonate while on the column. two different isomers are obtained, while for compound **B** only one species is produced in the synthetic process. The first observation indicates, that two isomers obtained for compound **A** are coordinated to the nitrogen atoms **N1** and **N2** of the triazole and pyridine ring, while at the same time compound **B** only shows a major peak is obtained since no free nitrogen atom is available because of steric reasons hinderence. These observations are of considerable importance in the further study of ruthenium containing 1,2,4-triazole compounds. Coordination through the ^{1}HNMR spectroscopy the **N2'** atom of compound **B** is confirmed, of particular interest is that the results show that compound **A** loses its proton when deprotonated on the HPLC, however, no deprotonation of compound **B** is observed. particular importance is that the results show that compound **B** loses its proton when deprotonated on the HPLC.

Subsequently the separation of the isomers of compound **A** isomer was carried out using semi-preparative HPLC techniques. The compound used was $[Ru(bpy)_2(ptr)](PF_6)$, as shown in Figure 2.2. As an example, the NMR spectra of both isomers, the **N4** isomer and the **N2** isomer are shown in Figure 2.3 below. Using HPLC as a purification method for the isolation of a photochemical intermediate obtained by photolysis was clearly established [3,4]. With the HPLC method applied up to 100 mg of pure compounds can be obtained.

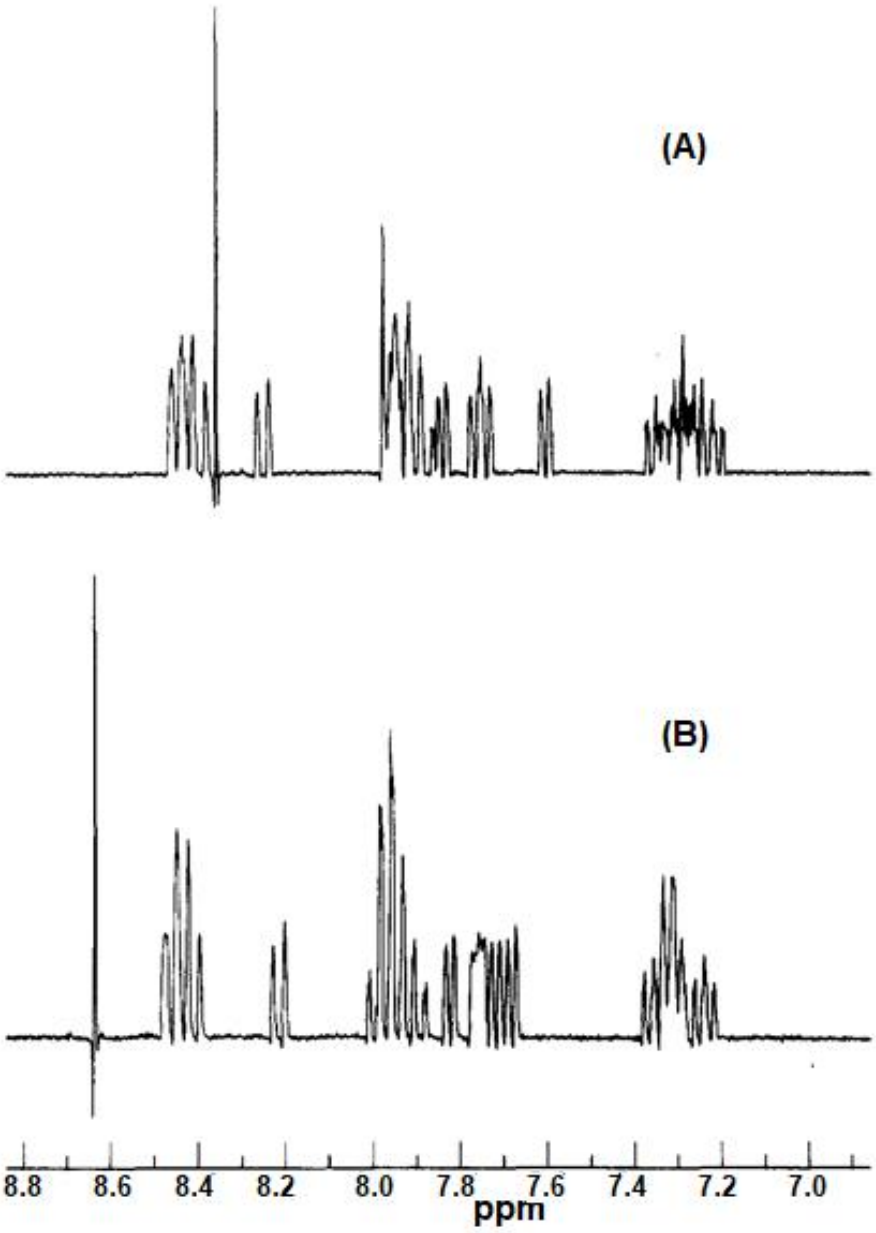

Figure 2. 3: Proton NMR spectroscopy of the two separated isomers of compound $[Ru(bpy)_2(ptr)](PF_6)$ under acid conditions. The spectra of the protonated isomers A, N4 and **B**, N2, are obtained using semi-preparative HPLC at pH of 2.37 N4 (**B**) and N2 0.60 respectively

The photoactive behaviour of related ruthenium triazole compounds was also studied with HPLC techniques. In this study the photophysical and photochemical properties of the ruthenium $[Ru(bpy)_2(4Mptr)](PF_6)_2$ triazole compounds were investigated in detail. The results indicate that the presence of coordinating

counter ions yields the cis-anion complex with loss of the pyridyl triazole ligand. However, the protonated form is photostable [5,6]. The thermal and photochemical properties of pyridyltriazole complexes was further investigated. These studies were again supported by semipreparative HPLC. A typical example is shown in Fig 2.4 below for the compound $[Ru(bpy)_2(4Mptr)](PF_6)_2$ [5] where 4Mptr is the 4-methyl-l - (pyridin-2-yl)-l,2,4-triazole.

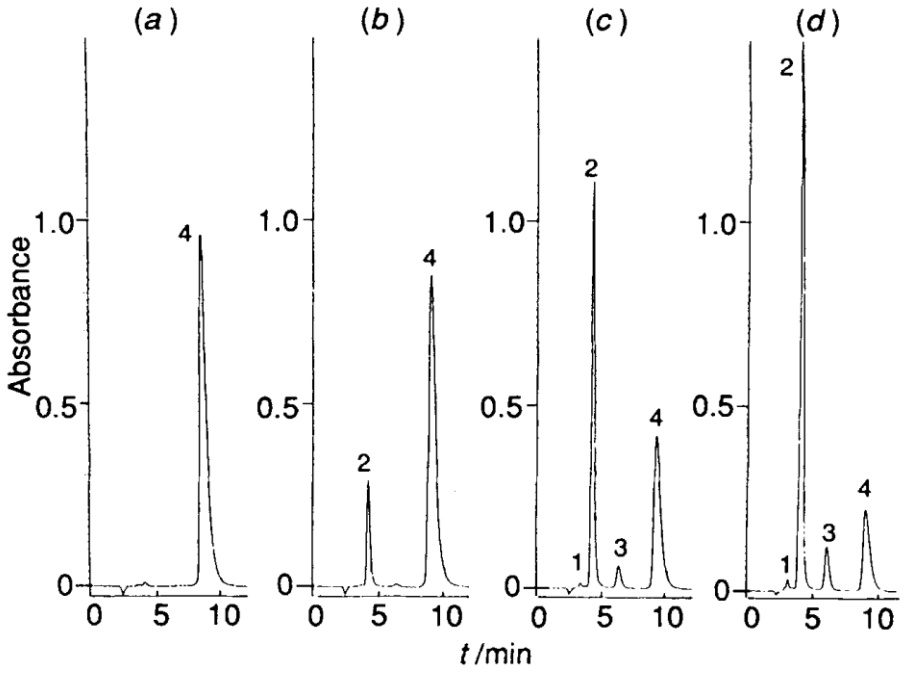

Figure 2.4: HPLC traces taken during the photolysis of compound $[Ru(bpy)_2(4Mptr)](PF_6)_2$ in acetonitrile . Photolysis times, (a) 0s, b 60s, c 360s, d 660 s, Columns SCX, Flow rate 2.0 cm^3/min mobile phase acetonitrile: water 80:20 containing 0.1 $mol.dm^{-3}$ $LiClO_4$. Detection wavelength 280 nm.

From the HPLC analysis it is clear that upon photolysis of compound **1** (peak 4) a number of main products are formed. The most important of these are the two products $[Ru(bpy)_2(MeCN)_2]^{2+}$ and $[Ru(bpy)_2(4Mptr)(MeCN)]^{2+}$, were identified by comparison with an authentic sample. This compound is also the expected final

photoproduct. From the fact that no free ligand is formed during the formation of Peak 2, this species is identified as $[Ru(bpy)_2(4Mpt)(MeCN)]^{2+}$.

Semipreparative HPLC is therefore found to be useful for the separation, identification and quantification of isomers in case of ruthenium complexes with asymmetrical ligands like 3-(pyridin-2'-yl)-1,2,4-triazole [3,4,5,6] 1-methyl-3-(pyridin-2'-yl)-1,2,4-triazole or 2-(4'*H*-[1,2,4]triazol-3'yl)pyrazine [7,8] and for the separation of isomers deriving from dimeric ruthenium complexes with ligands like 3,5-bis(pyridin-2'-yl)-1,2,4-triazole [9,10,11,12] or 3,5-bis(pyrazin-2'-yl)-1,2,4-triazole [3,4,5,6,13,14].

Several other multinuclear ruthenium complexes were analysed using cation exchange HPLC of which compounds containing ligands such as 2-phenyl-pyridine [15] and 2,5-bis(5'-methyl-4'H-[1,2,4]triaz-3'-yl)-pyrazine [16]. This technique was also used in characterising bipyridine complexes with metals other than ruthenium, for example, iron and nickel [17], which proves its wide ability to purify and characterize metal complexes with bipyridyl-based ligands. The isomerisation of two possible coordination isomers for the $[Ru(bpy)_2(Hpytr)]^{2+}$, complex has been reported, the different coordination isomers where separated by semi-preparative HPLC [18,19], In this compound the Hpytr ligand is attached *via* either the **N2** or the **N4** nitrogen atom of the triazole ring as illustrated in Figure 2.5

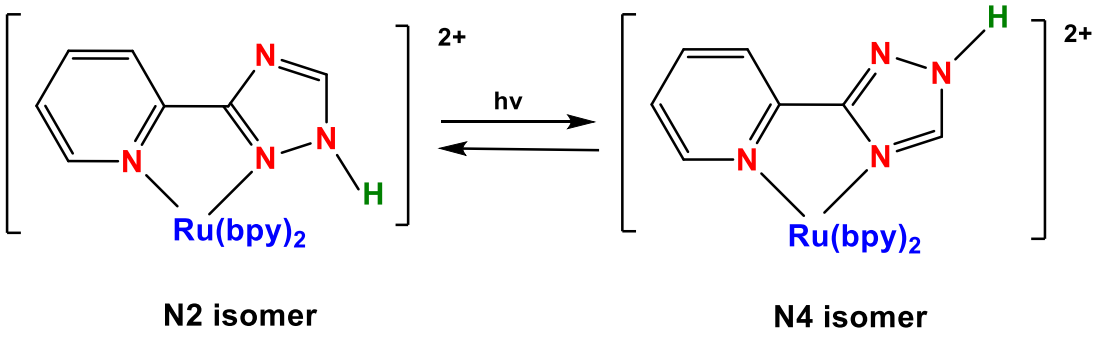

Figure 2. 5: The Hpytr ligand is bound via either the **N2** or the **N4** nitrogen atom of the triazole ring.

For this experiment, HPLC was of value in the separation and identification of the two isomers. The HPLC traces of the photolysis of these isomers in CH_2Cl_2 produced (aside the peak due to solvent) two peaks, the first was due to **N2** isomer and peak 3 was of the **N4** isomer [18,19].

HPLC was also used in the characterisation of the products of photolysis obtained from irradiation of related polypyridyl compounds [13,14,20,21,22]. In particular, the study of the photoreactions of the dinuclear complex using HPLC. Those compounds include $[Ru(bpy)_2(bpt)Ru(phen)_2](PF_6)_3$ (bpt = 3,5-bis-(pyridin-2'-yl)-1,2,4-triazole; phen = 1,10-phenanthroline) and its isomer $[Ru(phen)_2(bpt)Ru(bpy)_2](PF_6)_3$. This study allowed the characterisation and identification of the fragmentation products such as $[Ru(bpy)_2(CH_3CN)_2]^{2+}$, $[Ru(bpy)_2(CH_3CN)Cl]^{+}$ and $[Ru(bpy)_2Cl_2]$ and $[Ru(bpy)_2(bpt)]^{+}$, [13,14], while in case of $[Ru(bpy)_2(tbmbpy)]Cl_2$ irradiation {tbmbpy = *trans*-1,2-bis[4-(4'-methyl)-2,2'-bipyridyl] ethane}, HPLC verified the process of a light-driven dimerization [20,21,22].

At present we concentrate on the use of HPLC for the separation and analysis of the photoreaction products produced from the irradiation of the binuclear

complexes of ruthenium {$[Ru(bpy)_2]_2L]^{3+}$ with L = bpt (see Figure 2.1) [23,24] and bpzt [bpzt = 3,5-bis-(pyrazin-2'-yl)-1,2,4-triazole] [3,4] and of related mononuclear pyrazinetriazole compounds. The photochemistry of binuclear systems is very interesting because it is possible to induce *intramolecular* transfer of excitation and/or charge between the two metal centres [6,7,25,26] by irradiating the compound with light that has the frequencies of metal-to-ligand charge transfer (MLCT) transitions. $[(Ru(bpy)_2)_2L]^{3+}$ complexes are considered as supramolecular systems in which the metal centres perform different functions in the photoactivation processes [27,28,29]. However, in this study our interest is on the photochemical behaviour of dinuclear compounds that are able to split water into its elemental components and produce hydrogen from water and solar light.

High performance liquid chromatography (HPLC) is an essential research tool used for the qualitative and quantitative analysis of synthetic and natural products and polymers by separating different compounds to fractions depending on different physical and chemical properties of the substances including hydrophobicity, chemical composition, molecular weight, functional groups, charge etc. Similar to other chromatographic techniques, separation in HPLC results from the partitioning of the different chemicals present in the sample components between the mobile phase and stationary phase. The difference between HPLC and other chromatographic techniques is that this process takes place in solution (hence called liquid) inside the chromatographic column that is packed with stationary phase. This stationary phase can be inorganic (usually, silica-based) or organic (synthetic resin, such as polystyrene–divinyle benzene and acrylic-based materials) porous particles, that is both mechanically and

chemically stable in high pressure applied on the moving liquid (mobile phase) which is pumped mechanically through the column. There are different types of HPLC according to the mobile phase composition, isocratic (in which the mobile phase does not change its composition) or gradient (the composition of the mobile phase changes by time), this significantly expands the capabilities of the technique [30]. Separating different components is due to their differences in migration rates through the stationary phase column as shown in Figure 2.6 [31,32].

2.1.1 Classification of HPLC Methods

There are different ways to categorise HPLC. This classification can be based on the type of the stationary phase and the separation process, three modes can be specified [31].

2.1.1.1 Adsorption Chromatography

In this type, the stationary phase is an adsorbent (as silica gel or any other silica based packing) and the separation between components is based on their repeated adsorption- desorption steps.

2.1.1.2 Partition or Distribution

Those similar terms used to describe the equilibrium process that is attained between the concentration of the analyte in the mobile phase and the stationary phase.

2.1.1.3 Size Exclusion

In this technique, the separation between species is based on their relative size or three dimensional shape. Where the bigger sized molecule moves faster than smaller, also the shape affects the relative retention times.

2.1.1.4 Ion Exchange

This type involves the exchange of ions, (cation, or anion) during the process of separation [33].

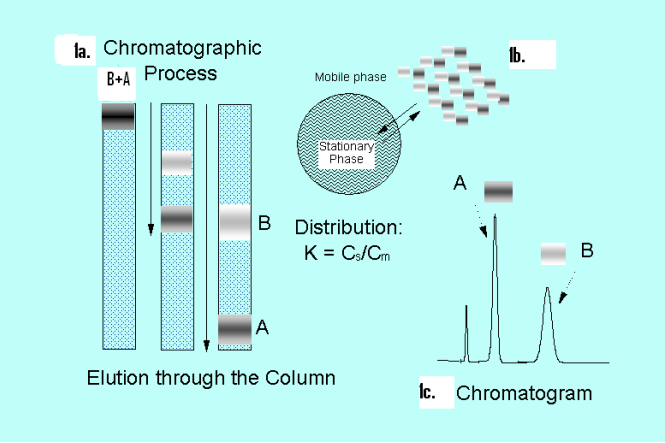

Figure 2. 6**:** (a) Schematic of the chromatographic process showing the migration of two bands of components down a column. (b) Microscopic representation of the partitioning process of analyte molecules A and B into the stationary phase bonded to a spherical solid support. (c) A chromatogram plotting the signal from a UV detector displays the elution components A and B. [33].

2.1.1.5 Ion- Exchange Chromatography (IEC)

In the ion-exchange chromatography [34,35], the separation theory is based on the exchange of ionic analytes with the ions of the same charge that is bound to ions of opposite charge immobilised on the surface of the stationary phase (Figure 2.7). Typical stationary phases which are cationic has (sulfonate), or anionic has (quaternary ammonium) groups bound to polymeric or silicacious

particles. The mobile phases consist of buffers, mostly with increasing ionic strength, to enhance the migration of the analytes. Among the most common applications are the analysis of ions and biological components such as amino acids, proteins/peptides, and polynucleotides.

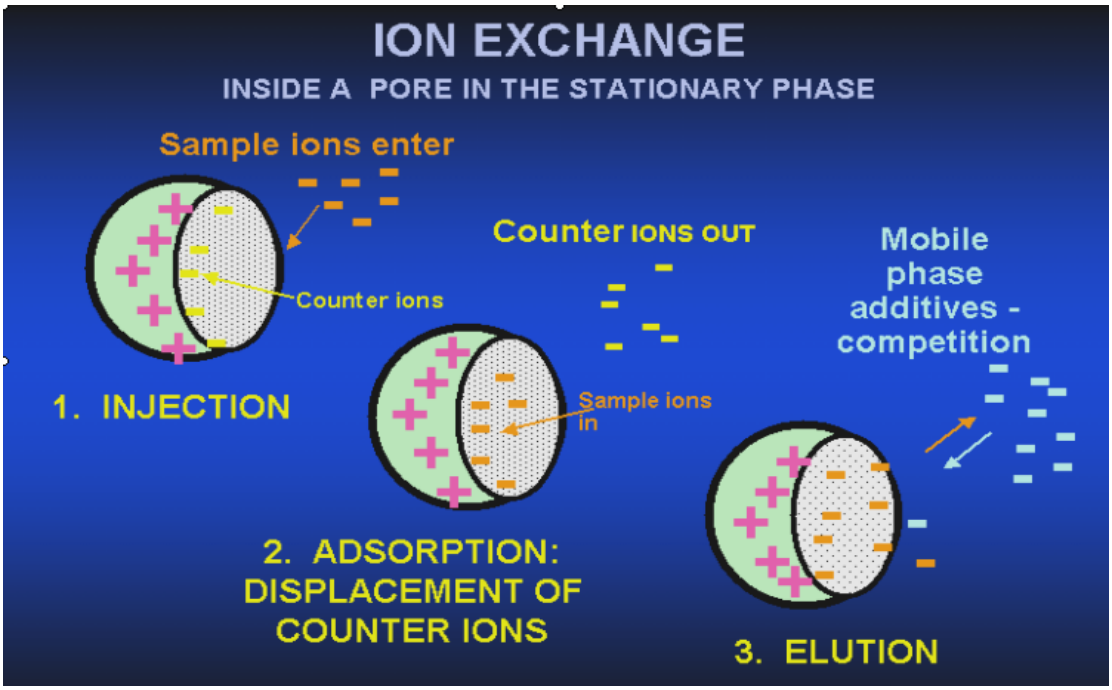

Figure 2. 7: a pore in the stationary phase in ion exchange chromatography [35].

Shortly after the introduction of commercial HPLC machines in 1968, ion-exchange chromatography (IEC) was an established HPLC method [34].

Over the next decade, however, its applications for the separation of many sample types were becoming fewer compared to other HPLC methods. Recently, it is used only for certain “special” samples. This includes samples of biological origin (amino acids, oligonucleotides, peptides, proteins, and nucleic acids), inorganic salts, and some organometallics.

2. 2 Theory of Ion Exchange

Ion exchangers as apparent in the name are insoluble solid materials that exhibit charge centers and replaceable counterions of opposite charge bounds by means of ionic bond. When the ion exchanger which is immobilised on a solid support (usually particles) is in contact with a solution (mobile phase) of an electrolyte, its counterions can be exchanged for the same amount of ions that carries the same charge which is contained in the electrolyte. If the exchangeable counterion provided by the insoluble solid substance (stationary phase) is a cation, the stationary phase is commonly referred to as a cation exchanger. If it is an anion, anion exchange is occurring and the stationary phase in this case is referred to as an anion exchanger [36]

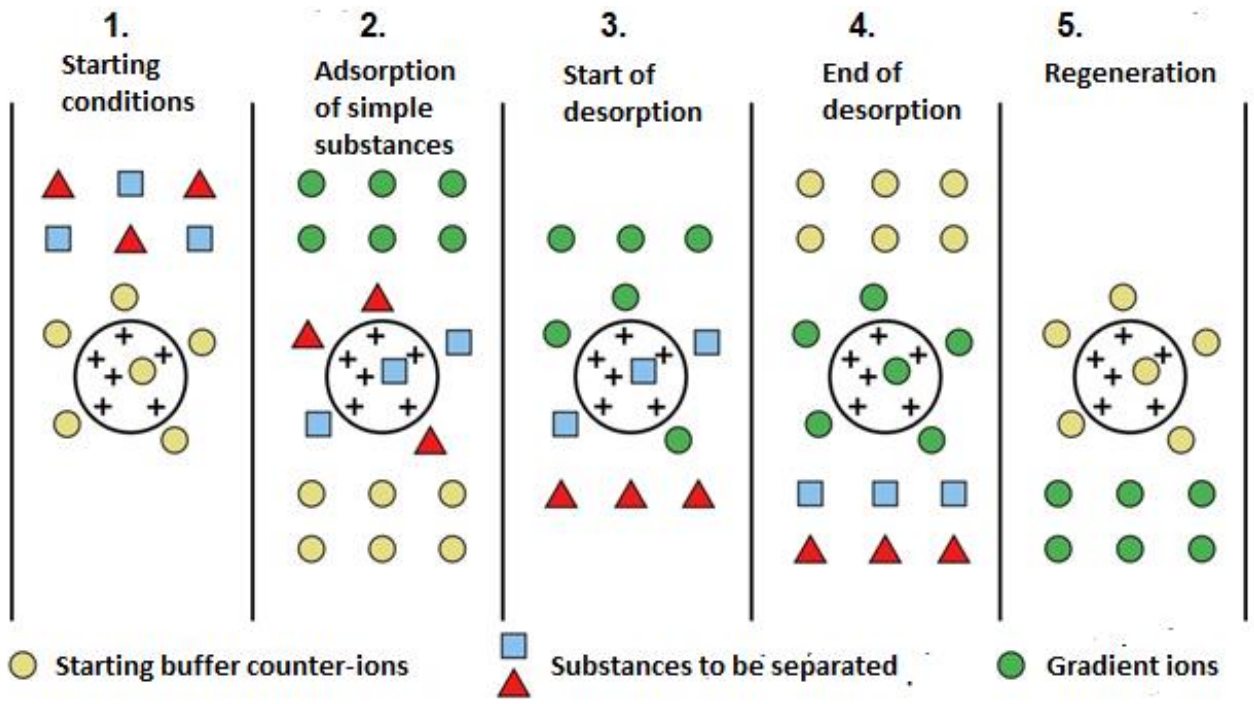

Figure 2.8**:** Principle of ion exchange chromatography [36].

The separation in ion exchange chromatography is theoretically attributed to the reversible adsorption process of charged solute molecules to an oppositely charged group that is immobilized on an insoluble solid support that constitutes the stationary phase. The general sequence of an ion exchange experiment has five main stages as depicted in the scheme below.

In the first stage the ion exchanger is equilibrated and brought to a starting state, in which the pH and ionic strength are relatively constant and allow the binding of the solute molecules with the right charge. The exchanger groups are associated at this stage with the exchangeable counter-ions (usually elemental anions or cations, such as chloride or sodium).

The second stage is sample injection and adsorption, in which the analyte molecules carrying the suitable charge exchange the counter-ions and reversibly associate to the exchanger group immobilised at the stationary phase. The unwanted molecules in the sample that does not have the right charge travels with the mobile phase without being associated with the stationary phase, thus being washed out from the exchanger column and separated from the desired analyte using starting buffer.

At this stage, the desired substances can be obtained from the column by rendering the elution parameters unfavourable for ionic bonding of the solute molecules thus weakening the ionic bond between the analyte and the stationary phase. This is normally attained by raising the ionic strength of the mobile phase or changing its pH. Figure 2.8 shows how desorption is achieved by gradually increasing the salt concentration of the eluting buffer and consequently solute

molecules are dissociated from the stationary phase ionic groups following their order of binding strengths with the stationary phase, so that the substances with lowest binding strength is eluted first.

The fourth and fifth stages are reconditioning the column by removing the substances that have not eluted under the stage 3 experimental conditions and equilibration of the stationary phase back to the starting conditions for the next run of purification.

The separation occurs successfully since different molecules have varying affinity to the ion exchanger stationary phase. These differences are in physical and chemical properties such as charges, charge densities, molecular weight and three-dimensional configuration of the molecule and their surface charge distribution. These interactions can be tuned by changing experimental conditions such as pH and ionic strength. The ionic properties of biological compounds are often considerably different and because ion exchange chromatography can separate species with very minute differences in structural properties that changes the overall charge, e.g. similar proteins that have only one different charged amino acid, this is considered a very powerful separation technique.

Also, it is possible in ion exchange chromatography to bind the desired substances to the column stationary phase and let the impurities or undesired substances to pass through the column, or to capture the impurities and allow the wanted substance to pass through. However, the first approach is more practical since it permits a higher degree of fractionation and concentrates the desired product.

Secondary to the ion exchange process, other forms of binding might occur. These effects are weak and are attributed mainly to van der Waals forces and non-polar interactions. Ion exchange separations may be performed in a column in a batch format, or by expanded bed adsorption. All these techniques are performed following the aforementioned stages of equilibration, sample adsorption etc. [37].

2. 2.1 Ion Exchangers for HPLC

In order to be a suitable and effective stationary phase material in HPLC settings, the material have to possess a number of physical and chemical properties, added to the properties that affect analyte-stationary phase retention which leads to a favourable flow of mobile phase and produces narrow, well-defined chromatographic peaks of high resolution. The more optimum those properties, the more efficient the column operation becomes and the better its ability to separate mixtures of analytes with high resolution provided that other factors that influence analyte-stationary phase interactions are optimised. Table1 summarizes the critical stationary phase physical properties that have to be fulfilled for an optimum and efficient column operation.

Table 2.1, Critical stationary phase physicochemical properties

1	Particle size uniformity and monodispersity.
2	Particles shape (ideally spherical)
3	Microsize particles
4	Particles rigidity
5	Physical strength to resist fracture due to column pressure drop
6	Porousity of the particles that provides access to retention sites and determines surface area.
7	Inertness and chemical stability toward a wide range of mobile phase conditions

A suitable ion exchange for HPLC applications should contain the following basic components:

1. An ionogenic surface group.
2. The ionogenic groups within the ion exchanger must be accessible.
3. A favourable number (ion exchange capacity) of the ionogenic groups should be present.
4. A preference of one analyte over another (ion exchange selectivity) should be present.
5. The ion exchange should be reversible and follow the effects of mass action
6. The kinetics of the in exchange (rate of exchange) should be rapid enough to permit a column operation.

Ion exchangers suitable for HPLC applications are of four basic types:

- Organic polymeric ion exchanger
- Bonded phase ion exchanger
- Pellicular ion exchanger
- Inorganic oxide ion exchanger

Figure 2.9 depicts their basic physical structure of a stationary phase particle. A macroporous structure is obtained by the packing of microspheres. Those microspheres are jointed together or by the channels in the matrix. Because the ionogenic groups are bound to the matrix, they are accessible due to porosity. Which leads to a positive effect on mass transfer and column efficiency. On the other hand, the pellicular-type ion exchanger has its macroporous network on the surface, which contains the ionogenic group. This reduces thickness over the inert core to be about 1-3 µm rather than throughout the bead, mass transfer in this case is even further improved. The positive effect, however, is partially reversed by the subsequent decrease in the number of ionogenic groups available for binding and the challenging fabrication of this type of particles in a <10µm size with the required monodispersity and narrow particle size distribution.

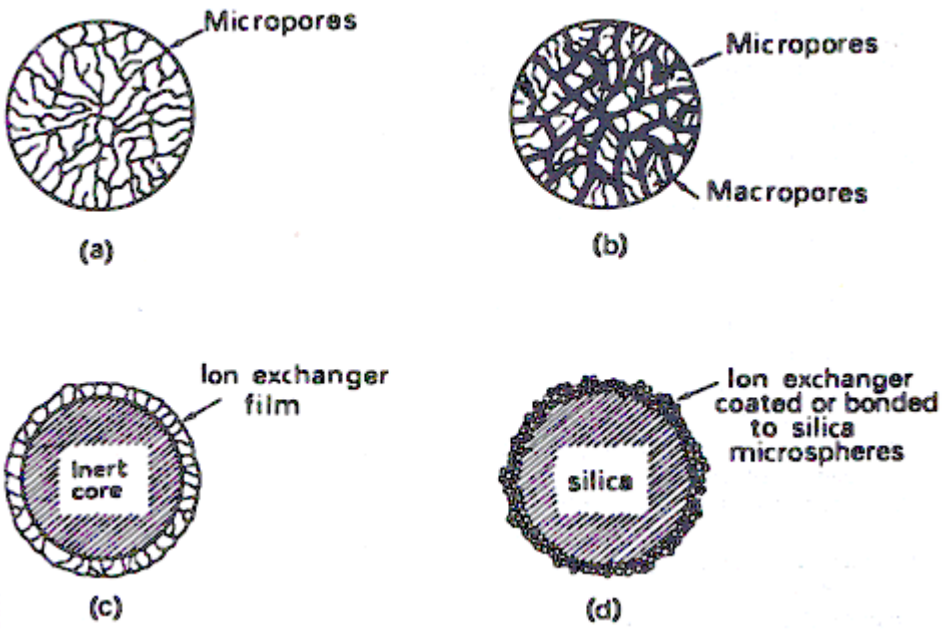

Figure 2. 9**:** Types of ion exchangers. (a) microporous or gel organic polymaeric ion exchangers; (b) macroporous organic polymeric ion exchanger; (c) pellicular ion exchanger; (d) bonded phase ion exchanger [31].

2. 2. 2 Bonded Phase Ion Exchanger

The introduction of the bonded stationary phase to HPLC stationary phases was a turning point in the advancement of HPLC. This type of stationary phase is used in the large majority of HPLC applications. The particles have the physical strength of an adsorbent and the coat provides the resolving power associated with a partitioning system of a stationary phase coated with a liquid layer. Since the bonded layer is chemically bound to the stationary phase particles via a stable covalent bond, it is stable enough and does not desorb during the elution of mobile phase. Bonded phases are fabricated by attaching hydrocarbon chains chemically to microsilica particles. Sometimes polar groups are added to the hydrocarbon, in this case, the bonded phase exhibits some of the normal phase

chromatographic properties. If those polar functional groups are absent, the stationary phaseexhibits reversed phase chromatographic features. Also, the hydrocarbon group can carry an ionogenic group or one can be chemically added to it in a subsequent reaction, then the bonded phase becomes an ion exchanger. The conjucation chemistry of these functional groups onto silica can be carried out in several ways [35,36]. One approach is based on converting the silanol by to silicate ester by reacting it with an alcohol as shown in Eq. 2.1. The silanol group will then undergo

$$\equiv Si-OH + ROH \rightarrow \equiv Si-OR \qquad \textit{Equation (2.1)}$$

reactions with organochlorosilanes easily (Eq. 2.2). If an organodichlorosilane is used, a terminal –OH group is obtained which can then be reacted with another type of organochlorosilane.

$$\equiv Si-OH + R_3SiCl \rightarrow \equiv Si-O-SiR_3 \qquad \textit{Equation (2.2)}$$

The silanol can be substituted by chloride, e.g., by reaction with thionyl chloride, and the resulting chloride is then treated with a Grignard organolithium reagent to give the product as shown in eq.2.3.

$$\equiv Si-OH + SOCl_2 \rightarrow \equiv Si-Cl + LiR \rightarrow \equiv Si-R \qquad \textit{Equation (2.3)}$$

The silane chemistry in eq.3 provides a very versatile synthetic routes to the bonded phase ion exchangers. If aromatic groups are attached, then these can be sulfonated to yield a strong-acid cation exchanger [37].

Using silica as a solid support in Ion-exchange has many advantages over polystyrene based support. In addition to the difference in selectivity. The glass or silica core of the particles strengthen them structurally. Which reduces the occurrence of problems like swelling or bed settling. Generally, it is also possible to change buffer salts or even use mixed solvents without sacrificing column efficiency due to swelling of the particles. It is also possible to use high temperatures (up to 80°C) without a negative effect on the packings with bonded resin. However, extremely acidic (pH<2) or mildly basic (pH>8) solutions can lead to attacking the silica supporting the bonded phases and destroy the column resistance consequently decreasing column efficiency.

2. 2. 3 Inorganic Groups.

Having a charged functional group is one prerequisites of an ion exchanger. The nature of the charge and the type of the functional group determines the type and strength of the ion exchanger. Their total number (i.,e. Surface coverage of the particles) and availability (which is determined by the porosity of the particles) determines the capacity. A cationic ion exchanger has a strong acid or weak acidic inorganic group while an anionic exchanger has a strong base or weak basic group. There are many groups that have been use in ion exchangers; some of these are shown in Table 2.

Table 2.2, Functional groups used on ion exchangers.

Anion exchangers **Functional group**		
Quaternary ammonium	strong	$-O-CH_2N^+(CH_3)_3$
Diethylaminoethyl	weak	$-O-CH_2CH_2N^+H(CH_2CH_3)_2$
Diethylaminopropyl	weak	$-O-CH_2CHOHCH_2N^+H(CH_2CH_3)_2$
Cation exchangers **Functional group**		
Sulfopropyl	strong	$-O-CH_2CHOHCH_2OCH_2CH_2CH_2SO_3–$
Methyl sulfonate	strong	$-O-CH_2CHOHCH_2OCH_2CHOHCH_2SO_3–$
Carboxymethyl	weak	$-O-CH_2COO–$

Sulphonic and quaternary amino groups are considered strong ion exchangers; while the other groups form weak ion exchangers. The extent of variation of ionization with pH determines the strength or weakness of the exchanger and not the binding strength. Strong ion exchangers are ionized completely over a large pH range whereas with weak ion exchangers, the degree of dissociation and thus exchange capacity varies markedly with pH.

Properties of strong ion exchangers:

- Loading capacity does not decrease at high or low pH values due to loss of charge from the ion exchanger.
- A very simple mechanism of interaction exists between the ion exchanger and the solute.

2. 3 Basis of Retention

As mentioned earlier, columns used in ion exchange chromatography are characterized by the presence of charged groups covalently bonded to the particles of the stationary phase: anion-exchange columns exhibits a positive charge (normally a quaternary ammonium or amine group) and cation-exchange columns has a negative charge (usually sulfonate or carboxylate groups). Cation-exchange columns are used for the separation of cations such as protonated bases, and anion-exchange columns are used for anionic or acidic samples [38].

If the stationary phase is denoted R^- (cation exchanger) or R^+ (anion exchanger), and the sample is X^+ (cation) or X^- (anion), the retention in ion exchange chromatography can be represented as follows:

$$X^+ + R^-K^+ \Leftrightarrow X^+R^- + K^+ \qquad \textit{(cation exchange)} \qquad \textit{Equation (2.4)}$$

$$X^- + R^+Cl^- \Leftrightarrow X^-R^+ + Cl^- \qquad \textit{(anion exchange)} \qquad \textit{Equation (2.5)}$$

the assumption here is that the counterion in the mobile phase is either K^+ or Cl^-, and the sample ion is monovalent.

The concentration of the counterion affects the retention and this effect can be generalized for a sample ion of charge *z* and a monovalent counterion as follows:

$$k = \frac{\text{constant } t}{(counterion\ concentration)^z} \qquad \textbf{Equation (2.6)}$$

So, the increase in salt or buffer concentration in the mobile phase decreases retention (as seen from the inverse relationship between the concentration and the K) , and the effect is greater for more charged sample compounds (z >1). The ionic strength of the mobile phase is tuned to control analyte retention between 0.5 > k > 20, so the resolution between two compounds will depend on their difference in charge (Eq.2.6 See above).

2. 3.1 pH Effects

Ion-exchange chromatography is used to separate and purify acids and basis. Because retention (Eqs.2.4 and 2.5) necessitates that the analyte molecule carries a charge that is opposite to that on the column, only the ionized from of the acid or base will be retained significantly. That is why, pH of the mobile phase is a very essential factor in determining the separation between compounds. As in high pH, acids tend to be fully ionised (hence, more able to be retained on the anionic exchangers). While in solution of low pH value, alkaline compounds tend to be ionised [38,39].

2. 3.2 Salt or Buffer Types

Mobile-phase anions or cations are retained differently in terms of strength to an ion exchanger. Sometimes a particular salt is selected to provide stronger or weaker retention. Therefore, a strong displacer can reduce sample retention more than the same concentration of a weaker displacer. In general, the more charged displacers are stronger [40]. The relative strength of different displacers in anion-exchange chromatography is F^- (weak) < OH^- < acetate$^-$ < Cl^- < SCN^- < Br^- < NO_3^- < I^- < oxalate^{2-} < SO_2^{2-} < citrate^{3-} (strong)

Similarly, displacer strength in cation-exchange chromatography varies as

Li^+ (weak) < H^+ < Na^+ < NH_4^+ < K^+ < Rb^+ < Cs^+ < Ag^+ < Mg^{2+} < Zn^{2+} < Co^{2+} Co^{2+} < Cd^{2+} < Ni^{2+} < Ca^{2+} < Pb^{2+} <Ba^{2+} (strong) [40].

2. 3. 3 Organic Solvents

The addition of an organic solvent to the mobile phase causes the retention to decrease, similar to reversed-phase HPLC [32,39]. Solvents as methanol or acetonitrile are used usually in ion exchange to enhance selectivity.

2. 3. 4 Column Type

The ion-exchange column can be categorised to four main groups: weak and strong cation exchangers (WCX and SCX, respectively) and weak and strong anion exchangers (WAX and SAX, respectively).

Strong ion exchangers carry a strongly ionic group whose ionisation does not change over the most used pH range (2 < pH < 12) [e.g., $-SO_3^-$ groups for cation exchange and $–N(CH_3)^{+3}$ groups for anion exchange]. Weak ion exchangers lose their charge and the ability to retain samples for certain pH ranges (e.g., $^-COO^-$ groups for cation exchange show a progressive loss in charge for pH< 5) [32,38,39].

Most of the applications of ion- exchange chromatography (except the separation of biological samples) uses strong ion exchangers. Weak ion-exchange columns can be used as a means of changing selectivity or for reduced retention.

2. 4 Resolution in Ion Exchange Chromatography

This section explains the main theoretical factors that affect separation in ion exchange chromatography. One of the main parameters in evaluating a chromatographic separation in general and ion exchange chromatography is included is the resolution between the different compounds peaks. The resolution (R_s) is calculated from the chromatogram as shown in Figure 2.10 [36,37,40].

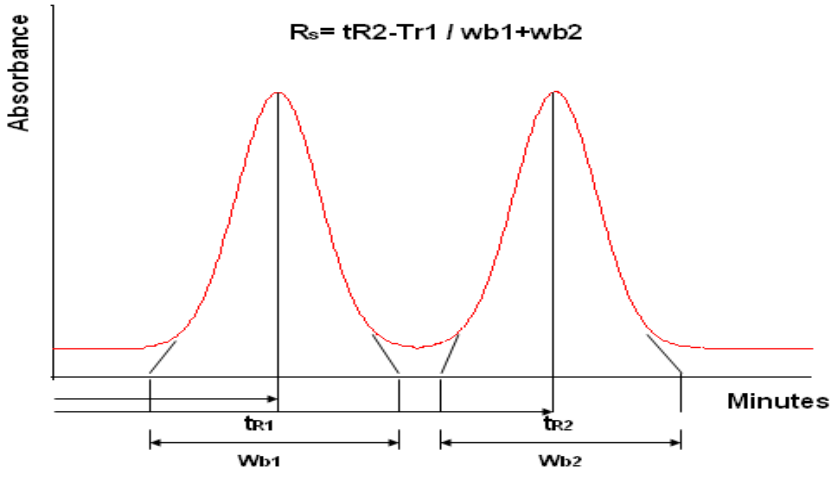

Figure 2. 10: Determination of the resolution (R_s) between two peaks.

The definition of resolution is the distance between peak maxima compared with the Average base width of the two peaks. Peak widths should be determined using the same units so as theresolution is dimensionless. R_s is a critical measure of the relative separation between two peaks and can be used to determine if more optimization of the chromatographic procedure is needed. If R_s = 1.0 (Fig.2.10) then 98% purity has been achieved at 98% of peak recovery, provided the peaks are Gaussian and approximately equal in size. Baseline resolution requires that R_s =1.5. At this value purity of the peak is 100%. Note: A completely resolved peak is not equivalent to a pure substance. This peak may represent a series of components that are not resolvable using the selected separation parameter. The resolution achievable in a system is proportional to the product of the selectivity,

The efficiency and the capacity of the system are the two most important parameters to control column chromatography performance. The analytical expression for R_s is:

$$R_s = \frac{1}{4}\frac{\alpha - 1}{\alpha} \text{ X } \sqrt{N} \text{ X } \frac{k}{k+1} \qquad \textbf{Equation (2.7)}$$

Selectivity expressed as Separation factor (α).
Retention of later eluted compound expressed as Capacity factor (k.)
Efficiency expressed as number of effective plates (N).

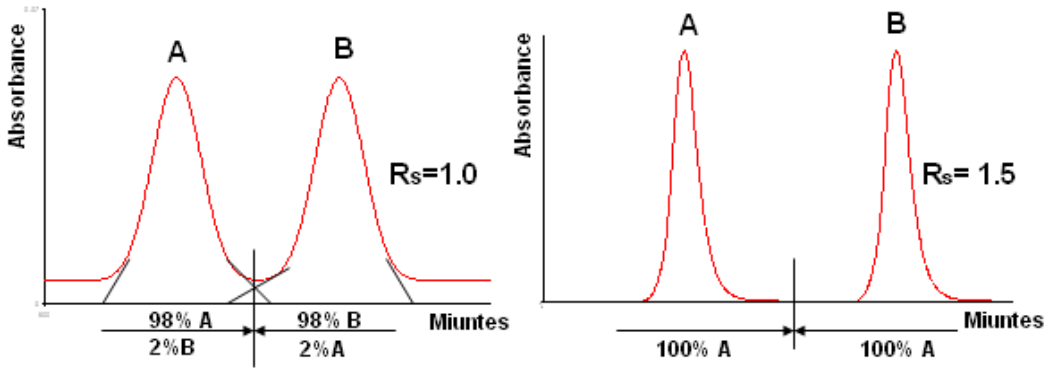

Figure 2. 11: *Separation results with different resolutions.*

2. 4. 1 Retention Factor

The capacity or retention factor k is a measure of the retention of a component and should not be confused with loading capacity (mg sample/ml) or ionic capacity (mmol/ml). The capacity factor is calculated for each individual peak. For example, k for peak1 in (Figure 2.11) is derived from the equation:

Capacity factor k= $\frac{V_R - V_0}{V_0}$ ***Equation (2.8)***

V_R is the retention time of the peak, V_0 is the dead time of the column.

In the equation for R_s, k is the average of k_1 and k_2. The quantities V are the retention times of the solutes and can be measured almost always time. Adsorption techniques such as ion exchange chromatography can have high capacity factors since experimental conditions can be chosen which lead to peak retention volumes greatly in excess of V_0. This can be seen in contrast with the technique of gel filtration where capacity is limited since all peaks must elute within the volume (V_t - V_0).

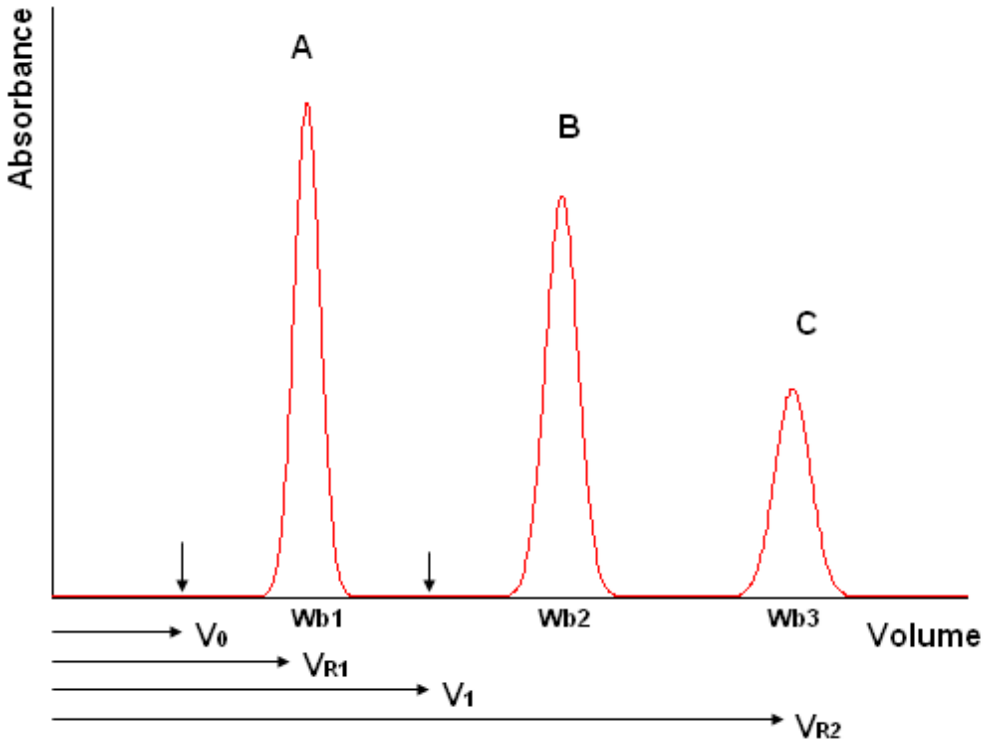

Figure 2. 12: Hypothetical chromatogram.

V_0 = void volume.

V_{R1} = elution volume for peak 1, wb1 = peak width for peak 1

V_{R2} = elution volume for peak 2, wb2 = peak width for peak 2

V_t = total volume.

2. 4. 2 Column Efficiency

The column efficiency is related to the zone broadening which occurs on the column and can be calculated from the expression:

$$N = 16\left(\frac{V_R}{w}\right)^2 \quad \text{or} \quad N = 5.54\left(\frac{V_R}{w_{1/2}}\right)^2 \qquad \textit{Equation (2.9)}$$

(Where w and $w_{1/2}$ are respectively the peak width and the peak width at half peak height) and is expressed as the number of theoretical plates (N) for the column under specified experimental conditions.

The plate model supposes that the chromatographic column is contains a large number of separate layers, called theoretical plates [23,37,41].

Separate equilibrations of the sample between the stationary and mobile phase occur in these "plates". The analyte moves down the column by transfer of equilibrated mobile phase from one plate to the next.

It is important to remember that the plates do not really exist; they are a figment of the imagination that helps us understand the processes at work in the column. They also serve as a way of measuring column efficiency, either by stating the number of theoretical plates in a column, N (the more plates the better), or by stating the plate height; the Height Equivalent to a Theoretical Plate (the smaller the better). If the length of the column is L, then the HETP is

$$HETP = L / N$$

A more realistic description of the processes at work inside a column takes account of the time taken for the solute to equilibrate between the stationary and mobile phase (unlike the plate model, which assumes that equilibration is infinitely fast). The resulting band shape of a chromatographic peak is therefore affected by the rate of elution. It is also affected by the different paths available to solute molecules, since they travel between particles of stationary phase. If we consider the various mechanisms that contribute to band broadening, we arrive at the Van Deemter equation for plate height [40].

$HETP = A + B / u + C.u$

Where u is the average velocity of the mobile phase. A, B, and C are factors which contribute to band broadening.

A - Eddy diffusion

The mobile phase moves through the column that is packed with stationary phase. Solute molecules will take different paths through the stationary phase at random. This will cause broadening of the solute band, because different paths are of different lengths.

B - Longitudinal diffusion

The concentration of analyte is less at the edges of the band than at the center. Analyte diffuses out from the center to the edges. This causes band broadening. If the velocity of the mobile phase is high then the analyte spends less time on the column, which decreases the effects of longitudinal diffusion.

C - Resistance to mass transfer.

The analyte takes a certain amount of time to equilibrate between the stationary and mobile phase. If the velocity of the mobile phase is high, and the analyte has a strong affinity for the stationary phase, then the analyte in the mobile phase will move ahead of the analyte in the stationary phase. The band of analyte is broadened. The higher the velocity of mobile phase, the worse the broadening becomes Van Deemter plots [40].

A plot of plate height vs. average linear velocity of mobile phase.

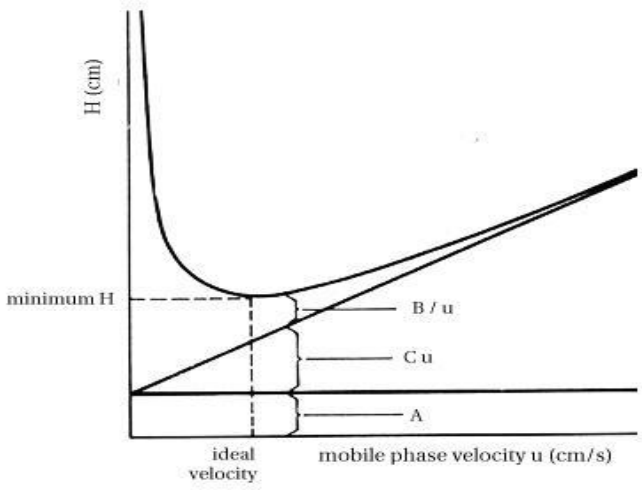

Figure 2. 13: Van Deemter plot [40].

Such plots are of considerable use in determining the optimum mobile phase flow rate. Since the observed value for N depends on experimental factors such as flow rate and sample loading, it is important that comparisons are done under identical conditions. In the case of ion exchange chromatography, efficiency is measured under isocratic conditions, using a substance that does not interact with the matrix, e.g. acetone. One of the main causes of zone broadening in a chromatography bed is longitudinal diffusion of the solute molecules. The effect is minimized if the distances available for diffusion, in both the mobile phase and stationary phase, are minimized. In practice this is achieved by using small uniform bead sizes and important developments in ion exchange chromatography have been the introduction of 10 μm and 15 μm diameter particles. The highest efficiency is achieved with the non-porous, 3 μm diameter, designed for analytical and micropreparative applications. After bead size, the second major contributory factor to efficiency is good experimental technique. Badly, unevenly packed chromatography beds and air bubbles will lead to channelling, zone broadening and loss of resolution. Good separations require well packed columns and the

importance of column packing increases in direct proportion to the performance required.

2. 4. 3 Selectivity

The selectivity (α) can be defined as the ability of the chromatographic system to separate peaks i.e. the distance between two peaks. The selectivity factor can be calculated from the chromatogram (Figure 2.14) using the expression [41].

$$\alpha = \frac{k_2}{k_1} = \frac{V_{R2} - V_0}{V_{R1} - V_0} \qquad \textit{Equation (2.10)}$$

Good selectivity is a more important factor than high efficiency in determining

Resolution (Figure 2.14) since Rs is linearly related to selectivity but quadratically related to efficiency. This means that a fourfold increase in efficiency is required to double the resolution under isocratic conditions.

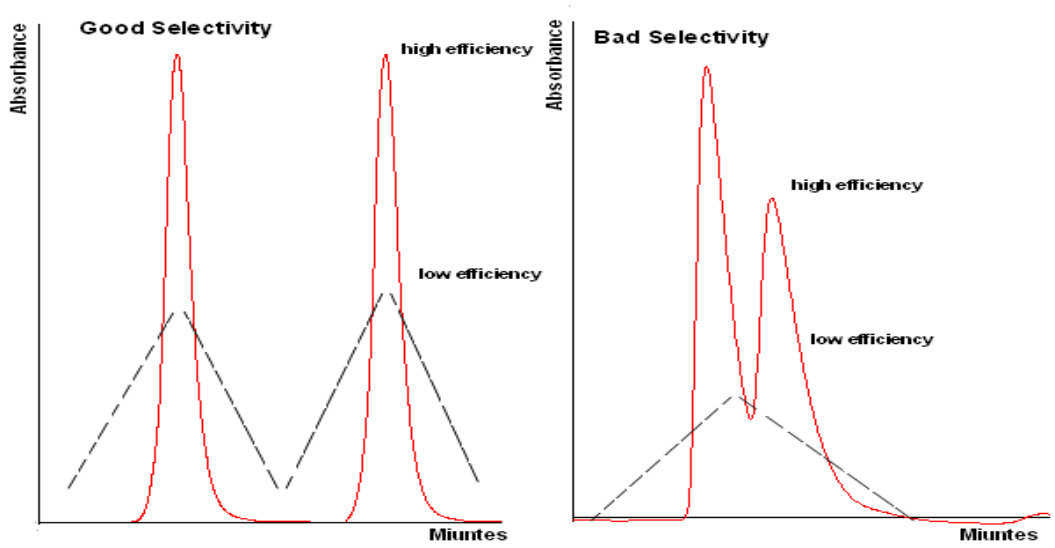

Figure 2. 14: Effects of selectivity and efficiency on retention

Selectivity in ion exchange chromatography depends not only on the nature and number of the ionic groups on the matrix but also on the experimental conditions, such as pH and ionic strength. It is the case and predictability with which these experimental conditions, and thus the selectivity, can be manipulated which gives ion exchange chromatography the potential of extremely high resolution.

2. 4.4 Capacity

The capacity of an ion exchanger is a quantitative measure of its ability to take up exchangeable counter-ions and is therefore of major importance. The capacity may be expressed as total ionic capacity, available capacity or dynamic capacity. The total ionic capacity is the number of charged substituent groups per gram dry ion exchanger or per ml of swollen gel. Total capacity can be measured by titration with a strong acid or base. The actual amount of electrolyte that can be bound to an ion exchanger, under defined experimental conditions, is referred to as the available capacity for the gel. If the defined conditions include the flow rate at which the gel was operated, the amount bound is referred to as the dynamic capacity for the ion exchanger [42,43].

Available and dynamic capacities depend upon:

- The properties of the electrolyte.
- The properties of the ion exchanger.
- The chosen experimental conditions.

The properties of the electrolyte which determine the available or dynamic capacity on a particular ion exchange matrix are its molecular size and its charge/pH relationship. The capacity of an ion exchanger is thus different for different electrolytes [30,33,37].

2.5 Experimental Section

The photochemistry of compounds was monitored by HPLC, ^{1}H-NMR and UV-Vis spectroscopy.

2.5.1 Materials

The compounds which will be investigated were available from previous experiments and were synthesized by Ms Tanja Kowacs (Institute of Inorganic Chemistry I, University of Ulm, Germany). All samples were used as received, with no further purification. All solvents employed were of HPLC grade or better (Sigma-Aldrich). Water was prepared with water purification System model Milli-Q (Millipore, Bedford, MA, USA). All samples were filtered through Nylaflo® nylon membrane filter units of 0.45 µm pore diameter (Millipore). All mobile Phases were degassed prior to use.

2.5.2 Analytical HPLC:

Analytical High Performance Liquid Chromatography (HPLC) experiments were carried out on using a Varian Pro Star photodiode array as detecting system in conjunction with Varian Star software, a Varian 230.0 pump, (model 230.01) and Varian detector (Model 330.71), fitted with a 20µL injector loop and a strong

cation exchange Luna SCX column (25cm x4.6mm-100Å) provided by PHENOMENEX. This column is a silica-based sorbent derivatized with benzenesulfonic acid phase. The column is packed with 5μm particles and the operating pH range is between 2.0 and 7.0. The 280nm was chosen as the detection wavelength because the most intense band in the absorption spectrum for the compounds studied was between 270nm and 290nm.

2.5.3 Mobile phases used:

- Acetonitrile/water with volume ratio (50/50) mixture during 30 minutes to stabilise the column before use.
- Acetonitrile/water/methanol mixture containing potassium nitrate KNO_3 as a salt during 30 minutes (*the volume ratio of mobile phase and the potassium nitrate concentration changeable depending on experimental conditions required*). When the mobile phase needs to be changed the system was cleaned for 20-30 minutes.
- The Column was rinsed with an acetonitrile/water with volume ratio (50/50) mixture (30 min at least) after use.

All mobile phase was vacuum filtered through 0.5 μm membrane filters and then degassed in an Ultra Sonic batch for 15-20 minutes prior to use. The flow rate used was varied from between 1.5-3 mL/min and the pump pressure is highly depending on increasing of flow rate.

Figure 2. 15: Varian ProStar 230 HPLC System.

2.5.4 HPLC Setup:

The pump and UV/Vis detector were switched on. After washing the column with HPLC Grade acetonitrile/water (50/50 v/v) with a low flow change that suited the mobile phase for appropriately 20-30min until the pressure had stabilised. The injection loop was cleaned by placing the loop in the (load) position and injecting the mobile phase. This was repeated for every change of mobile phase and samples. The absorbance detection wavelength was 280 nm and depending on experiment and solvents.

2.5.5 Preparation of Samples for Photoanalysis

2.5.5.1 Photolysis of Compounds in the absence of TEA.

All samples were used as received, all measurements were performed at 24 °C (Used Column Thermostat). Preparation of sample solutions was carried out in the absence of ambient light and solutions were wrapped in aluminium foil and carefully sealed to avoid exposure to light, and evaporation. Samples were always prepared fresh, immediately prior to the measurements. A $1x10^{-4}$ M solution of compounds in acetonitrile, or in acetone, 5 ml sample of above concentration solution was take for irradiation at 470 nm (blue light) as shown in Figure 2.16. Displaying presence of fans to avoid heating of the solutions.

2.5.5.2 Photolysis of Compounds in the Presence of TEA.

Photolysis experiments were carried under inert conditions (N_2) at room temperature (24 °C) under constant irradiation of the sample, Acetonitrile HPLC grade and TEA used were freshly distilled under argon. The samples for the LED light irradiation experiments were prepared in GC vials and charged in the dark and under an argon stream. After adding of triethylamine (V = 0.6 ml) and (V = 0.2 ml) of degassed water. the final samples concentration in acetonitrile was 1 x 10^{-4} M. Subsequently, the GC vials were irradiated with blue LED light (470 nm, P = 30 – 40 mW). After irradiation, 20µl samples were drawn from the vials and injected immediately into the HPLC apparatus. All time intervals were measured by the same procedure that mentioned previously.

Figure 2.16: shows the reactor where the catalytic solutions were irradiated by blue LEDs (470 nm wavelength).[15]

2.6 UV-Vis Spectroscopy:

The UV-vis spectra of the products obtained after separation with HPLC were generated by the Photodiod Array (PDA) detector attached to the HPLC software.

2.7 ^{1}H-NMR spectroscopy:

^{1}H-NMR spectra were recorded on a Bruker Advance 600 MHz NMR spectrometer. Data were referenced to residual solvent absorptions.

2.8 References:

[1] S.J. Valently, P.E. Behnken, Anal. Chem. **1978**, 50, 834.

[2] B.E. Buchanan, E. McGovern, P. Harkin, J.G. Vos, The Application of High-Performance Liquid Chromatography in the Investigation of Reactions involving Ruthenium(II)bis(bypyridyl) compounds Inorg. Chim. Acta **1988**,154,1-4.

[3] Chromatographic Separation and Characterisation of Linkage Isomers of the 3-(Pyridin-2-yl)-1H-1,2,4-triazole complex of Ruthenium(II) bis(2,2'-bipyridyl). Inorg. Chem. **1990**, 29, 3263-3265.

[4] H.A. Nieuwenhuis, J.G. Haasnoot, R. Hage, J. Reedijk, T.L. Snoeck, D.J. Stufkens, J.G. Vos, pH-Control of the Photophysical Properties of Ruthenium Complexes Containing 3-(pyrazin-2-yl)-1,2,4-triazole ligands. Inorg. Chem, **1991**, 30, 48-64.

[5] R. Hage, R. Prins, J.G. Haasnoot, J. Reedijk, J.G. Vos, Synthesis, Spectroscopic and Electrochemical Properties of Bis(2,2'-bipyridyl) Ruthenium Compounds of some Pyridyl-1,2,4-triazoles. J. Chem. Soc. Dalton Trans. **1987**, 1389-1395.

[6] pH Control of Photoreactivity of Ru(II) Pyridyltriazole Complexes: Photoinduced Linkage Isomerism and Photoanation.R. Wang, J.G. Vos, R.H. Schmehl, R. Hage, J. Am. Chem. Soc. **1992**, 114, 1964-1970.

[7] Thermally and Photochemically Induced Coordination Changes in Ruthenium(II) Bis(2,2'-bipiridyl) Complexes Containing Pyridyltriazole Ligands. B.E. Buchanan, H. Hughes, P. Degn, J.M. Pavon Velasco, B.S. Creaven, C. Long, J.G. Vos, R. A. Howie, R. Hage, J.H. van Diemen, J.G. Haasnoot, and J. Reedijk. J. Chem. Soc., Dalton Trans., (1992), 1177-1183.

[8] W.R. Browne; D. Hesek, J.F. Gallagher, C.M. O'Connor, J.S. Killeen, F. Aoki, H. Ishida, Y. Inoue, C. Villani, J.G. Vos, Structural and Photophysical Characterisation of Coordination and Optical Isomers of Mononuclear Ruthenium(II) Polypyridyl 1,2,4-triazole Complexes. Dalton Trans. **2003**, 2597-2601.

[9] R. Hage, A.H.J. Dijkhuis, J.G. Haasnoot, R. Prins, J. Reedijk, B.E. Buchanan, J.G. Vos, Synthesis, Spectroscopic and Electrochemical Properties of tMononuclear and Dinuclear Bis(2,2'-bipyridyl)ruthenium Complexes Containing 3,5-Bis(pyridin-2-yl)-1,2,4-triazole. Inorg. Chem. **1988**, 27, 2185-2189.

[10 H.P. Hughes, D. Martin, S. Bell, J.J. McGarvey; J.G. Vos,. Photophysical and Photochemical Properties of Dinuclear Ruthenium(II) Complexes Containing 2,2'-Bipyridyl and 1,10-phenanthroline. Inorg. Chem. **1993**, 32, 4402-4408.

[11] R. Hage, J.G. Haasnoot, J. Reedijk, R. Wang, J.G. Vos, Mononuclear and Dinuclear Ruthenium Complexes with Triazole-Containing Ligands: Fine-Tuning of the Spectroscopic Properties. Inorg. Chem. **1991**, 30, 3263-3269.

[12] L. De Cola, F. Barigelletti, V. Balzani, R. Hage, J.G. Haasnoot, J. Reedijk, J.G. Vos, Electronic Energy Transfer in Bimetallic Ru-Os Complexes Containing the 3,5-bis (pyridin-2-yl)-1,2,4-triazolate Bridging Ligand.Chem. Phys. Lett. **1991**, 178, 491-496.

[13] H.P. Hughes, J.G. Vos, The Control of Photosubstitution in Dinuclear Ruthenium Polypyridyl Complexes by the Choice of Bridging ligand Inorg. Chem. **1995**, 34, 4001-4003.

[14] W.R. Browne, C.M. O'Connor, C. Villani; J.G. Vos, Separation and Photophysical Properties of the ΔΔ, ΛΛ, ΔΛ, and ΛΔ Stereoisomers of a Dinuclear Ruthenium(II) Complex Inorg. Chem. **2001**, 40, 5461-5464.

[15] J.H. Van Diemen, R. Hage, J.G. Haasnoot, H.E.B. Lempers, J. Reedijk, J.G. Vos, L. De Cola, F. Barigelletti, V. Balzani, Electrochemical and Photophysical

Properties of New Triazole-Bridged Heterobi-metallic Ruthenium-Rhodium and Ruthenium-Iridium Complexes. Inorg. Chem. **1992**, 31, 3518-3522.

[16] W.R. Browne, N.M. O'Boyle, W. Henry, A.L.. Guckian, S. Horn, Fett, T.; O'Connor, C.M.; Duati, M.; De Cola, L.; Coates, C.G.; Ronayne, K.L.; McGarvey, J.J. J.G. Vos, Ground and Excited state electronic structure of an Emissive Pyrazine bridged Ruthenium(II) dinuclear complex. J. Am. Chem. Soc. **2005**, 127, 1229-1241.

[17] A. Mangia, M.T. Lugari, J. Liq. Chromatogr. Rel. Techn. **1983**, 6, 1073.

[18] S.Fanni, T.E. Keyes, C.M. O'Connor, H. Hughes, R. Wang and J.G. Vos. Excited State Properties of Ruthenium(II) Polypyridyl Complexes Containing Asymmetric Triazole Ligands. Coord. Chem. Rev. **2000**, 208, 77-86.

[19] S. Fanni, S. Murphy, J. S. Killeen and J.G. Vos Site-specific Methylation of Coordinated 1,2,4-triazoles: A Novel Route to Sterically Hindered $Ru(bpy)_2$ Complexes. Inorg. Chem. (2000) 39, 1320-1301

[20] H. Zhang, C.S. Rajesh, P.K. Dutta, J. Phys. Chem. A **2008**, 112, 808-;

[21] M. Thomalla, H. Tributsch, Compt. Rend. Chimie **2006**, 9, 659;

[22] Y. Cho, Y. Park, W. Choi, J. Ind. Eng. Chem. **2008**, 14, 315-.

[23] P. Passaniti, W.R. Browne, F.C. Lynch, D. Hughes, M. Nieuwenhuyzen, P. James, M. Maestri, J.G. Vos, Synthesis, spectroscopic and electrochemical properties of mononuclear and dinuclear bis(bipy)ruthenium(II) complexes containing dimethoxyphenyl-(pyridin-2-yl)-1,2,4-triazole ligands. J. Chem. Soc. Dalton Trans. **2002**, 1740-1746.

[24] W.R. Browne, C.M. O'Connor, H.P. Hughes, R. Hage, O. Walter, M. Doering, J.F. Gallagher, J.G. Vos, Ruthenium(II) and Osmium(II) Polypyridyl Complexes of asymmetric pyrazinyl- and pyridinyl-1,2,4-triazole based ligands. Part 1: Connectivity

and physical properties of mononuclear complexes J. Chem. Soc. Dalton Trans. **2002**, 4048-4082.

[25] J.G. Vos, J.M. Kelly, Ruthenium Polypyridyl Chemistry, from Basic research to Applications and Back Again Dalton Trans. **2006**, 4869 – 4883.

[26] H.M.Y. Ahmed; N. Coburn, D. Dini J.J.D de Jong, C. Villani, W.R. Browne, J.G. Vos, Application of Circular Dichroism Spectroscopy in the Study of Mixed-Valence Asymmetric Ruthenium Polypyridyl Complexes Inorg. Chem. (2011), 50, 5861-5863.

[27] S. Rau, B. Schaefer, D. Gleich, E. Anders, M. Rudolph, M. Friedrich, H. Goerls, W. Henry, J.G. Vos, A Supramolecular Photocatalyst for the Production of Hydrogen and the Selective Hydrogenation of Tolane. Angew. Chem. Int. Ed. **2006**, 45, 6215-6218;

[28] B. Gholamkhass, H. Hiroaki Mametsuka, K. Koike, T. Tanabe, M. Furue, O. Ishitani, Inorg. Chem. **2005**, 44, 2326-;

[29] S. Sato, K. Koike, H. Inoue, O. Ishitani, Photochem. Photobiol. Sci. **2007**, 6, 454.-

[30] W. R. Brown, HPLC and CE Principles and Practice, USA, **1997**.

[31] L. R. Snyder, J. L. Glajch, J. J. Kirklan, Practical HPLC Method Development second edition Wiley & Sons, USA **1997**.

[32] D. A. Skoog, D. M. West, F. J.Holler, Fundamental of Analytical Chemistry, seventh edition, USA, **1996.**

[33] M. W. Dong, Modern HPLC for Practicing Sciences, Wiley & Sons, USA, **2006.**

[34] K. Unger, Packings and Stationary Phase in Chromatographic Techniques (Chromatographic Science), Marcel Dekker, New York, **1990**.

[35] K. Unger, Porous Silica , Journal of Chromatography Library, Volume 16, Elesevier Scientific Publishing Co., New York, **1979**.

[36] D. A. Wellings, A Practical Handbook of Preparative HPLC, Elsavier Ltd **2006**.

37] J. Barnes, High Performance Liquid Chromatography, John Wiley & Sons **1992**.

[38] A. Pryde, J. Chromatographie. Sci., **1974**, 12, 438.

[39] D. C. Harris, Quantitative Chemical Analysis, seventh edition,. W. H. Freeman & Company. USA, **2007**.

[40] Ion Exchange Chromatography Principle and methods. Handel Book Amersham Biosciences.**2004**.

[41] D. A. Skoog, F. J. Holler, T. A. Nieman, Principles of Instrumental Analysis, fifth edition, USA, **1998**.

[42] R. E. Majors and M. J. Hopper, J**.** Chromatography. Sci., **1974**, 12, 974.

[43] S. Ahuja, Chromatography and Separation Science, V4, **2003**.

Chapter 3

An investigation of the photostability of ruthenium based photocatalysts, based on the 2,3-di(pyridyl-2-yl) pyrazine bridging ligand.

The purpose of Chapter 3 is the characterisation and the investigation of the stability of the complexes $[(bpy)_2Ru(2,3dpp)]^{2+}$ **(A-I)**, $[(bpy)_2Ru(2,3dpp)PtCl_2]^{2+}$ **(A-II)**, and $[(bpy)_2Ru(2,3dpp)PtI_2]^{2+}$ **(A-III)** when irradiated with visible light using HPLC, UV-vis spectroscopy and NMR techniques. The NMR experiments indicate that when the compounds are irradiated with visible light compound **A-I** and **A-II** are photostable after 24 hour of irradiation, while **A-III** shows a small decrease of stability at longer irradiation times. In the absence of TEA, the thee compounds are mostly stable. The effect of the platinum catalytic centres and the halogen terminal species ($PtCl_2$ or PtI_2) are also considered. A study of the stability of the complexes in acetonitrile, with TEA as an electron donor in the presence light was carried out. The results obtained indicate that in the presence of TEA compounds studied are not stable but are highly photo reactive. They may however have the potential of being developed as supramolecular photocatalysts in the future.

3.1 Introduction.

As outlined in the introduction (chapter-1), the purpose of this thesis is the investigation of the stability of a range of ruthenium based metal complexes as precursors for potential photocatalysts for hydrogen generation from water using solar light. The DCU group has carried out a range of experiments investigating the efficiency of various peripheral[1,2,3] and bridging ligands.[5,6,7,8] These studies are aimed at further optimisation of potential solar devices in the future. In this section, assessment and characterization of the three compounds containing the ligands shown in Figures 3.1 and 3.2 is carried out. These techniques will be also being used in later chapters to characterise the other groups of compounds. The effect of triethylamine, TEA, on the stability of these compounds will also be investigated. In this study we will refer to the present group of compounds called Group A, where each ligand plays a different role as a photocatalytic molecular device. In this particular group, the peripheral ligand utilised is 2,2'-bipyridine **(bpy)** and the bridging ligand is 2,3-di(pyridyl-2-yl) pyrazine **2,3dpp.** The structures of the **bpy** bidentate (N^N) chelating ligand and the **2,3dpp** bridging ligand are illustrated in Figures 3.1and 3.2. All compounds studied were obtained from earlier studies, but their stability with respect to irradiation and potential to act as photocatalysts have not yet been investigated. The bridging ligand 2,3dpp is needed to connect the ruthenium photosensitiser centre to the platinum catalytic centre in order to create dinuclear Ru/Pt compounds as shown in Figure 3.3. As shown in this Figure, one compound is a mononuclear precursor and the

other two compounds are dinuclear complexes that can be tested as potential solar driven photocatalysts.

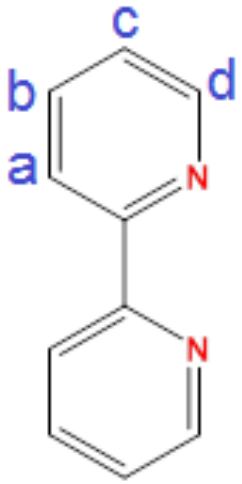

bpy

Figure 3.1: Structures of the peripheral ligand bpy, which are used in this part.

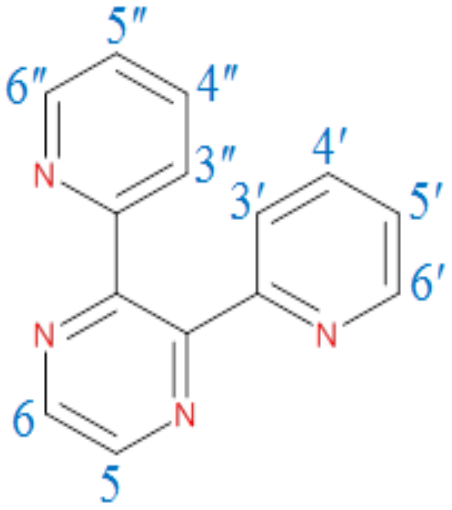

2,3dpp

Figure 3.2: Structure of the bridging ligand 2,3-di(pyridyl-2-yl)pyrazine, 2,3dpp.

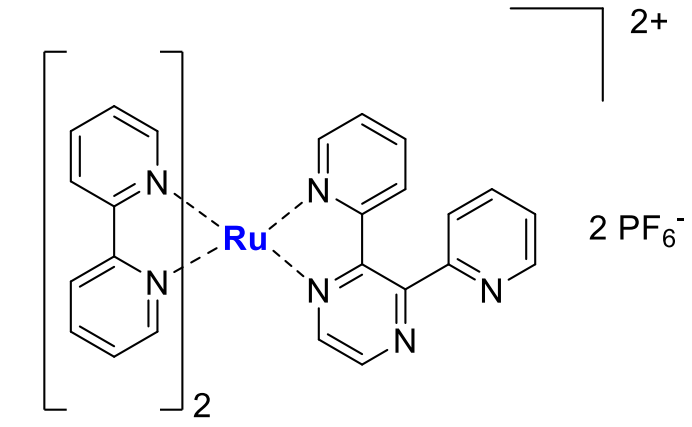

A-I

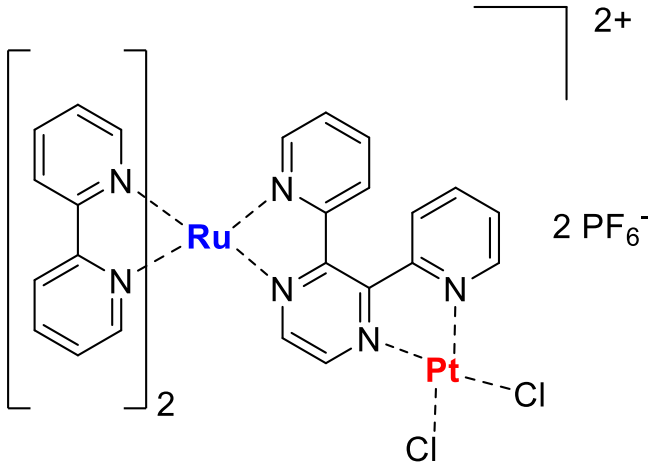

A-II

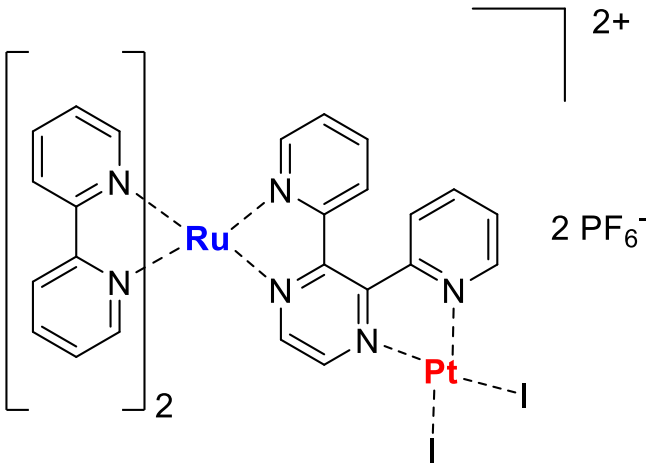

A-III

Figure 3.3: Structures of the dinuclear Ru/Pt compounds and Ru(II) monomers with 2,3dpp as bridging ligand with two bpy based peripheral ligands.

3.2 Results and Discussion

3.2.1 Chromatographic HPLC Assessment.

The HPLC chromatograms obtained for the mononuclear $[(bpy)_2Ru(2,3dpp)]^{2+}$ complex (**A-I**) species and the dinuclear compounds $[(bpy)_2Ru(2,3dpp)PtCl_2]^{2+}$ (**A-II**) and $[(bpy)_2Ru(2,3dpp)PtI_2]^{2+}$ (**A-III**) compounds that are shown in Figures (3.4 a,b,c). A strong peak is observed for all 3 compounds at retention time at 10.47, 4.83 and 3.42 min respectively. There are a small peaks appearing before and also after the main peak in compound (**A-III**) probably due a small amount of synthetic impurity as shown in Figure 3.4c.

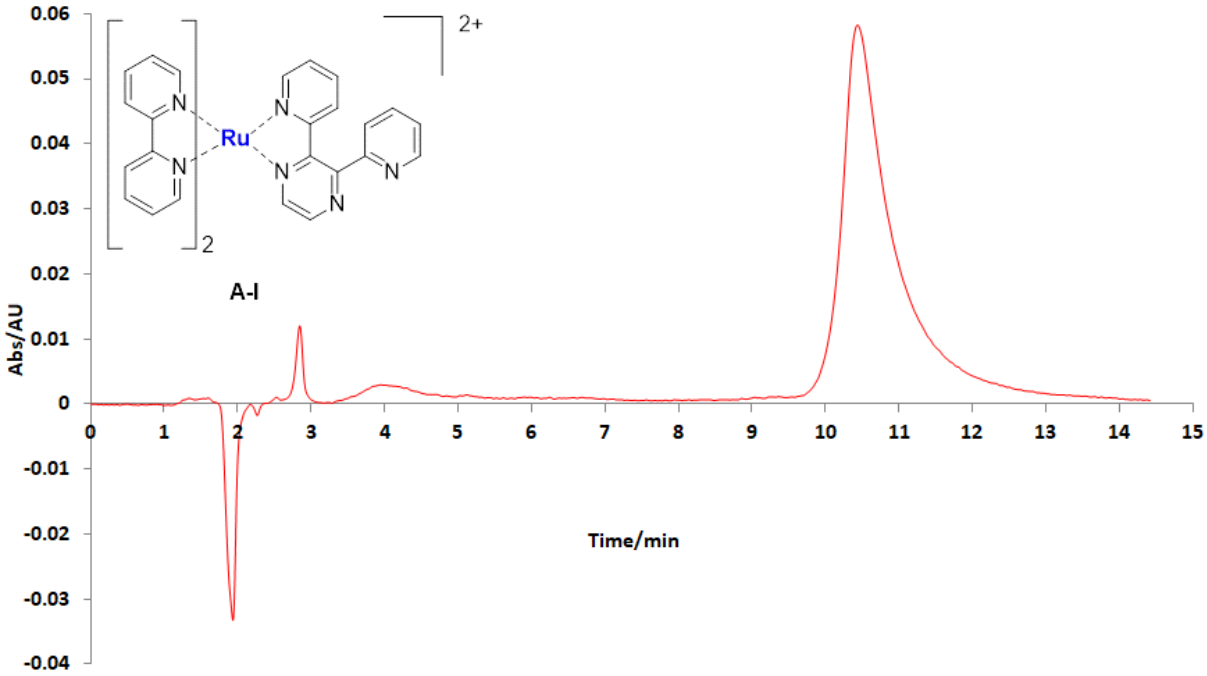

Figure 3.4(a): HPLC trace for $[(bpy)_2Ru(2,3dpp)]^{2+}$ in CH_3CN ($1x10^{-4}$ M), mobile phase CH_3CN: H_2O: CH_3OH with volume ratio 75:20:5 containing 0.12 M KNO_3. Flow rate: 2.0 cm^3 min^{-1}; detection wavelength at 280 nm, T=24^0C

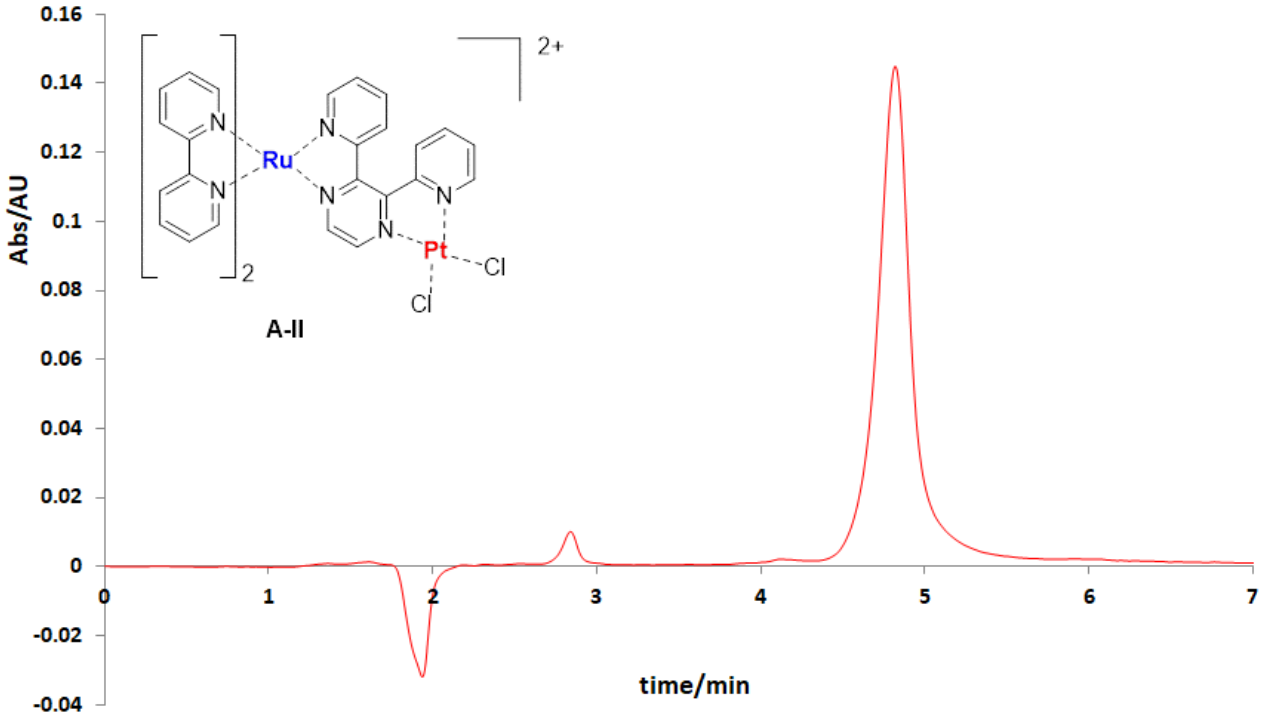

Figure 3.4(b): HPLC trace for $[(bpy)_2$ Ru (2,3dpp)$PtCl_2]^{2+}$ in CH_3CN ($1x10^{-4}$ M), mobile phase CH_3CN: H_2O: CH_3OH with volume ratio 75:20:5 containing 0.12 M KNO_3. Flow rate: 2.0 cm^3 min^{-1}; detection wavelength at 280 nm, T=24^{0}C

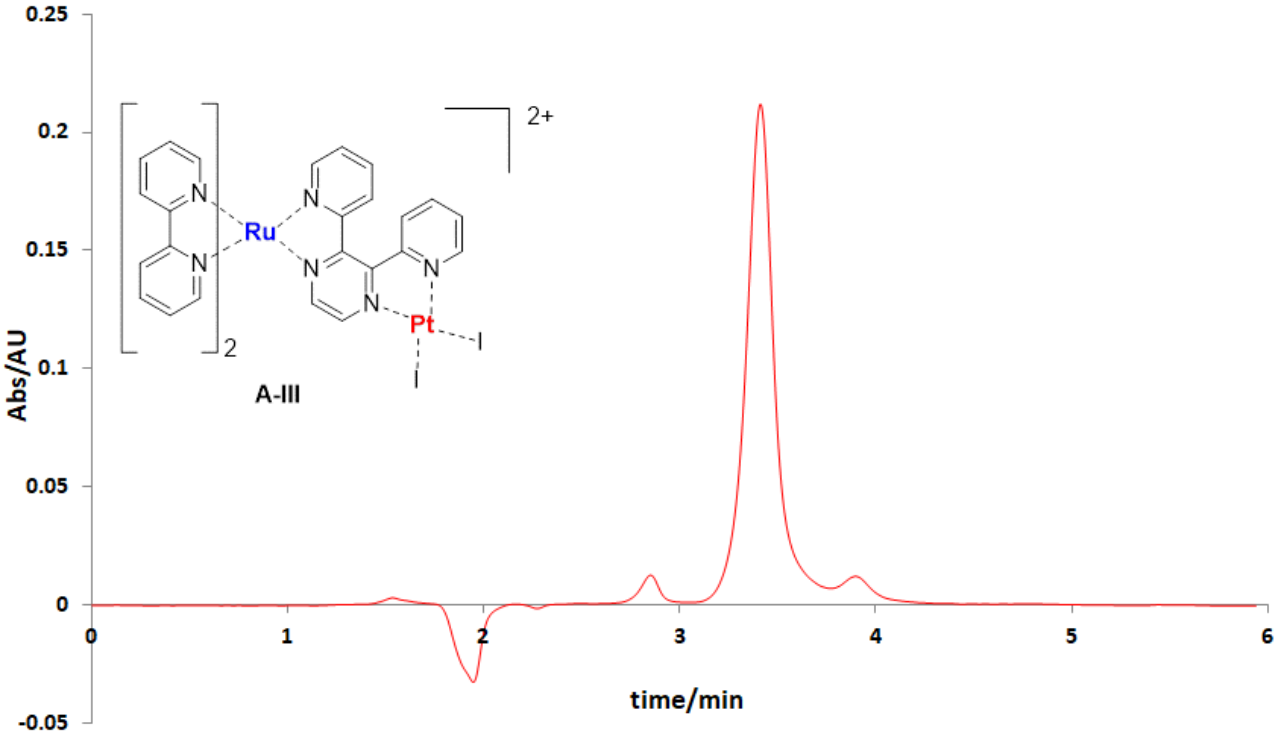

Figure 3.4(c): HPLC trace for $[(bpy)_2$ Ru (2,3dpp)$PtI_2]^{2+}$ in CH_3CN ($1x10^{-4}$ M), mobile phase CH_3CN: H_2O: CH_3OH with volume ratio 75:20:5 containing 0.12 M KNO_3. Flow rate: 2.0 cm^3 min^{-1}; detection wavelength at 280 nm, T=24^{0}C

Comparison between the three chromatograms shows a clear difference in retention time for the compounds as shown in Table 3.1 It also shows that compounds **A-II** and **A- III** have similar retention times, but are different from compound **A-I**. One proposed explanation for that difference is that the presence of platinum catalytic centre with highly electronegative atoms (**Cl^-** and **I^-**) at the bridging ligand of the compounds **A-II** and **A-III** affects the charge of the compound and renders it less positive that affect the retention behaviour on the column. This is further discussed in the NMR section below. It is important to note that without irradiation the three compounds are stable for long periods.

Table 3.1:Retention times and absorption maximum of compounds **A-I, A-II** and **A-III** in mobile phase with detection wavelength at 280 nm, T=24°C

Compound	***Retention time (min)***	***UV/vis spectrum/ λ_{max} (nm)***
$[(bpy)_2Ru(2,3dpp)]^{2+}$	*10.47*	*442*
$[(bpy)_2Ru(2,3dpp)PtCl_2]^{2+}$	*4.83*	*415, 508.*
$[(bpy)_2Ru(2,3dpp)PtI_2]^{2+}$	*3.42*	*415, 514*

3.2.2 ^{1}H NMR characterisation.

To obtain further information about the structural features of the compounds further analysis of three compounds was carried out using ^{1}H-NMR. The ^{1}H-NMR spectra of the monomer $[Ru(bpy)_2(2,3dpp)]^{2+}$ and the dinuclear compounds $[Ru(bpy)_2(2,3dpp)PtCl_2]^{2+}$ and $[Ru(bpy)_2(2,3dpp)PtI_2]^{2+}$ in acetonitrile-d_3 are shown below in Figure 3.5.

These three compounds shown were obtained from [9] have been analysed before, but their behaviour with respect of stability with respect to TEA and irradiation have not been reported. It is important to note that that the doublet signals of H5 and H6', have only one adjacent proton that splits the signal to a single doublet. The presence of highly electro negative atoms such as the chloride and the iodide that attach to the platinum molecule may result in an increase the chemical shift of the adjacent proton (H5, H6'), as is shown by the electronegativity of the halogens in the Table 3.2 below.

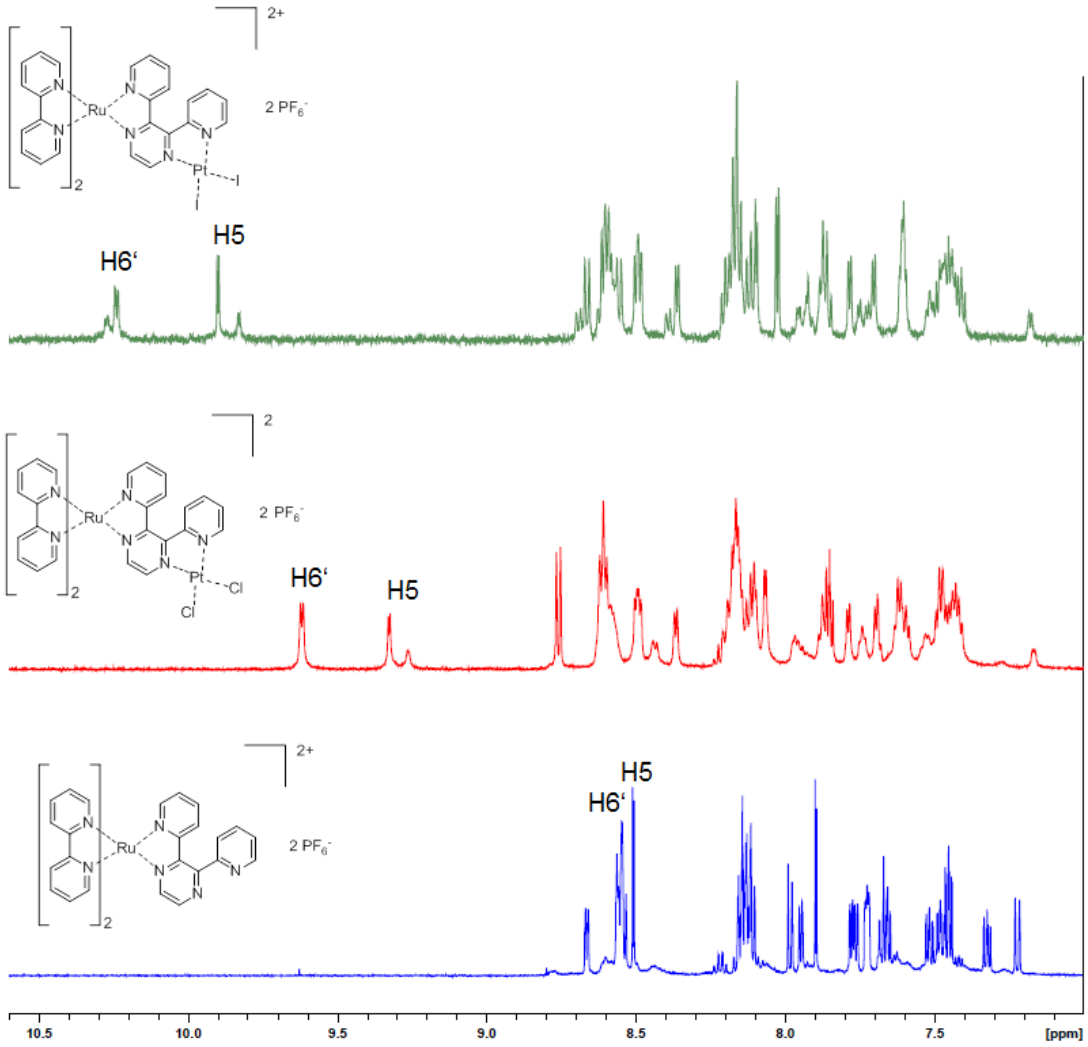

Figure 3.5: ^{1}H-NMR of $[Ru(bpy)_2(2,3dpp)]^{2+}$ **A-I** (bottom), $[Ru(bpy)_2(2,3dpp)PtCl_2]^{2+}$ **A-II** (middle) and $[Ru(bpy)_2(2,3dpp)PtI_2]^{2+}$ **A-III** (top) in d_3-acetonitrile.

Table 3.*2* Electronegativity of Halogen atoms. [9]

Halogen	Electronegativity
Chloride	3.16
Iodide	2.66

The table shows that the electronegativity of the coordinated chloride ion is higher than its iodide equivalent. Therefore, in the case of chloride complexes, chloride atoms are expected to have a more significant effect on the chemical shift of the protons. In addition, the ^{1}H-NMR results also show that the protons of the iodide compounds are more shifted upfield than the protons in chloride compound.

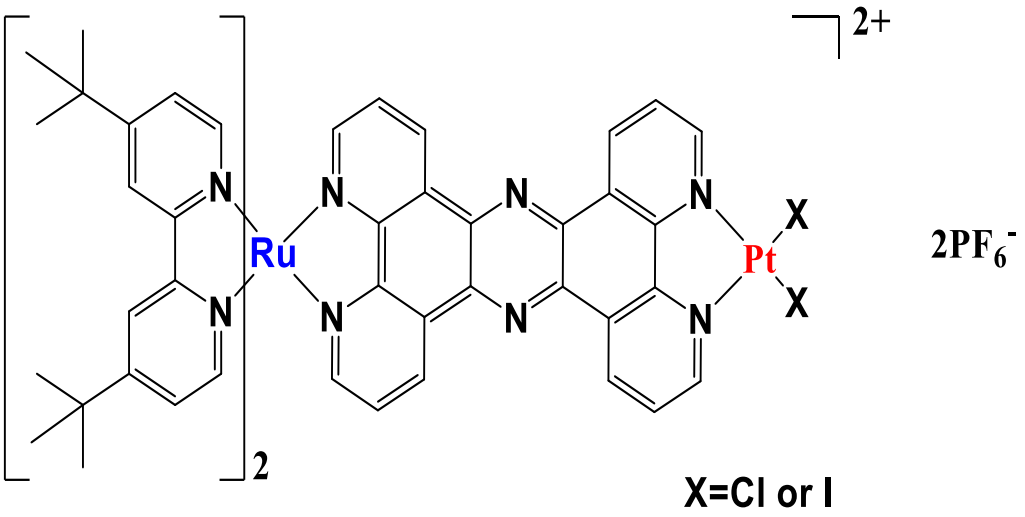

Figure 3.6 Structure of photocatalytic assemblies based on $PtCl_2$ or PtI_2 as $[(tbbpy)_2Ru(tpphz)PtCl_2]^{2+}$ or $RuPtI_2$, where tbbpy=4,4'-di-tert-butyl-2,2'-bipyridine and tpphz=tetrapyrido[3,2-a:2',3'c:3'',2'',- h:2''',3'''-j]phenazine).

Similar arrangements have been observed for related photocatalysts. An example is shown in Figure 3-6 above.[10] For this platinum based photocatalysts the iodide analogue $RuPtI_2$ has the highest **TON** values of this type with a value of 276. This increase in hydrogen generation is most likely associated with the electron negativity of the Iodide moiety that is observed in the ^{1}H-NMR at 10.13 (Ha) and 10.06 (Hb) ppm. DFT studies have indicated that there is a negative charge on the Pt centre which induces the presence of a softer iodide ligand respected to the chloride ion. This in agreement with other studies.[11]

The main peaks in the spectra of compounds **A-II** and **A-III** are observed at around 9.30 ppm, 9.35 ppm and 9.60 ppm for $Ru/PtCl_2$ and 9.80 ppm. 9.90 ppm,10.25 ppm and 10.30 ppm for Ru/PtI_2 can be assigned to the protons neighbouring the nitrogen atoms involved in the coordination of the Pt metal centres. No such features are observed for the mononuclear compound **A-I**. For both dinuclear compounds, it is observed that the downfield shift is stronger in case of the iodide compounds compared with the values obtained for the chloride compound. Table 3.3 below displays the chemical shifts of H5 and H6' for the monomers and dinuclear compound.

Table 3.3: Assignment of the signals of H5 and H6' with respect to chemical shifts (ppm) for the monomer and Ru/Pt dinuclear species in acetonitrile-d_6.

H5			H6'		
monomer	Ru/Pt-Cl_2	Ru/Pt-I_2	monomer	Ru/Pt-Cl_2	Ru/Pt-I_2
8.5 ppm	9.35, 9.30 ppm	9.99, 9.80 ppm	8.6 ppm	9.6 ppm	10.30, 10.25 ppm

This was also observed for other similar Ru/Pt compounds for example: [Pt(tbbpy)Cl_2] tbbpy (tbbpy = 4,4′-di-tert-butyl-2,2′-dipyridyl) and [Pt(tbbpy)I_2] in d_6-dmso confirmed the observed shifts (See figure 3.7).

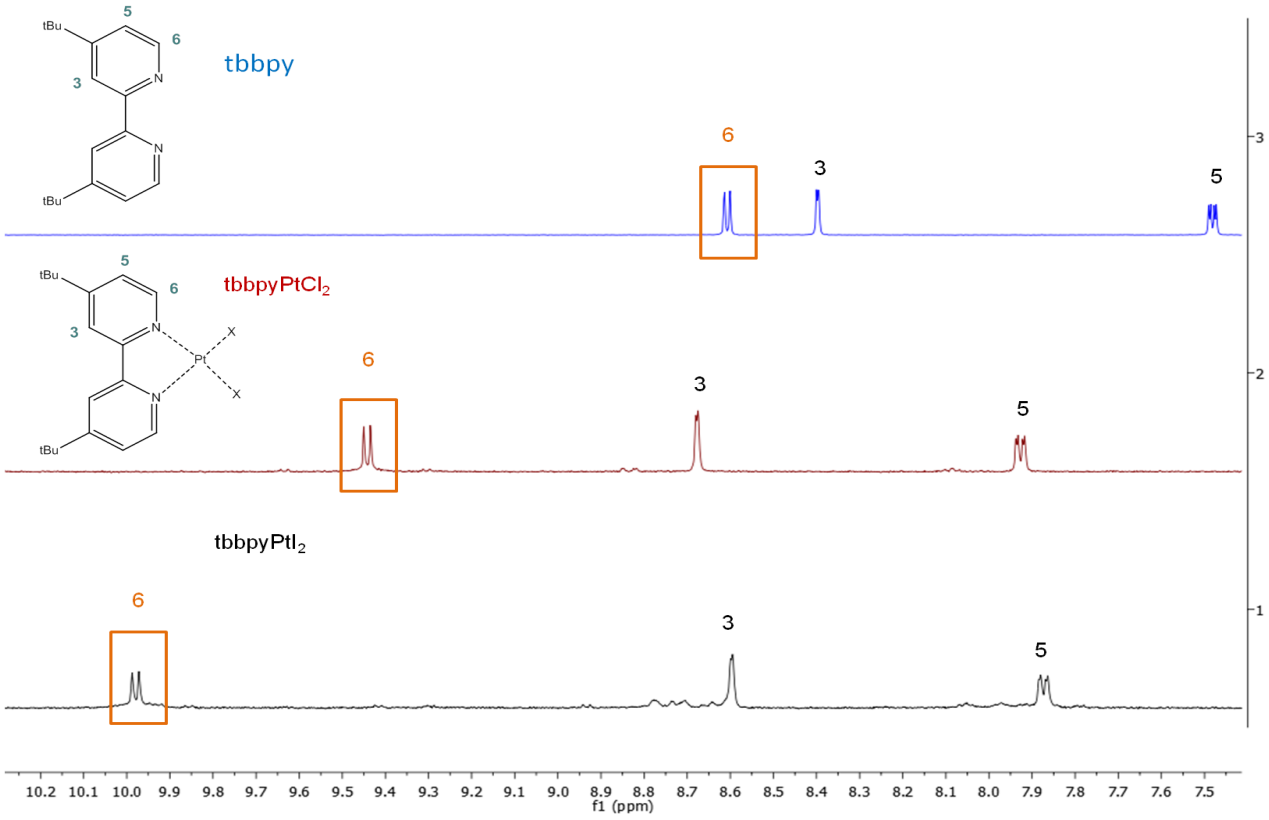

Figure 3.7**:** Comparison of the ^{1}H-NMR spectra of the reference compound [Pt(tbbpy)Cl_2] in dmso-d_6, (c = 3 mM; red: X= Cl, black: X=I)[10]

This is opposite to what is expected as a higher electronegativity atom like Cl should exert a stronger inductive effect on the neighbouring H atoms and cause them to be deshielded, thus appearing more upfield as shown in Table 3.1. The tetrahedral structure of platinum centre excludes the possibility of a π-stacking effect that explains the unusual deshielding of the neighbouring H atoms. Another more plausible explanation for the unusual up field shifts in case of the iodide

complexes is the direct deshielding of hydrogen atoms by the relatively large Iodine atoms in terms of atomic radius compared to Cl atoms. Another alternative for the differences observed is the loss of $\mathbf{I^-}$ or $\mathbf{Cl^-}$ anion from the Pt metal. This anion loss has been observed earlier in the literature for similar RuPtPtPtRu pentanuclear compounds see below.

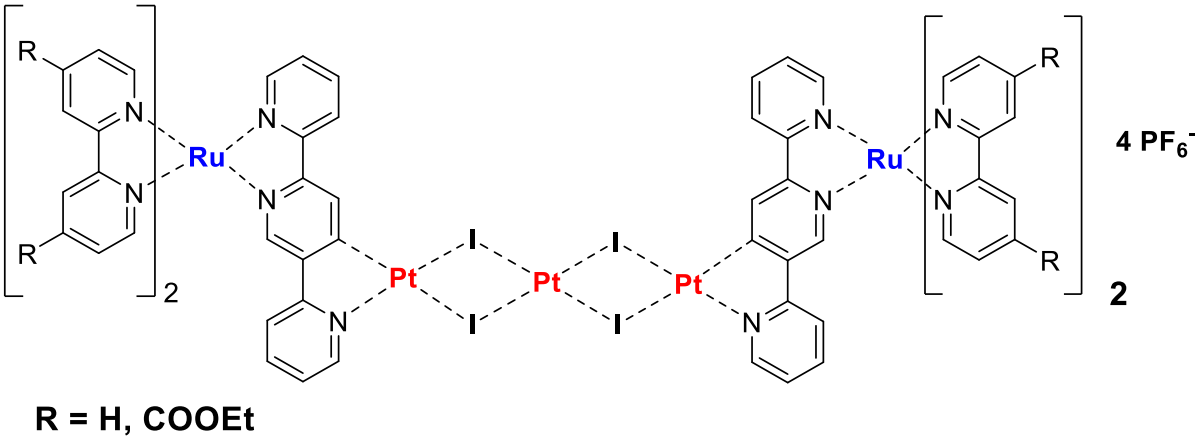

Figure 3.8 Potential structure for pentanuclear photocatalysts.[12]

3.2.3 UV/Vis Absorption spectroscopy

As shown in Chapter 1 the UV/Vis spectra of ruthenium compounds are of considerable importance and can be used to consider the absorption and emission properties of the compounds obtained.

UV/vis absorption properties have been studied for both the Ru(II) monomers and the dinuclear species for the compounds in question. The electronic spectra of the compounds were taken in acetonitrile and the obtained results are shown in Table 3.3. The UV-Vis spectra of the three compounds together with the retention times are shown in Figure 3.9. The UV/Vis spectra were obtained for compound (**A-II**) and compound (**A-III**) using the Photodiod Array (PDA) detector attached to

the HPLC device are more similar to each other than to compound **A-I** as shown in Figure 3-9. However, it is likely that the differences observed for the two Pt

compounds may depend on the potential interaction with the catalytic centre and the presence of the halogen terminal species, i.e. $PtCl_2$ or PtI_2. It also needs to be considered that both chloride and iodine atoms may be labile and could be replaced readily by solvent molecules (see Table 3.1 above).

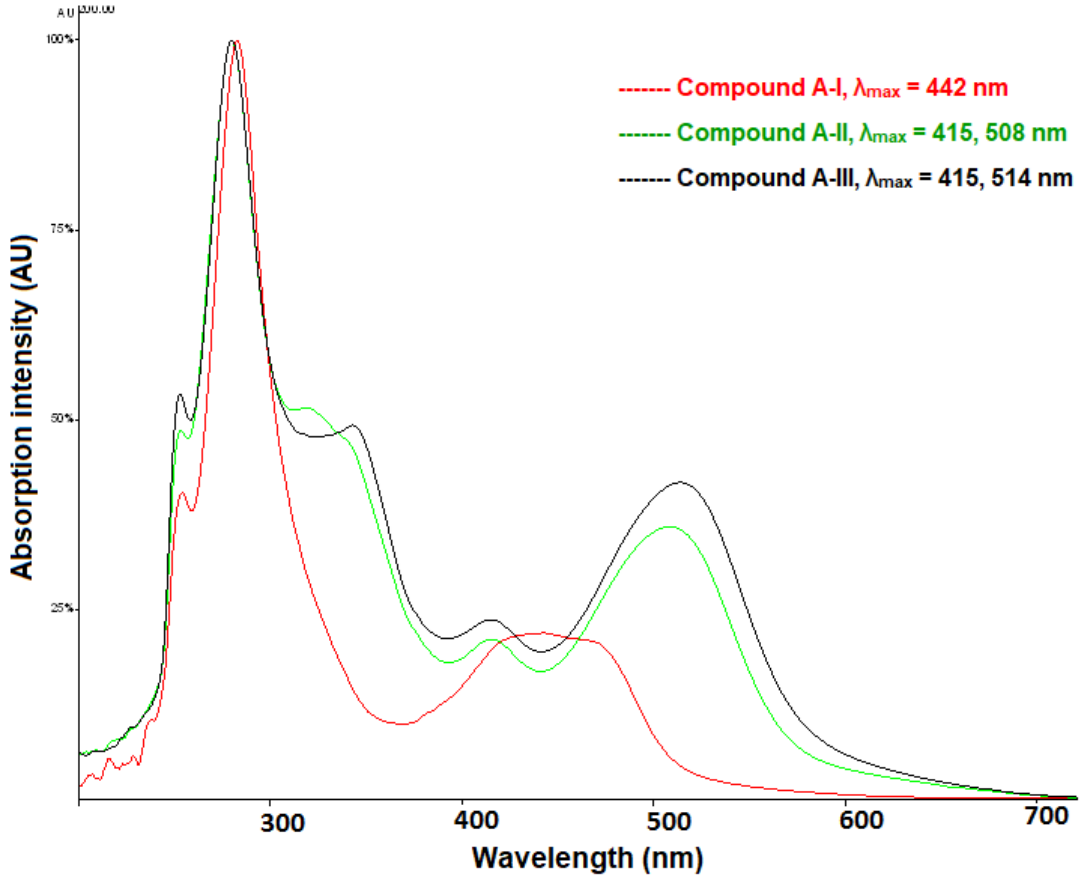

Figure 3.9**:** Absorption spectra (normalized) spectra of $[Ru(bpy)_2(2,3dpp)]^{2+}$ (red), $[Ru(bpy)_2(2,3dpp)PtCl_2]^{2+}$ (green) and $[Ru(bpy)_2(2,3dpp)PtI_2]^{2+}$ (black) at T=24^{0}C in acetonitrile shown in Figure 3.4 a,b,c.

The UV-Visible absorption spectra of the complexes **A-II** and **A-III**, are similar to each other but different from the spectrum obtained with **A-I**. They show two

absorption peaks at λ_{max} of 415,508 nm and 415,514 nm respectively. This is in accordance with lowering the energy of pyrazine based MLCT states.[13,14] There is however no significant difference between the spectra of the iodo and chloro species which suggests that the nature of the halogen component has a relatively small influence on the lowest ^{1}MLCT states after the stabilisation of the pyrazine based states. **A-III** shows a small red shift of the π/π* shoulder at about 340 nm, and the Ru → 2,3dpp transition is slightly stronger for compound **A-II**. The broad absorption area in the UV region (the plateau between 300 nm and 360 nm) is assigned to ligand centred π/π* transitions of the bridging ligand.

The results considered so far, apart from the HPLC data are, in agreement with those observed in the literature [7]. This is important since in the next sections the stability of the three compounds in acetonitrile and in the presence of triethylamine (TEA) will be considered. The results obtained so far indicate that in the dark the compounds are stable and this is especially important for the two dinuclear photocatalytic compounds.

3.3 Photolysis of Compounds.

The aim of this section is to study the photochemical behaviour of both the mononuclear and dinuclear complexes characterised previously in this chapter (compounds **A-I, A-II** and **A-III**, with and without a sacrificial agent. Upon irradiation in acetonitrile with LED 470 nm visible light are carried out, both in the presence of TEA and without. Another purpose also is to investigate the stability of these compounds in light. Since those compounds are under investigation as photocatalysts in a photocatalytic hydrogen generation cells, their photochemical behaviour need to be thoroughly investigated. All the compounds were irradiated

for up to 3 hours in acetonitrile in case of the absence of the TEA. However, in the presence of TEA the irradiation was carried out in much shorter times, as will be specified in the experiment. To minimise the influence of temperature on the chromatographic separation all experiments were carried out at an isothermal system maintained at 24^{o}C.

3.3.1 Photolysis of Compounds in Acetonitrile.

All compounds were photolysed in acetonitrile, after irradiating the compounds for up to 3 hours, it was found that compound **(A-I)** is photo-reactive and compound **(A-II)** is photo stable. The compound (**A-III)** is slightly photo-reactive under these conditions. The photochemical processes were followed by characterisation with HPLC, UV-Vis spectroscopy and ^{1}H-NMR spectroscopy as shown in the following Figures. It has been established that acetonitrile can undergo light-induced ligand exchange reactions. [15,16,17]

3.3.1.1 Compound A-I

The photolysis of the mononuclear compound **A-I** is addressed by using analytical techniques, such as, HPLC, UV-Vis spectroscopy and ^{1}H-NMR spectroscopy. The results of compound **A-I** upon irradiation before and after the irradiation are outlined in Figures (3.10), (3.11) and (3.12).

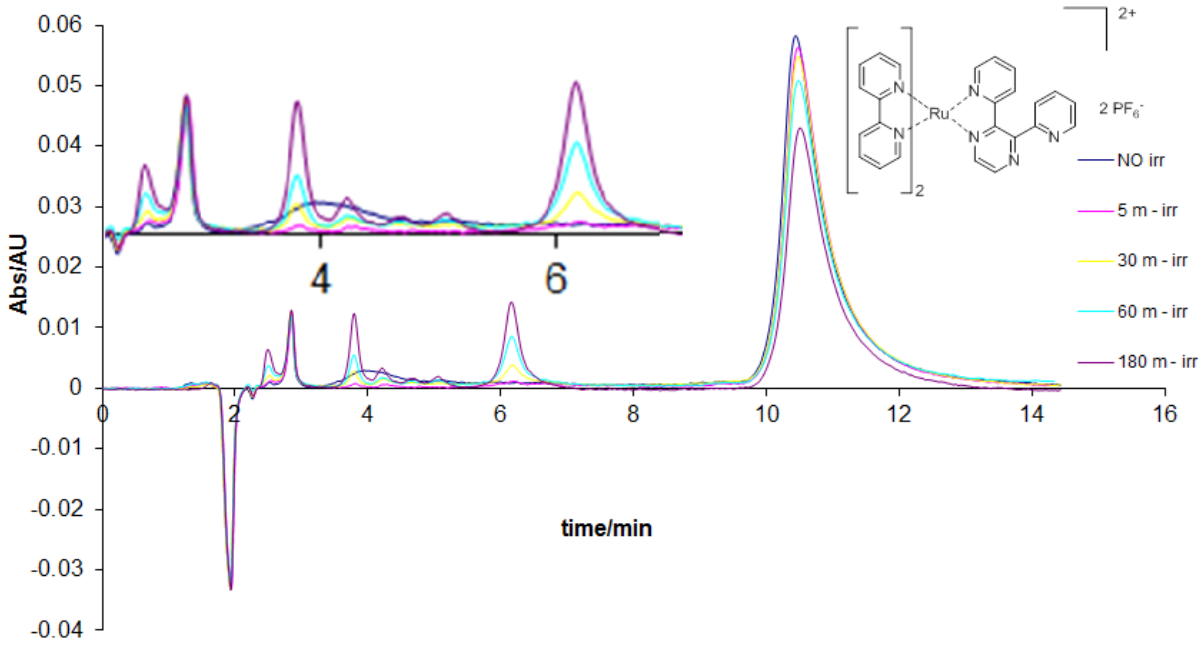

Figure 3.10(a): HPLC trace during Photolysis of $[(bpy)_2Ru(2,3dpp)]^{2+}$ in CH_3CN (mobile phase CH_3CN: H_2O: CH_3OH with volume ratio 75:20:5 containing 0.12 M KNO_3). Flow rate: 2.0 cm^3 min^{-1}; detection wavelength at 280 nm, T=24 ^oC

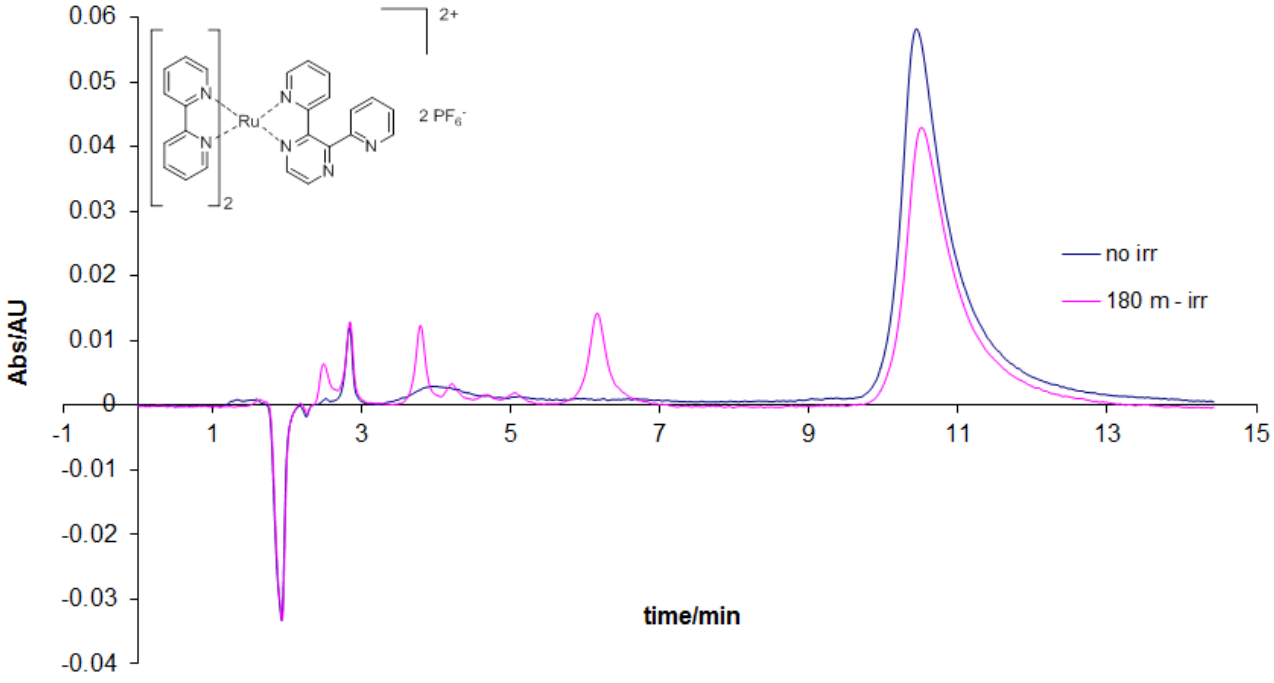

Figure 3.10(b): HPLC trace before and after Photolysis for $[(bpy)_2Ru(2,3dpp)]^{2+}$ in CH_3CN (mobile phase CH_3CN: H_2O: CH_3OH with volume ratio 75:20:5 containing 0.12 M KNO_3). Flow rate: 2.0 cm^3 min^{-1}; detection wavelength at 280 nm, T=24 ^oC

These figures show that the retention time observed for (compound **A-I**) is 10.47 minutes and that the retention time has not changed significantly upon irradiation. However, four different peaks are observed and they increase with the irradiation time. They appear at retention times of 2.54, 3.81, 4.24 and 6.20 minutes and the main peak's area is reduced by increasing the irradiation time. The UV-Vis absorption spectrum of the first product is shown in Figure 3.9 in has a retention time of 3.81 min has a λ_{max} at 435 nm and the second product with retention time of 6.20 has a λ_{max} at 424 nm. and these are in agreement with the formation of the compound - $[Ru(bpy)_2(CH_3CN)_2]^{2+}$ is staple compound no other materials are observed. [14] The absorption spectra of the two new peaks present after 3 hours of irradiation are shown in Figure 3.11 below.

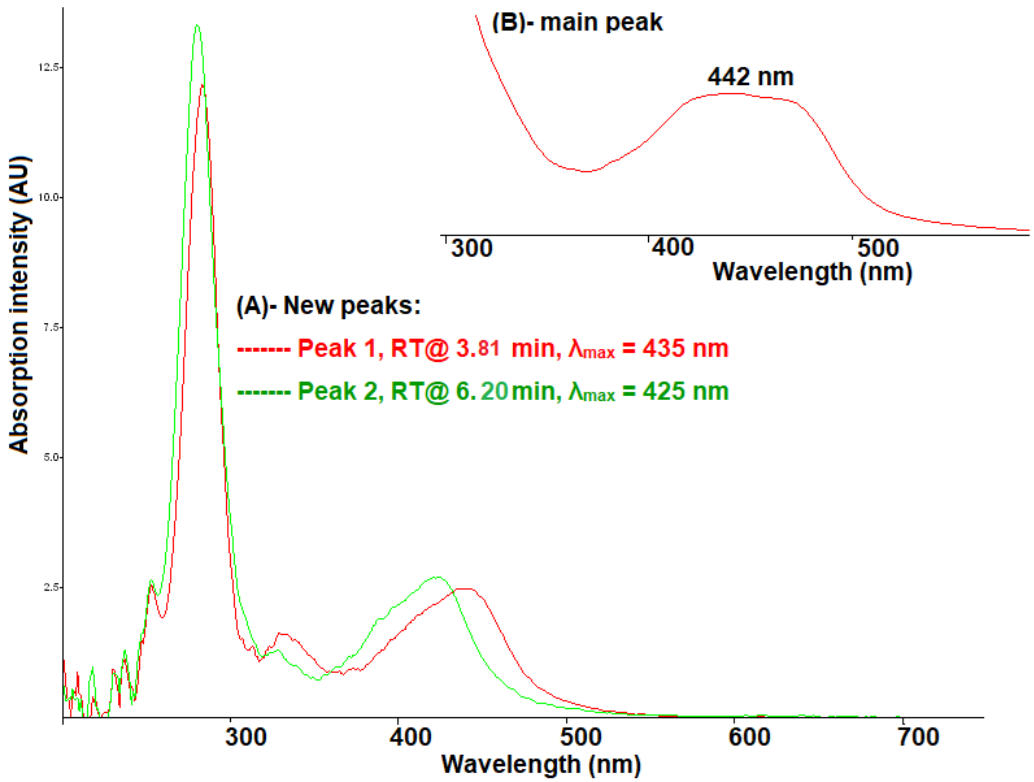

Figure 3.11 Absorption spectra of species detected in compound A-I After irradiation (A) and main peak (B) in Figure 3.10 (a, b) above. Detection wavelength 280 nm.

The ^{1}H-NMR spectroscopic experiments were carried out to obtain further information on the photochemical changes made in the compounds and the ^{1}H-NMR spectroscopic results obtained for the photolysis of compound **A-I** in acetonitrile are shown in Figure 3.12.

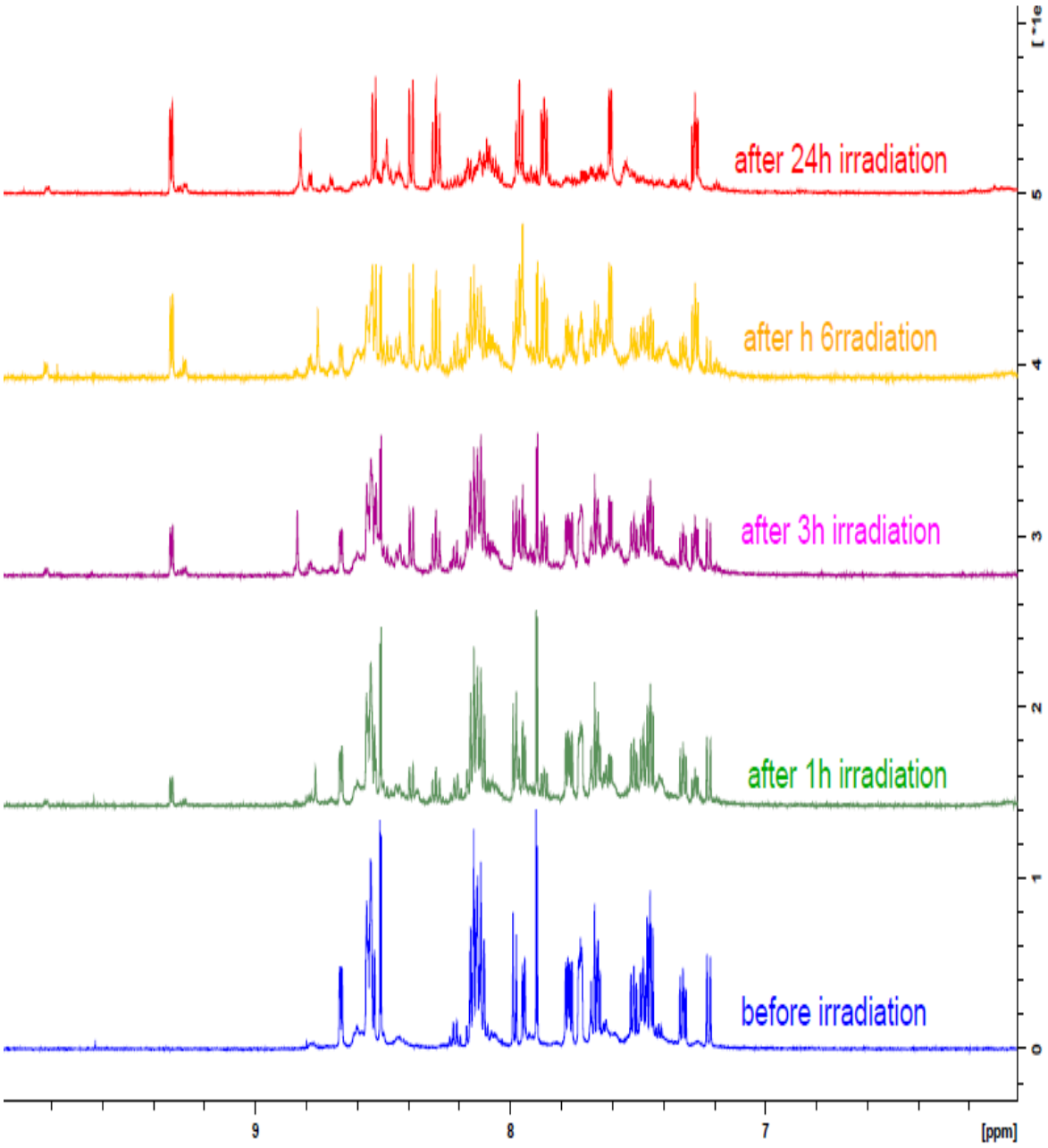

Figure 3.12: ^{1}H-NMR spectroscopy of compound **A-I** during Photolysis in acetonitrile-d_3

In the ^{1}H-NMR spectroscopy results obtained during 24 hours of irradiation, the more than a few signals are growing at 9.4 ppm, 8.8 ppm, 8.4ppm and 8.3 ppm while other processes are observed as well several signals are disappearing at 8.1ppm, 7.7ppm and 7.5 ppm. These signals are found in the region expected for a complex with the general formula; $[Ru(bpy)_2(L)_2]^{2+}$. The λ_{max} observed in the UV-vis spectrum in Figure 3.11 for the species with a retention time of 2.54 minutes indicates the presence the solvent (acetonitrile). This is not unexpected as this is the solvent used for the photolysis experiments The change of the ^{1}H-NMR result is consistent with the photolysis leading to the loss of the (2,3dpp) ligand with subsequent replacement by CH_3CN during the irradiation time and that the following reaction has taken place as (See chapter 6) outlined above [14];

$$[Ru(bpy)_2(2,3dpp)]^{2+} \xrightarrow{h\nu} [Ru(bpy)_2(CH_3CN)_2]^{2+} + 2,3dpp$$

This reaction can be confirmed with ^{1}H-NMR spectrum obtained after 24 hours of photolysis are typical for the bisacetonitrile compound $[Ru(bpy)_2(CH_3CN)_2]^{2+}$ and these features are very similar to those observed in the ^{1}H NMR spectrum for $(Ru(bpy)_2(CH_3CN)_2(PF_6)_2$ in Figure 3-13. Note that the stability of compound A-1 is much stronger that that of the reference below.

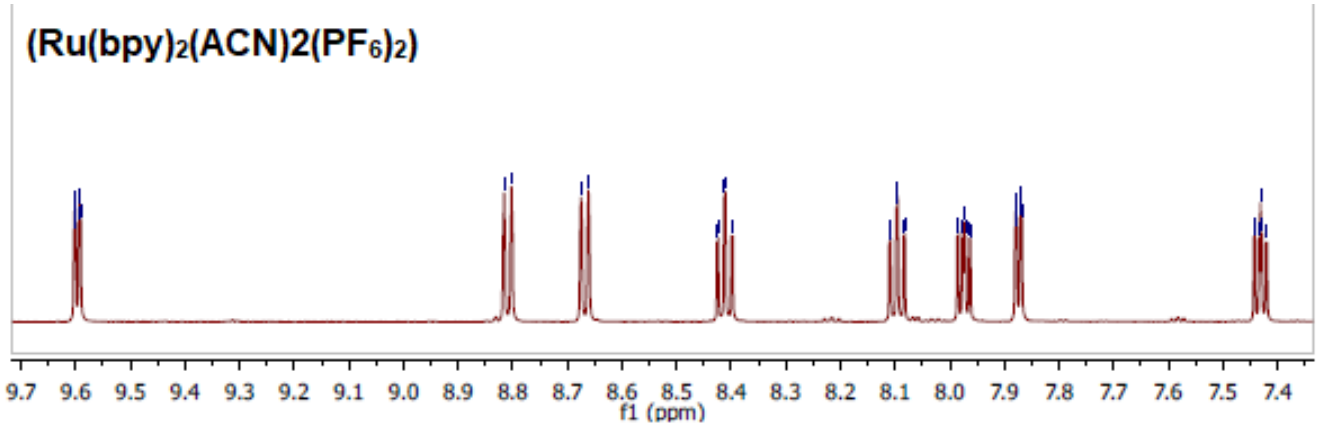

Figure 3.13: ^{1}H-NMR spectroscopy of $(Ru(bpy)_2(CH_3CN)_2(PF_6)_2)$ in d_3-acetone.

^{1}H-NMR (600 MHz, Acetone) δ 9.60 (ddd, J = 5.5, 1.4, 0.7 Hz, 1H), 8.81 (d,J = 8.1 Hz, 1H), 8.67 (d,J = 8.0 Hz, 1H), 8.41 (td,J = 7.9, 1.5 Hz, 1H), 8.12 – 8.07 (m, 1H), 7.97 (ddd, J = 7.6, 5.5, 1.3 Hz, 1H), 7.87 (ddd, J = 5.7, 1.4, 0.6 Hz, 1H), 7.45 – 7.41 (m, 1H), 2.49 (s, 3H)

3.3.1.2 Compound A-II

The photoreaction of compound **A-II** is investigated using HPLC, UV/Vis spectroscopy and ^{1}H-NMR spectroscopy. Irradiation of the compound was carried out in the same conditions prescribed above for compound **A-I**. The compound was irradiated for 3 h. The HPLC results obtained after photolysis of this compound is shown in Figures 3.14

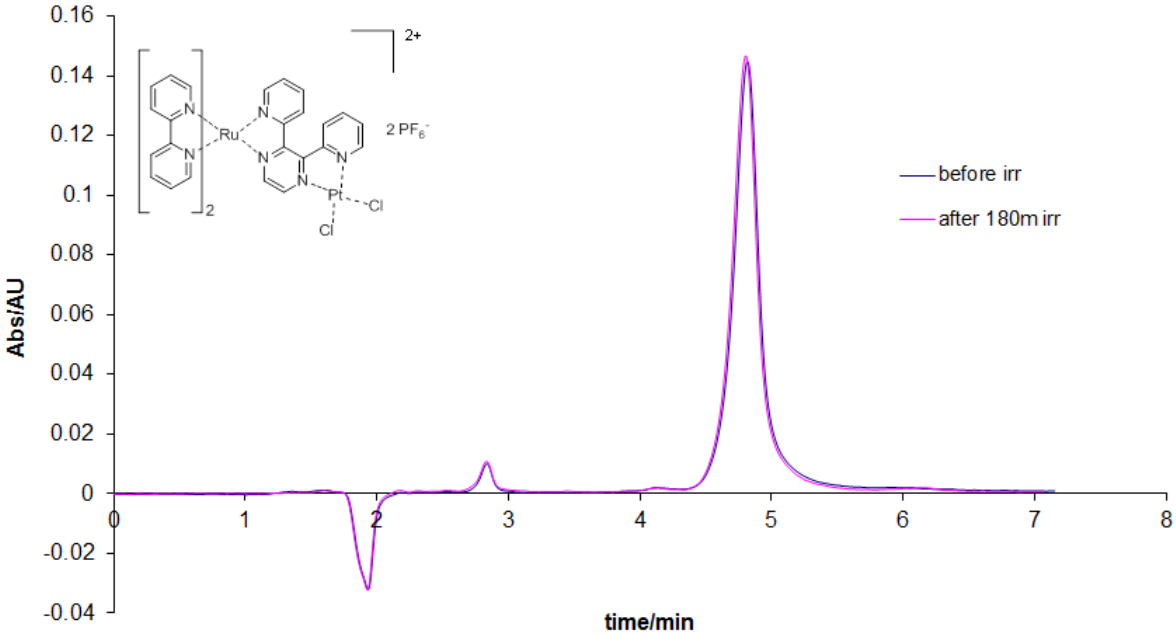

Figure 3.14: HPLC trace during Photolysis of $[(bpy)_2$ Ru (2,3dpp)PtCl$]^{2+}$ in CH_3CN (mobile phase CH_3CN: H_2O: CH_3OH with volume ratio 75:20:5 containing 0.12 M KNO_3). Flow rate: 2.0 cm^3 min^{-1}; detection wavelength at 280 nm, T=24 ^oC

It seems somewhat surprising that the HPLC trace shown in Figure 3-14 during photolysis shows that under the conditions used compound is largely photostable for irradiation up to 3 hours period. The ^{1}H-NMR results show that under the conditions used in these experiments the compound **A-II** is photostable for up to 24 hours as shown in Figure 3-15.

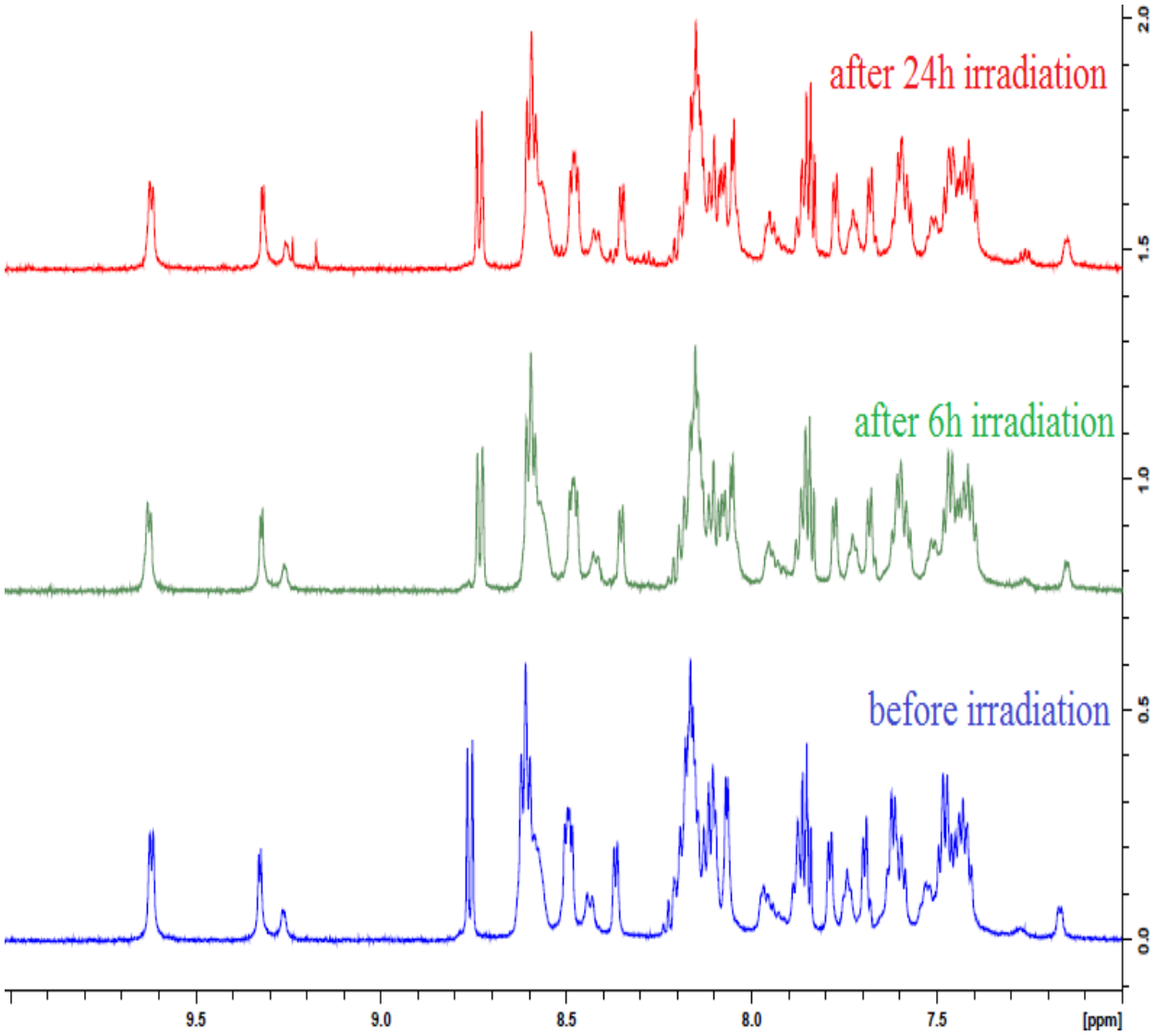

Figure 3.15: ^{1}H-NMR during Photolysis of $[Ru(bpy)_2(2,3dpp)PtCl_2]^{2+}$ in d_3-acetonitrile.

The compound was irradiated in ^{1}H-NMR solvent (CH_3CN-d_3) at much higher concentrations. Since the concentration of NMR solution is higher than the amount used in the HPLC studies by at least three times, longer irradiation times were applied for the compound to compensate for the higher expected absorption. Even tough, the compound is found to be still very stable.

The ^{1}H-NMR results are in agreement with HPLC results. Clearly, the results show that the compound **A-II** is photostable under the conditions used in these experiments.

3.3.1.3 Compound A-III

The compound **A-III** was photolysed by irradiation for up to 3 hours in acetonitrile. The photochemical behaviour processes were monitored by HPLC, UV/Vis spectroscopy and ^{1}H-NMR spectroscopic, the results obtained are shown in Figures 3.16(a,b)

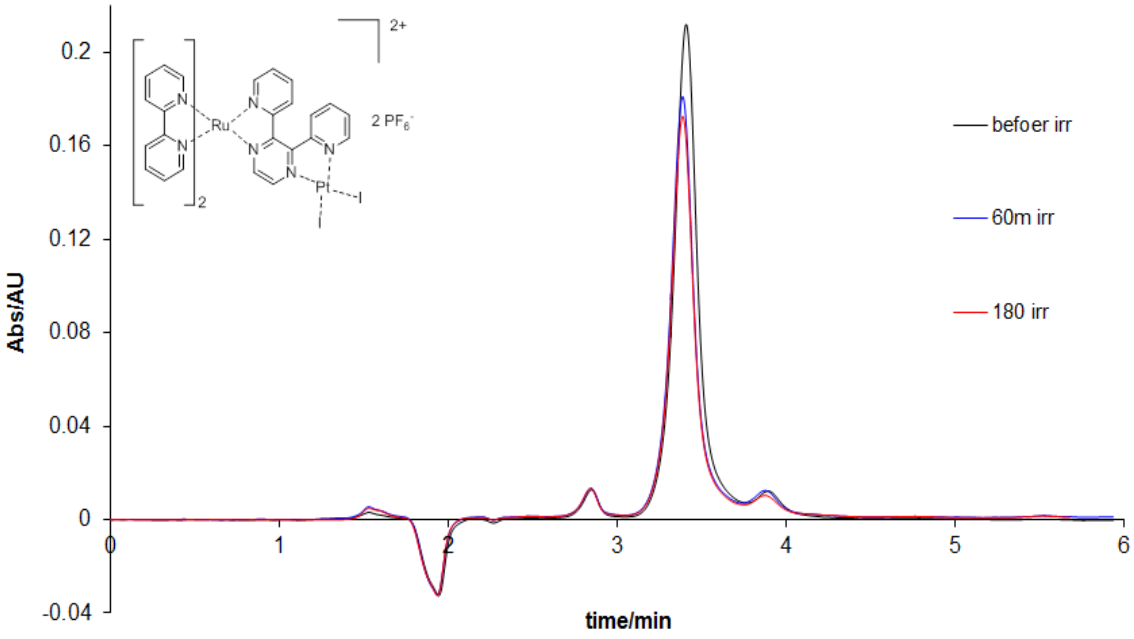

Figure 3.16(a): HPLC trace during Photolysis of $[(bpy)_2Ru(2,3dpp)PtI_2]^{2+}$ in CH_3CN (mobile phase CH_3CN: H_2O: CH_3OH with volume ratio 75:20:5 containing 0.1 M KNO_3). Flow rate: 2.0 cm^3 min^{-1}; detection wavelength at 280 nm, T=24 ^{o}C

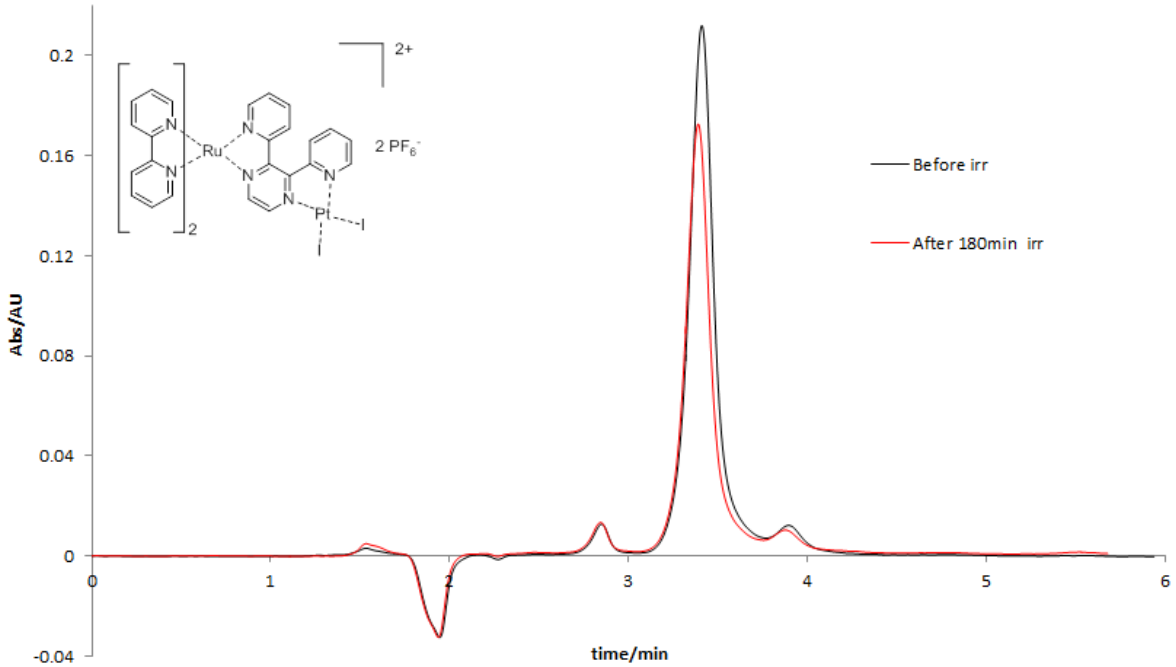

Figure 3.16(b): HPLC trace before and after Photolysis for $[(bpy)_2Ru(2,3dpp)PtI_2]^{2+}$ in CH_3CN (mobile phase CH_3CN: H_2O: CH_3OH with volume ratio 75:20:5 containing 0.12 M KNO_3). Flow rate: 2.0 cm^3 min^{-1}; detection wavelength at 280 nm, T=24 ^oC

These figures show that compound **A-III** undergoes photolysis under the irradiation condition described for this experiment. Surprisingly, there are limited photo detectable degradation products produced during the irradiation time. After 3 hours the main peak was only slightly decreasing in area under curve. The UV/Vis absorption spectrum of the main peak is found at 514 nm while a second peak is observed at 415 nm and these are shown in Figure 3.17 below. The features observed are the same as those measured in solution see also Table 3.3 and therefore stability of the compound is excellent.

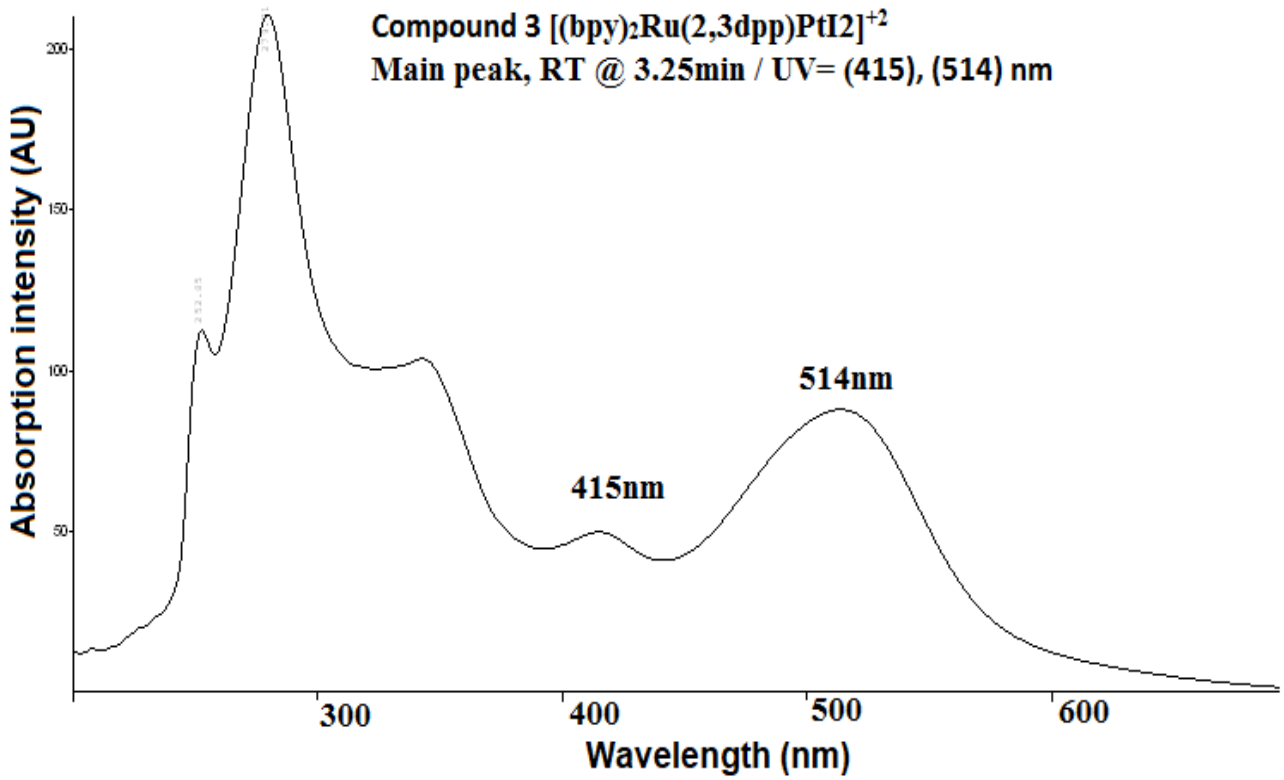

Figure 3.17*:* Absorption spectra of species detected in compound **A-III** $Ru(bpy)_2(2,3bpp)PtI_2](PF_6)_2$ in Figure 3.16 above at RT 3.25 min (main peak). Detection wavelength 280 nm.

To further investigate the photolysis process, sample **A-III** was also followed by ^{1}H-NMR spectroscopy in order to try to determine any possible by products produced upon photolysis. The evolution of the ^{1}H-NMR data for the sample during its irradiation in d_3-CH_3CN is shown in Figure (3.18). Between 12-24 hours of irradiation the ^{1}H-NMR spectrum a number of peaks appear between 9.0 and 9.6 ppm.

No significant new peaks appeared in the spectrum, but there might be a formation of a small amount of intermediates. Observed are a number of weak signals one at 9.17 ppm, one signal at 8.2 and also one signal at 7.2 ppm. This illustrates that the photolysis of **A-III** does create some intermediates but these

cannot be determined, clearly the amounts of these species produced are too low to allow for definitive assignment. for further details, discussed in Chapter 6.

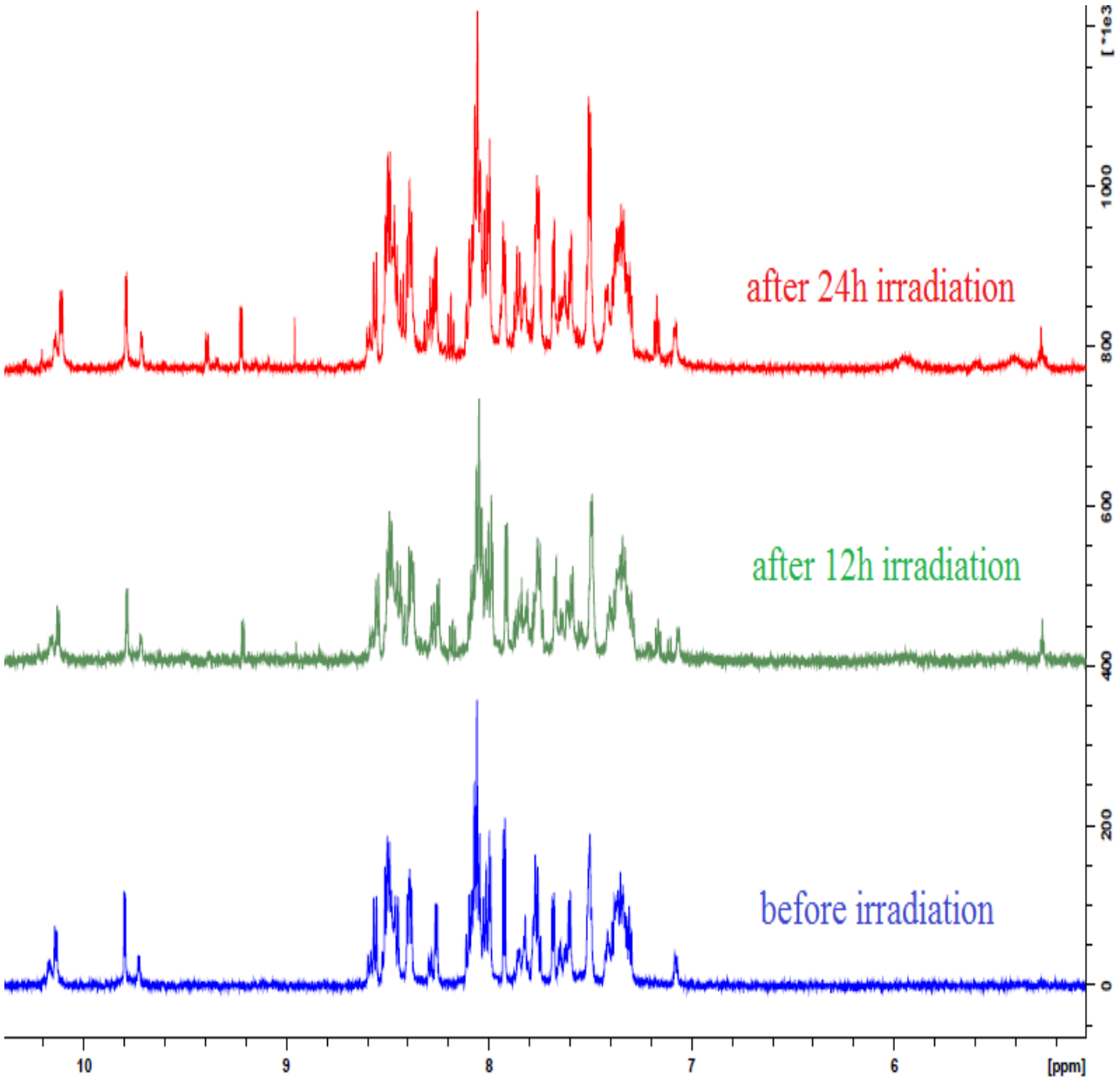

Figure 3.18: ^{1}H-NMR spectroscopy of compound **A-III** during photolysis in d_3-acetonitrile.

3.3.2 Photolysis of Compounds A-1, A-II and A-III in the Presence of TEA.

In the last section, it has been shown that in acetonitrile the compounds **A-I** and **A-III** are photoreactive but that compound **A-II** is photostable for up to 3 hours under irradiation with visible light. In this section, the photostability of the compounds after irradiation in the presence of TEA is considered. The major difference between the two experiments is adding triethylamine (TEA) in the solvent which acts as a sacrificial reductant agent in the photocatalytic process as mentioned in the literature review. Moreover, during the sample preparation, solutions were deaerated with argon or nitrogen prior to irradiation to mimic the conditions at which the photocatalytic process is conducted.

3.3.2.2 Results

The photochemical behaviour of **A-I** with TEA is outlined in Figure (3.19 a,b). These figures show the HPLC results of the compound **A-I** during the irradiation and display the initial and final compound after irradiation in the presence of TEA and MeCN. It is clear that the compound is not stable and the features observed are similar to those obtained for the compound in only acetonitrile, but the amount of decomposition observed is large under these conditions.

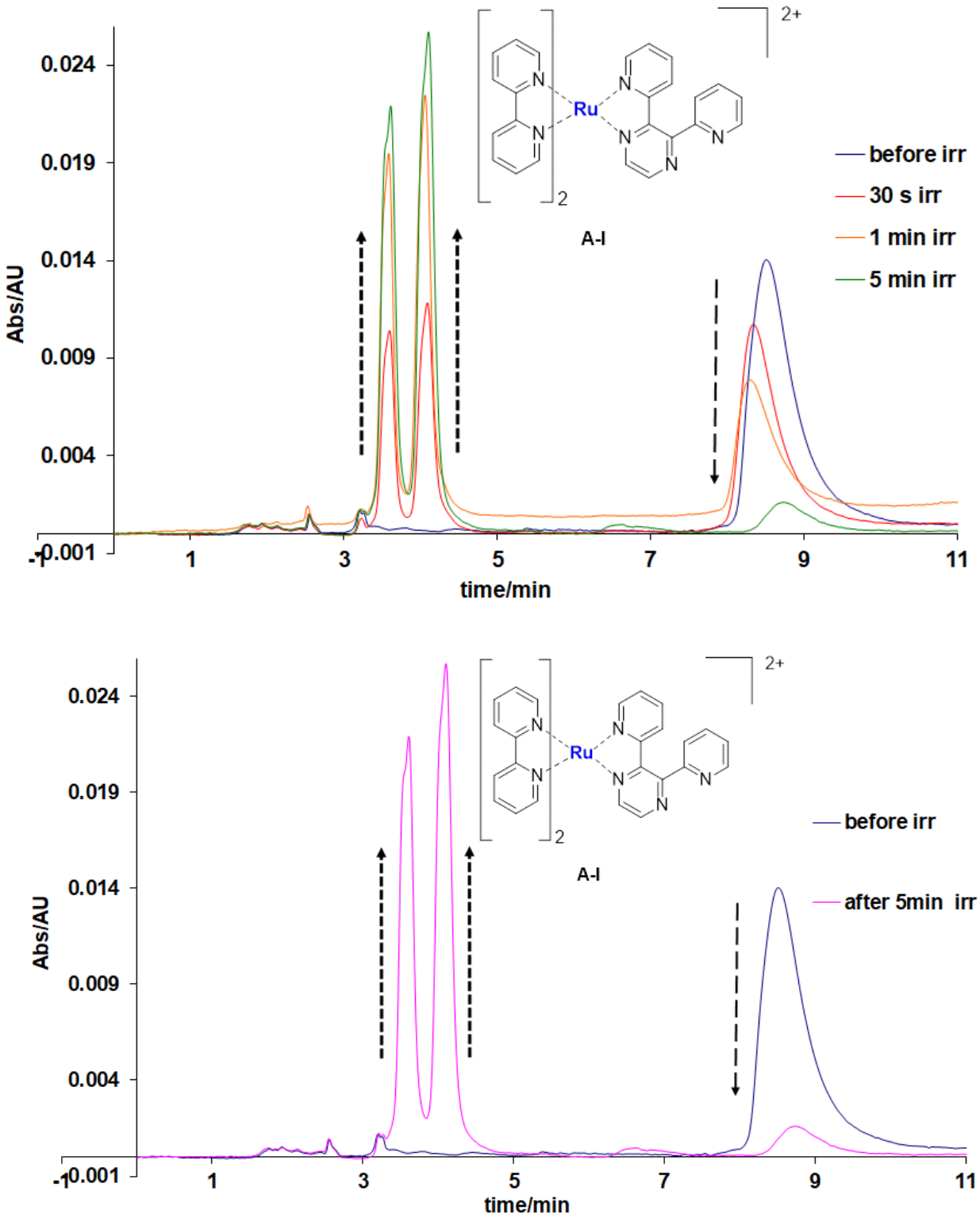

Figure 3.19(a,b): HPLC traces obtained upon photolysis of compound 1. Temperature 24° C. Irradiated in CH_3CN in presence of TEA (15%) and H_2O (10%) using 470 nm LED irradiation from (0-5min) degassing with Ar before irradiation detection wavelength; 470 nm, Mobile Phase CH_3CN:H_2O:CH_3OH with volume ratio 75:20:5 containing 0.12 M KNO_3 Flow rate 2.0 cm^3 min^{-1}

A small shift of the baseline is also observed due to minor variations in temperature during the experiments. The $[(bpy)_2Ru(2,3dpp)]^{2+}$ peak appears at a retention time of 8.55 minutes accompanied with a small amount of three different products is observed at 2.0, 2.57 and 3.22 minutes retention times before irradiation. The height of the main peak decreased within 30 seconds of irradiation from (14.0m AU) to (10.7m AU). It is approximately 23.57 % of peak height. While after 5 minutes it further decreased to (1.6m AU) which is more than 88.58 % from the compound concentration.

The decomposition process is resulting in appearance of two new products in the chromatograms during of irradiation at retention times of 3.69 and 4.14 minutes which found to increase by irradiation time. The absorption spectrum of the $[(bpy)_2Ru(2,3dpp)]^{2+}$ peak before irradiation and of products after 5 minutes of irradiation shown in figure 3.20 below, the red line of compound before irradiation, the red line of the product at retention time 3.60 minutes and green line of the product at retention time 4.10 minutes. The spectrum observed for the two new products with a retention time at 3.60, 4.10 min have a very similar absorption maximum at 442nm and can be identified from related studies as $[Ru(bpy)_2(CH_3CN)_2]^{2+}$. [14] As before A-1 the ruthenium compound was measured before for a period of 5 minutes without the presence of TEA. The formation of these compounds indicates that upon irradiation a 2,3dpp ligand is replaced by two CH_3CN molecules. further discussed in Chapter 6. After 5 minutes of photolysis, two new products were obtained for the compound at the retention time at 3.60, 4.10 minutes with peak heights of 21.9 mAU and 25.7mAU respectively, while the HPLC result shows a near-total breakdown of the compound.

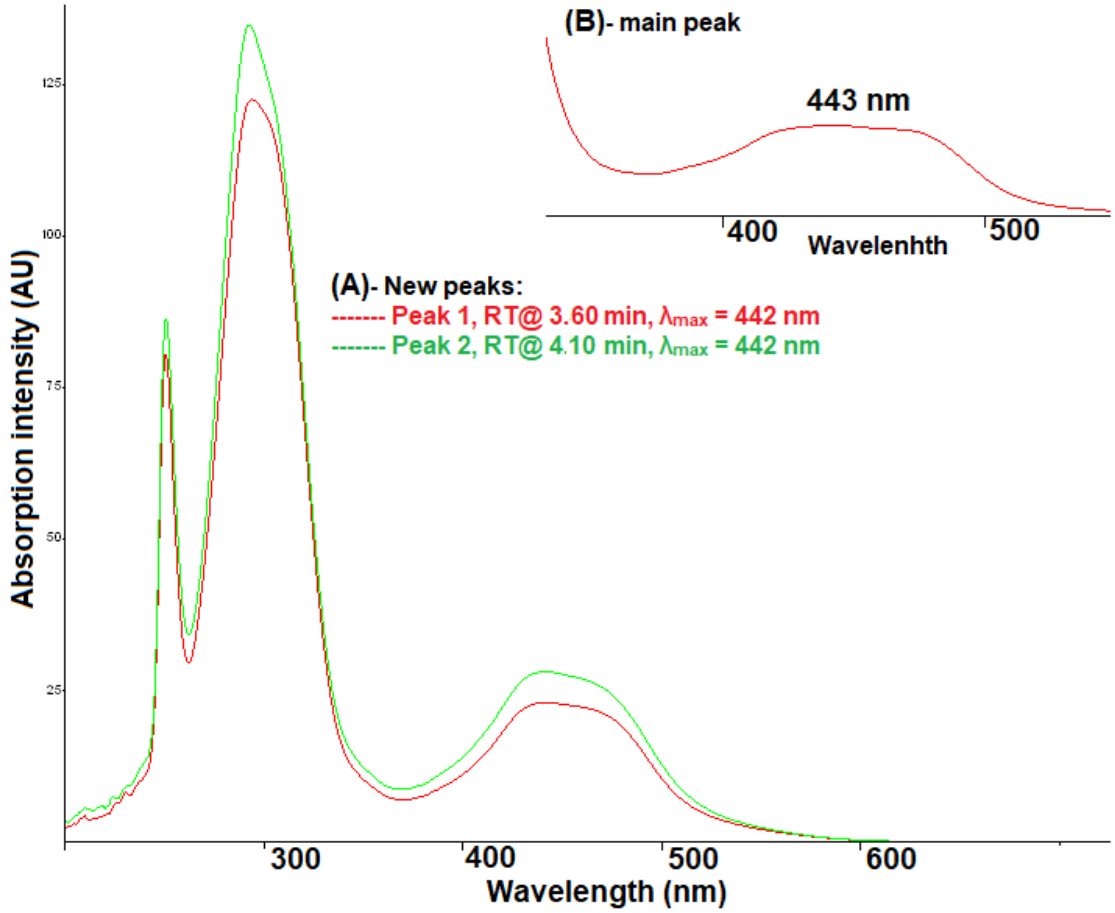

Figure 3.20: Absorption spectra features of all species identified above after 5 minutes of irradiation (A) and Absorption spectra of the main peak (B) in Figure 3.19. Detection wavelength 470 nm.

b - **Photoreaction of $[(bpy)_2Ru(2,3dpp)PtCl_2]^{2+}$ in the presence of TEA**

The HPLC traces obtained before irradiation and upon irradiation of this compound **A-II** in the presence of TEA are shown in Figures (3.21), (3.24a,b) below. The $[(bpy)_2Ru(2,3dpp)PtCl_2]^{2+}$ peak is detected at a retention time of 4.49 minutes and five small peaks of impurities or related compounds detected at the following retention times 1.72, 1.99, 2.23, 2.64 and 4.17 minutes directly before irradiation. The UV-spectra of these unidentified compounds in addition of the main compound are shown below in Figure 3.22 and 3.23.

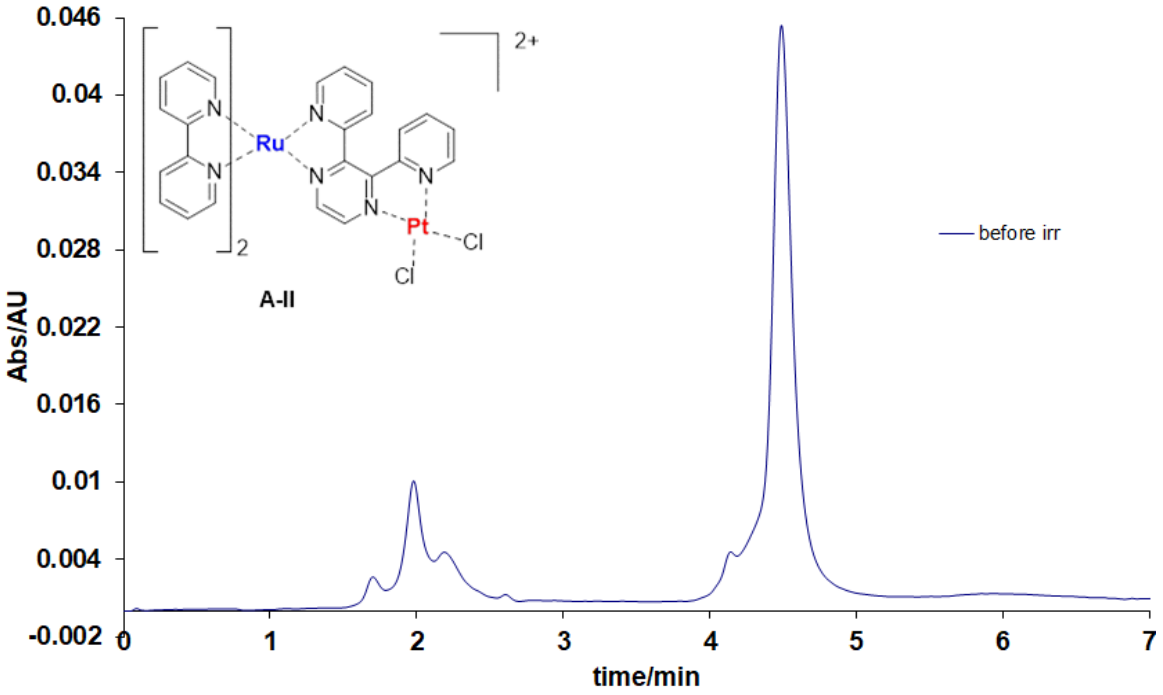

Figure 3.21: HPLC traces obtained before irradiation time of compound **A-II** in CH_3CN, presence of TEA (15%) and H_2O(10%) detection wavelength; 470 nm, Mobile Phase CH_3CN:H_2O:CH_3OH with volume ratio 75:20:5 containing 0.12 M KNO_3 Flow rate 2.0 cm^3 min^{-1}

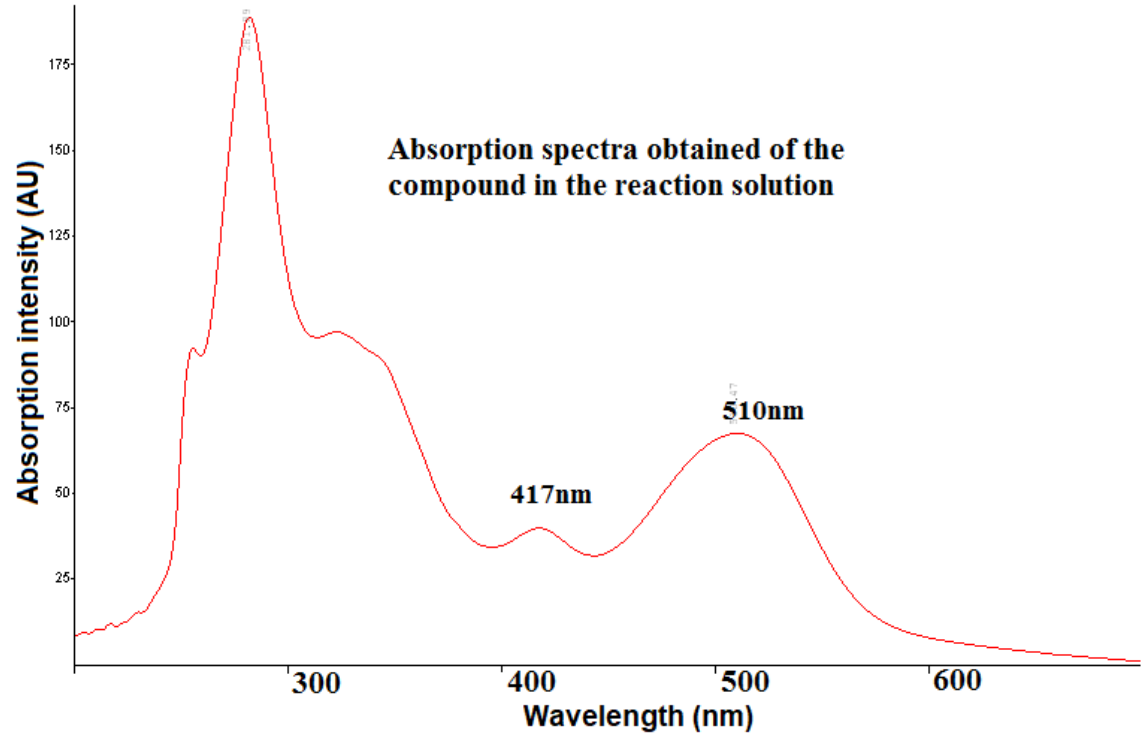

Figure 3.22: Absorption spectra obtained from compound **A-II** in the reaction solution before irradiation.

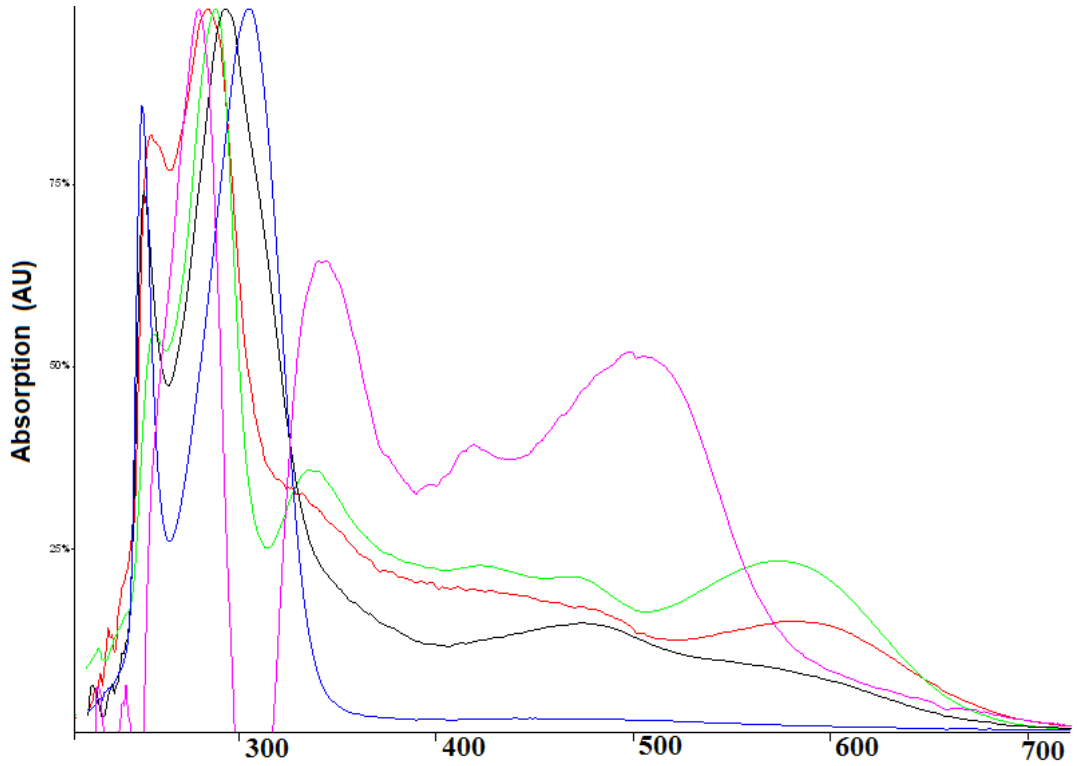

Figure 3.23*:* Normalized absorption spectra of small peaks in solution before irradiation. The red line of the peak at 1.72min, the green line of the peak at 1.99min, the black line of the peak at 2.23min, the blue line of the peak at 2.64min and the pink line of the peak at 4.17 min.

During the photolysis the $[(bpy)_2Ru(2,3dpp)PtCl_2]^{2+}$ peak of the product was decreased from 45.3 mAU to 27.5 mAU after 30 seconds irradiation which represent about 39.3 % of the compound concentration with appearance of two new products at the retention times of 1.97, 2.16 minutes and a peak at 5.70 minutes. On the other hand, the peaks at retention time 1.72, 2.64 and 4.17 minutes are found to be stable with no change in their peaks during the irradiation time.

The absorption spectra and the appropriate chromatogram obtained for peaks at 1.97, 2.16 min retention time indicate a strong overlap between the different species after photolysis for 5 min and are therefore not that informative. the results is shown below in Figure 3.24(a,b) and 3.25.

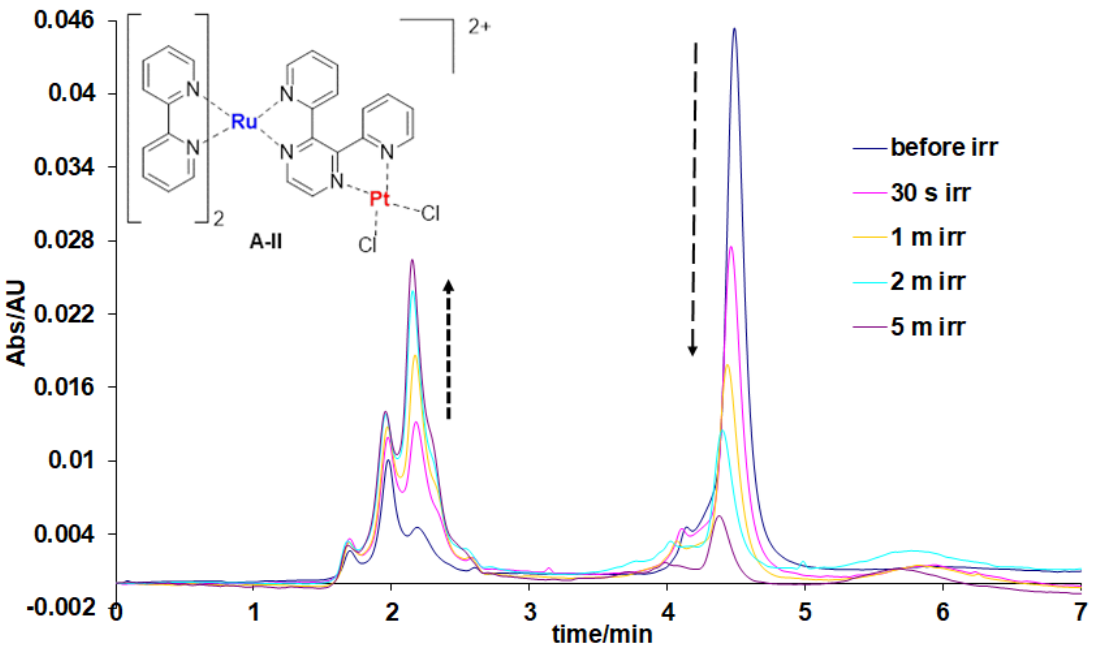

Figure 3. 24a: HPLC traces obtained upon photolysis of compound A-II. Irradiated in CH_3CN, presence of TEA 15% and H_2O 10% using 470 nm LED irradiation from (0-5min) degassing with Ar before irradiation detection wavelength;470 nm,Mobile Phase $CH_3CN:H_2O:CH_3OH$ with volume ratio 75:20:5 containing 0.12 M KNO_3 Flow rate 2.0 cm^3 min^{-1}

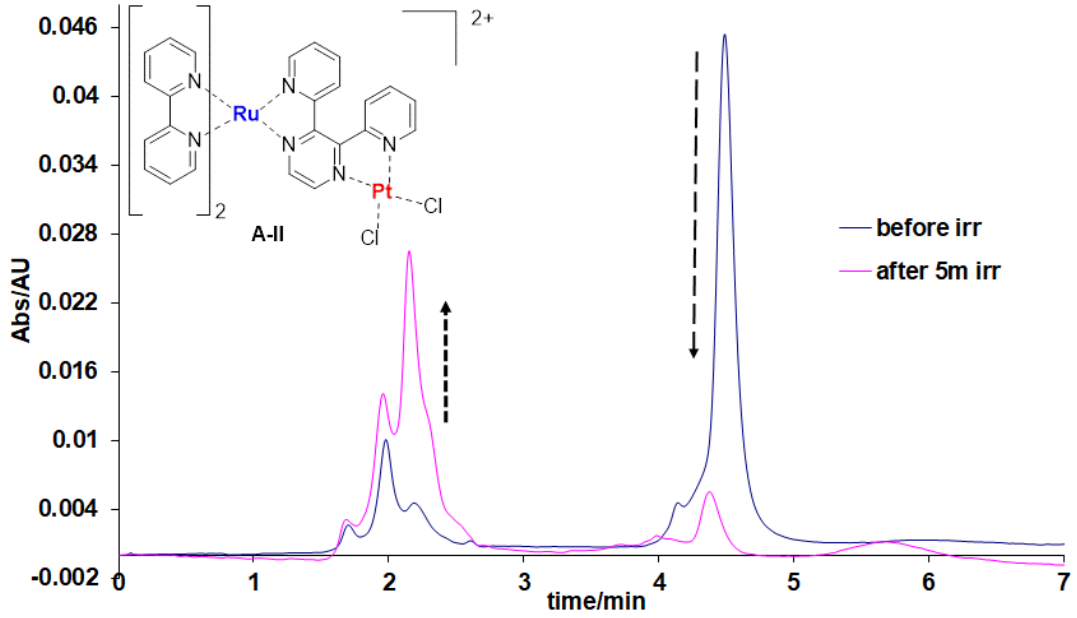

Figure 3.24b: HPLC traces obtained before and after photolysis of compound **A-II**. Irradiated in CH_3CN, presence of TEA (15%) and H_2O(10%) using 470 nm LED irradiation from (0-5min) degassing with Ar before irradiation detection wavelength; 470 nm,Mobile Phase $CH_3CN:H_2O:CH_3OH$ with volume ratio 75:20:5 containing 0.12 M KNO_3 Flow rate 2.0 cm^3 min^{-1}

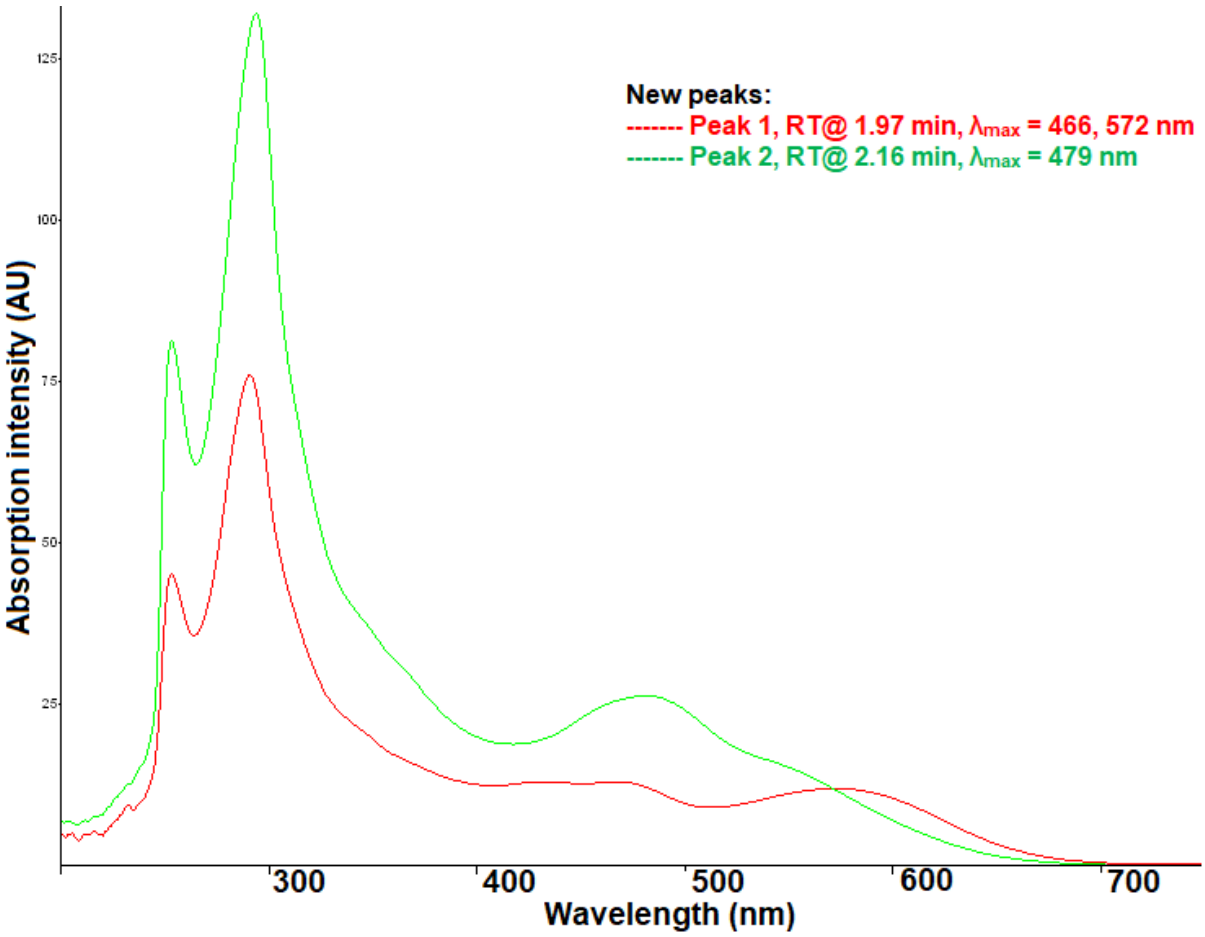

Figure 3.25**:** Absorption spectra features of new peaks identified above after 5 minutes of irradiation in Figure (3.24a, b). Detection wavelength 470 nm.

The presence of absorption peak at about 479 nm (retention time 2.16 min) may indicates the presence of $[Ru(bpy)_2Cl_2]$ or associated $[Ru(bpy)_2ClS]^+$ (S= solvent) compounds. Other species could not be determined with certainly, but the presence of free (2,3dpp) bridging ligand and $[Ru(bpy)_2(CH_3CN)_2]^{2+}$ (retention times of 1.8 and 2.2 respectively) are likely to be present. (See also Chapter 6)

For this part, the chromatogram explains that the **A-II** product is greatly unstable after 5 minutes of irradiation forming 3 different compounds with only 40% remained in the solution while the related compounds are found to be stable after the irradiation process.

C - Photoreaction of $[(bpy)_2Ru(2,3dpp)PtI_2]^{2+}$ A-III in the presence of TEA

To investigate the photostability of the $[(bpy)_2Ru(2,3dpp)PtI_2]^{2+}$, HPLC analysis of the photolysis in the presence of TEA was carried out. Traces were taken during the photolysis of the compound in the presence of TEA. Surprisingly, after 5 seconds of irradiation the main peak of **A-III** at Figure 3.26, was found to take a different shape at 3.70 min and a minor change in the retention time.

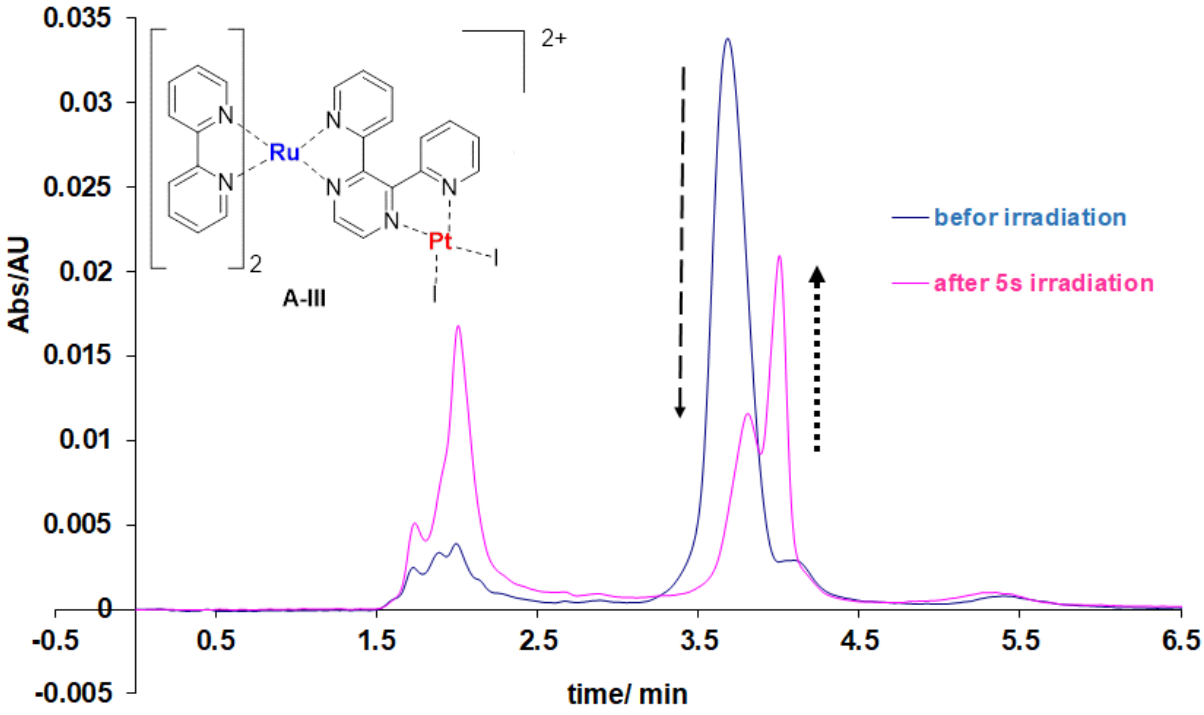

Figure 3.26**:** HPLC traces obtained upon photolysis of $[(bpy)_2Ru(2,3dpp)PtI_2]^{2+}$. Irradiated in CH_3CN, presence of TEA (15%) and H_2O(10%) using 470 nm LED irradiation from (only 5 seconds) degassing with Ar before irradiation detection wavelength; 470 nm, Mobile Phase CH_3CN:H_2O:CH_3OH with volume ratio 75:15:10 containing 0.12 M KNO_3 Flow rate 2.0 cm^3 min^{-1}

Interestingly a **RuPt$_3$Ru** compound has been observed recently as shown in Fig 3.6 [14] It is possible that this compound will decompose in 5 seconds and as a result a second species is obtained. Such a pentanuclear structure, was obtained during the synthesis of a novel supramolecular photocatalysed based on a **RuPt$_3$Ru** catalyst (Figure 3.8). This photocatalyst is able to create high turnover numbers for solar hydrogen generation, of up to 650 after 56 hours of irradiation. It is therefore possible that within seconds the iodine bridge is that is present in Figure 3.6 is dissociated and a number of different species are formed. Further experimental work is needed to further investigate these observations.

In addition to the degradation peak observed at around 3.70 min an increasing feature is observed at about 2.0 minutes in Figure 3.26. At the same time UV/Vis-absorption spectra recorded at Figure 3.27 for the photocatalyst show two similar spectra. Both features have an absorbance at about 500 nm in the ^{3}MLCT range and a minor feature at about 350 nm. For the **A-III** compound similar absorption features are observed at 483 nm this may indicate that if a supramolecular species is formed by decomposition it seems possible that two **"A-III"** type photocatalyst may be formed.

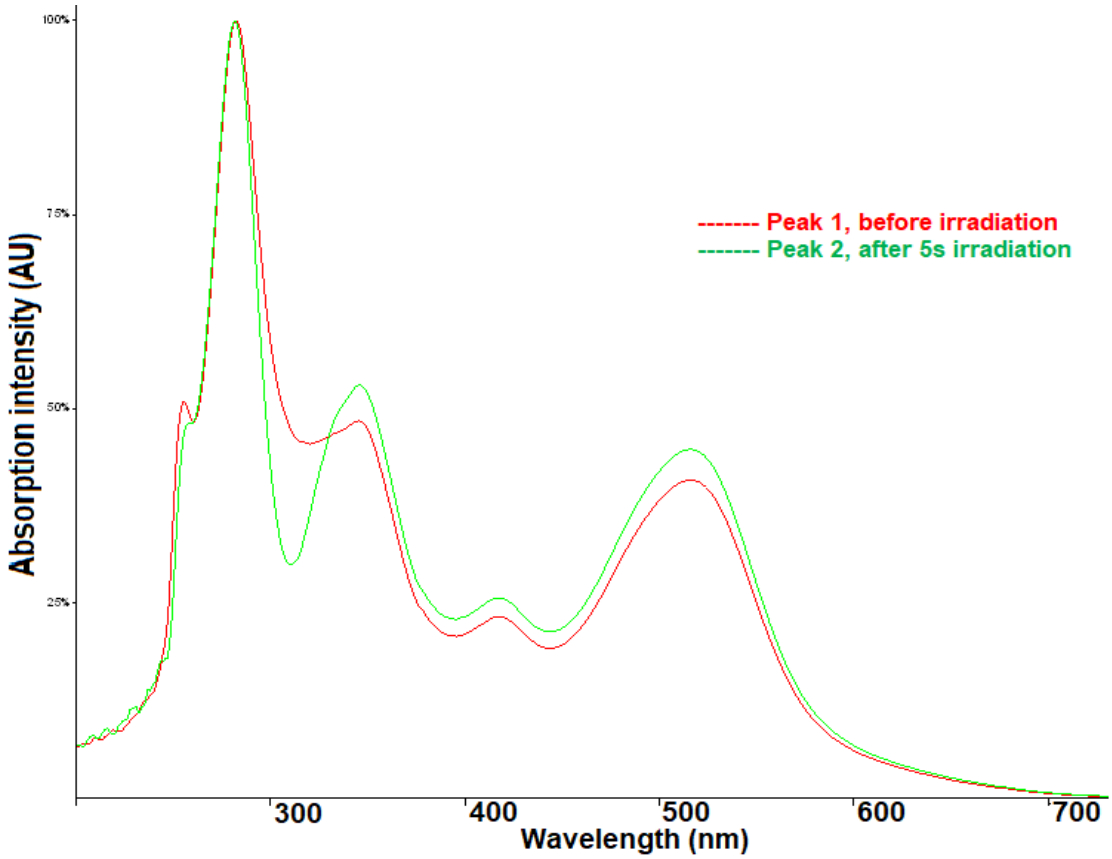

Figure 3.27: The absorption spectra obtained for the main peak of **A-III** (3.70 min) and the new peak (4.00 min) which appear beside the main peak within 5 seconds.

During the irradiation time the main peaks decrease and the new peak increases at retention time 2.0 minutes at outlined above. After 20 seconds the $[(bpy)_2Ru(2,3dpp)PtI_2]^{2+}$ peak and the peak beside it are decreased within 20 second of irradiation to (5.17mAU) and (5.67mAU) and the peak height of new peak is (27.4 mAU). The peak at 5.42 min of retention time did not increase or change during the irradiation time. Figure 3.28a gives a very nice illustration of the chromatograms of compound $[(bpy)_2Ru(2,3dpp)PtI_2]^{2+}$, **A-III**, during the irradiation time , while Figure 3.28b summarises the chromatogram of the compound before and after irradiation. Figure 3.29 shows the UV/Vis-spectra obtained after 20 sec of irradiation that are associated with a new peak (A)

observed at about 2.0 min, while a second peak is observed at about 4 min. The new spectra obtained at about 2 min are in the ^{3}MLCT range and the product obtained may be associated with loss of the 2,3dpp ligand and the generation of a $[(bpy)_2Ru(H_2O)_2]^{2+}$ or $[(bpy)_2Ru(H_2O)(CH_3CN)]^{2+}$ or $[(bpy)_2Ru(H_2O)I]^{2+}$ or $[(bpy)_2Ru(CH_3CN)I]^{2+}$ at λ_{max} 484 nm. Alternatively the formation of the photocatalysts discussed earlier may be considered.[12] The nature of the new peak is more difficult to determine. The presence of TEA and exposure to light willlead to a very fast decomposition of the compound the formation of a number of new compounds.

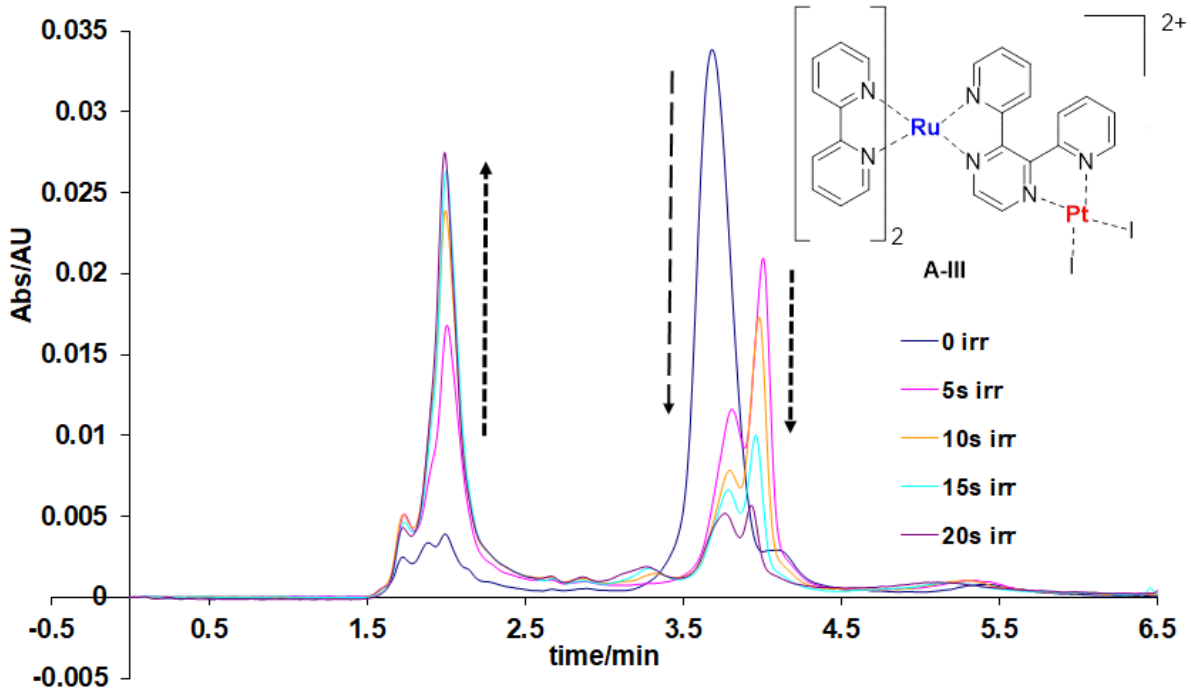

Figure 3.28a: HPLC traces obtained upon photolysis of $[(bpy)_2Ru(2,3dpp)PtI_2]^{2+}$. Temperature 24^o C. Irradiated in CH_3CN in presence of TEA (15%) and H_2O(10%) using 470 nm LED irradiation from (0-20s) degassing with Ar before irradiation detection wavelength; 470 nm, Mobile Phase CH_3CN:H_2O:CH_3OH with volume ratio 75:15:10 containing 0.12 M KNO_3 Flow rate 2.0 cm^3 min^{-1}

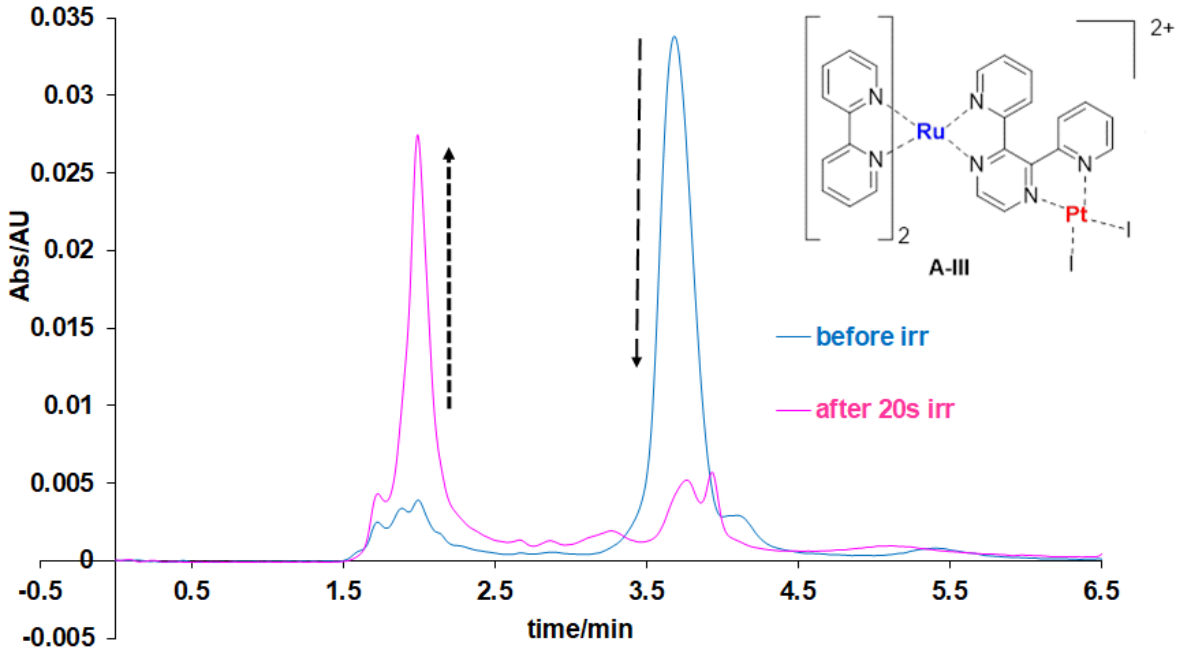

Figure 3.28b: HPLC traces obtained before and after 20s photolysis of $[(bpy)_2Ru(2,3dpp)PtI_2]^{2+}$. Temperature 24° C. Irradiated in CH_3CN in presence of TEA (15%) and H_2O(10%) using 470 nm LED, degassing with Ar before irradiation detection wavelength; 470 nm, Mobile Phase $CH_3CN:H_2O:CH_3OH$ with volume ratio 75:15:10 containing 0.12 M KNO_3 Flow rate 2.0 cm^3 min^{-1}

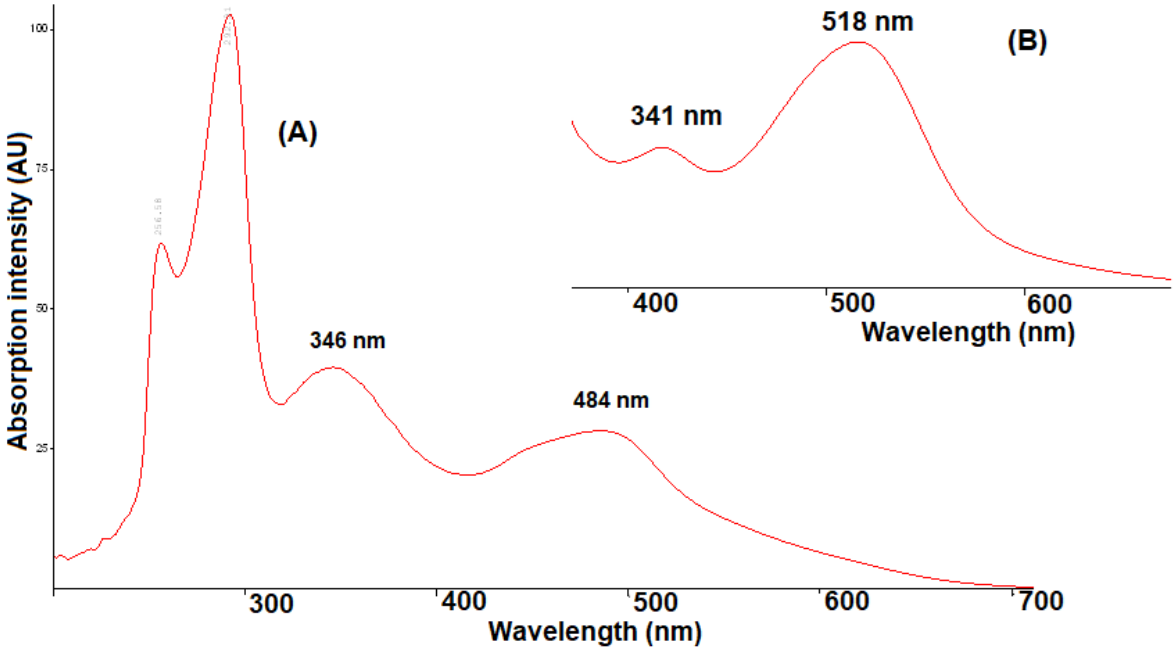

Figure 3. 29**:** Absorption spectra features of new species identified after 20 seconds of irradiation (A) and absorption spectra of the main peak (B) in Figure 3.28. Detection wavelength 470 nm.

3.4 Summary and conclusions

In this work, the characterisation and the stability of photocatalysts of $[(bpy)_2Ru(2,3dpp)]^{2+}$, $[(bpy)_2Ru(2,3dpp)PtCl_2]^{2+}$ and $[(bpy)_2Ru(2,3dpp)PtI_2]^{2+}$ were studied using HPLC, UV/vis absorption spectra and ^{1}H-NMR. The compounds were recorded to obtain information about the structural features and stability of the compounds. The HPLC results indicate, there is one dominant peak in all compounds, for compounds **A-II** and **A-III** the HPLC results of the dinuclear compounds showed changes in the retention time that might be due to the presence of the catalytic states and the nature of the halogen containing peripheral species.

The ruthenium monomers and the two dinuclear were studied using ^{1}H-NMR spectroscopy and it was observed that the ^{1}N-MR spectra of the dinuclear compounds show a significant change. Absorption spectra for the Ru(II) monomer and the dinuclear compounds have been obtained as well and all the compounds show clear absorption spectra. Changes in the properties of the compounds can be observed when the peripheral ligands at the Ru centre differ. The stability of the compounds has been investigated in acetonitrile. The chromatographic behaviour obtained indicates clearly that upon irradiation in both in acetonitrile and in acetonitrile containing Triethylamine further discussed in Chapter 6. The photochemical behaviour of the compounds has been investigated for up to 3 hours in acetonitrile. The results obtained indicate clearly that under this condition irradiation the monomer is photoreactive, the dinuclear $Ru/PtCl_2$ centre is photostable and the dinuclear Ru/PtI_2 centre is photoreactive but at a lower frequency than the monomer as shown in Figure (3,30).

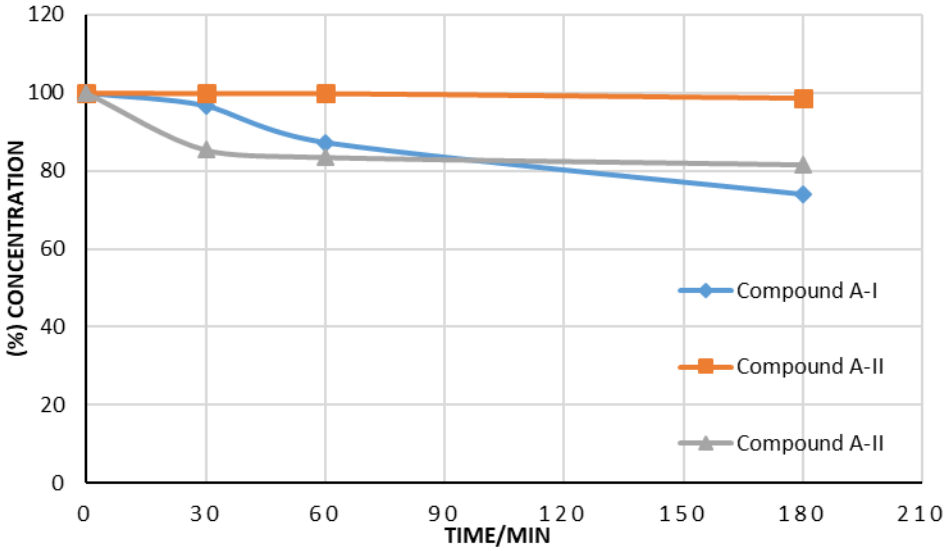

Figure 3.30: The rate of photo-degradation of compound **A-I**,**A-II** and **A-III** in the Absence of TEA.

The chromatograms described in this work show that the metal complexes are decomposing fast in the presence of TEA under irradiation. Importantly the $[(bpy)2Ru(2,3dpp)PtI_2]^{2+}$ species seem to be the faster these compounds under this condition. On the basis of the data obtained in this study, it could be said that TEA is a very reactive reagent that leads to the decomposition of Ruthenium complexes and acts as an electron donor in the presence light as shown in Figure (3,31).

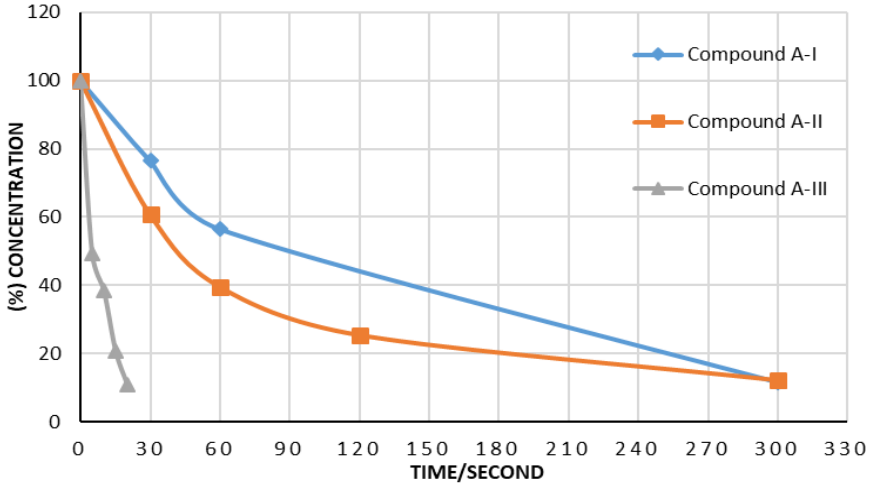

Figure 3.31: The rate of photo-degradation of compound **A-I**,**A-II** and **A-III** in the presence of TEA.

3.5 References

[1] M. Schulz, M. Karnahl, M. Schwalbe and J. G. Vos, The role of the bridging ligand in photocatalytic supramolecular assemblies for the reduction of protons and carbon dioxide. Coord. Chem. Rev (2012) 256, 1682– 1705.

[2] S. Rau, D. Walther, J.G. Vos, Inspired by nature: Light driven organometallic catalysis by heterooligonuclear Ru(II) complexes. Dalton Trans., (2007), 915-919

[3] G. S. Bindra, M. Schulz, A. Paul, S. Soman, R. Groarke, J. Inglis, M.T. Pryce, W. R. Browne, S. Rau, B. J. Maclean, J. G. Vos , The effect of peripheral bipyridine ligands on the photocatalytic hydrogen production activity of Ru/Pd catalysts, Dalton Trans, (2011), 40, 10812-10814

[4] M. Schulz, M. Karnahl, M. Schwalbe and J. G. Vos, The role of the bridging ligand in photocatalytic supramolecular assemblies for the reduction of protons and carbon dioxide. Coord. Chem. Rev (2012) 256, 1682– 1705.

[5] G. S. Bindra, M. Schulz, A. Paul, R. Groarke, S. Soman, J. L. Inglis, W., R. Browne, M. Pfeffer, S. Rau, B. J. MacLean, M. T. Pryce, J. G. Vos, The role of bridging ligand in hydrogen generation by photocatalytic Ru/Pd assemblies. Dalton Trans (2012) 41, 13050-13059

[6] D. Dini, Y. Halpin, J. G. Vos, E. A. Gibson, Coord. The influence of the preparation method of NiOx photocathodes on the efficiency of p-type dye sensitised solar cells. Chem. Rev. (2015), 304–305, 179–201. doi:10.1016/j.ccr.2015.03.020.

[7] T. Kowacs, Q. Pan, P. Lang, L. O'Reilly, S. Rau, W. R. Browne, M. T. Pryce, A. Huijser, J. G. Vos. Supramolecular Bimetallic Assemblies for Photocatalytic Hydrogen Generation from Water.Faraday Discuss. (2015),185, 143 - 170 DOI: 10.1039/C5FD00068

[8] Q. Pan, L. Freitag, T. Kowacs, J. C. Falgenhauer, J. P. Korterik, D.Schlettwein, W. R. Browne, M. T. Pryce, S. Rau, L. Gonzalez, J G. Vos, A. Huijser, Peripheral ligands as electron storage reservoirs and their role in enhancement of photocatalytic hydrogen generation. Chem. Commun. (2016), 52, 9371-9374. DOI: 10.1039/C6CC05222C

[9] T. Kowacs, Bachelor Thesis, Optimisation of Photocatalytic Hydrogen Generation by Variation of the Molecular Components in a Supramolecular Ru/Pt Assembly. University of Ulm, Institute of Inorganic Chemistry. 2012

[10] M. G. Pfeffer, T. Kowacs, M. Wächtler, J. Guthmuller,B. Dietzek, J. G. Vos and Sven Rau, Angew. A new avenue for the optimization of hydrogen evolving photochemical molecular devices. Chem. Int. Ed. Engl. (2015), 54, 6627-6631.

[11] P. S. Pregosin, Annual Reports on NMR Spectroscopy, Vol. 17 (Ed.:G.Webb), AcademicPress,London, 1986,p p. 285–349.

[12] T. Kowacs, L. O'Reilly, Q. Pan, A. Huijser, P. Lang, S. Rau, W. R. Browne, M. T. Pryce and J. G. Vos, Subtle Changes to Peripheral Ligands Enable High Turnover Numbers for Photocatalytic Hydrogen Generation with Supramolecular Photocatalysts, Inorg. Chem. (2016), 55, 2685−2690.

[13] R. Hage, H.E.B. Lempers, J.G. Haasnoot, J. Reedijk., F.M. Weldon and J.G. Vos. Homo- and Heteronuclear Ruthenium and Osmium Complexes Containing an Asymmetric Pyrazine Based Bridging Ligand. Inorg. Chem. (1997), 36, 3139-3145;

[14] B.E. Buchanan, H. Hughes, P. Degn, J.M. Pavon Velasco, B.S. Creaven, C. Long, J.G. Vos, R. A. Howie, R. Hage, J.H. van Diemen, J.G. Haasnoot, and J. Reedijk. J. Chem. Soc., Dalton Trans., 1992, 1177.

[15] B.P. Sullivan, T. J. Meyer, Comparisons of the physical and chemical properties of isomeric pairs. 2. Photochemical, thermal and electrochemical cis-trans isomerizations of M(Ph2PCH2PPh2)2Cl2 (M = RuII, OsII)

Inorg. Chem. 1982, 21, 1037,

[16] B. Durham, J.V. Caspar, J.K Nagle, T.J. Meyer, J. Am. Photochemistry of Ru(bpy)/sub 3//sup 2 +/Chem. Soc. 1982, 104,

[17] B. Durham, S. R. Wilson, D. J. Hodgson, T. J. Meyer, J. Am. Chem. Soc 1980, 103, 600;

Chapter 4

An investigation of the photostability of ruthenium photocatalysts, based on the 1,10-phenanthroline (phen) peripheral ligand and the 2,3-di(pyridyl-2-yl) pyrazine (2,3dpp) bridging ligand

In this section, the assessment and characterization of the second group of photocatalysts, which are composed of three complexes one mononuclear $[(phen)_2Ru(2,3dpp)]^{2+}$ (B-I) and two dinuclear $[(phen)_2Ru(2,3dpp)PtCl_2]^{2+}$ (B-II), and $[(phen)_2Ru(2,3dpp)PtI_2]^{2+}$ (B-III), will be discussed. Cation exchange HPLC columns will be employed to separate and quantify the compounds and the possible photodegradation products. ^{1}H-NMR will be used to try to identify the chemical changes in the structure of the molecules upon exposing it to light. Of the three compounds in this series compound B-I is photolabile B-II is photostable and B-III is partially photostable upon irradiation without the presence of TEA. In the presence of TEA a very fast conversion of the compounds is observed by HPLC and by UV/Vis spectroscopy and as a result changes in the coordination of the bridging ligands are observed.

4.1 Introduction.

In this chapter the peripheral ligands that are coordinated to Ru(II) are tricyclic 1,10-phenanthroline (phen) compounds. It is somewhat surprising that in the literature there are limited Ru(II) studies including phen ligands compared the bpy compounds reported.[1,2,3,4,5,6]. This is partly associated with the fact that both ligands have similar photochemical and structural properties. Some applications of the [Ru(phen)3]2+ species in the area of photochemistry group have recently been reported.[7,8] However, the photochemical behaviour of the different compounds can be different and compounds have been reported that are associated with 1,2,4-triazole bridging ligands. [9,10,11]. An example of the photochemical assembly of a dinuclear Ru(II) assembly based on the bridging ligand 3,5-bis(pyridin-2-yl)-1,2,4-triazole, Hbpt, in combination with both 2,2'-bipyridine and 1,10-phenanthroline containing complexes $[Ru(phen)_2(bpt)Rubpy)_2)]^{3+}$ and $[Ru(bpy)_2(bpt)Ru(phen)_2]^{3+}$ is shown in Figure 4.1 below.[10] Note that the nitrogen atoms of the triazole ring are not equivalent and are therefore numbered. The studies carried out indicate that the emitting 3MC state of the bpy/phen compound is bpy based. Furthermore, upon photolysis in acetonitrile only the metal centre bound to the N4 site of the triazole ring (See Figure 4.1) is labilised. However, both the N1 and the N4 position of the triazole are photolabile in the presence of Cl^- ions. These examples indicate that by variation in the nature of the metal centre and/or the peripheral or bridging ligands variations in the photochemical behaviour may be obtained, a number of extensive overviews that are of interest for these compounds are listed below. This observation is important for the further study of the photocatalysts under investigation. [11,12]

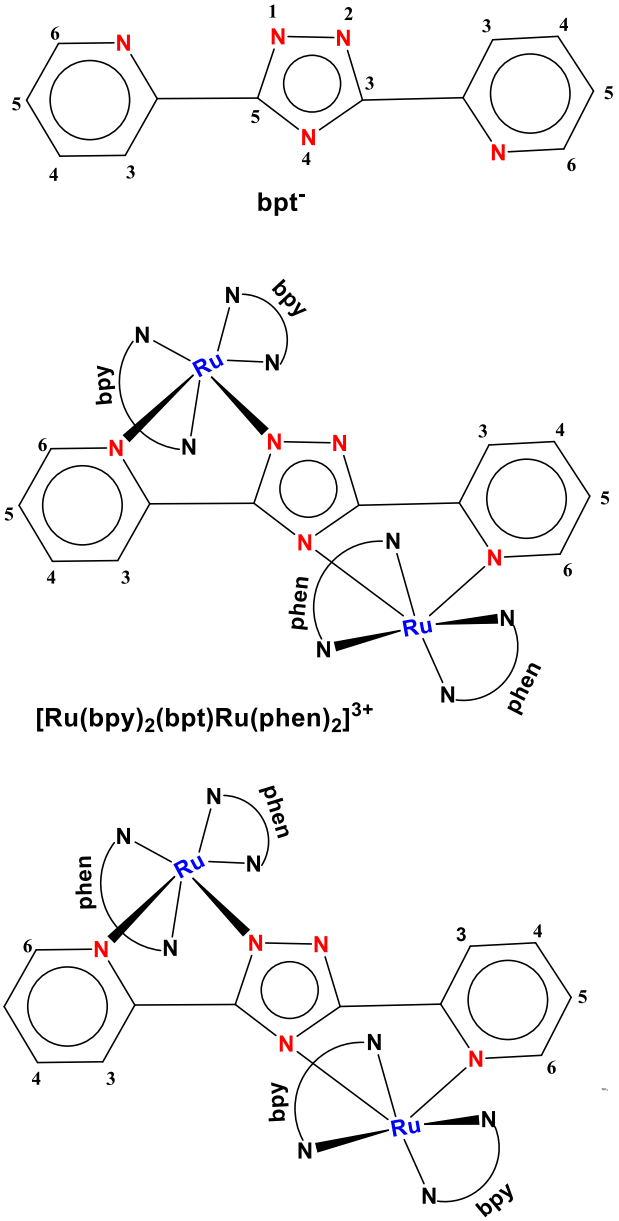

Figure 4. 1: Structure of the 3,5-bis-(pyridy-2-yl)-1,2,4,-triazole (Hbpt) ligand and phen compounds $[Ru(bpy)_2(bpt)Ru(phen)_2)]^{3+}$ and $[Ru(bpy)_2(bpt)Ru(phen)_2(bpt)]^{3+}$ [10].

In the present study, bidentate complexes based on the 1,10-phenanthroline (N^N) chelating ligand and the bridging ligand 2,3-bis(2'-pyridyl)pyrazine (2,3dpp) are displayed in Figures 4.2 and 4.3. The function of the bridging ligand is to connect the Ru(phen)2-photosensitiser to the platinum catalytic centre in order to produce dinuclear Ru/Pt complexes as shown in Figure 4.4.

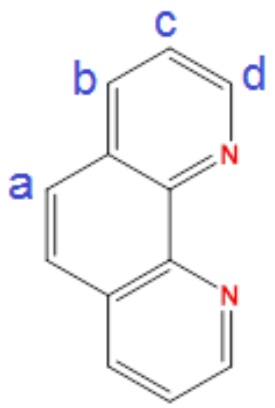

phen

Figure 4. 2: Structure of the peripheral ligand phen, which is used in this part.

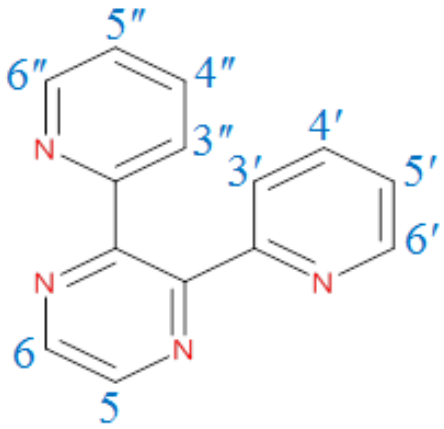

2,3dpp

Figure 4. 3: Structure of the bridging ligand 2,3dpp.

Three different compounds can be designed by different combinations of these ligands together with the Ru(II) and $PtCl_2$ and PtI_2 centres; one monomer and two binuclear organometallic complexes as illustrated in Figure 4.4. These compounds are designated as in Group B with phen as the peripheral, bidentate ligands and 2,3dpp as the bridging ligand. The structures of the monomer compound $[Ru(N\hat{}N)_2(2,3dpp)](PF_6)_2$ (N^N = phen) and the dinuclear Ru/Pt compounds,$[Ru(N\hat{}N)_2(2,3dpp)PtX_2](PF_6)_2$,where X = Cl^-, I^-), the behaviour of which will be discussed in this part, are displayed in Figure 4.4.

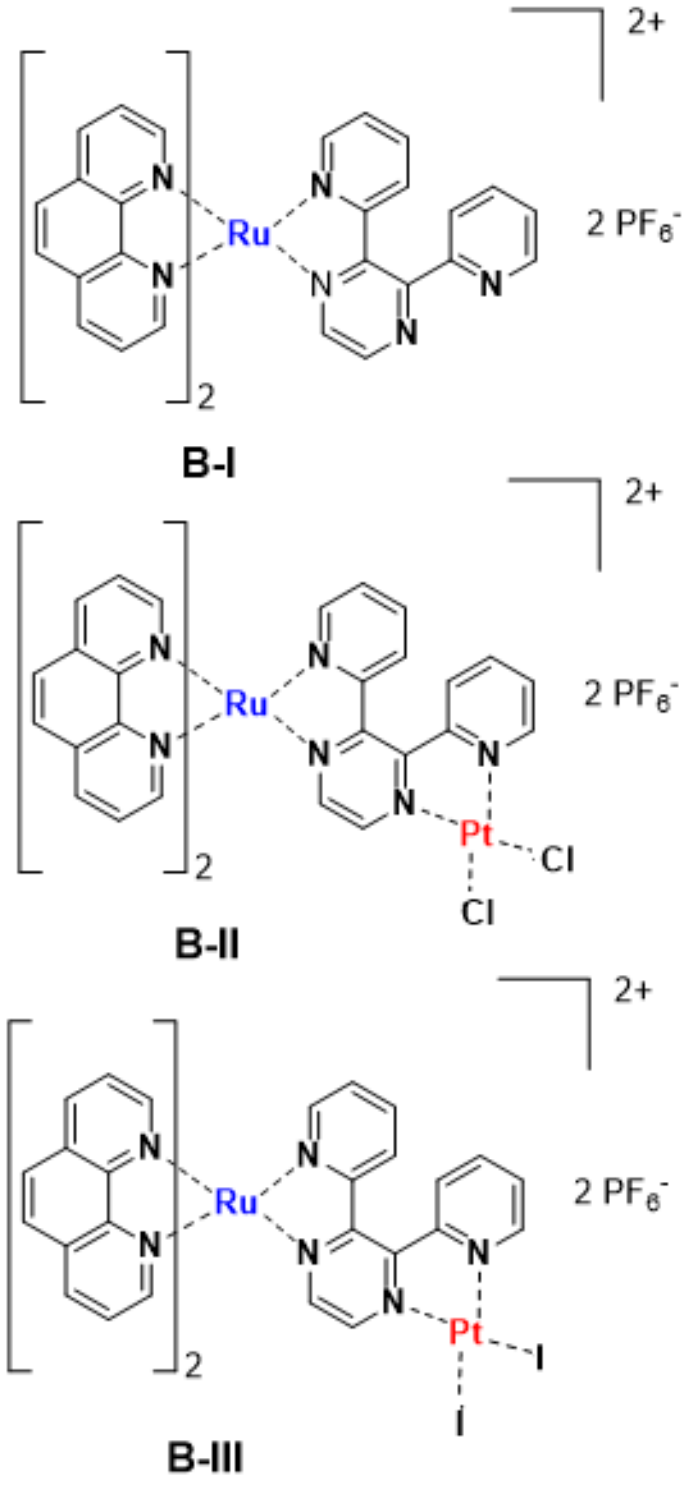

Figure 4. 4: Structures of the dinuclear Ru/Pt compounds and Ru(II) monomers with phen as a peripheral ligand and 2,3dpp as a bridging ligand.

4.2 Chromatographic, ^{1}H-NMR and UV-Vis spectra Behaviour of Compounds for group B.

4.2.1 Chromatographic characterisation

The chromatographic behaviour of the Group **B** compounds discussed in this section is similar to that observed for the compounds in Group A. In Group **A**, the peripheral ligand is composed of a bicyclic aromatic molecule, while the group B has tricyclic aromatic rings which suggests an increase of the aromaticity of the compound and consequently increasing the hydrophobicity.[9] Initially the retention time for those complexes was found to be higher. This increase in retention time was accompanied by peak tailing, poor peak separation and low resolution. In order to improve the retention times, the organic acetonitrile modifier in the mobile phase was increase to 80% from 75% to improve the elution and adjust the peak shape. Regardless the presence of $PtCl_2$ or PtI_2, the peak shape has not changed, as it does not affect the compound's hydrophobicity.

The chromatograms obtained for the mononuclear $[(phen)_2Ru(2,3dpp)]^{2+}$ (**B-I**) and the dinuclear compounds $[(phen)_2Ru(2,3dpp)PtCl_2]^{+2}$ (**B-II**), and $[(phen)_2Ru(2,3dpp)PtI_2]^{2+}$ (**B-III**) are shown in Figures 4.5 a,b,c.

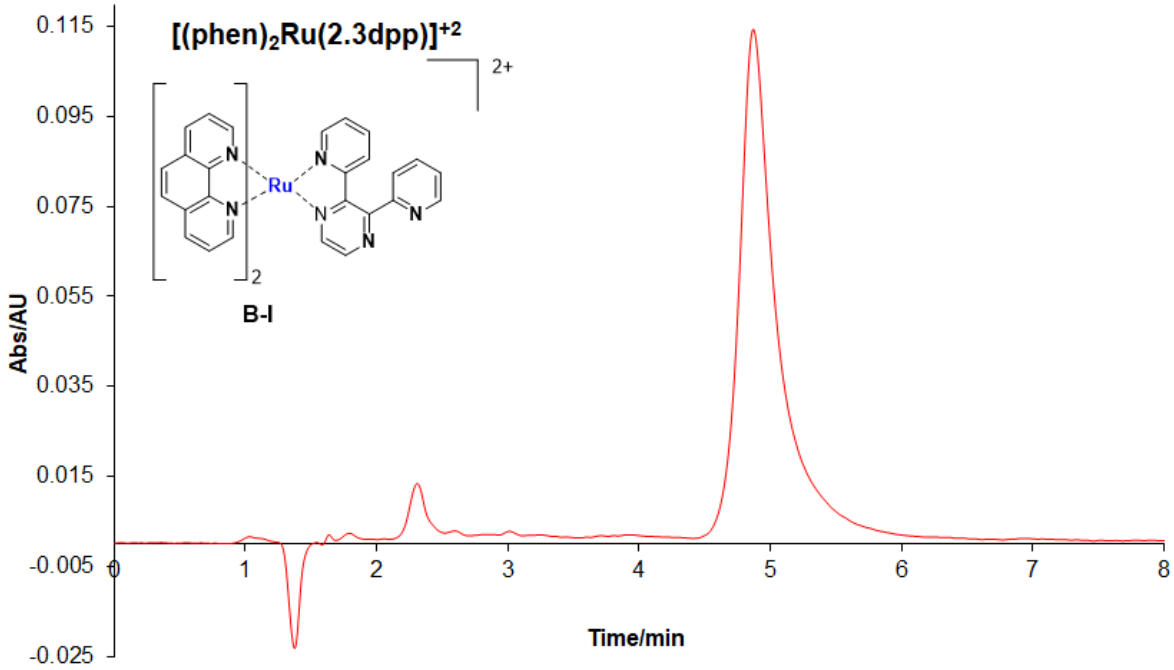

Figure 4. 5(a): HPLC trace for [(phen)2 Ru (2,3dpp)]$^{2+}$ in Mobile phase CH_3CN:H_2O:CH_3OH with volume ratio 80:15:5 containing 0.10M(KNO_3),Flow rate: 2.0 cm3 min-1, Detection wavelength at 280 nm, T=24 ^oC

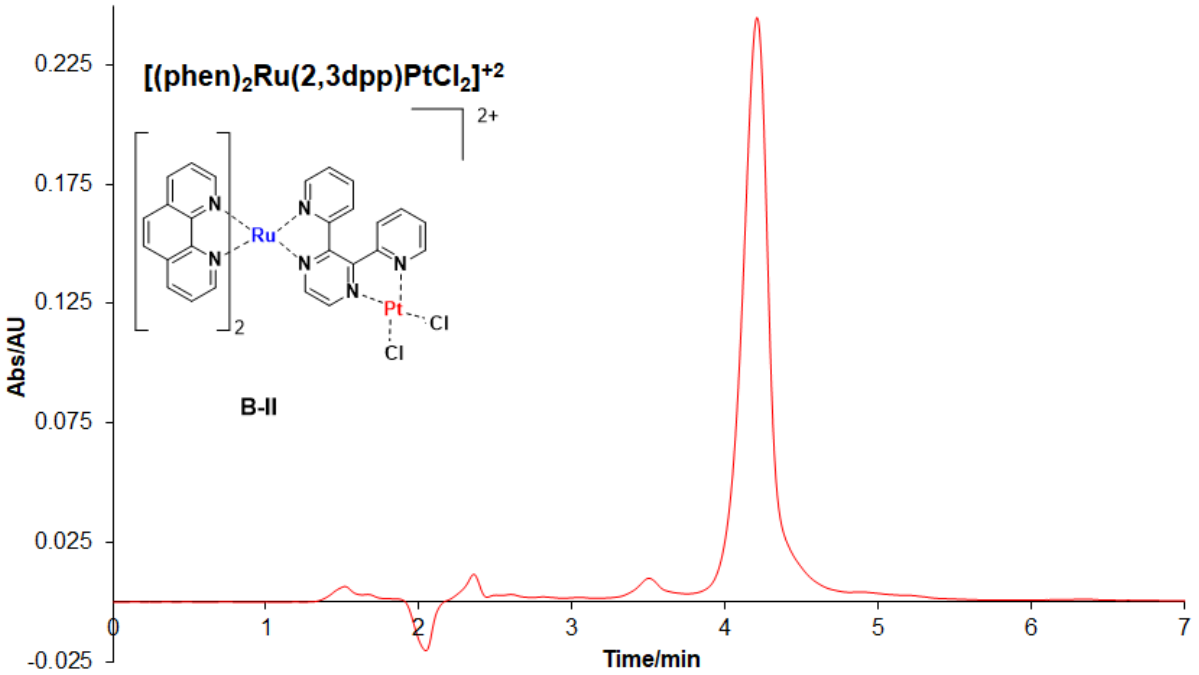

Figure 4- 5(b): HPLC trace for [(phen)$_2$ Ru (2,3dpp)$PtCl_2$]$^{2+}$ in Mobile phase CH_3CN:H_2O:CH_3OH with volume ratio 80:15:5 containing 0.10M(KNO_3),Flow rate: 2.0 cm^3 min^{-1}, Detection wavelength at 280 nm, T=24 ^oC

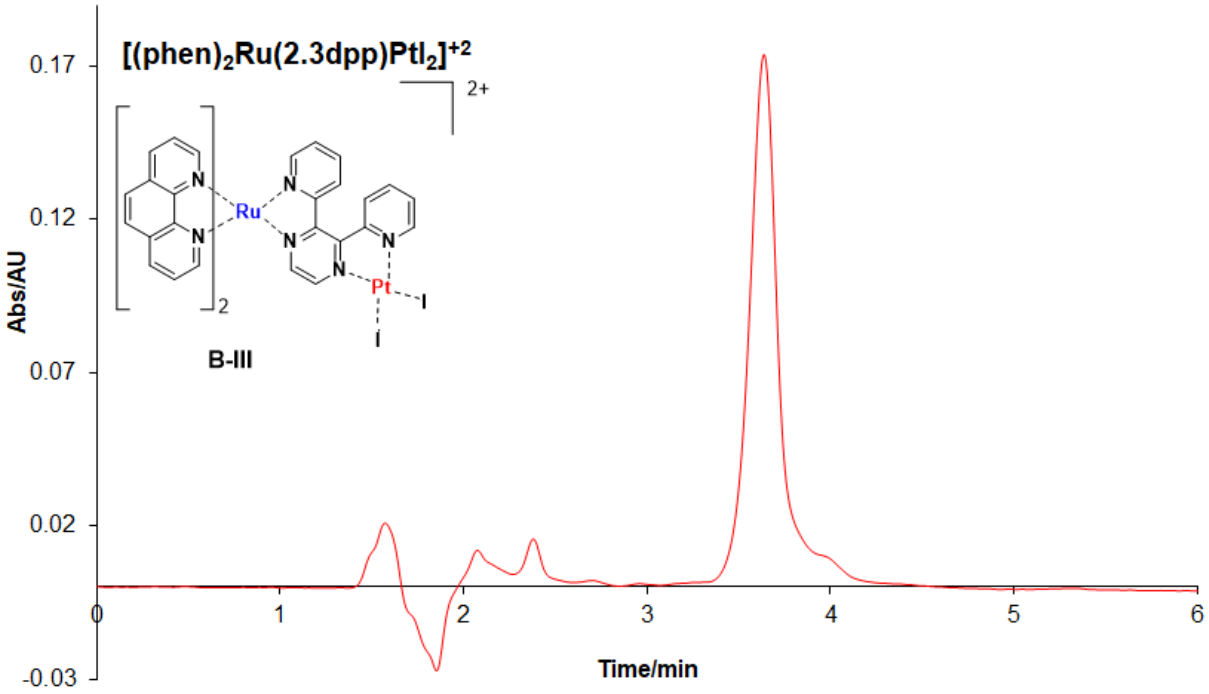

Figure 4-5(c): HPLC trace for [(phen)2 Ru (2,3dpp)PtI_2]$^{2+}$ in Mobile phase CH_3CN:H_2O:CH_3OH with volume ratio 80:15:5 containing 0.10M(KNO_3),Flow rate: 3.0 cm^3 min^{-1}, Detection wavelength at 280 nm, T=24 ^oC

A strong peak is observed for all compounds **B-I, B-II** and **B-III** at about 4.87, 4.20, 3.65 min respectively. The retention times observed are rather short for the mononuclear compound, especially when compared with that observed for the mononuclear compounds in group **A.** That there is a small variation of retention times observed between the three compounds partly depends on the nature of the halogen terminal species ($PtCl_2$, or PtI_2) and this is also noted in Table 4-1.

Table 4-1: Retention times and absorption maximum of B compounds (**I,II** and **III**) in acetonitrile with detection wavelength at 280 nm, T=24°C.

compound	Retention time (min)	UV/vis spectrum/ λ_{max} (nm)
$[(phen)_2Ru(2,3dpp)]^{+2}$	**4.87**	**435**
$[(phen)_2Ru(2,3dpp)PtCl_2]^{+2}$	**4.20**	**416, 510**
$[(phen)_2Ru(2,3dpp)PtI_2]^{+2}$	**3.65**	**413, 515**

This Table shows that there is no significant difference of the retention time of peaks obtained for the supramolecular compounds in this group compared with those in the group **A**. There is however a significant difference between the two mononuclear compounds **A-I** (Retention time = 10.26 min) and **B-I**, as shown in Table 4-1.

4.2.2 ^{1}H NMR characterisation

The monomer and the binuclear compounds were again dissolved in acetonitrile-d3 and all compounds were subjected to ^{1}H-NMR analysis. The compounds were treated under the same conditions as in group **A.** The results obtained are comparable with those obtained at group A as discussed above. (See Figure 4-6) The NMR data observed at high ppm values in the experiment with group B are in agreement with those shown in group **A**. Table 4.2 displays the chemical shifts of the two compounds H5 and H6' and for the monomer, 8.62 and 8.67 ppm (**A-I**).

The two signals for compound **B-II** and **B-III**, show chemical shifts of 9.10, 9.30 and 9.60, 9.70 ppm in Ru/PtCl2 and 9.70, 9.6 and 10.25 ppm in Ru/PtI2 respectively.

Table 4.2: Assignment of the signals of H5 and H6' with respect to chemical shifts (ppm) for the monomers and Ru/Pt dinuclear compounds in d_3-acetonitrile.

H5			H6'		
monomer	Ru/Pt-Cl2	Ru/Pt-I2	monomer	Ru/Pt-Cl2	Ru/Pt-I2
8.62	9.30, 9.10	9.85, 9.75	8.67	9.70 - 9.60	10.30, 10.25

These spectra are consistent with the hypothesis that the presence of platinum catalytic centres at the bridging ligand and the nature of the halogen terminal species in the dinuclear compounds will substantially affect the properties of the 2,2'-bipyridyl complexes of the A-group as discussed in chapter 3.[13]

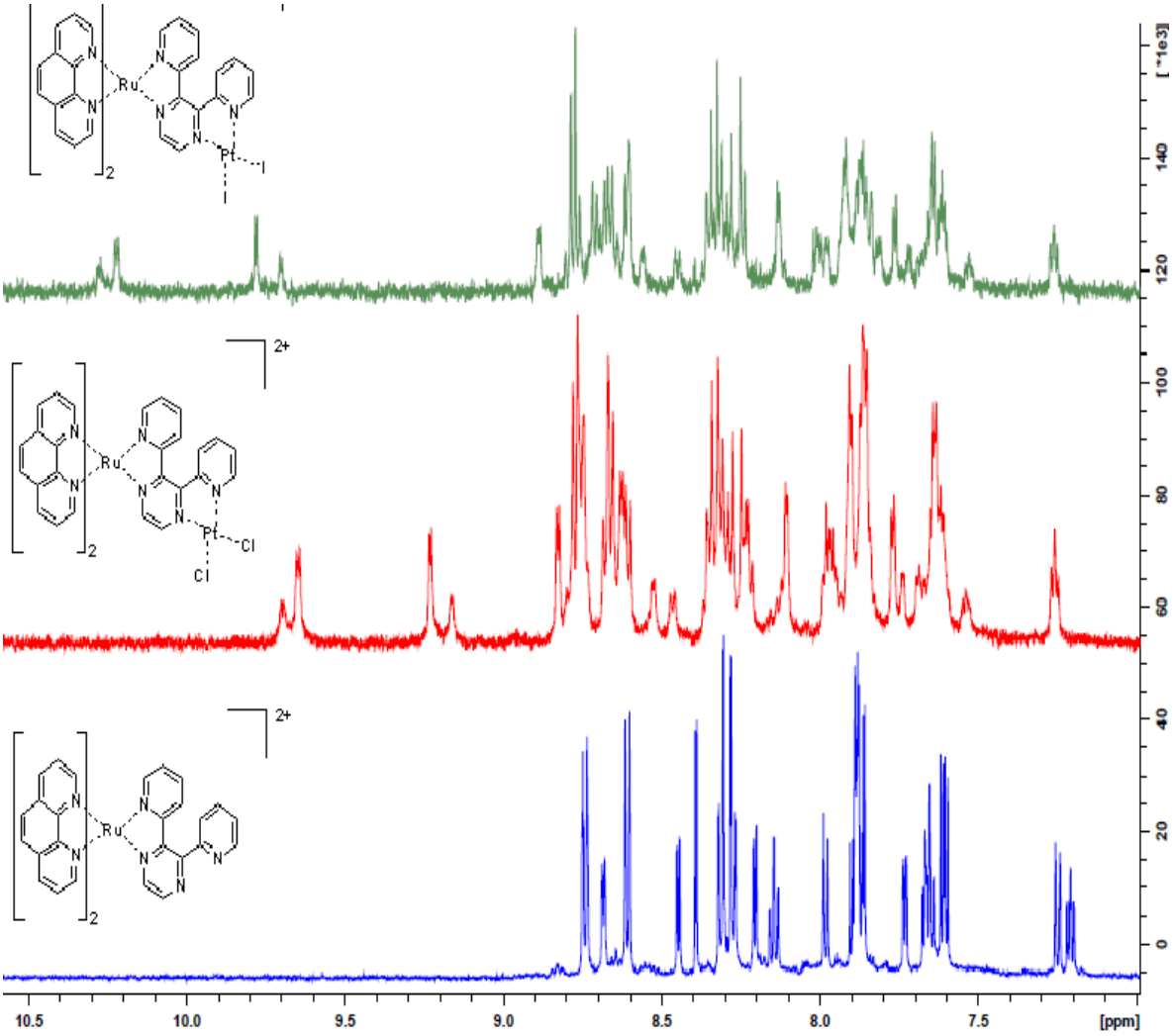

Figure 4.6: 1H-NMR of $[Ru(phen)_2(2,3dpp)]^{2+}$ B-I (bottom), $[Ru(phen)_2(2,3dpp)PtCl_2]^{2+}$ B-II (middle) and $[Ru(phen)_2(2,3dpp)PtI_2]^{2+}$ B-III (top) in d6-acetonitrile.

4.2.3 UV-Vis Absorption spectroscopy

UV/vis absorption spectra have been studied for the B-I monomer and the dinuclear compounds B-II and B-III. The spectra were measured using acetonitrile as a solvent. The UV-Vis spectra of the three compounds are shown in Figure 4.7. The UV-Vis spectrum of $[Ru(phen)_2(2,3dpp)]^{2+}$, compound, B-I, shows a broad peak with an irregular plateau region between 340 and 470 nm (λmax = 465 nm). This observation is in agreement with other similar phen containing

compounds. [5,10] The spectrum shows a considerable change upon introduction of the Pt sections of the compounds as shown. It is clear that the absorption of the other two other molecules $[Ru(phen)_2(2,3dpp)PtCl_2]^{2+}$ **B-II** and $[Ru(phen)_2(2,3dpp)PtI_2]^{2+}$ **B-III** are similar. Both compounds show 2 separate absorptions in the visible region, the first one is observed at λmax= 340 nm a second feature at λmax= 515 nm. These features can be identified as ruthenium based ^{1}MLCT transitions.[5,14] However, for **B-I**, there is only a broad ^{1}MLCT absorption at 415 nm as was also observed for **A-I**. This indicates that the photophysical and photochemical properties of these two compounds are considerable different when compared with the mononuclear compound **B-I**.

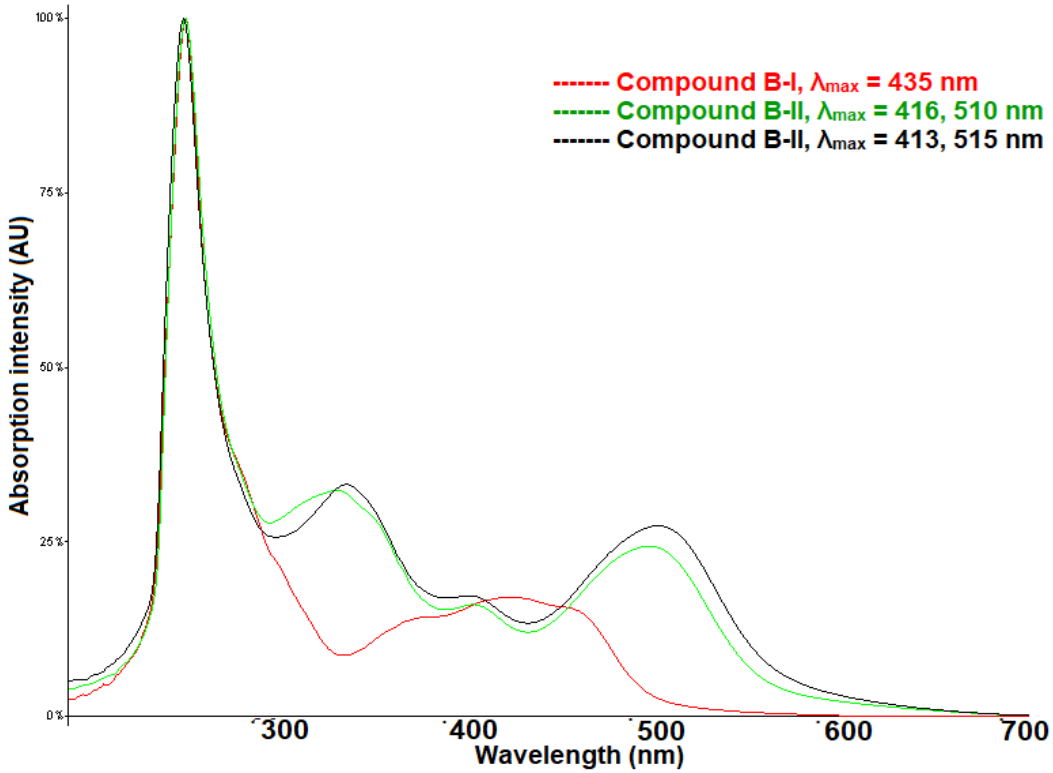

Figure 4.7: Absorption spectra (normalised) of $[(phen)_2Ru(2,3dpp)]^{2+,}$ $[(phen)_2$ Ru (2,3dpp)$PtCl_2]^{2+}$ and [(phen)2 Ru (2,3dpp)$PtI_2]^{2+}$ in CH_3CN shown in Figure (4.3 a, b, c).

4.3 Photolysis of Compounds in Acetonitrile without TEA.

The purpose of this section is to discuss the photochemical behaviour of the same complexes characterised previously in this chapter (compounds **B-I, B-II** and **B-III**). Upon irradiation with LED 470 nm visible light acetonitrile is used as a solvent, both in the presence and absence of triethylamine (TEA) as a sacrificial reducing agent. The aim of this approach is to investigate the stability of these compounds in light. First the compounds are irradiated for up to 3 hours in acetonitrile in the absence of TEA. Subsequently, in the presence of TEA, the decomposition of the compounds was was carried out as shown in Section 4.3.2. To minimise the influence of temperature on the chromatographic separation all experiments were carried out at an isothermal chromatographic system maintained at 24 ^{o}C. The photochemical processes were followed by characterisation with HPLC, UV-Vis spectroscopy and ^{1}H-NMR spectroscopy as discussed below. In these experiments it has be considered that acetonitrile can undergo light-induced ligand exchange reactions. [7,15], As observed for the previous group of compounds, Group **A**, when irradiating of the compounds of group B for up to 3 hours, it was found that compound **B-I** is photo reactive while compound **B-II** is photostable and the third compound **B-III** is slightly photoreactive under these conditions.

4.3.1 Photolysis of Compounds in Acetonitrile, Compound B-I

All compounds were photolysed in acetonitrile, after irradiating the compounds for up to 3 hours, it was found that compound **B-I** is photo-reactive, compound **B-II** is photo stable and the compound **B-III** is slightly photo-reactive under these conditions. The photolysis of the mononuclear compound **B-I** is characterised by

using different analytical techniques HPLC, UV-Vis spectroscopy and ^{1}HNMR spectroscopy and outlined in Figure 4.8 (a, b).

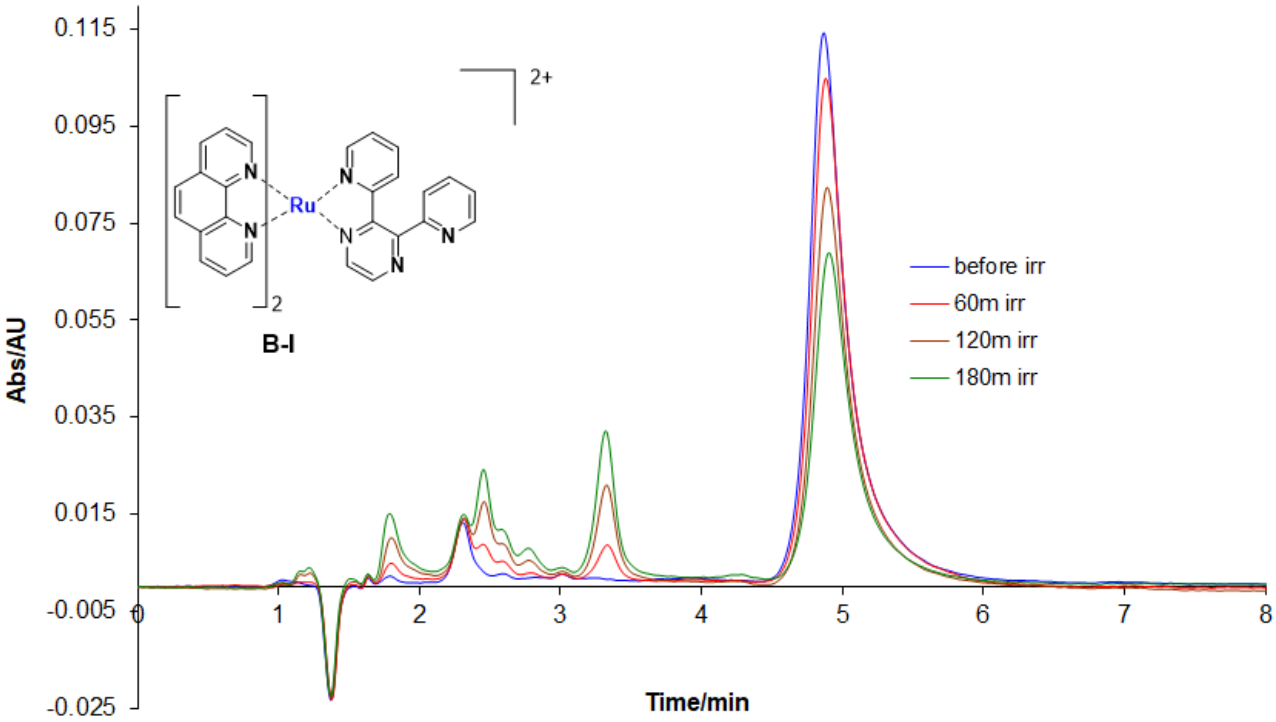

Figure 4.8(a): HPLC trace during photolysis for $[(phen)_2Ru(2,3dpp)]^{2+}$ B-I in CH_3CN. Mobile phase, $CH_3CN:H_2O:CH_3OH$ with volume ratio 80:15:5 containing 0.10M KNO_3),Flow rate: 2.0 cm^3 min^{-1}, Detection wavelength at 280 nm, T=24 ^{o}C.

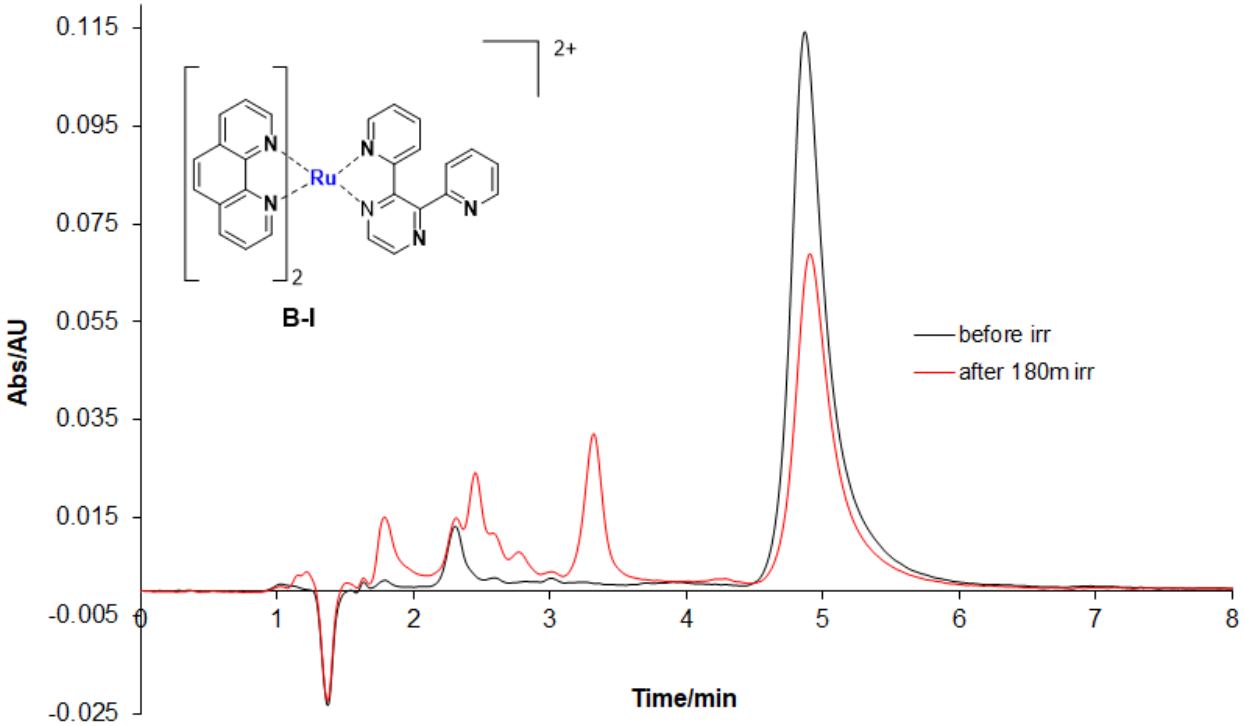

Figure 4.8(b): HPLC trace before and after photolysis for $[(phen)_2\ Ru\ (2,3dpp)]^{2+}$ in CH_3CN. Mobile phase; $CH_3CN:H_2O:CH_3OH$ with volume ratio 80:15:5 containing 0.10M(KNO_3),Flow rate: 2.0 $cm^3\ min^{-1}$, Detection wavelength at 280 nm, T=24 ^oC.

The HPLC traces during photolysis show that in figure 4.8a-b there is decreasing of the main peak and three different peaks appear and increase in peak area with the increase of irradiation duration appearing at retention times 1.48, 2.27 and 3.20 minutes. Since there is a significant amount of compound B-I remaining with a retention time of about 5 min. possible to identify the nature of this species. As shown in Figure 4.7 the spectrum of B-I is centred at about 420-430nm. The UV-Vis absorption spectrum of the products are shown in Figure 4.9, The first species with a 1.28 min retention time has a λmax at 469 nm (red line), the second product at 2.16 min retention time has a λmax at 437 nm (green line) and the third

product at 3.12 min retention time has a λmax at 384 and 420 nm (black line) and these are in agreement with the exchange of the compounds such as $[(Ru(phen)_2(CH_3CN)_2]^{2+}$, and $[(Ru(phen)_2(CH_3CN)(H_2O]^{2+}$ with the solvent, [11] The absorption spectra of all the new peaks present after three hours of irradiation are shown in Figure 4.9 below.

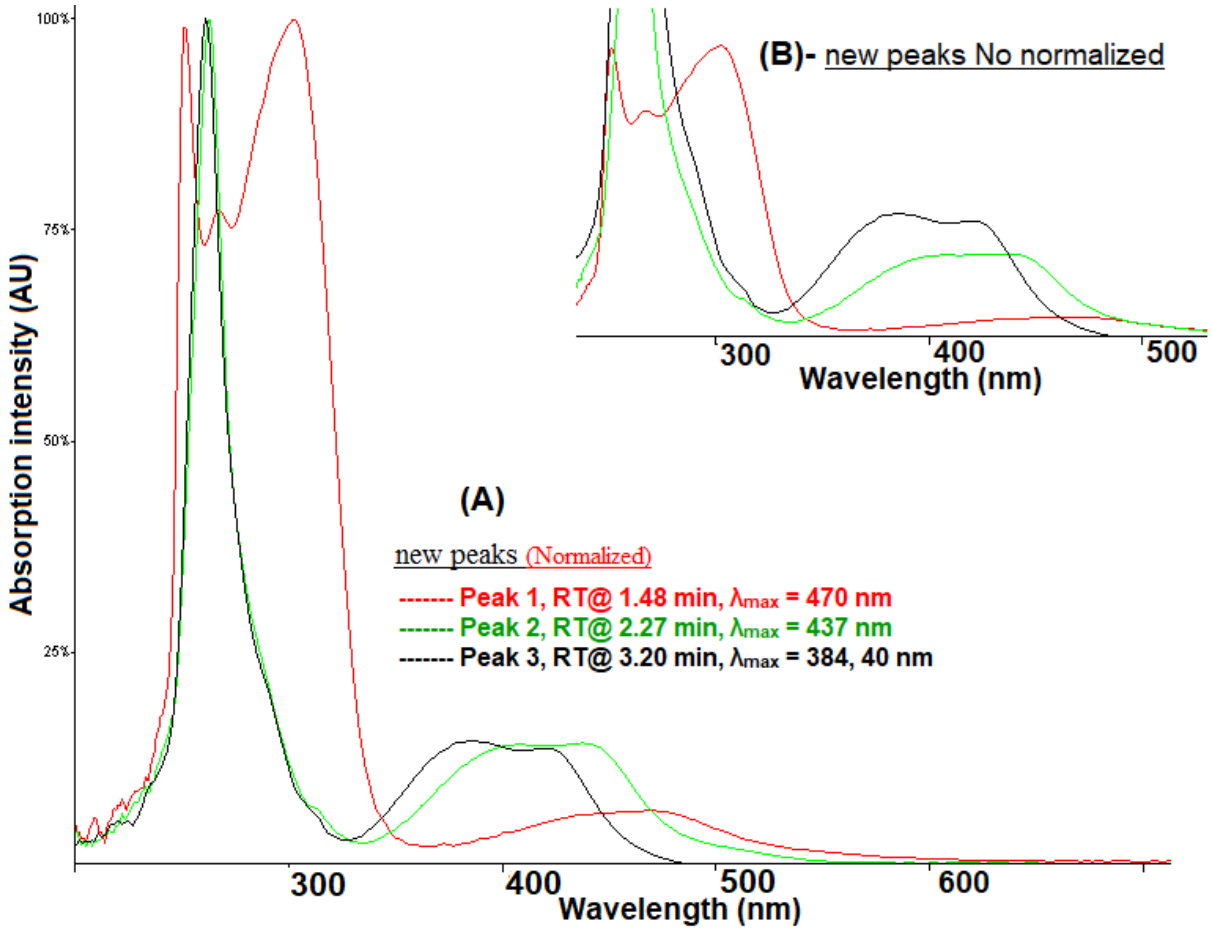

Figure 4.9: Absorption spectra features of new species identified in compound B-I after irradiation (normalized) (A) and (No normalized) (B) in Figure 4.8. Detection wavelength 280 nm.

The photolysis of B-I with increasing irradiation durations is also characterised by ^{1}H-NMR spectroscopy to obtain further information and monitor the appearance

and disappearance of peaks. The photolysis reaction of $[Ru(phen)_2(2,3dpp)]^{2+}$ suggests the loss of the bridging ligand as shown in Figures 4.10a.

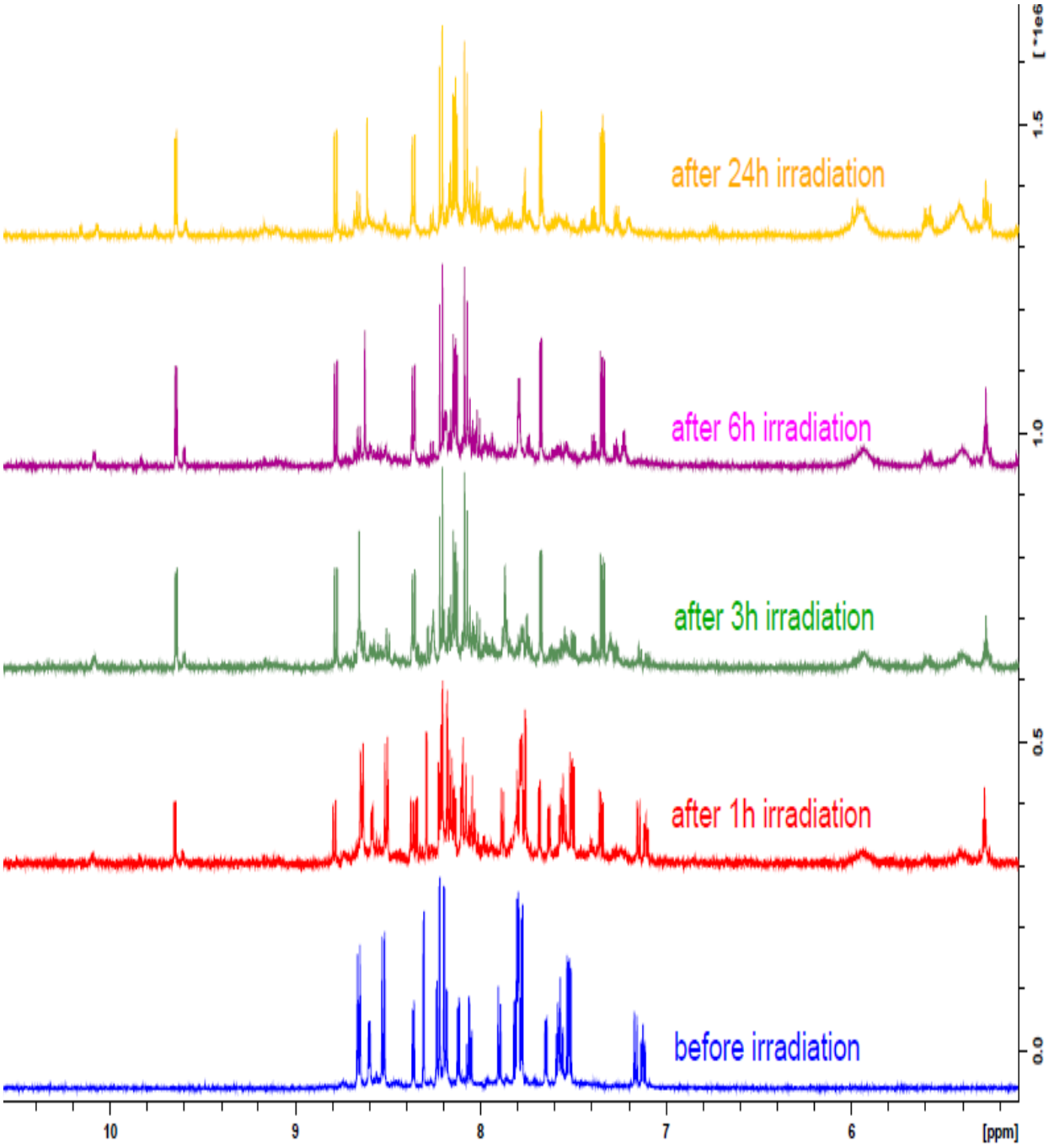

Figure 4.10a: ^{1}H-NMR spectroscopy of compound B-I during Photolysis in acetonitrile-d_3.

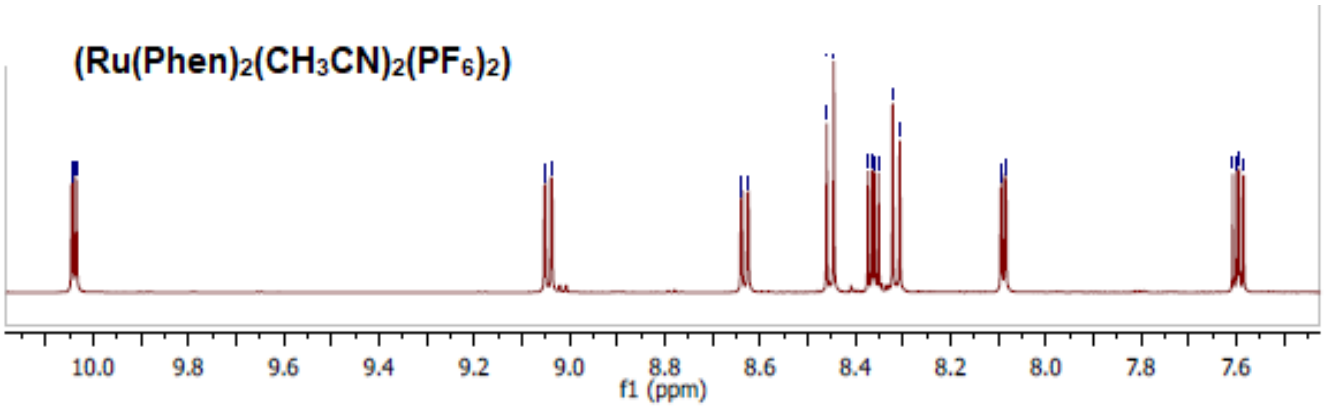

Figure 4-10b: ^{1}H-NMR spectroscopy of control sample [Ru(phen)$_2$(CH$_3$CN)$_2$(PF6)$_2$] in d$_3$-acetone.

^{1}H-NMR (600 MHz, Acetone) δ 10.04 (dd, J = 5.1, 1.2 Hz, 1H), 9.04 (dd, J = 8.3, 1.3 Hz, 1H), 8.63 (dd, J = 8.2, 1.1 Hz, 1H), 8.45 (d,J = 8.8 Hz, 1H), 8.36 (dd, J = 8.3, 5.1 Hz, 1H), 8.31 (d, J = 8.9 Hz, 1H), 8.09 (dd, J = 5.3, 1.2 Hz, 1H), 7.60 (dd, J = 8.1, 5.3 Hz, 1H), 2.44 (s, 3H).

To investigate this observation a sample was obtained as shown in Figure 4-10b. The spectrum obtained from **B-I** Figure 4-10a indicates that after 24 hours of radiation, degraded products were found in the region expected from a complex with the general formula; [Ru(phen)$_2$(CH$_3$CN)2(PF$_6$)$_2$]. In the HPLC experiment, two new peaks of a compound which has a retention time between 2.8 min and 3.25 min are observed. This feature observed in Figure 4.8 suggests, that in agreement with the ^{1}H-NMR spectrum shown in Figure 4-10a, that indicates that this process is therefore most likely related by the irradiation of **B-I**;

$$\mathbf{[Ru(phen)_2(2,3dpp)]^{2+}} \xrightarrow{h\nu} \mathbf{[Ru(phen)_2(CH_3CN)_2]^{2+} + 2,3dpp}$$

This reaction can be confirmed with ^{1}H-NMR spectra obtained after 24 hours of photolysis are typical for the bis-acetonitrile compound $[Ru(phen)_2(CH_3CN)_2]^{2+}$ and these features are very similar to those observed in the NMR spectrum of control sample $[(Ru(phen)_2(CH_3CN)_2(PF_6)]_2$ in Figures 4-10a and 4-10b above.

The ^{1}H-NMR results show in Figure (4.10b), large changes in the peaks with chemical shifts between 9.8 and 10.2 ppm. A number of signals are disappearing at 8.8 ppm, 8.42 ppm and 7.4 ppm. Other signals are decreasing at 8.7 ppm, 7.85 ppm and 7.6 ppm in increasing the irradiation duration. When these results of compound **B-I** are compared with compound **A-I**, it appears that this compound is less stable than **A-I** upon irradiation. Phenanthroline compounds are less studied and therefore it is more challenging to establish the nature of the photoproduct. However, it seems likely that the end product obtained from the irradiation of **B-I** is a $[Ru(phen)_2(CH_3CN)_2]^{2+}$ type compound as is observed for **A-I**. In general, ^{1}H-NMR results indicate that **B-I** is more photoactive than **A-I** (see Chapter 3 and Chapter 6) as the changes observed are more extensive and are observed earlier in the experiment as shown in the Figure above. Importantly it needs to be considered that most of compound **B-II** is not degraded and that most is still present.

4.3.2 Photolysis of Compounds in Acetonitrile, Compound B-II

The photoreactivity of compound **B-II** was investigated using HPLC, UV-Vis spectroscopy and ^{1}H-NMR spectroscopy. Irradiation of the compound was carried out following the same conditions described previously for **B-I**. The compound

was irradiated for up to 3 h. The HPLC results obtained after photolysis of this compound are shown in Figures 4.11.

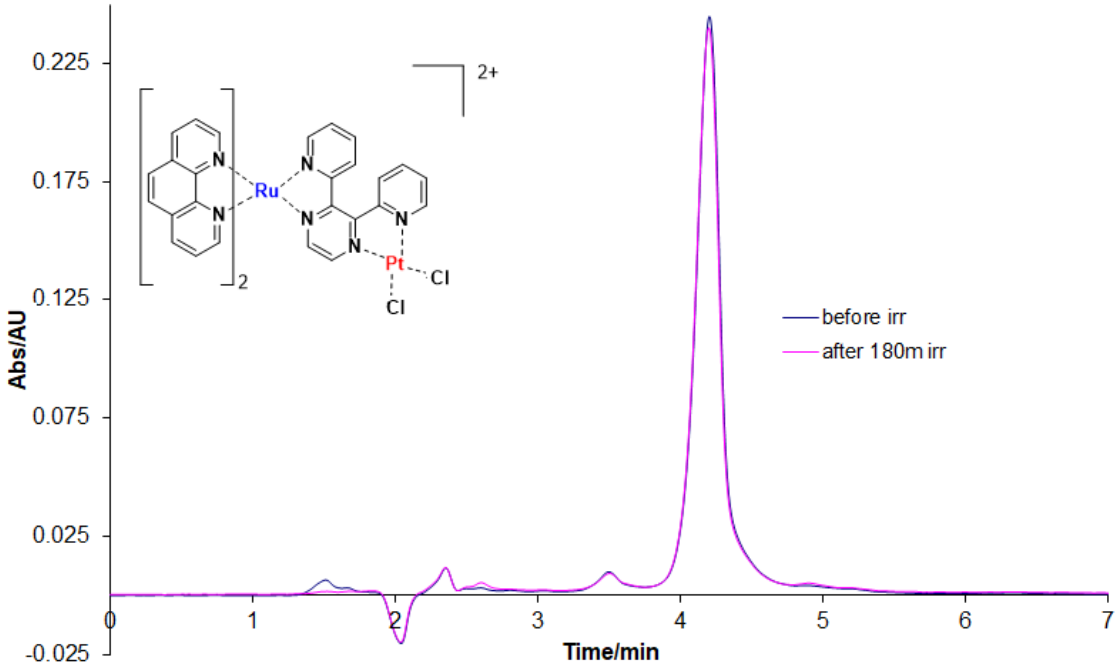

Figure 4.11: HPLC trace during Photolysis of $[(phen)_2$ Ru (2,3dpp)$PtCl_2]^{2+}$, B-II, in Mobile phase CH_3CN:H_2O:CH_3OH with volume ratio 80:15:5 containing 0.10M KNO_3,Flow rate: 2.0 cm^3 min^{-1}, Detection wavelength at 280 nm, T=24 ^oC.

The HPLC chromatograms during photolysis show that under the conditions used in these experiments the compound **B-II** is photostable upon irradiation for up to a 3 hours period and its behaviour shows the same HPLC results and the same stability as that observed for compound **A-II** in Chapter 3.

The ^{1}H-NMR spectroscopic results shown in Figure 4.12 indicate that under the conditions used in these experiments the compound is photostable for up to 24 hours. The compound was irradiated in ^{1}H-NMR solvent (d_3-CH_3CN) had higher

concentrations (Almost three times the user in the HPLC). Increased concentrations give rise to longer irradiation times of the compounds.

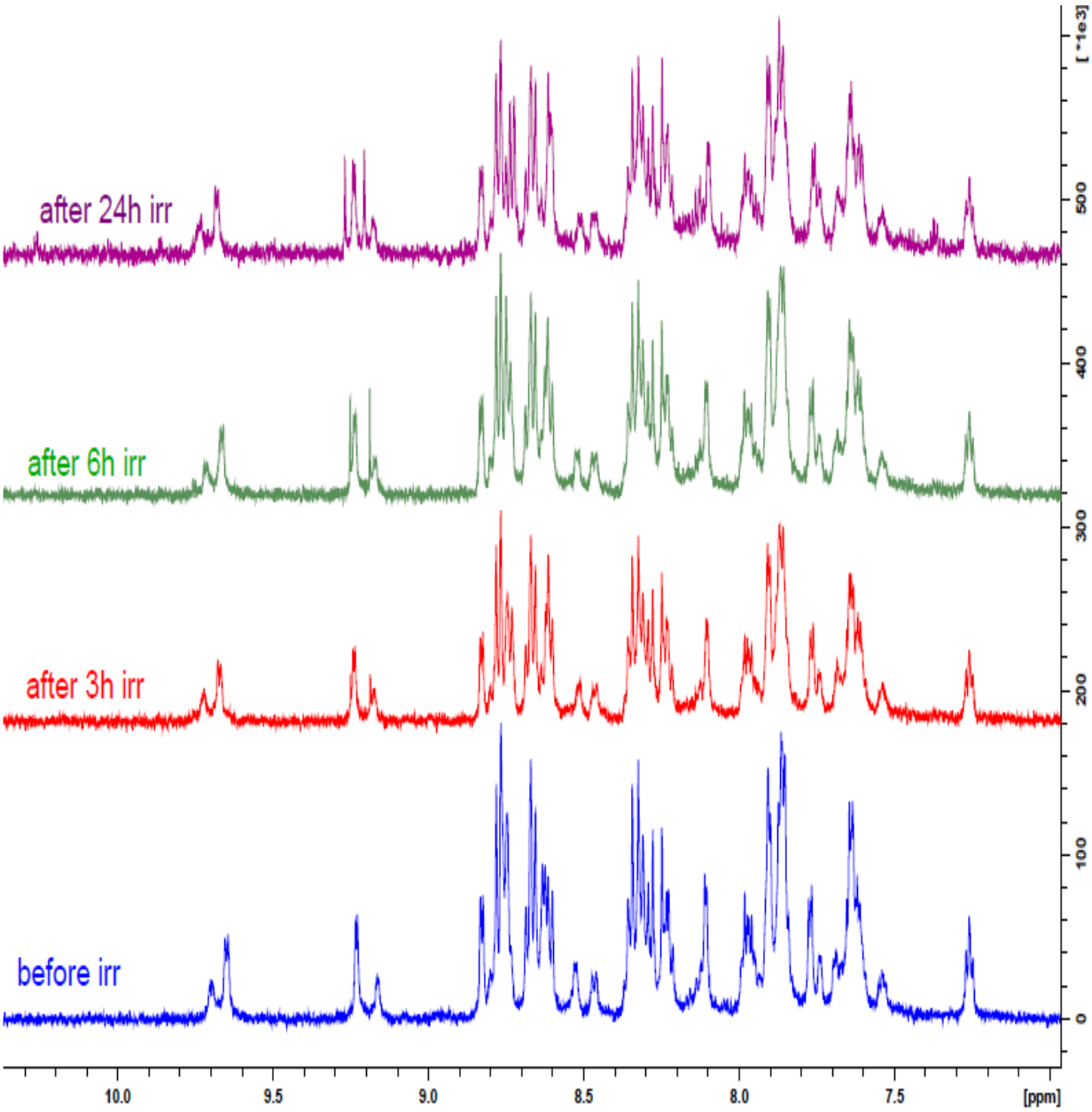

Figure 4.12: ^{1}H-NMR of the photolysis of [Ru(phen)2(2,3dpp)PtCl2]2+ in d_3-acetonitrile.

The ^{1}H-NMR results are also in agreement with the HPLC results. Clearly, the results show that compound **B-II** is HPLC stable under the conditions used in these experiments.

4.3.3 Photolysis of Compounds in acetone without TEA, Compound B-III

The next compound **B-III** was photolysed for duration of up to 3 hours in acetonitrile. The photochemical behaviour processes were followed by HPLC, UV/Vis spectroscopy and ^{1}H-NMR spectroscopic, the results obtained are shown in Figures 4.13 a,b, Figure 4.14

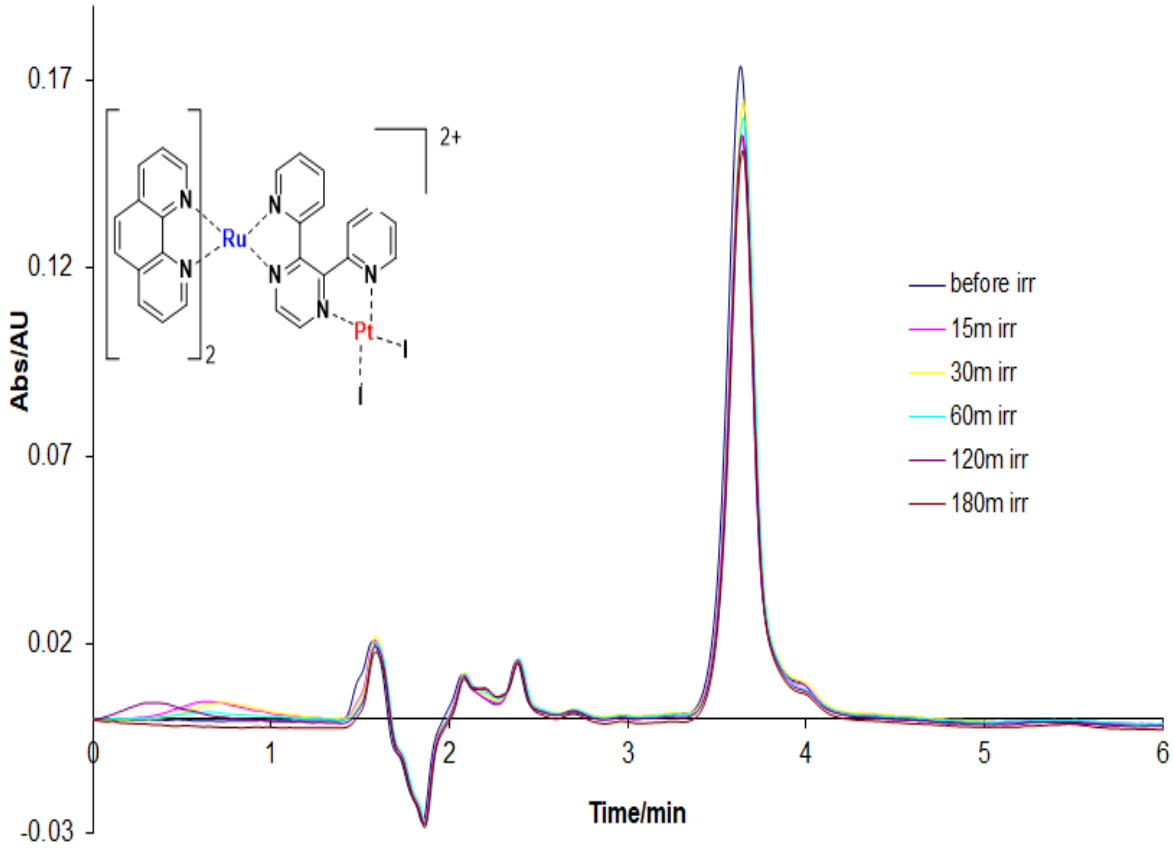

Figure 4.13(a): HPLC trace during Photolysis for $[(phen)_2$ Ru (2,3dpp)$PtI_2]^{2+}$ (B-III) in Mobile phase $CH_3CN:H_2O:CH_3OH$ with volume ratio 80:15:5 containing 0.10M KNO_3 Flow rate: 2.0 cm^3 min^{-1}, Detection wavelength at 280 nm, T=24 ^{o}C.

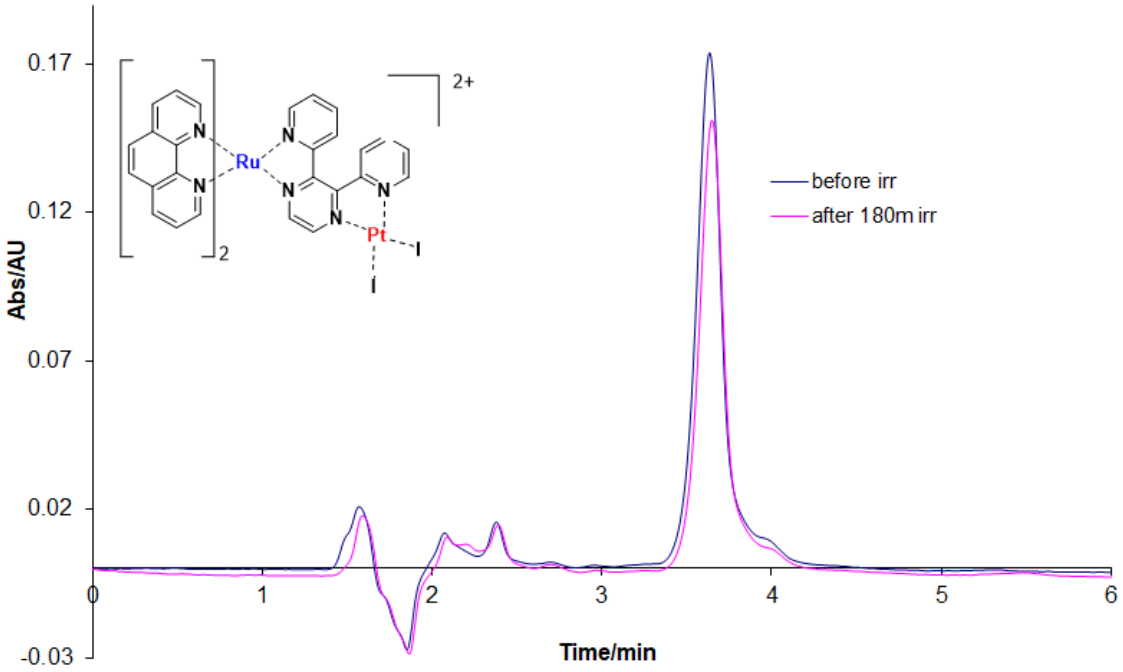

Figure 4.13 (b): HPLC trace before and after photolysis of $[(phen)_2$ Ru (2,3dpp)$PtI_2]^{2+}$ (B-III) in Mobile phase $CH_3CN:H_2O:CH_3OH$ with volume ratio 80:15:5 containing 0.10M(KNO_3),Flow rate: 2.0 cm^3 min^{-1}, Detection wavelength at 280 nm, T=24 ^oC.

The photolysis of compound **B-III** was carried out under the same conditions as that for compound group **A**. A small peak at retention time between 0.4 and 0.8 min appeared during the irradiation of the compound. It is noticeable that the small peak disappeared after about 1.48 min whilst the main peak was decreasing in increased duration.

The photolysis of the compound **B-III** is also monitored by ^{1}H-NMR spectroscopy to obtain more information about the changes and the results obtained are shown in Figure 4.14. The ^{1}H-NMR results show a number of peaks from about 7.4 to 8.8 ppm and 7.2 ppm as shown in the figure, that are decreasing with increasing radiation time. Also, new species that can be observed between 6.8 and 7.4 ppm.

There is also a fluctuation in signals from 9.6 ppm to 10.4 ppm which may suggest the formation of an intermediate.

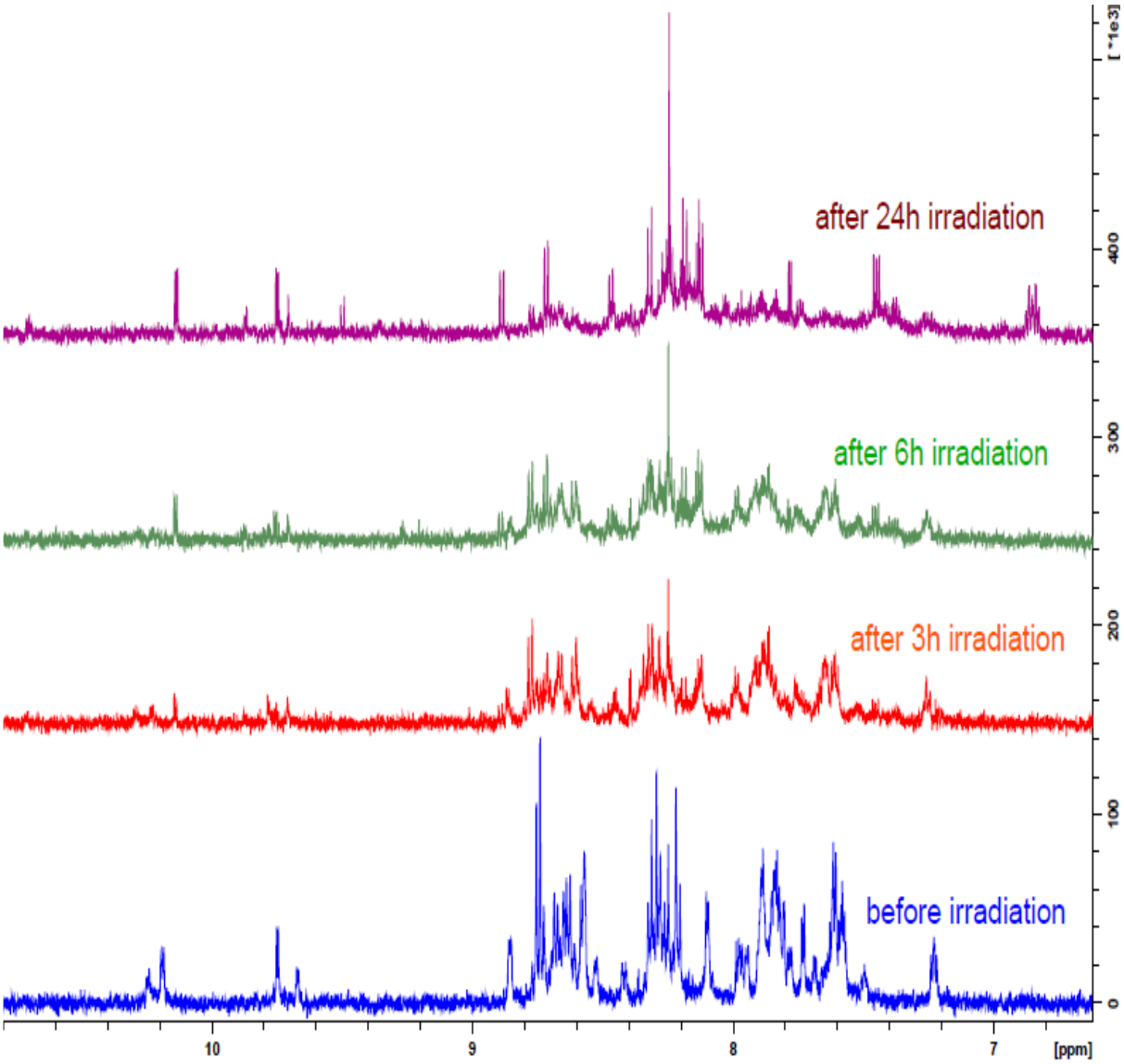

Figure 4.14: ^{1}H-NMR data of compound B-III during irradiation in d_3-acetonitrile.

This illustrates that the photolysis of A-III is not completed, since the irradiation creates create some intermediates. However, these cannot be determined at present, clearly the amounts of these species produced are too low to allow for definitive assignment. One possibility is the generation of a $[Ru(phen)_2(CH_3CN)_2]^{2+}$ type species as observed for the other compounds but

more studies need to be carried out to confirm this assessment. This feature will be discussed in Chapter 6.

4.4 Photolysis of Compounds in the Presence of TEA.

In the previous section it was shown that in acetonitrile the compounds B-I and B-III are photoreactive but the compound **B-II** is photostable for up to 3 hours under irradiation with visible light. In this section, the stability of the compounds against irradiation under catalytic conditions will be studied. The main difference between the two irradiation conditions is the presence of triethylamine (TEA) which acts as a sacrificial reductant as explained in the introduction. The samples were deaerated with argon before irradiation to reproduce the conditions used for the photocatalytic process.

4.4.1 Results

4.4.1.1 Irradiation of Compound B-I in the presence of TEA

The photochemical reaction between compound **B-I** with TEA is outlined as shown. The chromatograms of consider the photo reaction of compound **B-I** in the presence of TEA and CH_3CN. Before the irradiation process was taken place. The compound showed one identified peak at 6.30 minutes together with other negligible components as shown in Figure 4.15a.

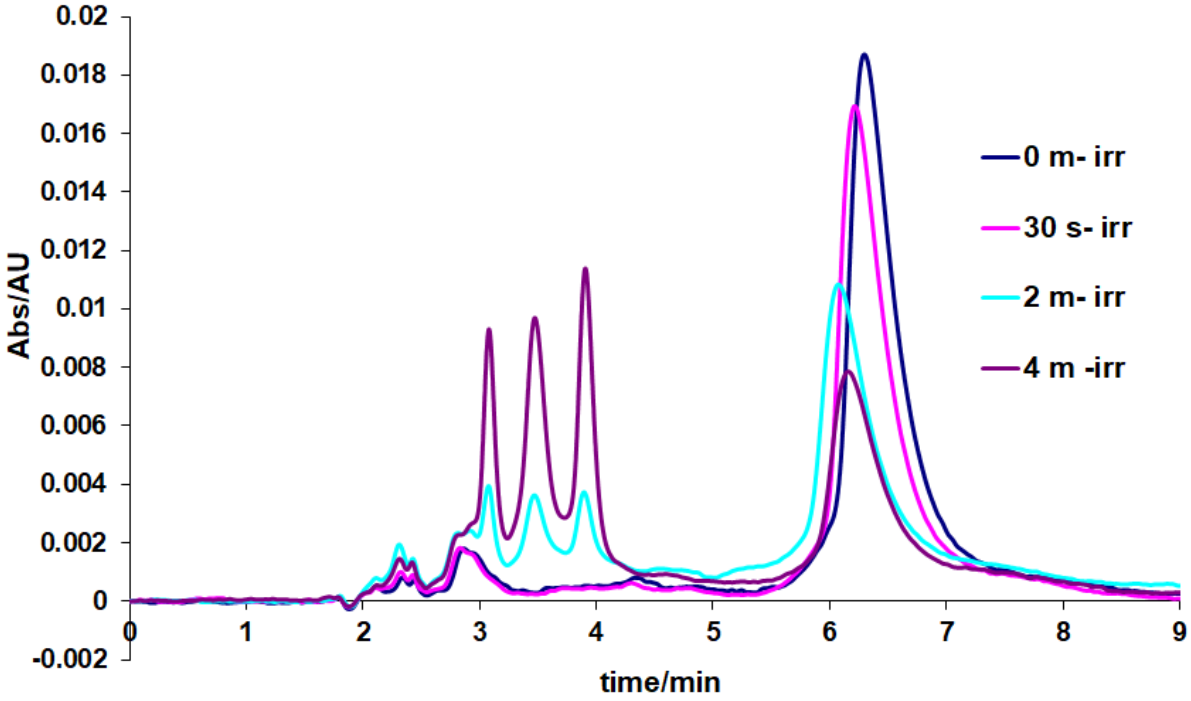

Figure 4.15: HPLC traces obtained upon photolysis of compound B-I. Temperature 24 ^{o}C. Irradiated in CH_3CN in presence of TEA (15%) and H_2O(10%) using 470 nm LED irradiation from (0-5min) degassing with Ar before irradiation detection wavelength; 470 nm, Mobile Phase CH_3CN:H^2O:CH_3OH with volume ratio 80:15:5 containing 0.12 M KNO_3 Flow rate 2.0 cm^3 min^{-1}.

It is of interest to note that without the presence of TEA compound **B-I** a peak at about 4.87 min as shown in Figure 4.8. This shows that there are considerable changes in the retention times in the presence of TEA in the reaction mixture. This is most likely related to a change in the reaction mixture.

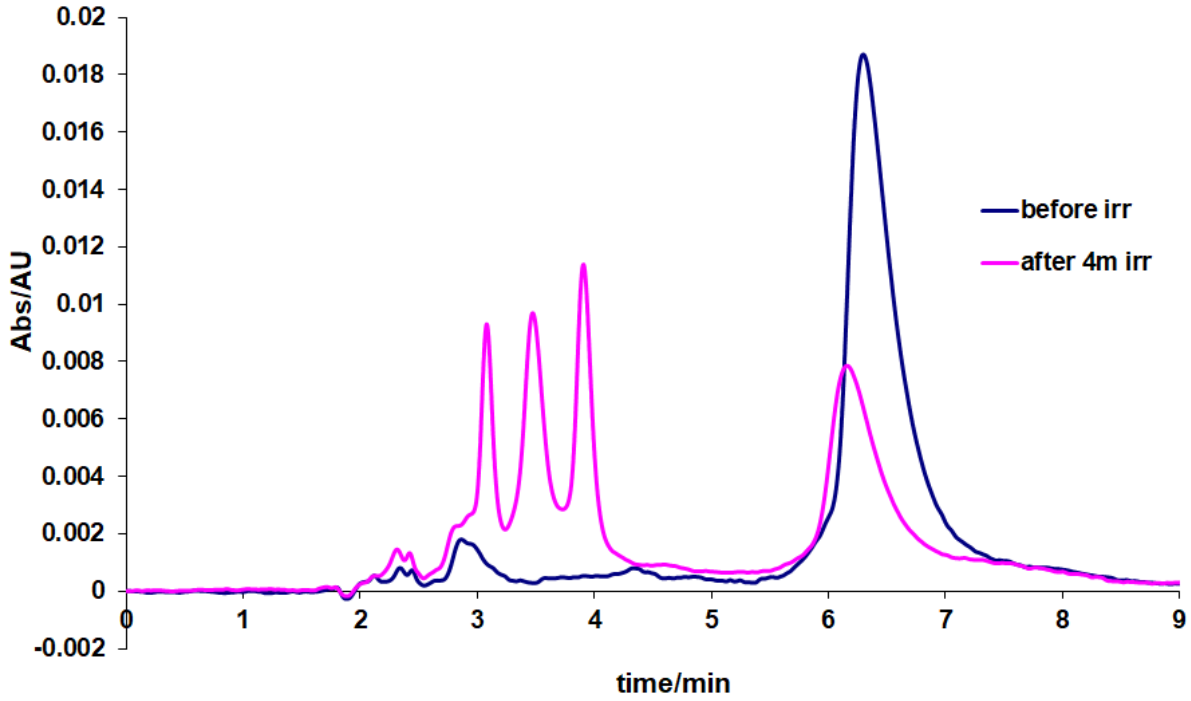

Figure 4.16: HPLC traces obtained before and after photolysis of compound B-I. Temperature 24 ^{o}C. Irradiated in CH_3CN in presence of TEA (15%) and H_2O (10%) using 470 nm LED irradiation from (0-5min) degassing with Ar before irradiation detection wavelength; 470 nm, Mobile Phase CH_3CN:H2O:CH_3OH with volume ratio 80:15:5 containing 0.12 M KNO_3 Flow rate 2.0 cm^3 min^{-1}.

During the irradiation the height of the main peak observed in Figure 4.16, the feature at 6.30 min, as slightly decreased after 30 s irradiation from (18.7 m AU) to (16.2m AU) approximately (13.4 %) with no significant change in the chromatogram. After continuous irradiation between 3 to 4 minutes, 3 new peaks in the range of 3-4 min irradiation appeared as HPLC traces and these were found to increase by irradiation time and reach their maximum with continuous photolysis process, followed by a significant decrease of the main product peak. As outlined in Figure 4.16 b this picture shows the difference between the initial solution and the final solution after 5 minutes of irradiation. It was found that upon irradiation three traces are observed without TEA between 1.7 and 3.5 min shown

in Figure 4.8a, without the presence of TEA, new features are observed between 2.7 and 4 min as shown in Figure 4.16. These peaks are observed in Figure 4.16 but the duration of the growing of these peaks is up to 180 min, indicating that direct irradiation is considerable slower as shown in Figures 14.8a and 14.8b. Nevertheless, it appears that these new species can be obtained even without the presence of TEA.

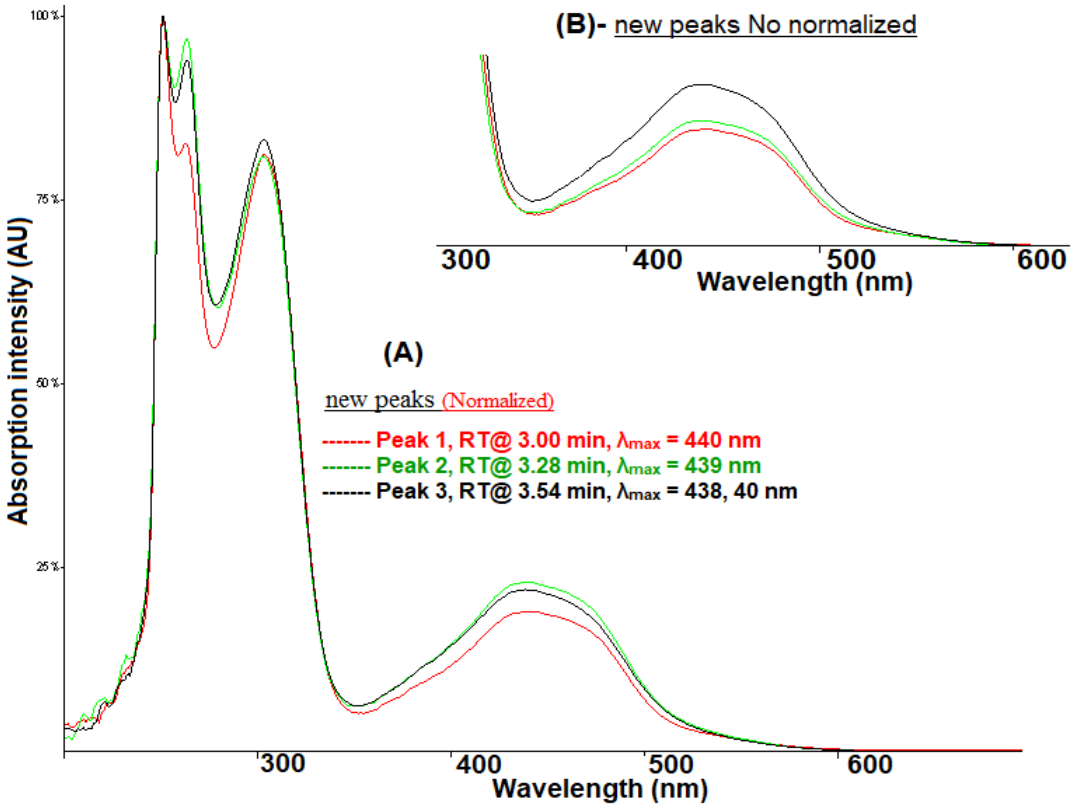

Figure 4.17: Absorption spectra features of new species identified in compound B- I after 4 minutes of irradiation (normalized) (A) and (No normalized) (B) in Figure 4.16. Detection wavelength 470 nm.

UV-spectra in Figure 4.17 found to have a rather broad absorption pattern λmax = between 420 and 480 nm, the red line of main peak before irradiation, the blue line of the product at 3.0 minutes, the green line of the product at retention time 3.48 minutes and black line of the product at retention time 3.90 minutes. This

suggests that these 3 compounds have very similar UV/Vis absorption spectra. This will be further discussed later in Chapter 6.

4.4.1.2 Irradiation of Compound B-II in the presence of TEA

In the reaction of B-II in the presence of TEA, the initial solution was found to have one major sharp peak with a retention time of 4.32 min in addition to two early peaks of impurities or related compounds at between 2 min and 2.5 min representing one third the height of the main peak. As shown in Figure 4.18a.

During the irradiation these early peaks are starting to increase and the height of the main peak significant decreased after 10 s irradiation from (33.7 m AU) to (22.1m AU) approximately (35 %). At the same time a new peak is observed at 3.2 min and the two early peaks increasing as well. The reaction was found to be very fast as only 60 second irradiation was enough to decompose up to 90 % of the main product. Compared with **B-I** product which required 4 min to decompose 60% of the product the peaks observed in for this compound obtained at about 60s, showing that decomposition of the species **B-II** is considerable faster. There are however also differences in the shape of these new peaks, indicating that the composition of these compounds is rather different as shown in Figures 4.18 and 4.19. The UV- vis spectra of new peak, main peak and the early peaks shown in Figures 4.19.

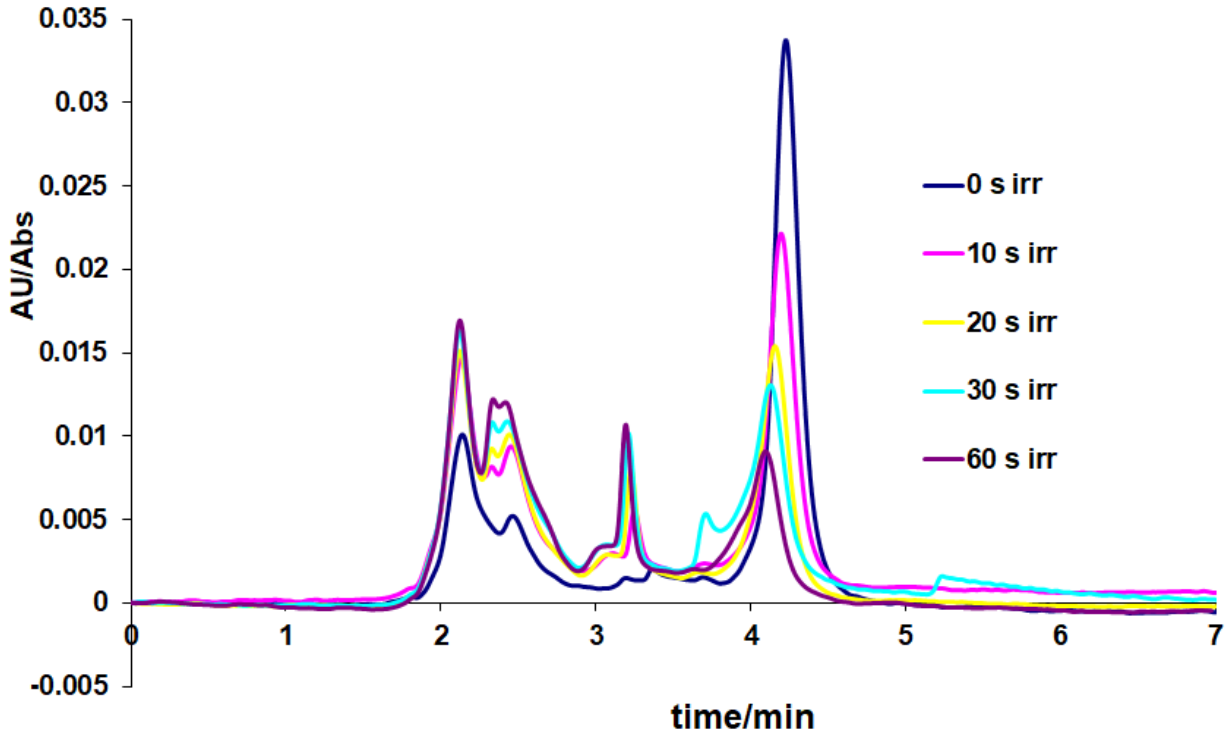

Figure 4.18a: HPLC traces obtained upon photolysis of B-II. Temperature 24 ^{o}C. Irradiated in CH_3CN in presence of TEA (15%) and H2O (10%) using 470 nm LED irradiation from (0-5min) degassing with Ar before irradiation detection wavelength; 470 nm, Mobile Phase CH_3CN:H_2O:CH3OH with volume ratio 75:15:10 containing 0.12 M KNO_3 Flow rate 2.0 cm^3 min^{-1}.

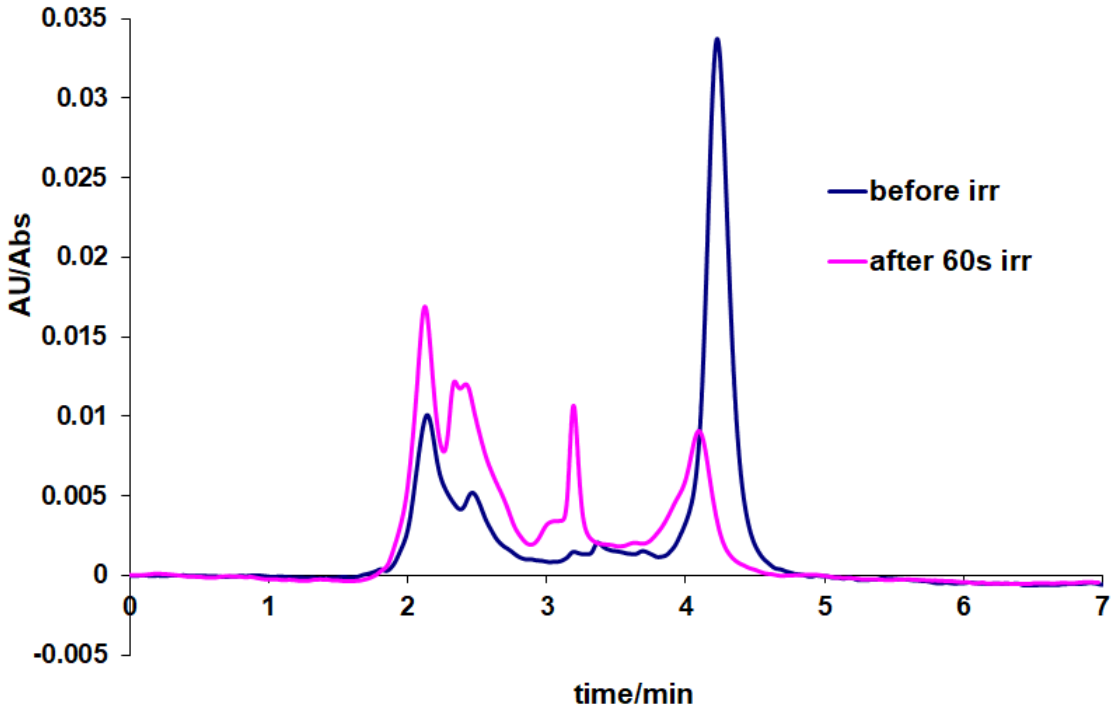

Figure 4.18b: HPLC traces obtained before and after photolysis of B-II. Temperature 24 ^{o}C. Irradiated in CH_3CN in presence of TEA (15%) and H_2O (10%) using 470 nm LED irradiation from (0-5min) degassing with Ar before irradiation detection wavelength; 470 nm, Mobile Phase CH_3CN:H_2O:CH_3OH with volume ratio 75:15:10 containing 0.12 M KNO_3 Flow rate 2.0 cm^3 min^{-1}.

Surprisingly irradiation of the compound **B-II** is rather fast and the traces observed for this compound are rather different from these shown in for **B-I**. For **B-II** there are HPLC traces of similar types between 2 - 3.5 min as observed for **B-I** and but no clear traces as observed for **B-I** are observed. The absorption spectra obtained from the HPLC traces are shown in Fig 4.19 shown below. It is clear that at least four types of spectra can be obtained. It seems that these spectra are complex and contain at least 2 different peaks containing maxima of ranging from 413 to 575 nm. This will be further discussed in Chapter 6.

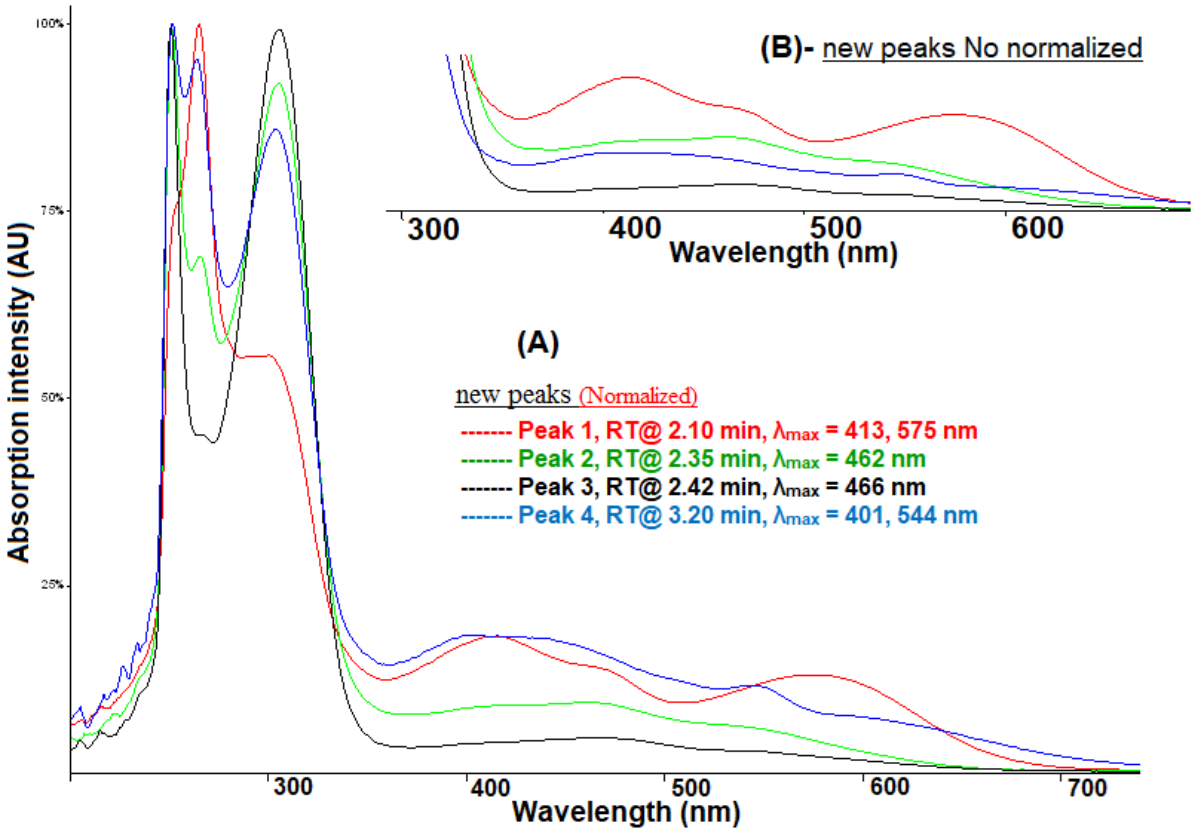

Figure 4.19: Absorption spectra features of new species identified in compound B- II after 60 seconds of irradiation (normalized) (A) and (No normalized) (B) in Figure 4.18. Detection wavelength 470 nm.

4.4.1.3 Irradiation of Compound B-III in the presence of TEA

In the case of the compound B-III as shown in Figure 4.20 the initial chromatogram has one sharp major peak at 3.5 min and another early forked peak at 2.1 min with an approximate ration 5:1. The reason for this behaviour as well as that observed for the compound B-II is unclear, but considering the fact that the photolysis as very fast, it may be the result of some irradiation by daylight. As Figure 4-20a,b shows the reaction was found to be very rapid

compared with the other 2 photocatalyst. This may also explain the role of iodine/chloride atoms on the photoreaction. The reaction was carried out for only 30 seconds, which was sufficient to decompose the compound almost completely. After 30 second of irradiation the early rather early peak become the major peak in the chromatogram with traces of the main compound observed at 3.5 min still in the solution.

The UV spectra of the new degraded products between 2,00 - 2.25 min due to the degradation of the main product which have maximum absorbance near 500 nm visible region as shown in Figure Figure 4.21.

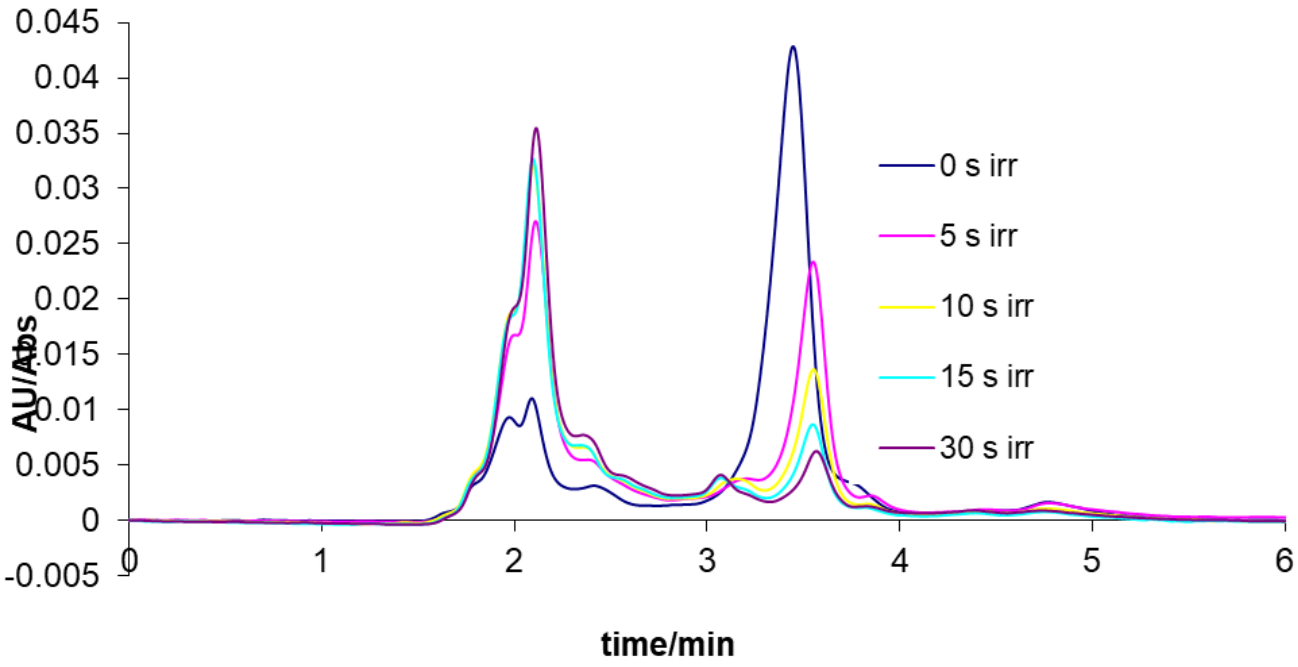

Figure 4. 20a: HPLC traces obtained upon photolysis of B-III. Temperature 24 ^{o}C. Irradiated in CH_3CN in presence of TEA (15%) and H_2O(10%) using 470 nm LED irradiation from (0-5min) degassing with Ar before irradiation detection wavelength; 470 nm, Mobile Phase CH_3CN:H_2O:CH_3OH with volume ratio 75:15:10 containing 0.12 M KNO_3 Flow rate 2.0 cm^3 min^{-1}.

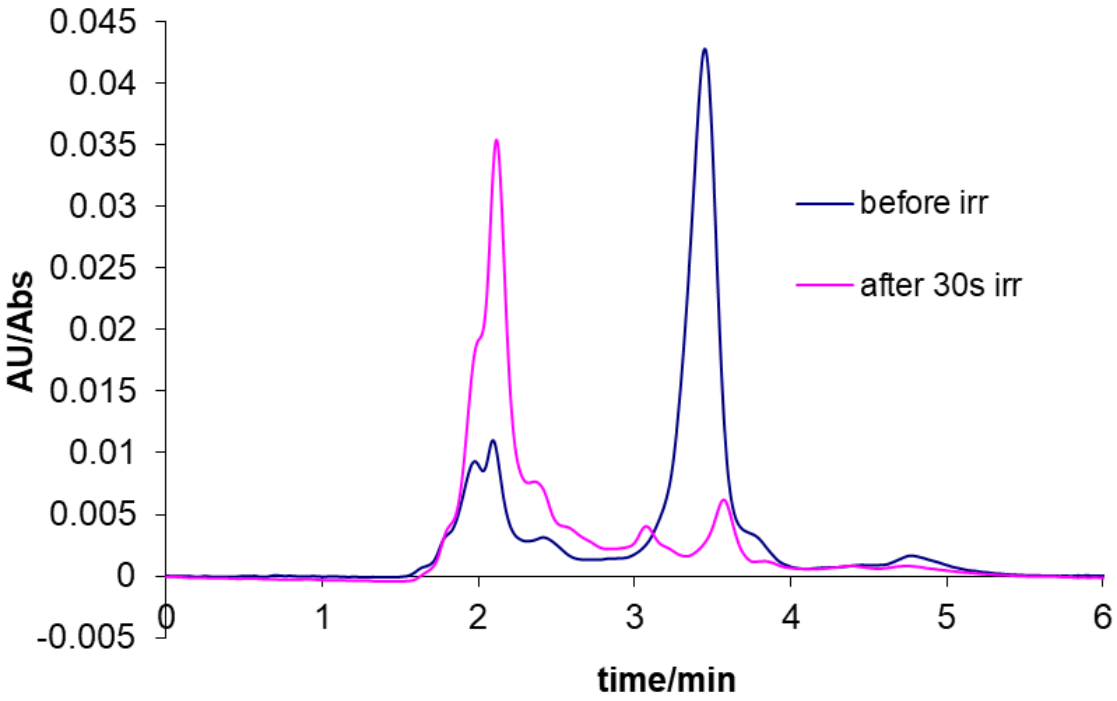

Figure 4.20b: HPLC traces obtained before and after photolysis of compound B-III. T 24 ^{o}C. Irradiated in CH_3CN in presence of TEA (15%) and H_2O (10%) using 470 nm LED irradiation from (0-5min) degassing with Ar before irradiation detection wavelength; 470 nm, Mobile Phase CH_3CN:H_2O:CH_3OH with volume ratio 75:15:10 containing 0.12 M KNO_3 Flow rate 2.0 cm^3 min^{-1}

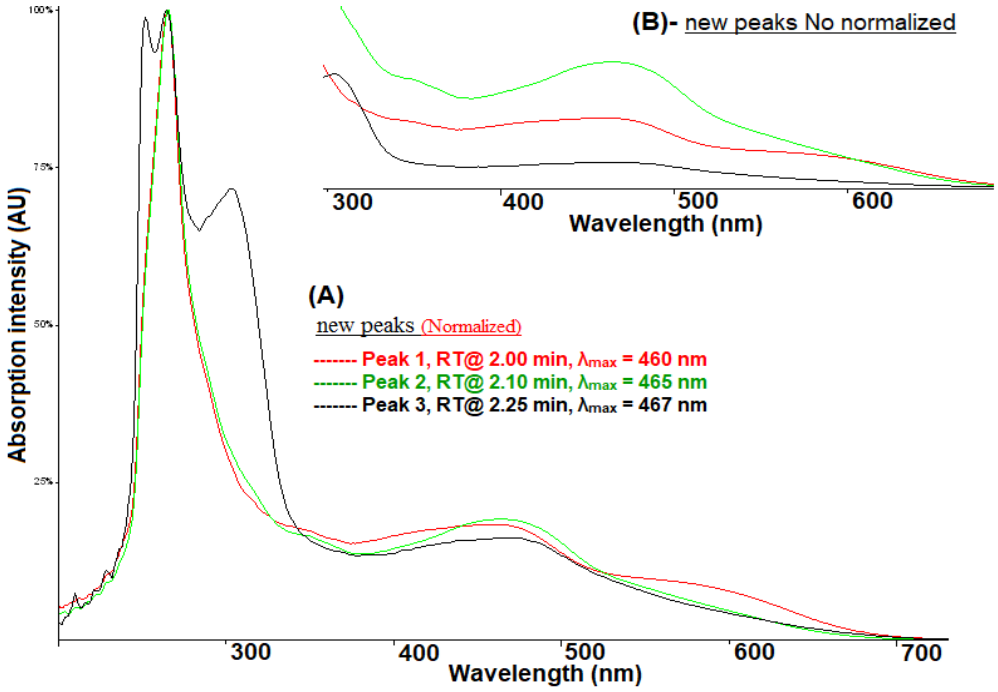

Figure 4.21: Absorption spectra features of new species identified in compound B- III after 30 seconds of irradiation (normalized) (A) and (No normalized) (B) in Figure 4.20. Detection wavelength 470 nm.

4.5 Summary

In this work, the characterisation and the stability of photocatalysts of $[(phen)_2Ru(2,3dpp)]^{2+}$, $[(phen)_2Ru(2,3dpp)PtCl_2]^{2+}$ and $[(phen)_2Ru(2,3dpp)PtI_2]^{2+}$ were studied. In this study HPLC, UV/vis absorption spectra and ^{1}H-NMR of the compounds were obtained to compare the structural features and investigate the stability of the three compounds. In HPLC results, the retention time of the three major peaks are different due to the presence of the catalytic states (monomer/dinuclear) and the nature of the halogen (Cl_2/I_2) containing peripheral species.

The stability of the compounds has been investigated in 2 conditions. The first condition is irradiation of compounds in acetonitrile solvent for 3 hours, together with the ^{1}NMR data, while the second condition was irradiation of the compounds in acetonitrile in the presence of TEA. last for only few minutes.

The obtained results indicate clearly that upon irradiation under the first condition the monomer is photo reactive, while $Ru/PtCl_2$ centre is photostable and the Ru/PtI_2 centre is photoreactive but at a lower extent than the monomer. The ^{1}H-NMR results are largely consistent with HPLC results as shown in Figure (4,22).

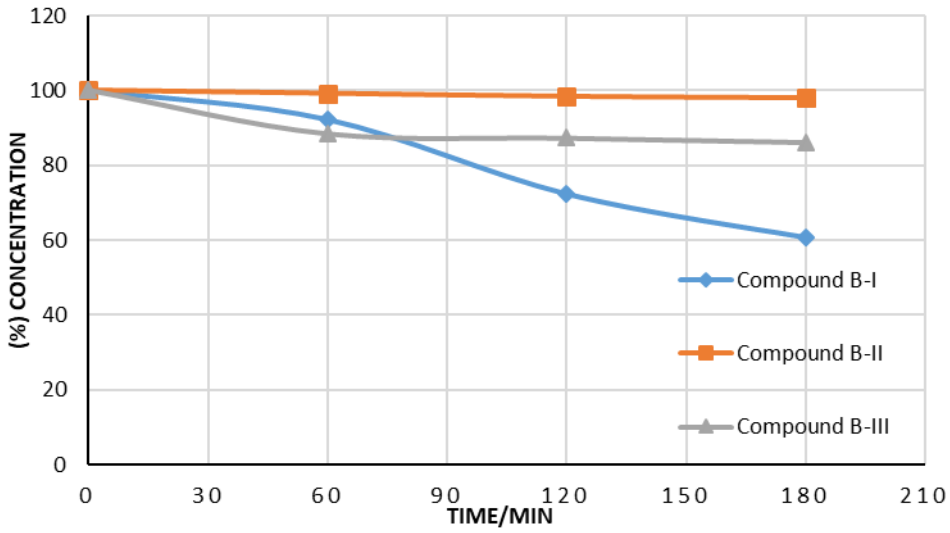

Figure 4.22: The rate of photo-degradation of compound B-I, B-II and B-III in the Absence of TEA.

Under the second condition the metal complexes are decomposing or rearranging rapidly. Especially the $[(phen)_2Ru(2,3dpp)PtI_2]^{2+}$ was found to be the fastest to decompose of these compounds under this condition as shown in Figure (4,23).

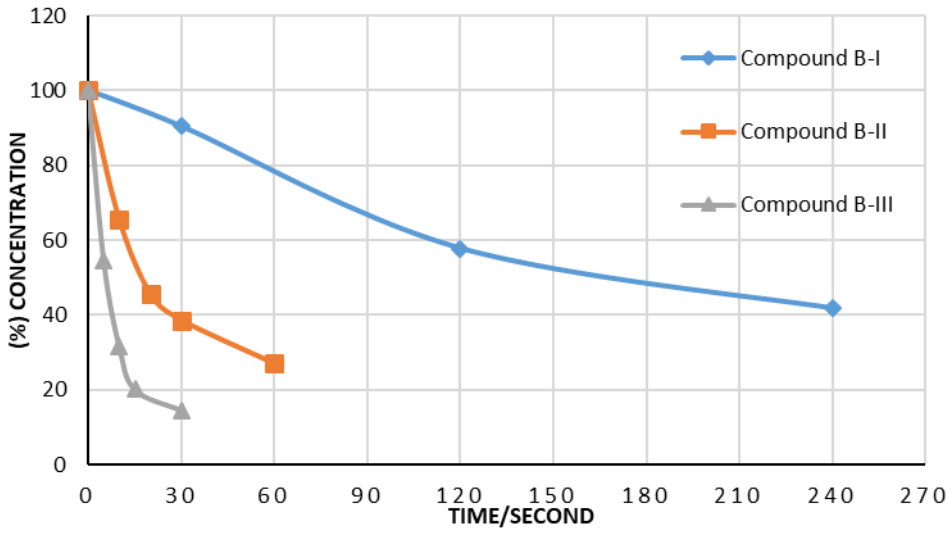

Figure 4.23: The rate of photo-degradation of compound A-I, A-II and A-III in the presence of TEA.

Apart from the disappearance of the three photocatalysts, some new and stable compounds are appearing. The HPLC studies indicate that the 3 compounds formed are very similar with absorption maxima from about 430 nm. It is furthermore unexpected that even in the presence of high concentrations of TEA these compounds are stable. It is possible that species form single bonds as shown in this diagram, where the ruthenium centre is only bound to a single bond associated to the bridging ligand and singly bound ligands such as S = CH_3 CN, Cl,$^-$ I^-. are possibly present as shown in Figure 22.

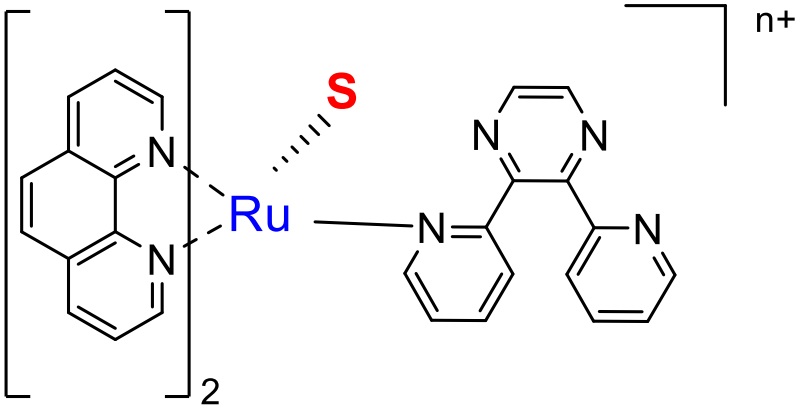

Figure 4. 22: Potential intermediate formed upon irradiation. S = CH_3CN, Cl^{-} I^-.

On the basis of the obtained data in this study, is seems clear that it is the high reactivity of TEA reagent that leads to the decomposition of ruthenium complexes. This will be further considered in Chapter 6.

4.6 References

[1] C Creutz, M.Chou, T.L. Netzel, M. Okumura, N. Sutin, J. Am. Chem. Soc., 1980, 102, 1309.

[2] A.T. Cocks, R.D. Wright, K.R. Seddon, Chem Phys. Lett, 1982, 83, 369.

[3] J. N. Demas and J. W. Addington J. Amer. Luminescence Quenching of the Tris(2,2/-bipyridine)ruthenium(II) and Tris(1,10-phenanthroline)ruthenium(II) Cations. Chem. Soc 5800-5806, 98, 1976.

[4] J. R. Schoonover, K. M. Omberg, J. A. Moss, S. Bernhard, V.J. Malueg, W. H. Woodruff, and T. J. Meyer, Interpretation of the Time-Resolved Resonance Raman Spectrum of [Ru(phen)3]2+ , Inorg. Chem 1998, 37 2585-2587

[5] P G. Sammes and G. Yahioglu, G. Lemercier , M. Four, S. Chevreux, Coord. Chem. Rev. 2018. 368, 1–12 b) 1,l0-phenanthroline: A versatile ligand. Chem. Soc. Rev, 1994, 327-334.

[6] L. Feng, Y. Wang, and J. Jia, Triplet Ground-State-Bridged Photochemical Process: Understanding the Photoinduced Chiral Inversion at the Metal Center of [Ru(phen)2(L-ser)]+ and its Bipy Analogues Inorg. Chem. 2017, 56, 14467−14476

[7] L Feng and Y. Wang, A Key Factor Dominating the Competition between Photolysis and Photoracemization of [Ru(bipy)3]2+ and [Ru(phen)3]2+ Complexes. Inorg. Chem. 2018, 57, 8994−9001

[8] R. Hage, J.G. Haasnoot, H.A. Nieuwenhuis, J. Reedijk, D.J.A. De Ridder and J.G. Vos. J. Am. Synthesis, X-Ray Structure, Spectroscopic, and Electrochemical Properties of Novel Heteronuclear Ruthenium-Osmium Complexes with an Asymmetric Triazolate Bridge. Chem. Soc., (1990), 112, 9245-.

[9] F. Barigelletti, L. De Cola, V. Balzani, R. Hage, J.G. Haasnoot, J. Reedijk, and J.G. Vos. Mononuclear and Dinuclear Osmium(II) Compounds Containing 2,2'-bipyridine and 3,5-bis(pyridin-2-yl)-1,2,4-triazole: Synthesis, Electrochemistry, Absorption spectra and Luminescence Properties. Inorg. Chem. (1991), 30, 641-.

[10] Hughes, D. Martin, S. Bell, J.J. McGarvey and J.G. Vos. Photophysical and Photochemical Properties of Dinuclear Ruthenium(II) Complexes Containing 2,2'-Bipyridyl and 1,10-phenanthroline. H.P. Inorg. Chem., (1993), 32, 4402-4408

[11] A. Juris, V. Balzani, F. Barigelletti, S Campagna P. Belser, and A von Zelewsky. Coord. Ru(II) polypyridine complexes - photophysics, photochemistry, electrochemistry, and chemiluminescence, Chem. Rev. Volume: 1988 ,84 85-277,

[12] J.G. Vos and J.M. Kelly, Ruthenium Polypyridyl Chemistry, from Basic research to Applications and Back Again. Dalton Trans. (2006), 4869 – 4883

[13] T. Kowacs, Q. Pan, P. Lang, L. O'Reilly, S. Rau, W. R. Browne, M. T. Pryce, A. Huijser, J. G. Vos. Supramolecular Bimetallic Assemblies for Photocatalytic Hydrogen Generation from Water. Faraday Discuss. (2015),185, 143 - 170

[14] A.C. Lees, C.J. Kleverlaan, C.A. Bignozzi and J.G. Vos, Photophysical Properties of TiO2 Surfaces Modified with Dinuclear RuRu and RuOs Polypyridyl Complexes. Inorg. Chem, (2001), 40, 5343-5349

[15] H.P. Hughes and J.G. Vos, The Control of Photosubstitution in Dinuclear Ruthenium Polypyridyl Complexes by the Choice of Bridging ligand.Inorg. Chem., (1995), 34, 4001-4003.

Chapter 5

An investigation of the photostability of ruthenium photocatalysts, based on the 4,4'-diethoxycarbonyl-2,2'-bipyridine (dceb) peripheral ligand and the 2,3-di(pyridyl-2-yl) pyrazine (2,3dpp) bridging ligand

In the present Chapter ruthenium based photocatalysts based on the presence of the peripheral ligand 4,4'-diethoxycarbonyl-2,2'-bipyridine (**dceb**) are discussed, During the sample preparation, solutions were deaerated with argon or nitrogen prior to mimic the conditions at which the photocatalytic process is conducted. In the absence of TEA, but in acetonitrile, the compounds **C-I** and **C-III** are photoreactive while that compound **C-II** is photostable, the latter for up to 3 hours under irradiation. Furthermore, the photostability of the compounds **C-I**, **C-II** and **C-III** during irradiation in the presence of TEA were measured. When the compounds **C-I**, **C-II** and **C-III** are tested under these conditions a fast degrading process is observed.

5.1 Introduction

As outlined in the introduction to the purpose of the investigation is to assess the stability of a number of photocatalysts capable of delivering hydrogen from water upon irradiation. These catalysts have been studied by the DCU group and it has been observed that the stability of the compounds and the amount of hydrogen formed depends on the conditions and the three components of the assembly; the peripheral ligand the bridging ligand and the catalytic centre. [1,2,3,4] In Chapters 3 and 4 two different peripheral ligands were used; bpy and phen respectively and the bridging ligand is 2,3-bis(2'-pyridyl) pyrazine (2,3,dpp). Both mononuclear, no catalytic centre, and dinuclear compounds are based on the platinum catalysts $PtCl_2$ and PtI_2. It has been shown that there are differences between bpy and phen as peripheral ligand and the dceb ligand. Recent studies have shown that the photophysics of the assemblies are greatly dependent on the arrangement of the catalytic components and that photocatalysts. With the dceb ligand as a peripheral ligand an increased hydrogen generation with other photocatalyst from 80, for a "bpy" based catalyst, to 650 after 6 hours of irradiation for the dceb complex. [5,6,7] Similar data were observed for another dceb complex with 2,2':5',3'':6",2'''quaterpyridine, bisbpy as the bridging ligand and $PtCl_2$ as the catalytic centre. For this compound hydrogen was formed at a rate of 513 turnover numbers over 6 hours.[8]

In the present Chapter 5, ruthenium based photocatalysts are studied with the peripheral ligand 4,4'-diethoxycarbonyl-2,2'-bipyridine (dceb), as shown in Figure 5-1, together with the 2,3 dpp bridging ligand. It should be noted that in this study

the 2,3 dpp ligand together with the Pt photocatalysts $PtCl_2$ and PtI_2 have been used in this study in order to create a range of compatible results. No catalytic centres are coordinated to the monomeric ruthenium 2,3 dpp compound.

5.2 *HPLC, UV-Vis and ^{1}H-NMR Characterisation of mononuclear and supramolecular Ru/Pt compounds.*

In this part, the characterization of the final group (**Group C**) is carried out and the photolytic properties of the compounds are assessed. This group is composed of three complexes, one mononuclear and two binuclear. The bidentate peripheral ligands that are coordinated to the Ru(II) centre as the 4,4'-diethoxycarbonyl-2,2'-bipyridine **(dceb)** component**.** The structure of the bridging ligand 2, 3-bis(2'-pyridyl) pyrazine **(2,3dpp)** are displayed in Figure 5.1. The chemical structures of these complexes are displayed in Figure 5.2. As mentioned before, the bridging ligand is essential for the connection to the ruthenium photosensitiser centre to the platinum catalytic centre in order to create the binuclear Ru/Pt compounds.

The binuclear compounds have different halogens attached to the Pt atom while the structures of the mononuclear compound $[Ru(N\hat{}N)_2(2,3dpp)](PF_6)_2$ (N^N = dceb) **C-I** and the dinuclear Ru/Pt compounds $[Ru(N\hat{}N)_2(2,3dpp)PtX_2](PF_6)_2$ (N^N = dceb, X = Cl-, or I-),called **C-II** and **C-III** respectively.

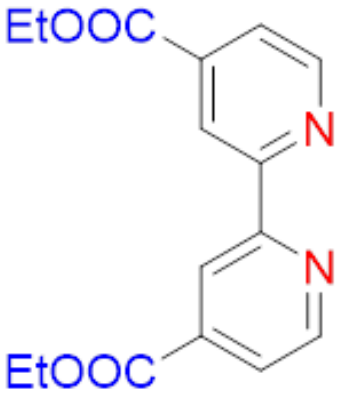

dceb

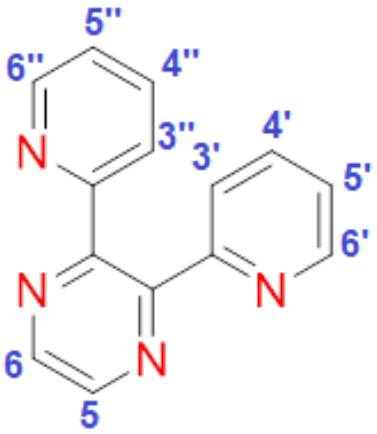

2,3dpp

Figure 5. 1**:** Structures of the peripheral ligand dceb and the bridging ligand 2.3dpp which are used in this part.

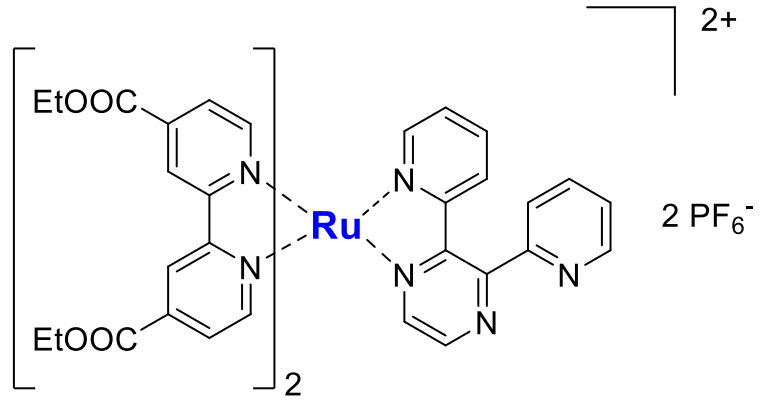

C-I

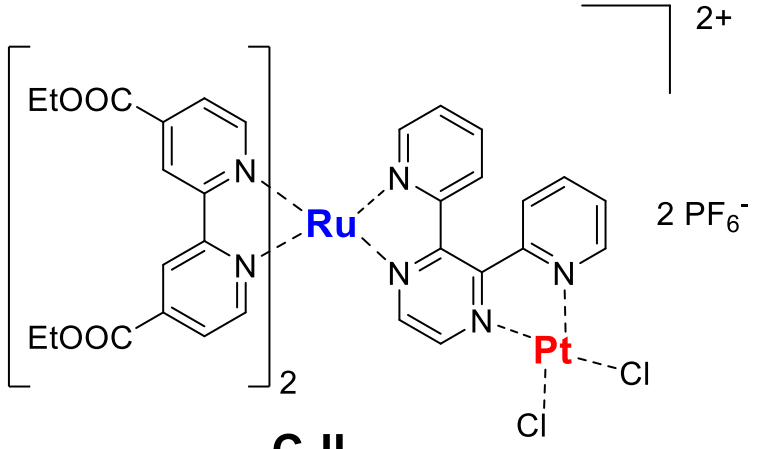

C-II

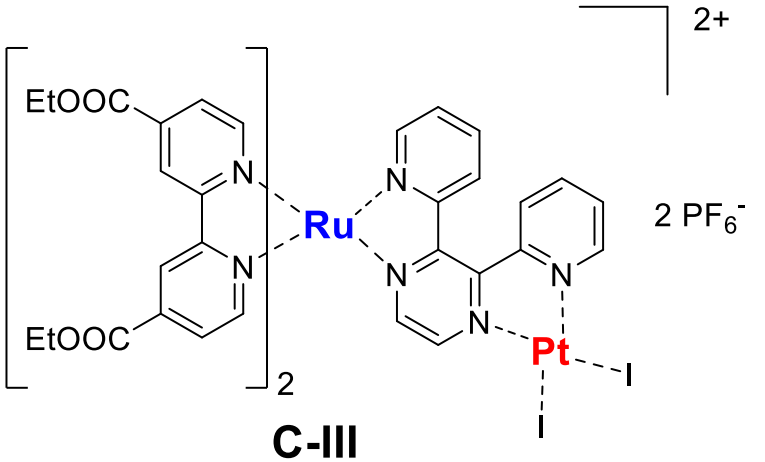

C-III

Figure 5.2**:** Structures of the dinuclear Ru/Pt compounds and Ru(II) monomer with 2,3dpp as bridging ligand and with dceb type peripheral ligands.

5.2.1 Chromatographic characterisation

The chromatographic characterisation of the **group C** compounds does not vary significantly from what was observed in previous chapters for groups **A** and **B**. The peripheral ligands for group **C** are similar in structure to Group **A** but has two additional ethyl ester moieties. It seems the HPLC experiments indicate that the retention time has changed considerably from group **A** results. The halogen atoms attached to the platinum centre do not affect the peak shape because as it seems to have limited effect on the compound hydrophobicity. The chromatograms obtained for the mononuclear $[(dceb)_2Ru(2,3dpp)]^{+2}$ **(C-I),** the dinuclear $[(dceb)_2Ru(2,3dpp)PtCl_2]^{2+}$ **(C-II)** and $[(dceb)_2Ru(2,3dpp)PtI_2]^{2+}$ **(C-III)** are shown in Figure (5.3 a, b, c). A strong peak is observed for all 3 compounds at retention times of about 4.18, 3.30 and 2.50 min**.**

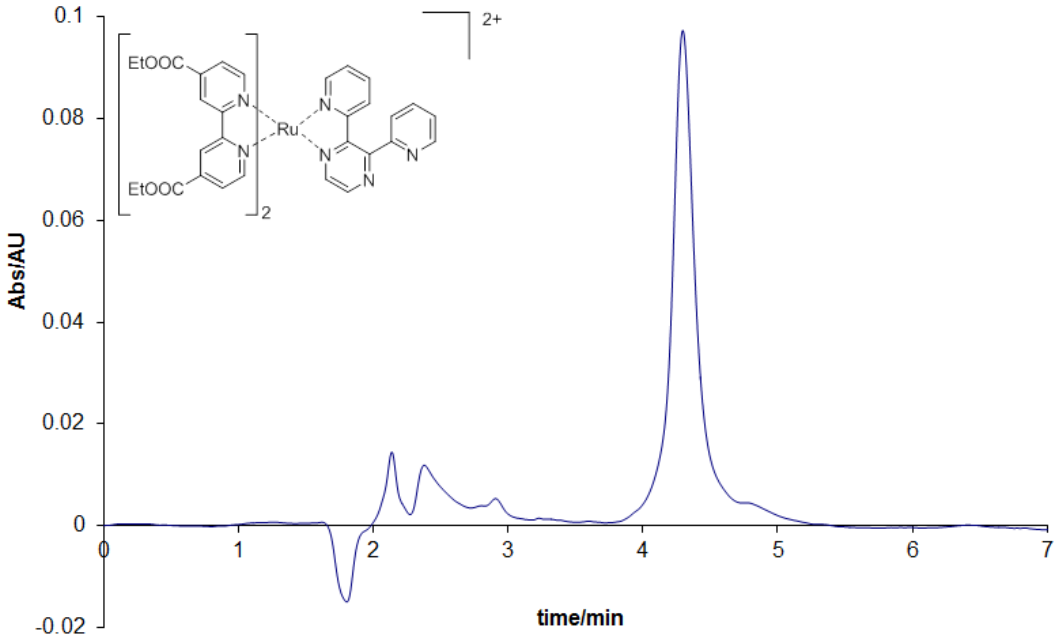

Figure 5.3a: HPLC trace for $[(dceb)_2Ru(2,3dpp)]^{2+}$ in CH_3CN (mobile phase CH_3CN: H_2O: CH_3OH with volume ratio 65:20:15 containing 0.05 M KNO_3) Flow rate: 2.0 cm^3 min^{-1}; detection wavelength at 280 nm, T=24 ^0C.

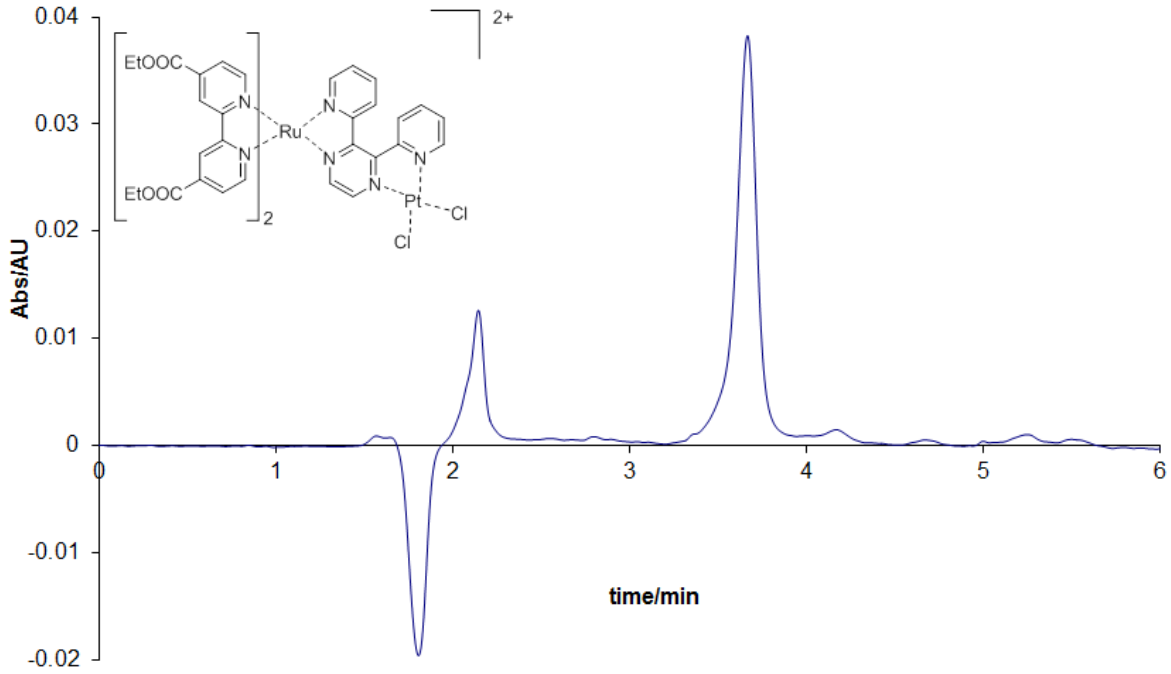

Figure 5.3 b: HPLC trace for $[(dceb)_2Ru(2,3dpp)PtCl_2]^{2+}$ in CH_3CN (mobile phase CH_3CN: H_2O: CH_3OH with volume ratios of 65:20:15 containing 0.05 M KNO_3, Flow rate: 2.0 cm^3 min^{-1}, detection wavelength at 280 nm, T=24 ^0C.

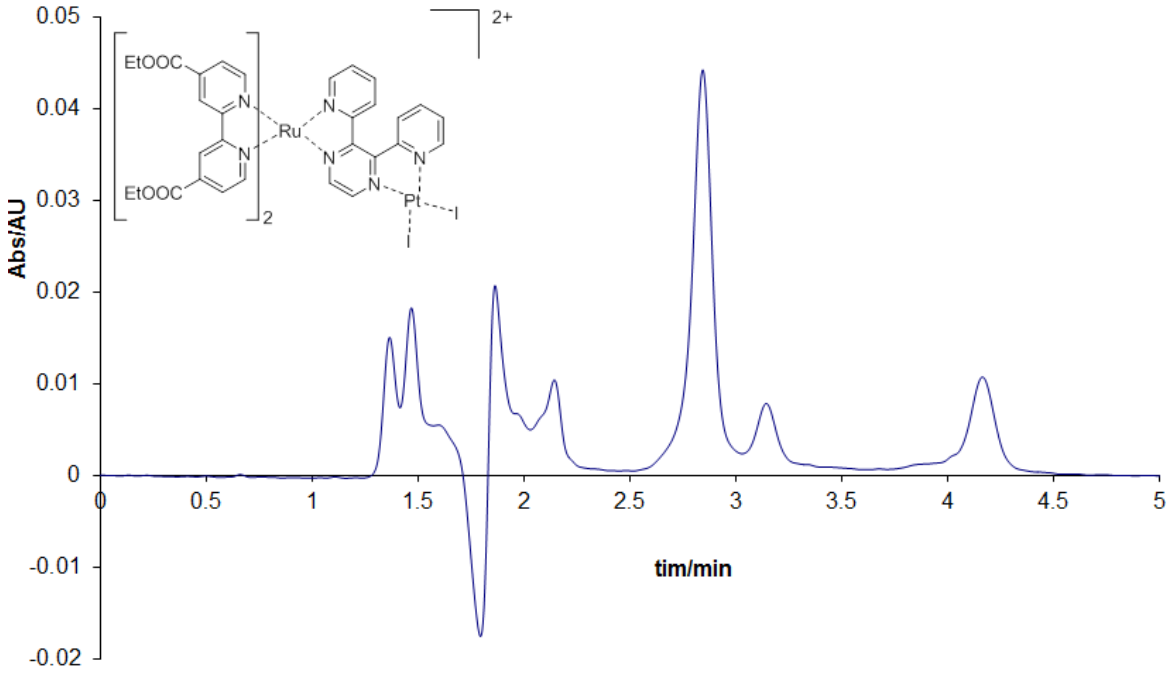

Figure 5.3 c: HPLC trace for $[(dceb)_2Ru(2,3dpp)PtI_2]^{2+}$ in CH_3CN (mobile phase CH_3CN: H_2O: CH_3OH with volume ratio 65:20:15 containing 0.05 M KNO_3, Flow rate: 2.0 cm^3 min^{-1}, detection wavelength at 280 nm, T=24 ^0C.

The retention times of the compounds **C-I** - **C-III** are short when compared with the mononuclear and dinuclear compounds. The dinuclear compound **C-III** show very short retention times. The small variation in retention times for the binuclear compounds may be attributed to the electron density of the attached halogen species ($PtCl_2$, or PtI_2). See Table 5.1

Table 5.1: Retention times and absorption maximum of compounds **C-I**, **C-II**, **C-III** in acetonitrile with detection wavelength at 280 nm, T=24 °C.

compound	**Retention time (min)**	**UV/vis spectrum/ λ_{max} (nm)**
$[(dceb)_2Ru(2,3dpp)]^{+2}$	4.18	464
$[(dceb)_2Ru(2,3dpp)PtCl_2]^{+2}$	3.30	466
$[(dceb)_2Ru(2,3dpp)PtI_2]^{+2}$	2.50	482

In order to further compare and contrast the compounds available in this study are listed in Table 5.2. In general, the retention times of compounds are based on the hydrophobicity of the material injected. As shown in Table 5-2 below the three mononuclear species have longer retention times. All the six dinuclear compounds with the highest value of 10.26 min obtained for compound **A-I**. The data also show that for the three dinuclear compounds **A-II, B-II** and **C-II** lower retention times are obtained ranging from 4.48 to 4.20 to 3.30 min. Therefore, for compound three the Group **C** -**III** compounds (see Table 5.1) the lowest charge is most likely located on the binuclear compounds. However, there is a considerable difference in retention times between the three mononuclear compounds **A-I** and

B-I and **C-I**, which suggests that the nature of the peripheral ligands is of paramount importance, however, the absence of catalytic centres may also play a role. For example, this difference between the chlorine and the iodine containing compounds has already been discussed with respect to the ^{1}H-NMR data. This is further discussed in the ^{1}H-NMR data shown in Figures 5.10 and 5.13. The differences between the chloride and iodide compounds are further studied by considering the UV/Vis data shown in Table 5.2.

Table 5.2: Retention times and absorption maximum of compounds group-**A**, group-**B** and group-**C** in mobile phase with detection wavelength at 280 nm, T=24°C.

Groups	compounds	Retention time (min)	UV/vis/ λ_{max} (nm)
Group A	$[(bpy)_2Ru(2,3dpp)]^{+2}$	10.26	442
	$[(bpy)_2Ru(2,3dpp)PtCl_2]^{+2}$	4.48	415, 508
	$[(bpy)_2Ru(2,3dpp)PtI_2]^{+2}$	3.25	415, 514
Group B	$[(phen)_2Ru(2,3dpp)]^{+2}$	4.87	435
	$[(phen)_2Ru(2,3dpp)PtCl_2]^{+2}$	4.20	416, 510
	$[(phen)_2Ru(2,3dpp)PtI_2]^{+2}$	3.65	413, 515
Group C	$[(dceb)_2Ru(2,3dpp)]^{+2}$	4.18	464
	$[(dceb)_2Ru(2,3dpp)PtCl_2]^{+2}$	3.30	466
	$[(dceb)_2Ru(2,3dpp)PtI_2]^{+2}$	2.50	482

The UV/vis value obtained by the 3 compounds **A-I**, **B-I** and **C-I** shown in the last row of Table 5.2 show absorption maxima of 442, 435 and 464 nm these are

typical for these type compounds have MLCT bands with maxima at around 450-500 nm [9,10,11]and indicate the presence of ^{3}MLCT transitions. This is as expected for mononuclear species of this type. Different observations are obtained when considering the dinuclear compounds of **A-II** and **A-III** values of 415 and 508 nm and 415 and 514 nm are observed, while for **B-II** and **B-III** two different ^{3}MLCT transitions are observed at 416 and 510 nm and 413 and 515 nm and these are typical for the types of compounds observed. However, for the compounds **C-II** and **C-III** singlet features with absorption maxima of 466 and 482 nm are observed as in Figure 5.5 as expected. [10]

5.2.2 ^{1}H NMR characterisation.

To carry out the ^{1}H-NMR analysis for compound of group **C**, the mononuclear and the dinuclear compounds were dissolved in acetonitrile-d_3 following similar procedures to what was carried out for Group **A** and **B**. The results obtained are, also comparable to those of group **A** and **B**. (See Figure 5-4) The same behaviour of the Iodide and chloride complexes in ^{1}H-NMR is repeated for Group **C**, where the hydrogen adjacent to the Pt centre of the iodide complex shows a more upfield signal than the one adjacent to the chloride complex. Since, iodine has more electronegativity and should deshield the adjacent hydrogen atom, this observation is seen for all the compounds investigated in this section. The two peaks at 9.30 and 9.60 ppm in Ru/$PtCl_2$) and 9.90 and 10.25 ppm in Ru/PtI_2 respectively. This is consistent with the hypothesis that the presence of platinum catalytic centres at the bridging ligand and the nature of the halogen terminal

species in the dinuclear compounds will substantially affect the properties of compounds as discussed above.

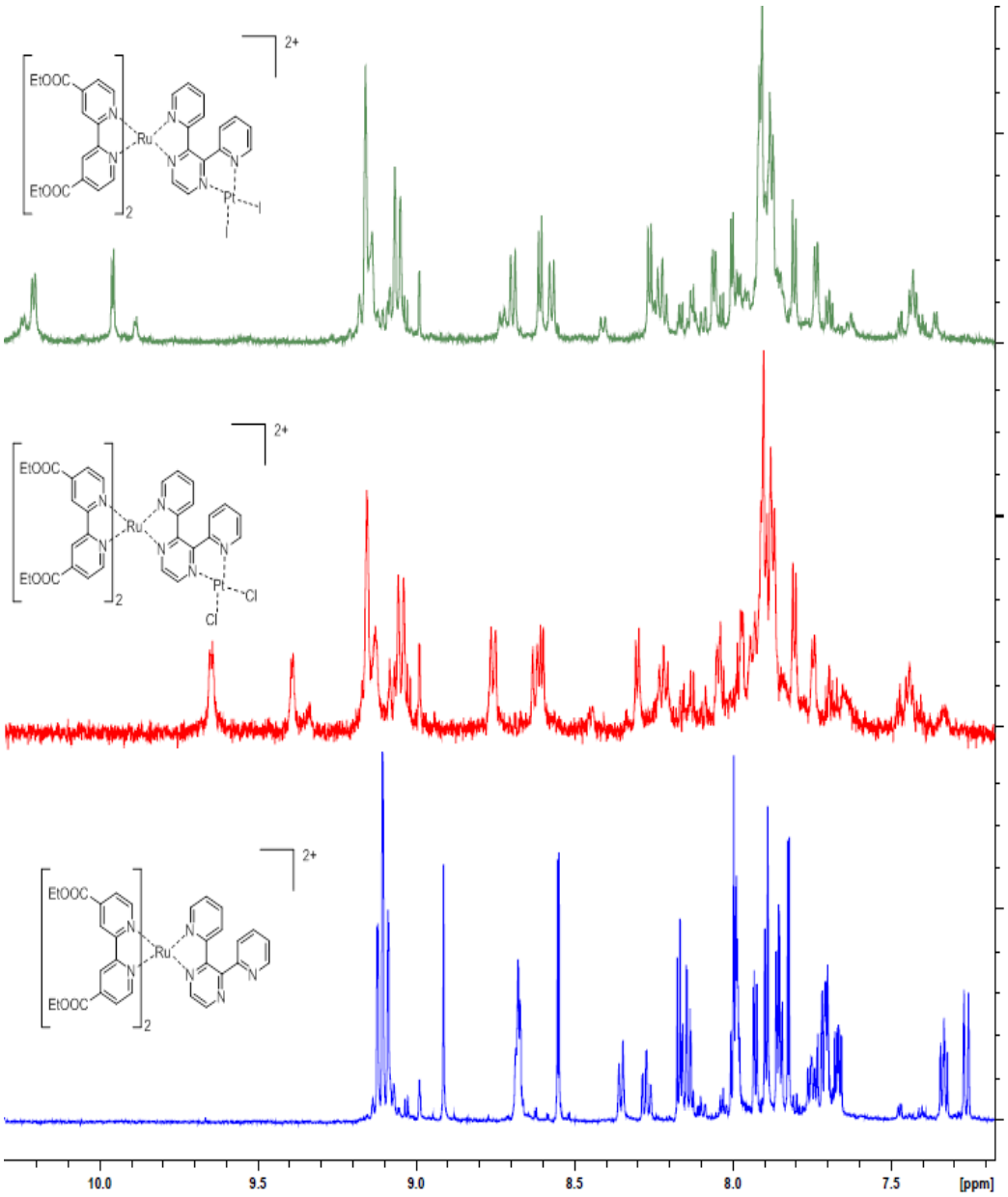

Figure 5.4: ^{1}H-NMR of $[Ru(dceb)_2(2,3dpp)]^{2+}$ **C-I** (bottom), $[Ru(dceb)_2(2,3dpp)PtCl_2]^{2+}$ **C-II** (middle) and $[Ru(dceb)_2(2,3dpp)PtI_2]^{2+}$ **C-III** (top) in d_3-acetonitrile.

5.2.3 UV/Vis Absorption spectroscopy

UV/vis spectra were determined for the mononuclear and the dinuclear Ru(II) compounds. Mobile phase was used as the solvent. The UV/Vis spectra of the three compounds are shown in Figure 5-5.

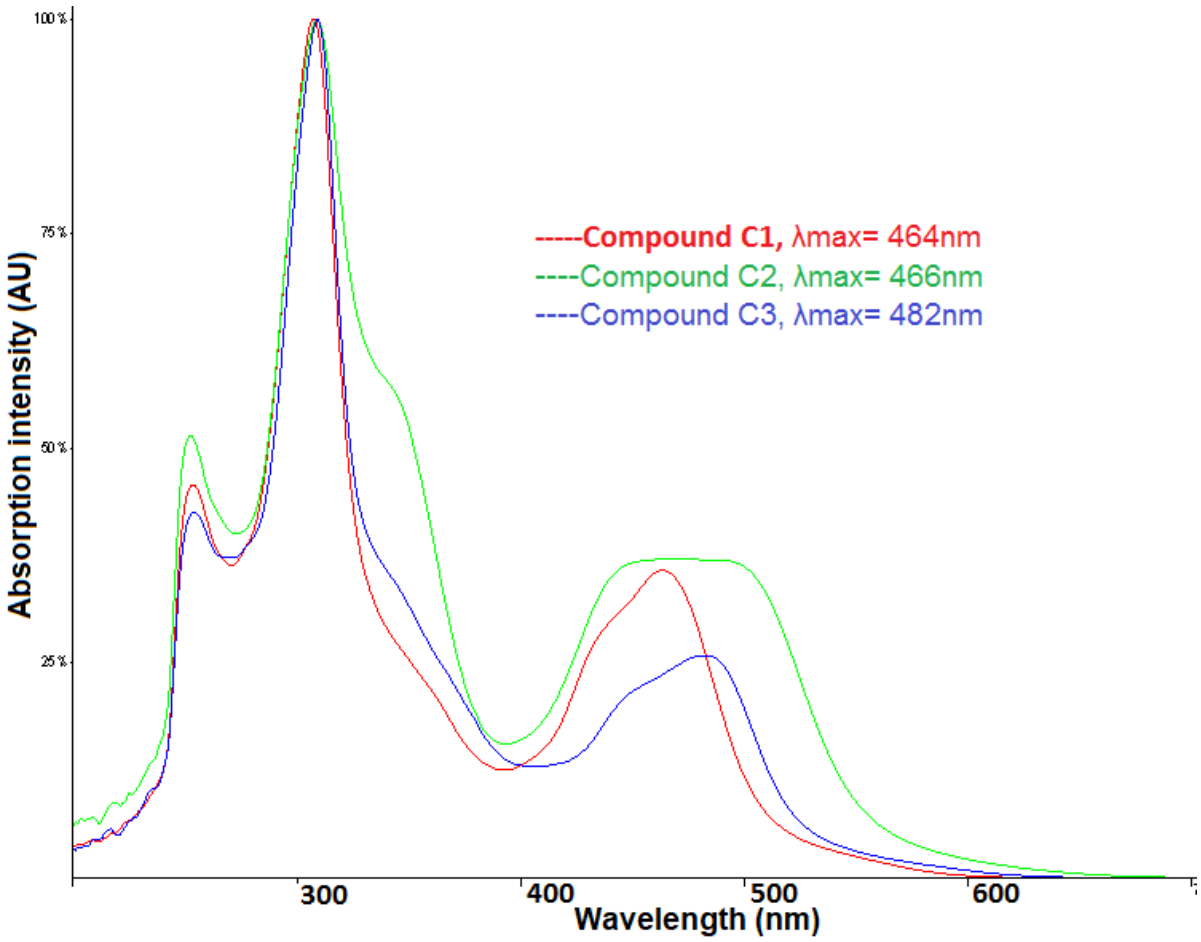

Figure 5.5: Absorption spectra (normalised) of $[(dceb)_2$ Ru (2,3dpp)$]^{2+}$ **C-I**, $[(dceb)_2$ Ru (2,3dpp)$PtCl_2]^{2+}$ **C-II** and $[(dceb)_2$ Ru (2,3dpp)$PtI_2]^{2+}$ **C-III** in CH_3CN, data obtained from Figure (5.3 a,b,c).

The absorption of the compounds group **C**, $[Ru(dceb)_2(2,3dpp)]^{2+}$ **C-I**, $[Ru(dceb)_2(2,3dpp)PtCl_2]^{2+}$ **C-II** and $[Ru(dceb)_2(2,3dpp)PtI_2]^{2+}$ **C-III** show in the visible region only one separate absorption at λ_{max}= 464nm, 466nm and 482nm respectively. Figure 5.5 and Table 5.1 indicate that **C-I** shows a broad band with a

λ_{max} at 464 nm and a shoulder at 432 nm. The absorption band at 464 nm is red shifted with respect to about give full band 420 nm compared to **A-I**. The absorption spectrum of **C-II** shows broad absorption bands between 440 to 520 nm with a maximum in the UV at 350 nm assigned to transitions of the 2,3-dpp ligand and possibly also Pt / 2,3-dpp ^{1}MLCT transitions.

Other than, the absorption of the **A-II**, **A-III** and **B-II**, **B-III** dinuclear compounds the visible region gives two separate absorptions of λ_{max}, first a feature at 415nm and a second feature at 515 nm approximately, while the mononuclear compounds in both groups give one separate absorptions of λ_{max} at about 464nm, the peaks are very similar to each other. Table 5.2 illustrates the UV/Vis absorption spectroscopy results.

5.3.1 Photolysis of Compounds in Acetonitrile.

Compounds **C-I**, **C-II** and **C-III** were dissolved and photolysed in acetonitrile without the presence of TEA and irradiated for up to 3 hours. They were analysed by HPLC using a mobile phase of $CH_3CN/H_2O/CH_3OH$ (65/20/15) % containing 0.05 M KNO_3 and detection wavelengths of 280 nm and a flow rate 2.0 cm^3 min^{-1}. The temperature control was set at 24^{o}C. It was found that compound **C-I** is photo reactive and compound **C-II** photo stable. However, compound **C-III** is slightly photo reactive under these conditions. The photochemical processes were followed by HPLC, UV-Vis spectroscopy and ^{1}H-NMR spectroscopy.

5.3.1.1 Compound C-I

The photolysis of the mononuclear compound **C-I** is shown in Figure 5-7 and is characterised by using several analytical tools such as HPLC, UV-Vis spectroscopy and ^{1}H-NMR spectroscopy. Irradiation of this compound was carried out under the same conditions as outlined above and is shown in Figure 5-6 (a, b).

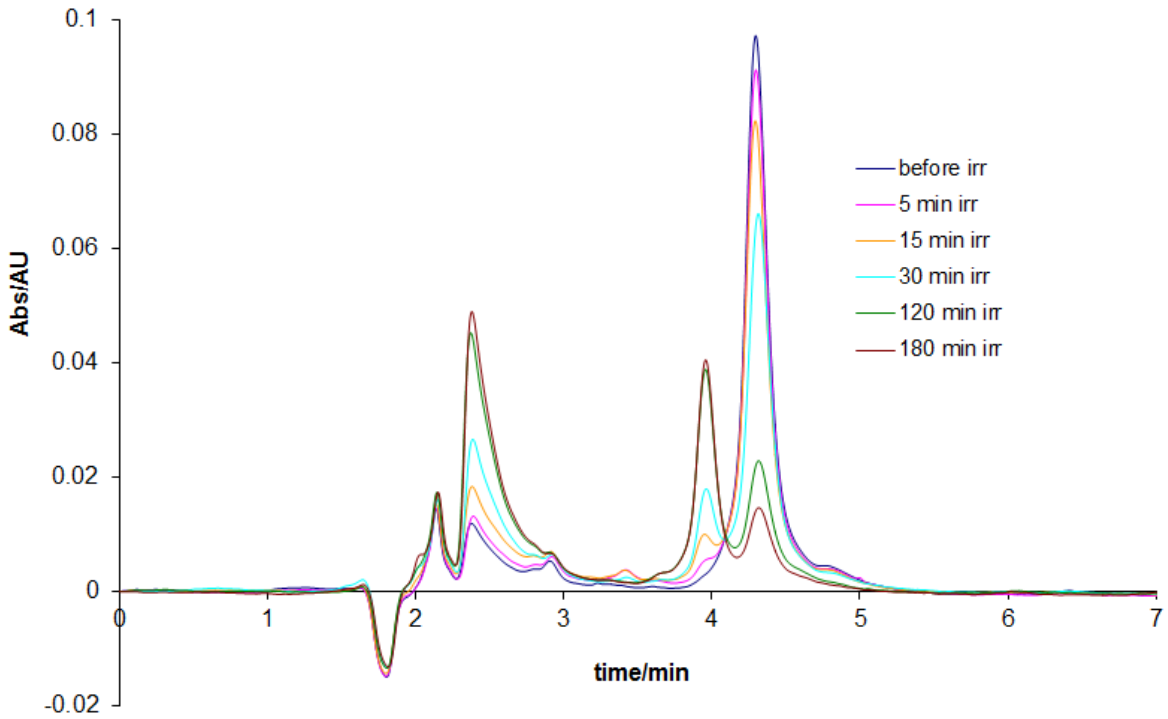

Figure 5. 6a: HPLC trace during Photolysis of $[(dceb)_2Ru(2,3dpp)]^{2+}$ in acetonitrile (mobile phase CH_3CN: H_2O: CH_3OH with volume ratio 65:20:15 containing 0.05 M KNO_3, Flow rate: 2.0 cm^3 min^{-1}; detection wavelength at 280 nm, T=24^{0}C.

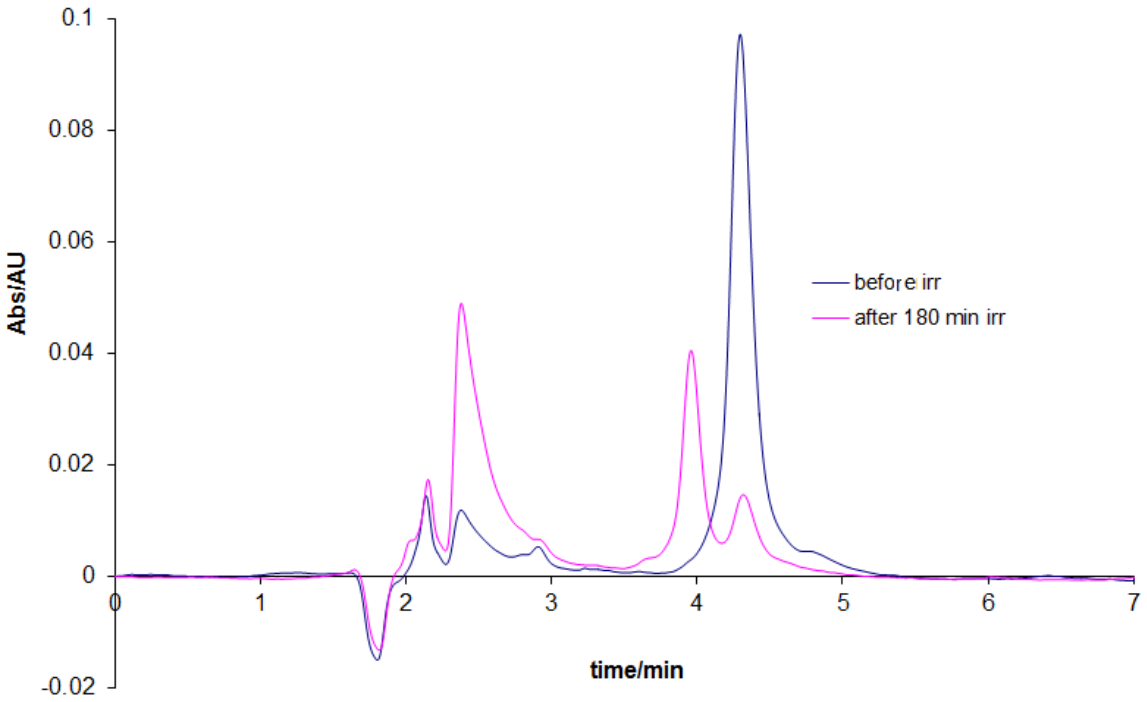

Figure 5.6 b: HPLC trace during Photolysis of $[(dceb)_2Ru(2,3dpp)]^{2+}$ acetonitrile (mobile phase CH_3CN: H_2O: CH_3OH with volume ratio 65:20:15 containing 0.05 M KNO_3 Flow rate: 2.0 cm^3 min^{-1}; detection wavelength at 280 nm, T=24^{0}C.

The HPLC chromatograms shown in Figure 5.6(a-b) at different time points during the irradiation, show clear signs of photolysis. There is constant reduction of the area of the main peak and two different peaks appear and keep increasing in area by increasing the duration of the irradiation. The UV-Visible absorption spectra of the all new peaks are shown in Figure 5.7. The main HPLC peaks appear at retention time of about 2.40 and 4.00 minutes and show UV/vis data at 464 nm for the main peak and a new signal at 452 nm. This may indicate that although the differences between the main and the new peaks are considerable, that both species have a similar detection wavelength.

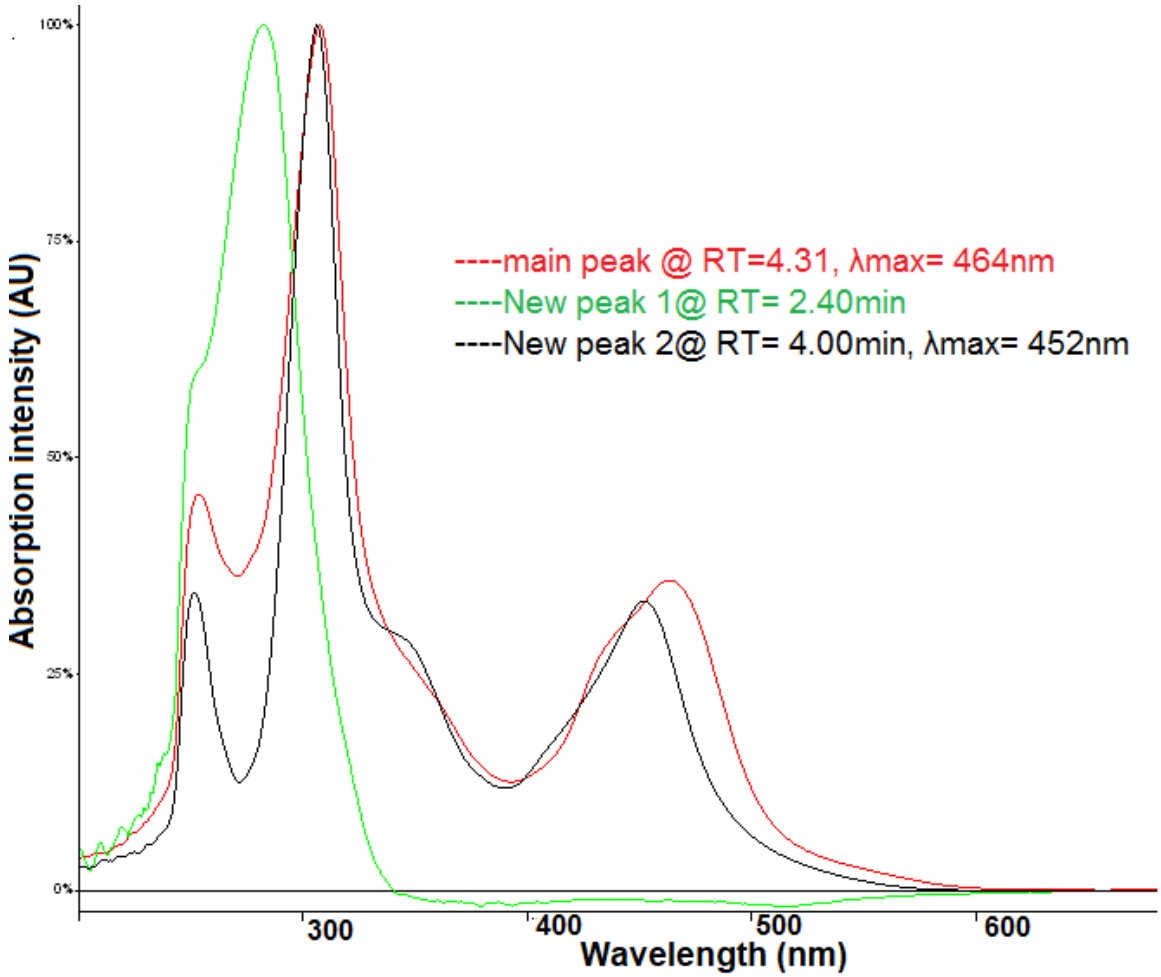

Figure 5.7**:** Absorption spectra of species detected in $[Ru(dceb)_2(2,3dpp)]^{2+}$ **C-I** after irradiation in Figure 5-6 (a, b) above. Detection wavelength 280 nm.

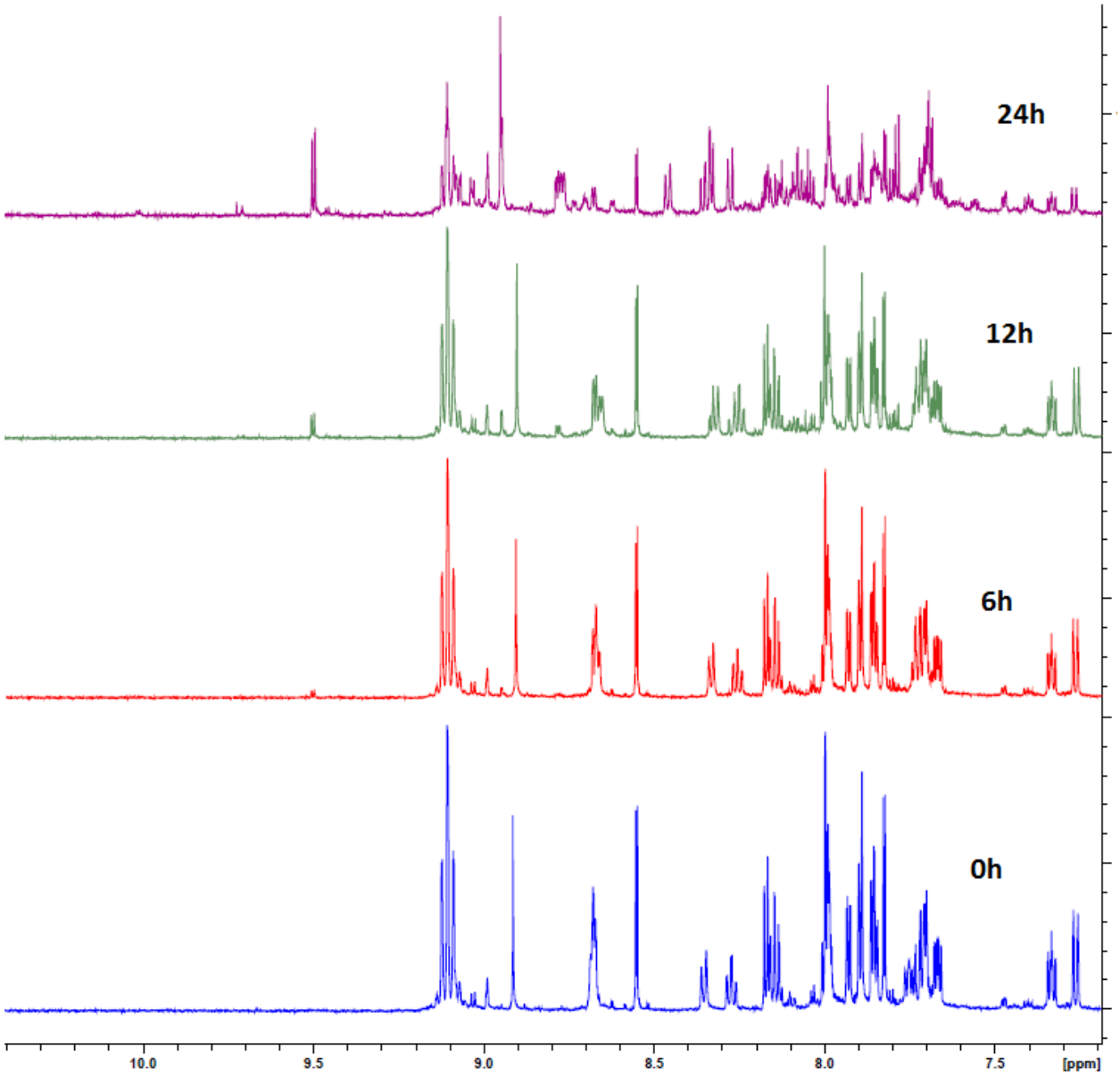

Figure 5. 8: ^{1}H-NMR study of $[Ru(dceb)_2(2,3dpp)]^{2+}$ **C-I** during 24 hours photolysis in acetonitrile-d_3.

^{1}H-NMR photolysis of compound **C-I** is shown in Figure 5-8 above. The obtained ^{1}H-NMR results shows some changes in chemical shift between 9.8 to 10.2 ppm and there are a number of signals that are increasing in height by the increase of the irradiation duration at 8.8 ppm, 8.42 ppm and 7.4 ppm. There are additional other peaks in the compounds that are decreasing as the irradiation time increases those can be seen at 8.7 ppm, 7.85 ppm and 7.6 ppm. When the

results of this group is compared with compound **A-I**, the compound **C-I** appears to be less stable upon irradiation. Unfortunately, not enough data are available to assign the various signals and further studies such as Mass spectrometry have to be carried out in order to fully understand the ^{1}H-NMR spectrum after irradiation. Overall the ^{1}H-NMR results indicate that **C-I** is more photoactive than **A-I** as the changes observed are more extensive and are observed earlier in the experiment as shown in Figure 5.8.

5.3.1.2 Compound C-II

The photoreactivity and stability of compound **C-II** is studied and the results obtained are shown in the Figure 5.9. The results obtained are were investigated using HPLC, UV-Vis spectroscopy and ^{1}H-NMR spectroscopy

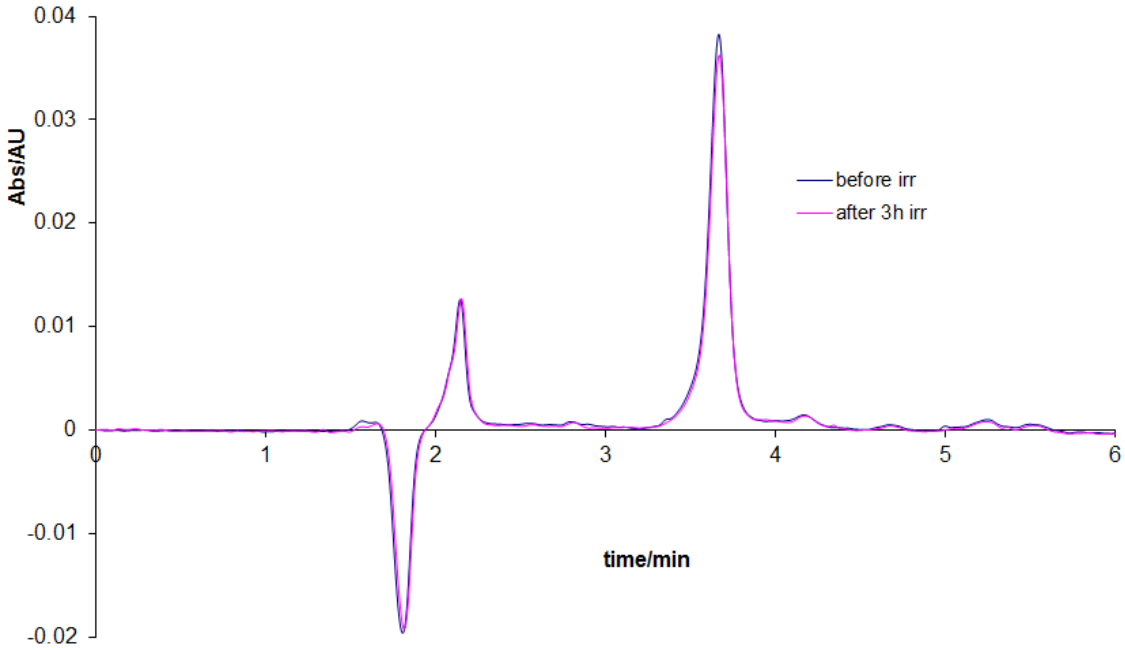

Figure 5.9**:** HPLC trace during Photolysis of for $[(dceb)_2Ru(2,3dpp)PtCl_2]^{2+}$ in CH_3CN mobile phase CH_3CN: H_2O: CH_3OH with volume ratio 65:20:15 containing 0.05 M KNO_3, Flow rate: 2.0 cm^3 min^{-1}; detection wavelength at 280 nm, T=24 ^{o}C.

Irradiation of the **C-II** compound was carried out in same conditions. The compound was irradiated for up to 3 hours.

The HPLC results obtained after photolysis of this compound is shown in Figures 5.9. As expected from the previous chapter, the HPLC trace during photolysis shows that under the conditions used in these experiments the compounds **C-II** is photostable for irradiation up to 3 hours period.

The ^{1}H-NMR spectra results shown in Figure 5-10 indicate that under the conditions used in these experiments **C-II** is photostable for up to 24 hours. The compound was irradiated in d_3-CH_3CN at higher concentrations. Increased irradiation times do not give any rise to longer irradiation times. The ^{1}H-NMR results are in agreement with HPLC results. Clearly, the results show that the compound **C-II** is photostable under the conditions used in these experiments.

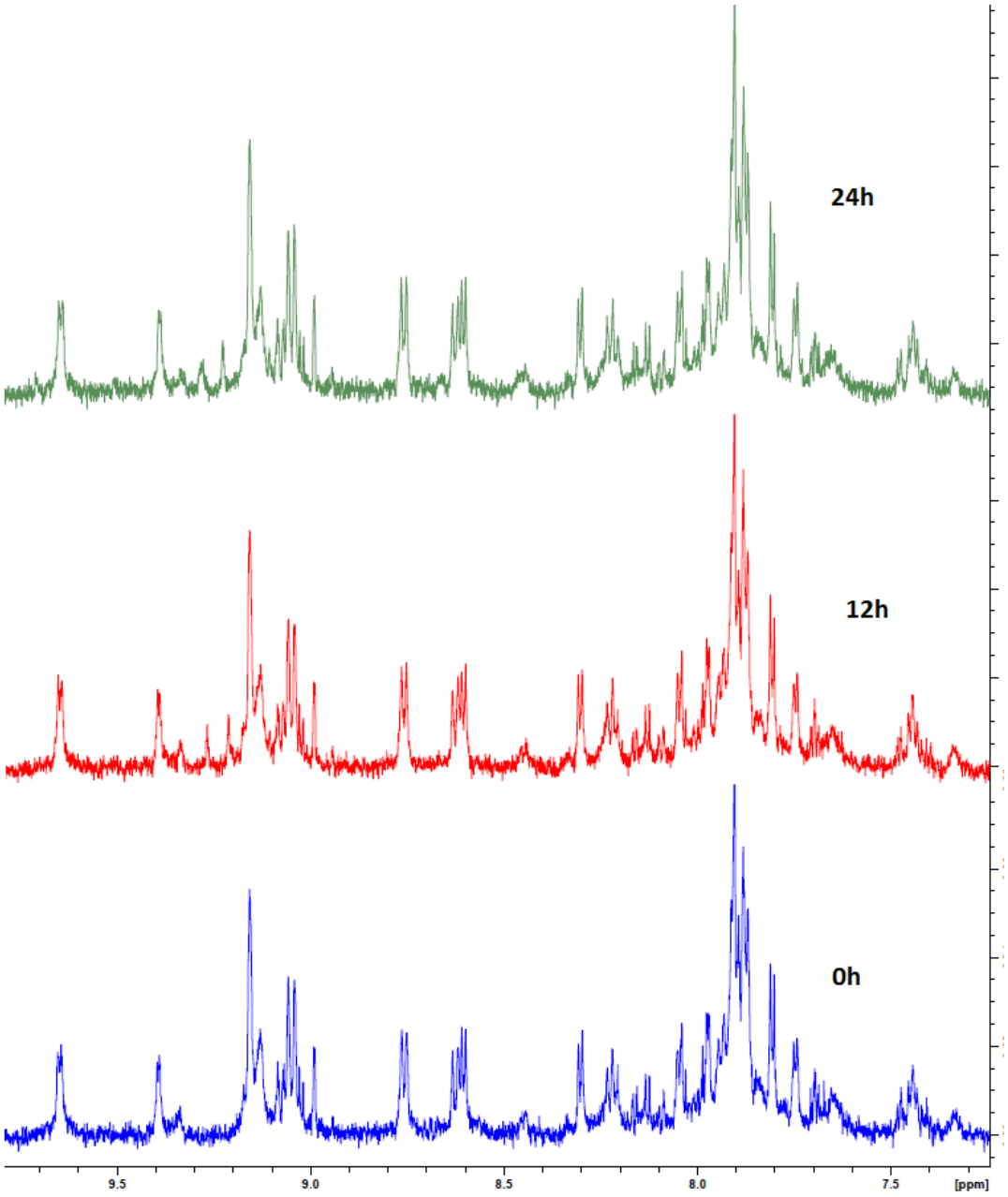

Figure 5.10: ^{1}H-NMR during Photolysis of $[Ru(dceb)_2(2,3dpp)PtCl_2]^{2+}$ **C-II** in acetonitrile-d_3.After 24 hours of radiation.

5.3.1.3 Compound C-III

Compound **C-III** was photolysed for up to 3 hours in acetonitrile. The photochemical processes were followed by HPLC, UV/Vis spectroscopy and ^{1}H-NMR spectroscopic, the results obtained are shown in Figure 5.11 a, b.

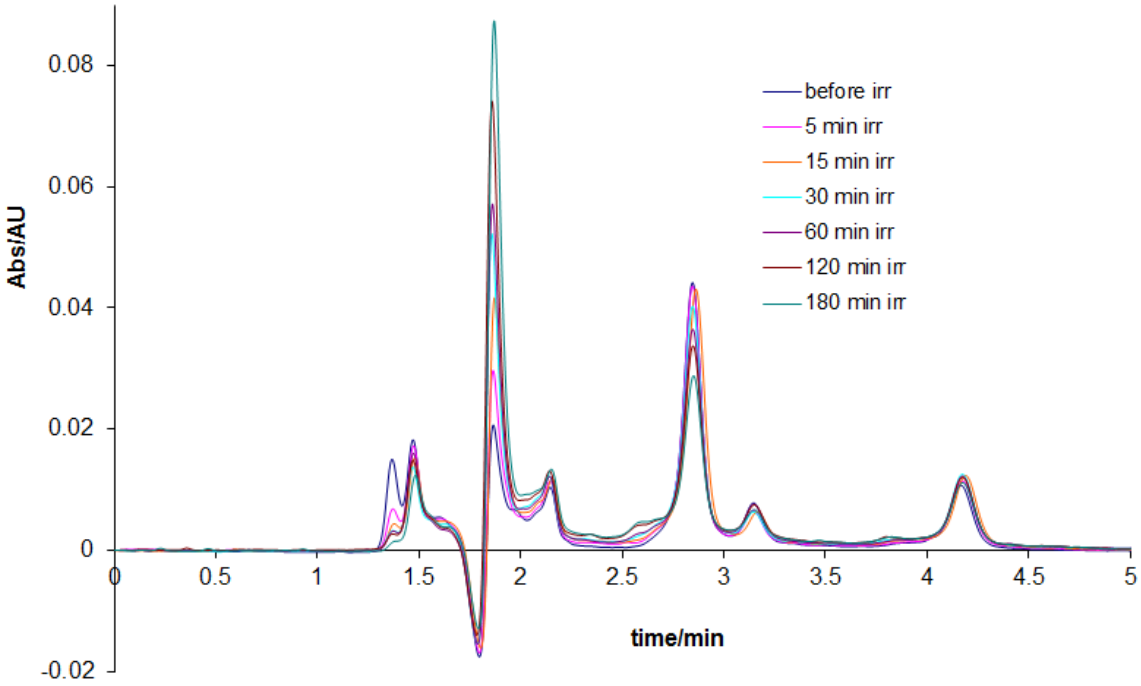

Figure 5.11a: HPLC trace during Photolysis of for $[(dceb)_2Ru(2,3dpp)PtI_2]^{2+}$ in CH_3CN (mobile phase CH_3CN: H_2O: CH_3OH with volume ratio 65:20:15 containing 0.05 M of KNO_3 Flow rate: 2.0 cm^3 min^{-1}; detection wavelength at 280 nm, T=24°C.

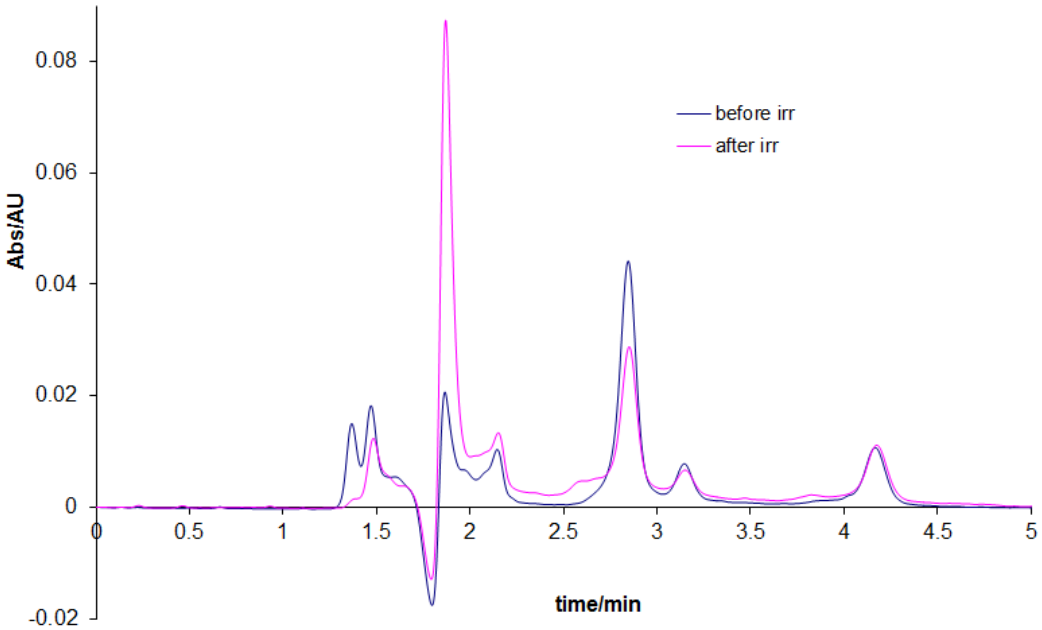

Figure 5.11b: HPLC trace during Photolysis of for $[(dceb)_2Ru(2,3dpp)PtI_2]^{2+}$ in CH_3CN (mobile phase CH_3CN: H_2O: CH_3OH with volume ratio 65:20:15 containing 0.05 M of KNO_3, Flow rate: 2.0 cm^3 min^{-1}; detection wavelength at 280 nm, T=24°C.

The photolysis of compound **C-III** was carried out under the same irradiation conditions as that of compounds **C-I** and **C-II.** The HPLC results at different time during the irradiation show that the compound clearly shows signs of photolysis. There is constant and quick reduction of the area of the main peak and very sharp peak appear at 1.87 minutes and continue increasing in the area by increasing the duration of the irradiation time. The UV/Vis absorption spectra of the new products is shown in Figure 5.12.

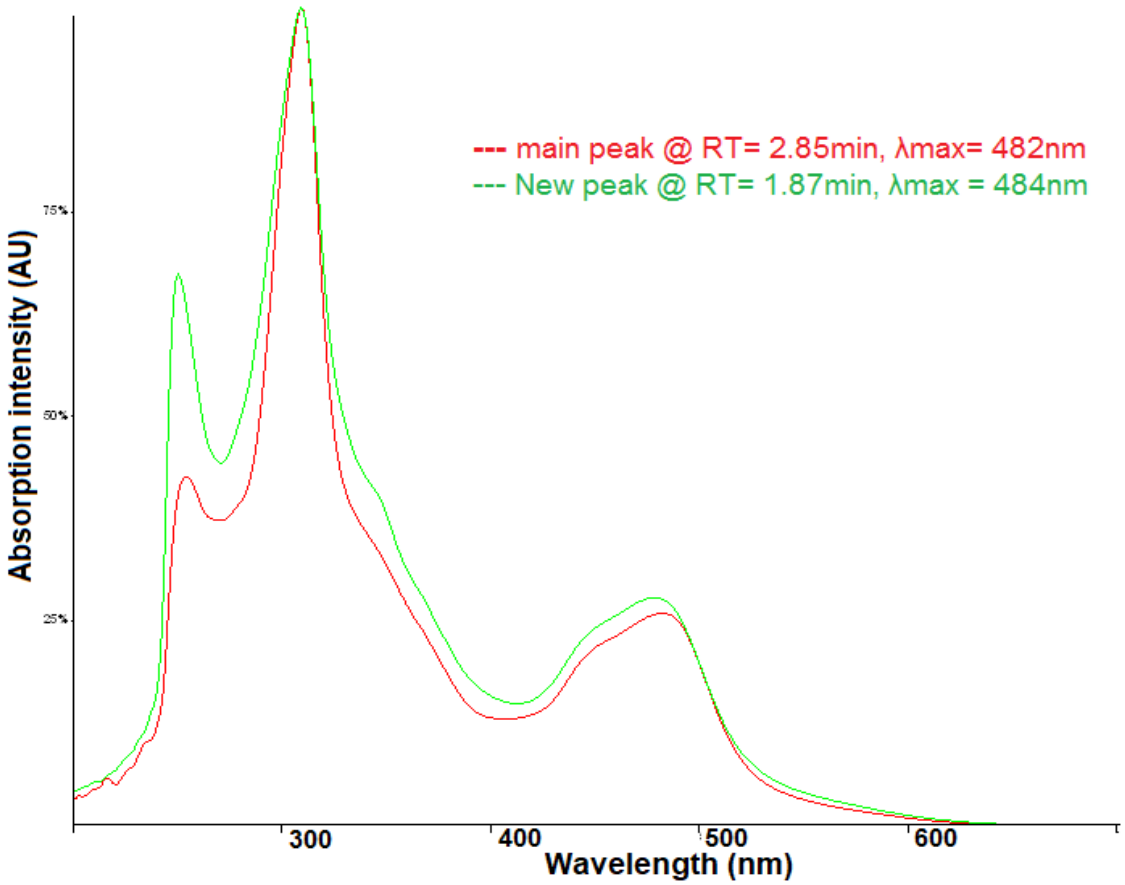

Figure 5.12: Absorption spectra of species detected in $[(dceb)_2Ru(2,3dpp)PtI_2]^{2+}$ **C-III** during irradiation in Figure 5-11 above. Detection wavelength 280 nm.

Two peaks are shown in Figure 5.12, both have a λ_{max} of 484 and 482 nm and retention times of 1.87 and 2.85 min respectively. Apart from these observations only a number of small amount of species are present as shown in Figure 5.12. Taking into account the similarity of the two peaks is seems likely that the original

pentanuclear compound $[((dceb)_2Ru(2,3dpp)PtI_2)_2Pt](PF_6)_4$ is transformed into a dinuclear compounds such as a $[(dceb)_2Ru(2,3dpp)PtIS)_2](PF_6)_2$ species, where S is a solvent as shown in Figure 5-13.[6]

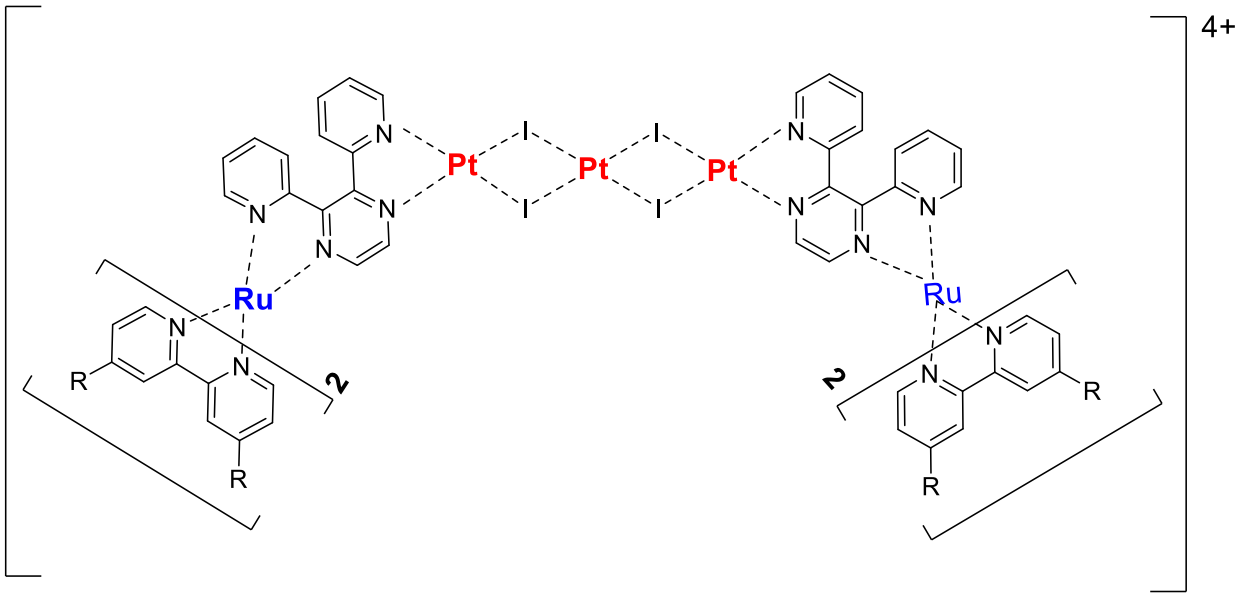

R= COOEt

---------- **tetranuclear compound** ----------

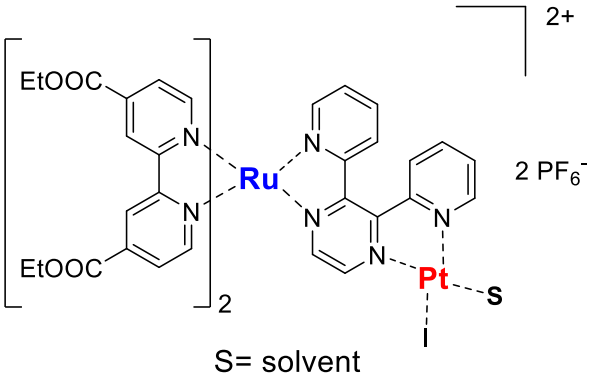

---------- **dinuclear compound** ----------

Figure 5. 13: The structure for the pentanuclear and dinuclear compounds.[6]

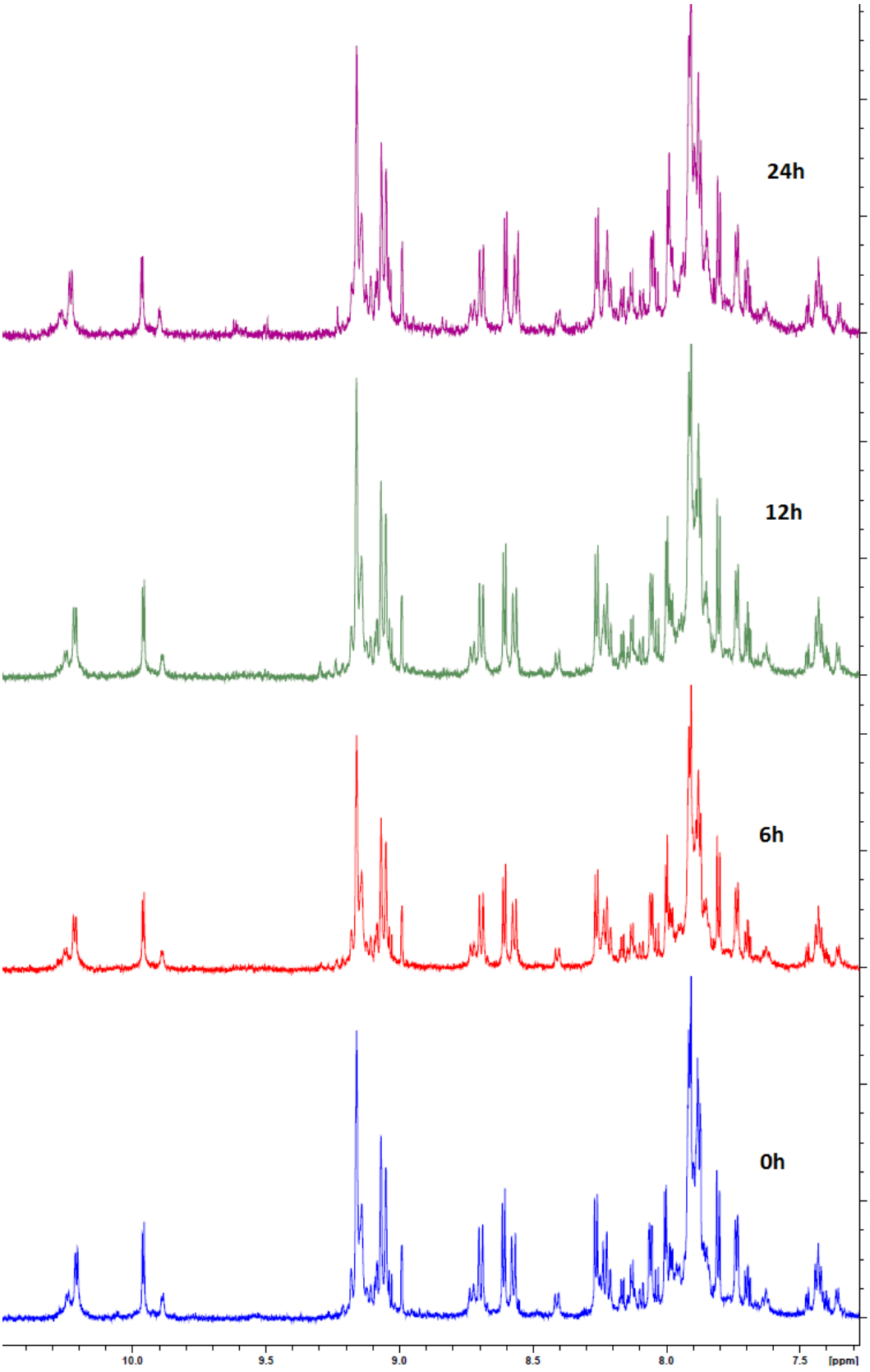

Figure 5.14: ^{1}H-NMR spectroscopy of $[(dceb)_2Ru(2,3dpp)PtI_2]^{2+}$ **C-III** during Photolysis in acetonitrile-d_3.

The photolysis of the compound was followed up by ^{1}H-NMR spectroscopy to obtain further information and results are shown in Figure 5.14. In addition, ^{1}H-NMR spectra indicate that after 24 hours **C-III** is still stable. No significant new peaks appeared in the spectrum. Observed are a number of very weak signals between 9.40-9.70 ppm with increasing radiation time as shown in the figure.
The ^{1}HNMR spectra illustrate that the photolysis of **C-III** does create some intermediates but these very difficult to determined. Obviously, the amounts of these species produced are too low to allow for definitive assignment.

The ^{1}H-NMR results are not in agreement with HPLC results. This is unexpected as the HPLC results show that the compound **C-III** is photoactive under the conditions used in these experiments.

5.3.2 Photolysis of Compounds C-I, C-II and C-III in the Presence of TEA.

The photolysis in absence of TEA has shown that only in acetonitrile the compounds **C-I** and **C-III** are photoreactive but that compound **C-II** is photostable for up to 3 hours under irradiation. In this section the photostability of the compounds **C-I**, **C-II** and **C-III** after irradiation in the presence of TEA is measured. The major difference between the two experiments is the addition of triethylamine to the solvent, which acts as a sacrificial reductant agent in the photocatalytic process.

5.3.2.1 Chromatographic Analysis

All compounds were dissolved in the eluent in CH_3CN) and filtered by a 0.45-micron filter prior to injection. The compounds $[(dceb)_2Ru(2,3dpp)](PF_6)_2$ (**C-I**) , $[(dceb)_2Ru(2,3dpp)PtCl_2](PF_6)_2$ (**C-II**), and $[(dceb)_2Ru(2,3dpp)PtI_2](PF_6)_2$ (**C-III**) were dissolved in CH_3CN with TEA and H_2O, were analysed using a HPLC mobile phase of $CH_3CN/CH_3OH/H_2O$ containing KNO_3. Where the percentage depends on the compound. HPLC detection wavelengths of 470 nm are used and a flow rate 2.0 cm^3 min^{-1}. The temperature control was set at 24ºC.

5.3.2.2 HPLC Behaviour of the Compounds Studied.

The chromatographic results of the compound **C-I**, compound **C-II** and compound **C-III** discussed in this chapter are similar to that observed for the compounds discussed in Chapters 3 and Chapters 4. It is clear that each of the compounds has a rapid reaction in the presence of the sacrificial agent TEA.

5.3.2.3 Results and discussion

5.3.2.3.1 Photoreaction of [(dceb)2Ru(2,3dpp)]2+ in the presence of TEA

The photochemical behaviour of **C-I** is outlined in Figure (5.15 a,b). The chromatographic shows that there is dominant peak at 3.27 minutes, attributed to compound **C-I.** There are however a number of small negligible peaks already present in the solution before irradiation. These are found at 1.54, 2.0, 2.23 and 5.18 minutes. Figure (5.15 a,b). shows the HPLC results of the compound **C-I** during the irradiation and display the initial and final compound after irradiation in the presence of acetonitrile and TEA. A small shift on the HPLC is also observed due to temperature variations. It is clear that the compound is not stable and the features observed are similar to those obtained for the compound in absence of TEA, but in the presence of TEA the amount of decomposition observed is large under this conditions, The peak height decreases to (65%) of concentration peak from (37mAU) to (24mAU) after 1 minutes and the broad peak at retention time (5.18 minutes) is growing up and shoulder at 4.80 minutes. In comparison with **A-I** and **B-I**, the chromatograms show that the products formed were shown as new well-defined peaks before the dominant peak of the main products as Figure 3.19 in Chapter 3 and Figure 4.16 in Chapter 4.

In addition, in the case of **C-I** the degraded products were found to have broad poorly-resolved peaks which can be justified by the role of ester group. It should be noted that the ratio of components of the mobile phases used for all compounds are different. At present there is no clear interpretation for the fast decomposition of the compounds, however, since the irradiation mixture used has

a considerable amount of which is basic decomposition can be expected.[ii] It is, therefore, likely that the peripheral ligands associated with the dceb ligands will present a considerable loss of ester components. In addition, the composition of the compounds generated is uncertain. As a result, further investigations such as Mass spectrometry, resonance Raman and electrochemical studies need to be carried out to further investigate these features. This may be the case for all three compounds investigated and it is unlikely that in the presence of TEA clear conclusions can be obtained. Therefore, the absorption spectra seen in Figure 5.16 cannot be interpreted.

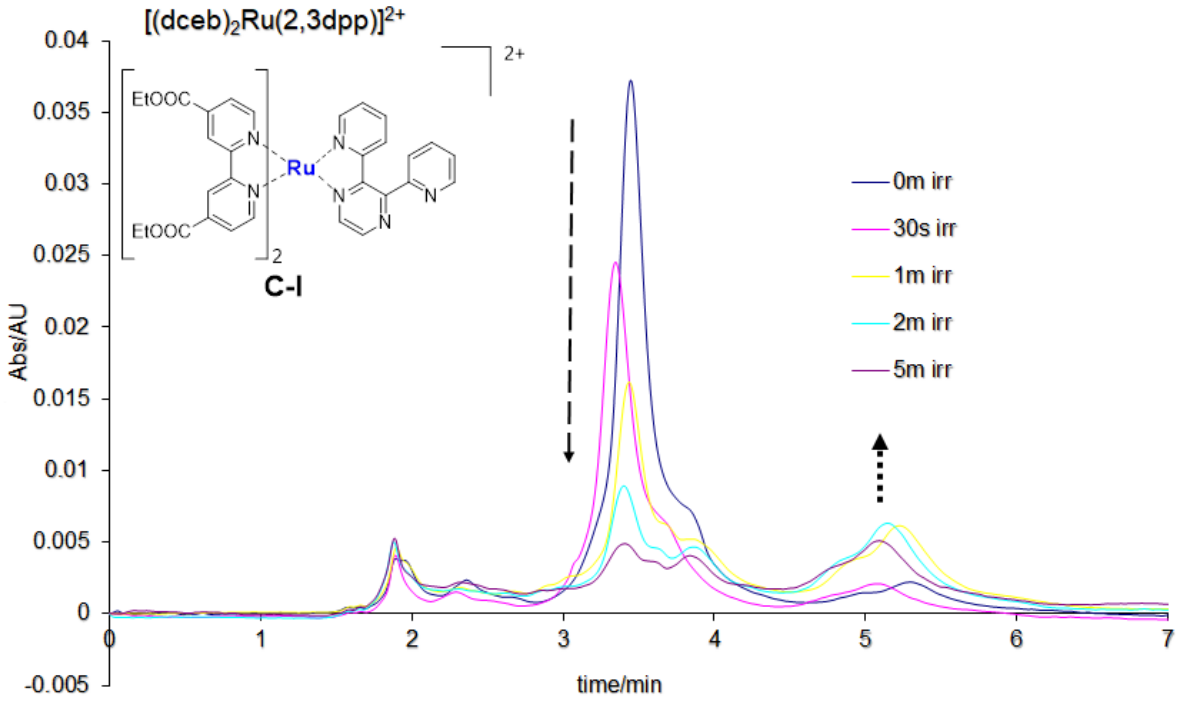

Figure 5.15a: HPLC traces obtained upon photolysis of compound **C-I**. Temperature 24ºC. Irradiated in CH_3CN in presence of TEA (15%) and H_2O (10%) using 470 nm LED irradiation; 5min degassing with Argon, irradiation detection wavelength; 470 nm, Mobile Phase CH_3CN:H_2O:MeOH 60:20:20 containing 0.06 M KNO_3 Flow rate 2.0 cm^3 min^{-1}.

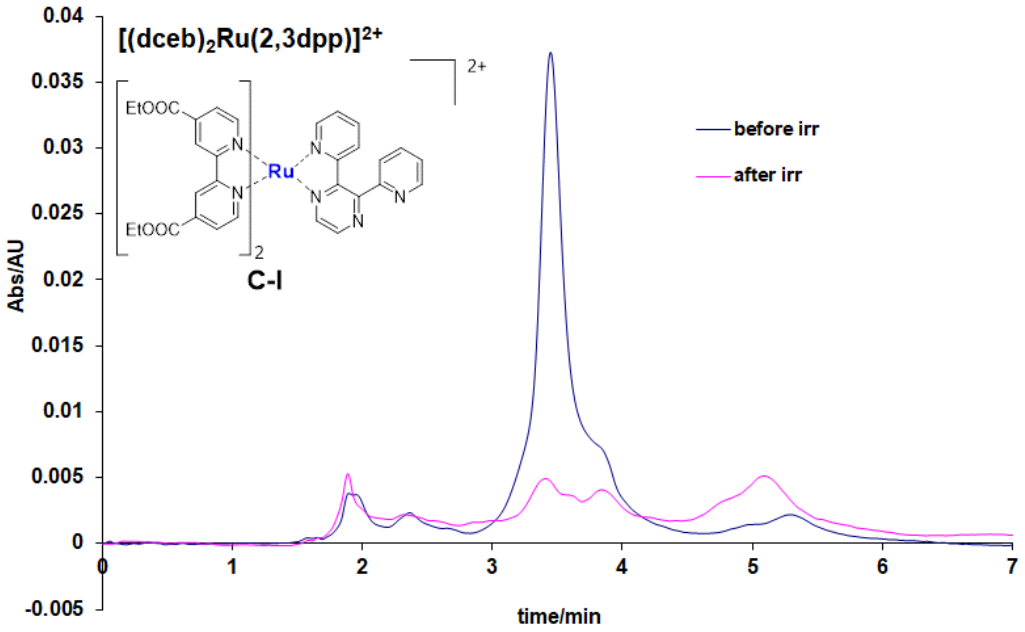

Figure 5.15b: HPLC traces obtained before and after photolysis of compound **C-I**. Temperature 24ºC. Irradiated in CH_3CN in presence of TEA (15%) and H_2O (10%) using 470 nm LED irradiation 5min) degassing with Ar before irradiation; detection wavelength; 470 nm, Mobile Phase CH_3CN:H_2O:MeOH 60:20:20 containing 0.06 M KNO_3 Flow rate 2.0 cm^3 min^{-1}.

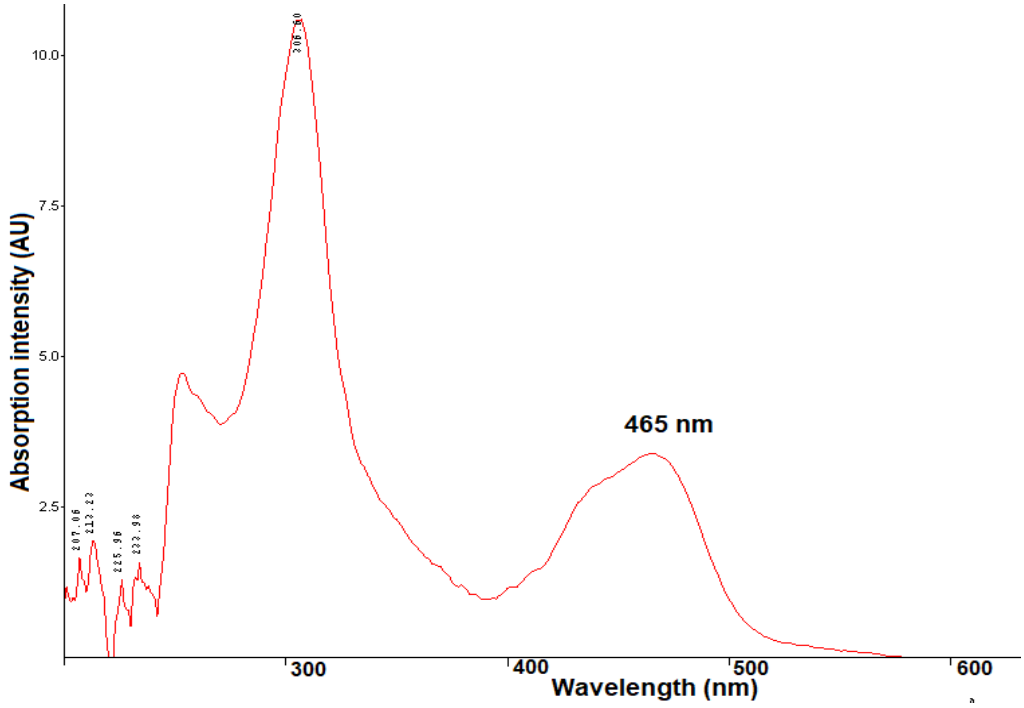

Figure 5.16 a.b: Absorption spectra of the new peak detected in compound **C-I**, RT @ 5.1 min After irradiation in Figure 5.15 above. Detection wavelength 450 nm.

The ^{1}H-NMR spectra results show in Figure 5-10 indicate that under the conditions used in these experiments **C-II** is photostable for up to 24 hours. The compound was irradiated in d_3-CH_3CN at much higher concentrations. Increased irradiation times do not give any rise to longer irradiation times. The ^{1}H-NMR results are in agreement with HPLC results. Clearly, the results show that the compound **C-II** is photostable under the conditions used in these experiments.

5.3.2.3.2 Photoreaction of [(dceb)2Ru(2,3dpp)PtCl2]2+ C-II in the presence of TEA

The chromatographic features observed for the compound **C-II** when sacrificial agent was added to the irradiated solution are shown in Figure 5.17 a,b below.

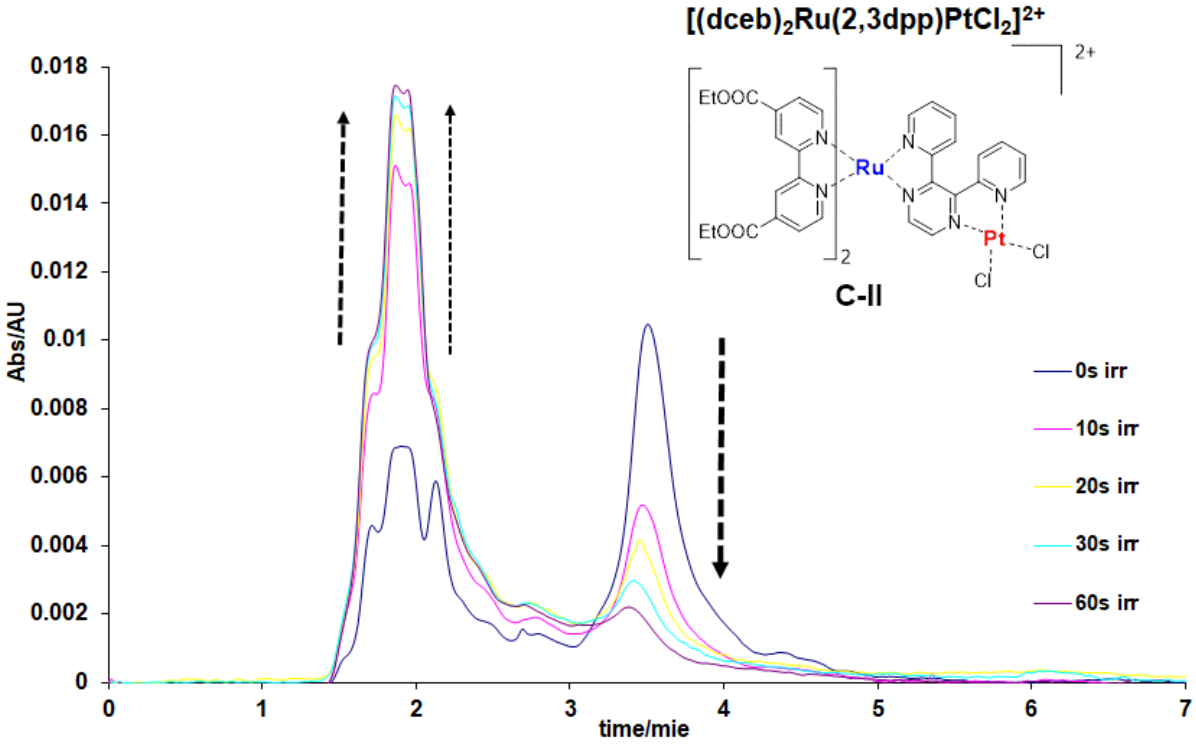

Figure 5.17a: HPLC traces obtained upon photolysis of **C-II**. Temperature 24^{o} C. Irradiated in CH_3CN in presence of TEA (15%) and H_2O(10%) using 470 nm LED irradiation; 5min degassing with Ar before irradiation detection wavelength; 470 nm, Mobile Phase CH_3CN:H_2O:MeOH 65:20:15 containing 0.04 M KNO_3 Flow rate 2.0 cm^3 min^{-1}.

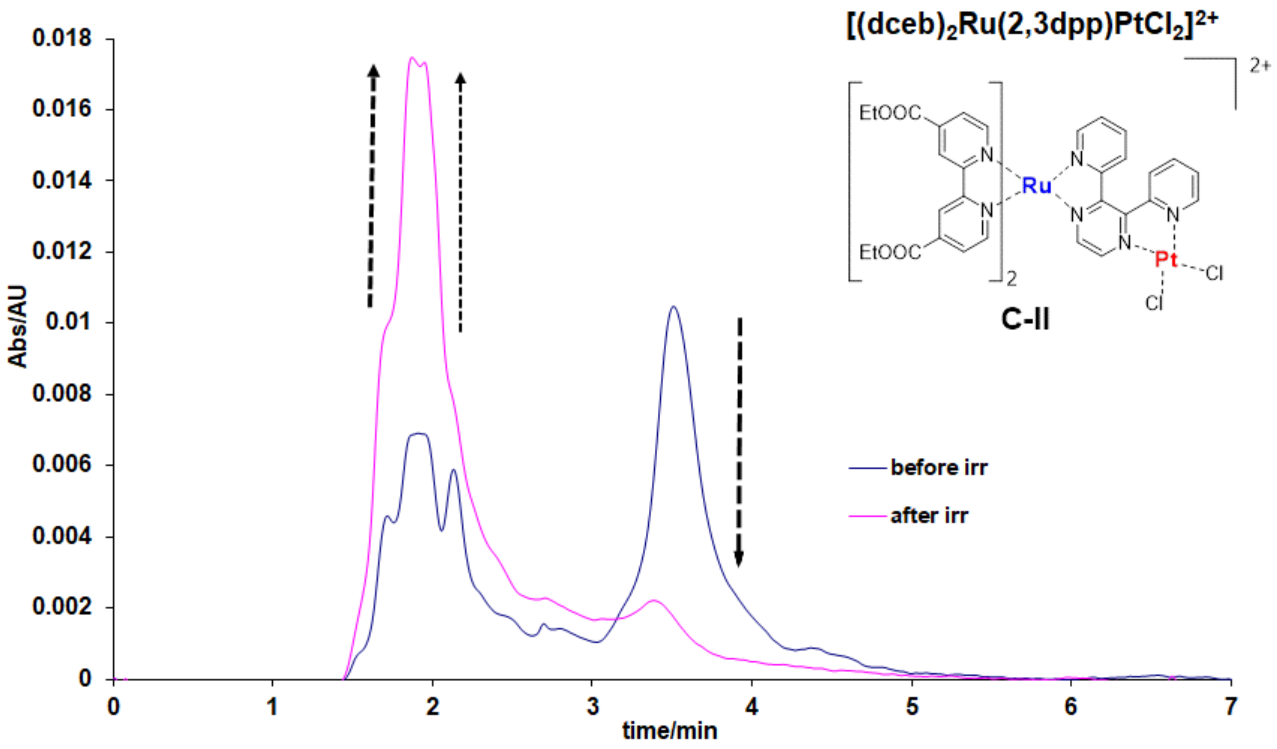

Figure 5.17b: HPLC traces obtained before and after photolysis of **C-II**. Temperature 24 ^{o}C. Irradiated in CH_3CN in presence of TEA (15%) and H_2O (10%) using 470 nm LED irradiation; 5min degassing with Ar before irradiation detection wavelength; 470 nm, Mobile Phase CH_3CN:H_2O:MeOH 65:20:15 containing 0.04 M KNO_3 Flow rate 2.0 cm^3 min^{-1}.

The chromatograms of compound **C-II** represent the photoreaction in the presence of TEA and CH_3CN before and after the irradiation process. The $[(dceb)_2Ru(2,3dpp)PtCl_2]^{2+}$ peak is detected at a retention time of 3.31 minutes together with number of synthesis related impurities that increased after the direct mix with the TEA [ii] and water even without irradiation at (1.41, 1.54, 2.00 and 2.10 minutes) of retention time and the absorption spectra of these species and main peak are show in Figure 5.18 below. After the irradiation, the impurities peaks increased significantly which result in more interference among them with

observable decrease in the main product concentration that resembles the degradation behaviour in **A-II** and **B-II** compounds. the absorption spectra of new products are show in Figure (5.18) below. However, as observed for the results obtained for compound **C-I** no significant features can be obtained as a result for the interaction of both the basic TEA and the contact with the HPLC column. [ii]

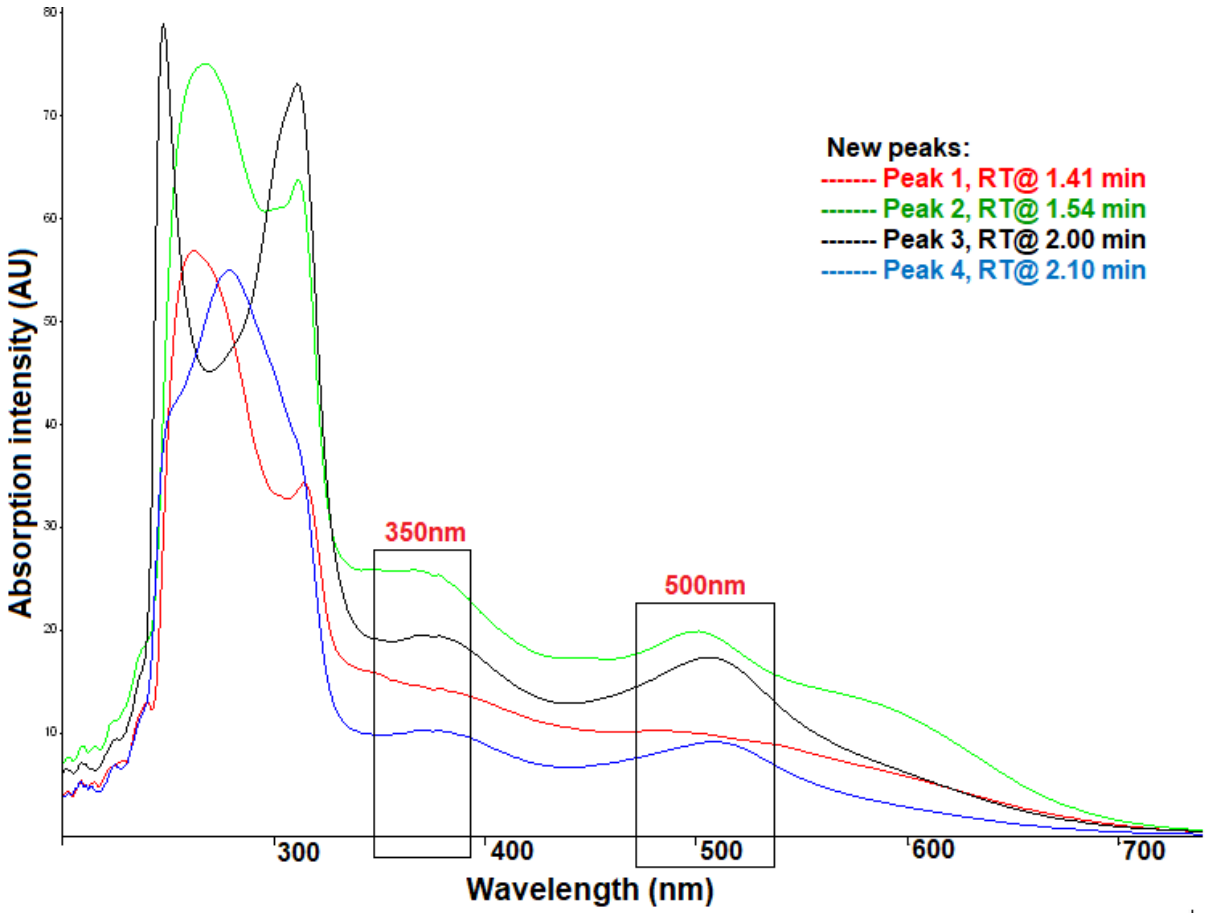

Figure 5.18: Absorption spectra of all new peaks detected in compound **C-II** After irradiation in Figure 5.17 (a, b) above. Detection wavelength 470 nm.

5.3.2.3.3 Photoreaction of [(dceb)2Ru(2,3dpp)PtI2]2+ C-III in the presence of TEA

The chromatographic features of **C-III** compound can show the dominant peak at retention time of 3.5 min. and three related impurities at 2.1, 2.5,2.8 min respectively and other minor impurities at 4.4min as shown in the Figure (5.19 a,b) and the absorption spectra of all small peaks detected and the main peak are show in Figure 5.20.

In the **C-III** compound, the chromatograms are quite different from the previous two compounds. Hence, the chromatograms show only the dominant peak of **C-III** compounds with other impurities which did not affect by the irradiation process. Only the main peak decreases to reflect the decrease of the concentration or the destruction of the product without the appearance of the degraded products as the Figure 5.19 shows. Also, these results can be considered different to **A-III** and **B-III** that the degradation products were detected on the chromatograms, this can be explained by the effect of the ester groups on the retention time of the degradation products.

Although, the chromatographic condition can detect the great change of the initial concentration before the irradiation and the almost completely degraded product (≈95%) after only 60 seconds of irradiation in the presence of TEA. However, in the absence of TEA the reaction is negligible after 3 hours of irradiation.

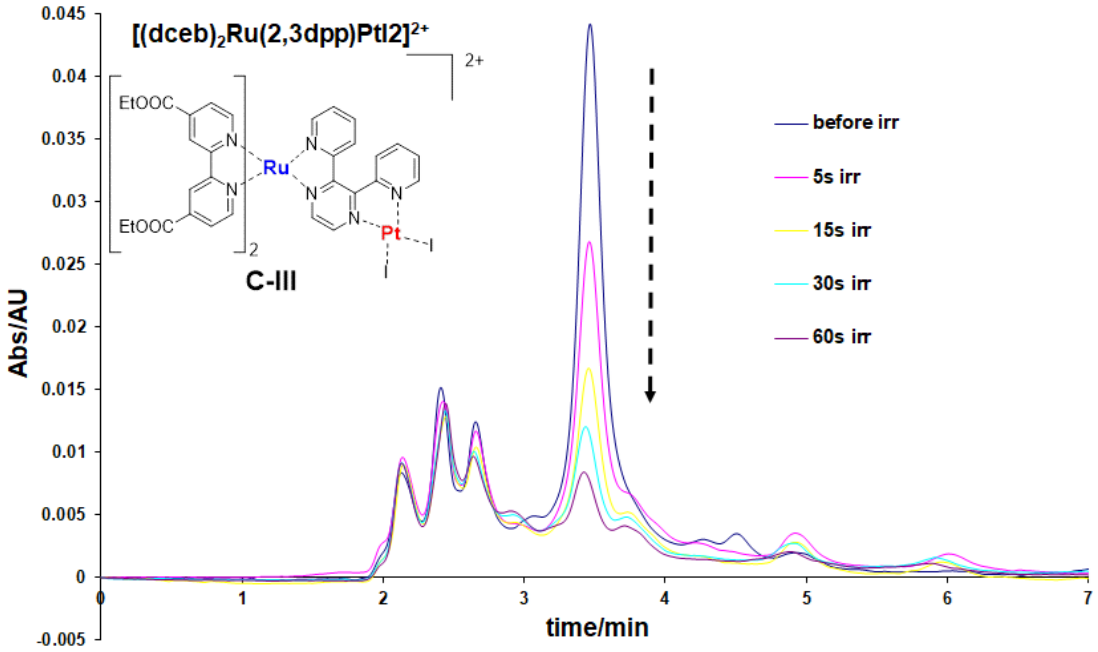

Figure 5.19a: HPLC traces obtained upon photolysis of **C-III**. Temperature 24 ^{o}C. Irradiated in CH_3CN in presence of TEA 15% and H_2O10% using 470 nm LED irradiation from (0-5min) degassing with Ar before irradiation detection wavelength; 470 nm, Mobile Phase CH_3CN:H_2O:MeOH 60:10:30 containing 0.06 M KNO_3 Flow rate 2.0 cm^3 min^{-1}.

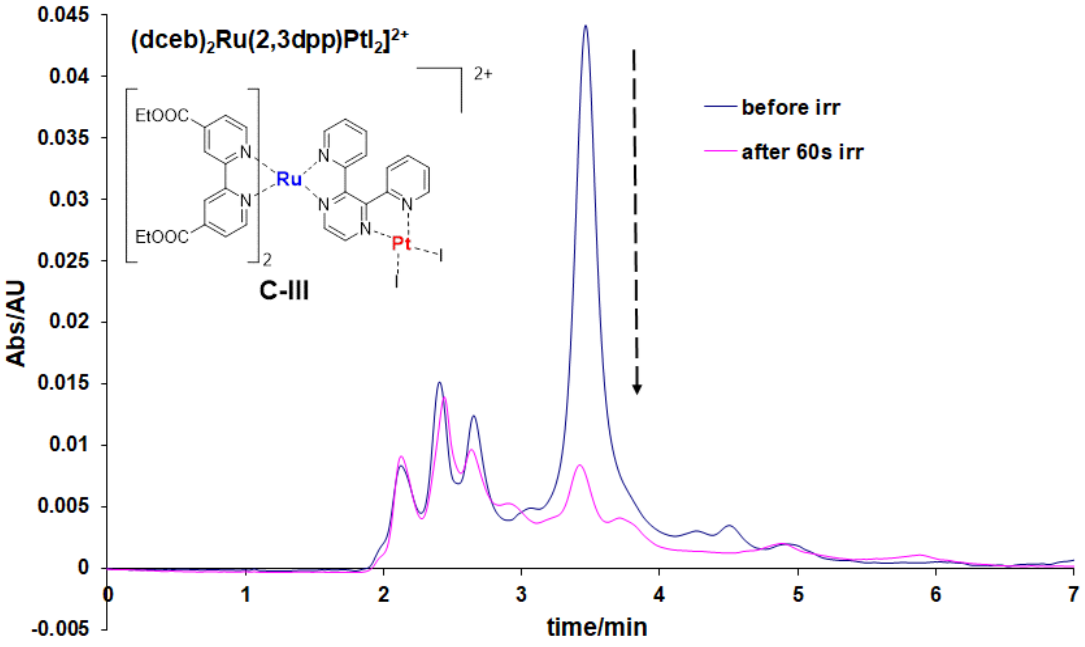

Figure 5.19 b: HPLC traces obtained before and after photolysis of compound **C-III**. T 24 ^{o}C. Irradiated in CH_3CN in presence of TEA 15% and H_2O 10% using 470 nm LED irradiation 5min degassing with Ar before irradiation detection wavelength; 470 nm, Mobile Phase CH_3CN:H_2O:MeOH 60:10:30 containing 0.06 M KNO_3 Flow rate 2.0 cm^3 min^{-1}.

5.4 Summary and conclusion

In this chapter, the characterisation and the stability of photocatalysts of $[(dceb)_2Ru(2,3dpp)]^{2+}$ **C-I**, $[(dceb)_2Ru(2,3dpp)PtCl_2]^{2+}$ **C-II** and $[(dceb)_2Ru(2,3dpp)PtI_2]^{2+}$ **C-III** were studied.

HPLC, UV/vis absorption spectra and ^{1}H-NMR of the compounds were obtained to compare the structural features and investigate the stability of the compounds as used in chapter 3 and chapter 4. In HPLC results, the retention time of the three major peaks are different due to the presence of the catalytic states (monomer/dinuclear) and the nature of the halogen (Cl^-/I^-) containing peripheral species. In the ^{1}H-NMR analysis for compound of group **C**, the same behaviour of the Iodide and chloride complexes is repeated, where the hydrogen adjacent to the Pt centre of the iodide complex shows a more upfield signal than the one adjacent to the chloride complex, these results have also been observed in previous chapters.

The stability of the compounds has been investigated upon irradiation in acetonitrile with LED 470 NM visible light, both in the presence and the absence of TEA as a sacrificial reducing agent. The compounds are irradiation for up to 3 hours in case of the absence of TEA. In the presence of TEA, the irradiation was carried out for varying durations but within minutes. Photolysis of Compounds in Acetonitrile in the absence of TEA found that the compound **C-I** is photo reactive and the compound **C-II** photo stable. However, the compound C-III is slightly a photo reactive under these conditions as shown in Figure (5,20).

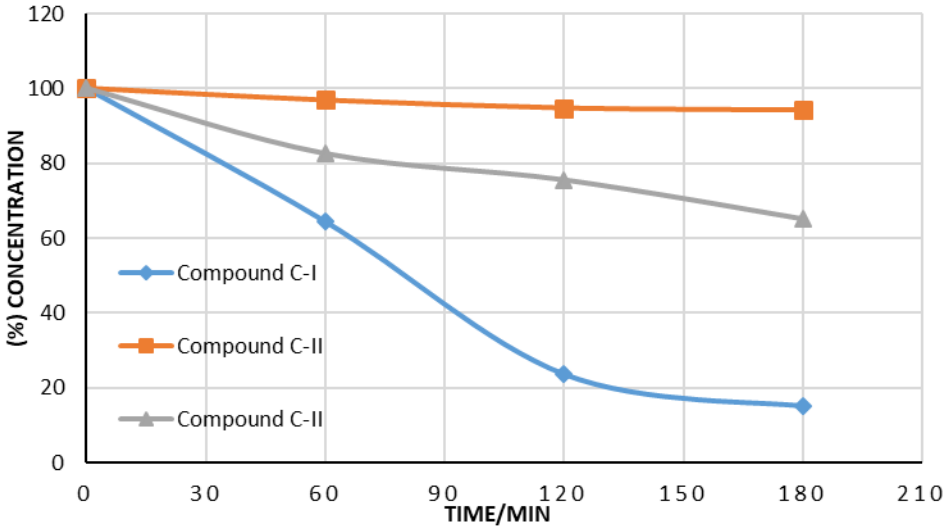

Figure 5.20: The rate of photo-degradation of compound **C-I**,**C-II** and **C-III** in the Absence of TEA.

The ^{1}H-NMR results are largely consistent with HPLC results for **C-I** and **C-II** and are not in agreement with **C-III**, this is unexpected as the HPLC results show that the compound **C-III** is photoactive under the conditions used in these experiments.

The photostability of the compounds **C-I, C-II** and **C-III** after irradiation in the presence of TEA is measured. The major difference between the two experiments is the addition of triethylamine to the solvent, the chromatographic results of the compounds discussed in this chapter is similar to that observed for the compounds discussed in Chapters 3 and Chapters 4. It was observed that each compound has a rapid reaction in the presence of sacrificial agent (TEA) as shown in Figure (5,21).

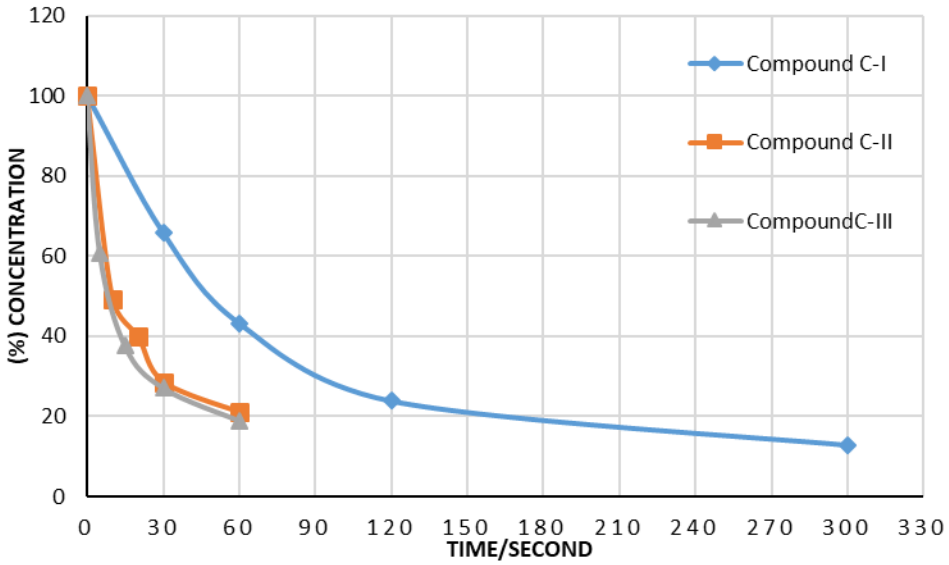

Figure 5.21: The rate of photo-degradation of compound **C-I**,**C-II** and **C-III** in the presence of TEA.

5.4 References

[1] J.G. Vos and M.T. Pryce, Photoinduced rearrangements in transition metal compounds ,Coord. Chem. Rev. (2010), 254, 2519–2532

[2] G. S. Bindra, M. Schulz, A. Paul, S. Soman, R. Groarke, J. Inglis, M.T. Pryce, W. R. Browne, S. Rau, B. J. Maclean, J. G. Vos, The effect of peripheral bipyridine ligands on the photocatalytic hydrogen production activity of Ru/Pd catalysts, Dalton Trans, (2011), 40, 10812-10814

[3] S. Soman, G. Singh Bindra, A. Paul, R. Groarke, J. C. Manton, F.M. Connaughton,, M. Schulz, D. Dini, C. Long, M. T. Pryce, J. G. Vos, Wavelength dependent photocatalytic H2 generation using iridium–Pt/Pd complexes. Dalton Trans (2012), 41, 12678-12680

[4] Q. Pan, F. Mecozzi, J. P. Korterik, D. Sharma, J. L. Herek, J. G. Vos, W. R. Browne, and A. Huijser, J Phys. Directionality of ultrafast electron transfer in a hydrogen evolving Ru-Pd based photocatalyst, Chem. (2014), 118, 20799-20806

[5] T. Kowacs, Q. Pan, P. Lang, L. O'Reilly, S. Rau, W. R. Browne, M. T. Pryce, A. Huijser, J. G. Vos. Supramolecular Bimetallic Assemblies for Photocatalytic Hydrogen Generation from Water. Faraday Discuss. (2015),185, 143 – 170

[6] T. Kowacs, L. O'Reilly, Q. Pan, A. Huijser, P. Lang, S. Rau, W. R. Browne, M. T. Pryce and J. G. Vos, Subtle Changes to Peripheral Ligands Enable High Turnover Numbers for Photocatalytic Hydrogen Generation with Supramolecular Photocatalysts, Inorg. Chem. (2016), 55, 2685−2690.

[7] Q. Pan, L. Freitag, T. Kowacs, J. C. Falgenhauer, J. P. Korterik, D.Schlettwein, W. R. Browne, M. T. Pryce, S. Rau, L. Gonzalez, J G. Vos, A. Huijser, Peripheral

ligands as electron storage reservoirs and their role in enhancement of photocatalytic hydrogen generation. Chem. Commun. (2016), 52, 9371-9374

[8] N. Das, G. Singh Bindra, A. Paul, J. G. Vos, M. Schulz and M. T. Pryce. Enhancing Photocatalytic Hydrogen Generation: The Impact of the Peripheral Ligands in Ru/Pd and Ru/Pt complexes. Chem Eur J (2017), 23, 1 – 9

[9] A. Paul, Ph.D. Thesis, Dublin City University, School of Chemical Science, 2011.

[10] F. Barigelletti, L. De Cola, V. Balzani, R. Hage, J. G. Haasnoot, J. Reedijk and J. G. Vos, 1989, 28, 4344–4350.

[11] W. R. Browne, M. T. Pryce, B. J. MacLean, M. G. Pfeffer, R. Groarke, G. S. Bindra, M. Schulz, S. Rau, J. G. Vos, S. Soman, A. Paul and J. L. Inglis, Dalt. Trans., 2012, 41, 13050–13059.

[12] J. Hu, J. Wang. H.Nguyen,N. Zheng, Beilstein J. The chemistry of amine cations produced by visible light photoredox catalysis. Org. Chem. 9, 1977-2001, 2013.

Chapter 6

Discussions, Conclusions and Potential Progress.

In this section a brief discussion about the results obtained in the thesis is given. The general behaviour of the compounds studied as given including the difficulties obtained. The behaviour of the compounds studied is described briefly and reasons for the decay of the varies compounds are discussed. For future work the use sacrificial agents is not recommended. Instead different approaches need to be developed for example by reducing the concentration of these agents that minimise the degradation of the photocatalysts studied. Without such an approach it is unlikely that stable solar cells well be developed unless the development of surface bound devices are developed. The immobilisation of surface bound photocatalysts is at present one of the most interesting options.

6.1 introduction

Over the last number of years there has been a great interest in the synthesis and characterisation of photosensitisers for the generation of hydrogen from sunlight. Most of these studies are carried out in solution and act as photocatalytic devices, based on the presence of a photosensitiser, a bridging ligand and a catalytic centre. However, sacrificial agents are required to re-reduce the metal centres that have been oxidised by photocatalytic devices. In most cases large amounts of sacrificial agents, such as triethylamine, TEA, are used in order to be able to investigate the amount of hydrogen that can be obtained. In these studies, the focus is more on the amount of hydrogen produced rather, than the effect that the sacrificial agent has on the stability of the photocatalysts. As a result, considerable amounts of decomposition do occur, for both the sacrificial agent TEA and the photocatalysts.

The purpose of these studies is to use three different photocatalysts that contain peripheral ligands but also metal centres, so that the behaviour of the compounds can be investigated systematically. It was hoped that by variation of the peripheral ligand the stability of the photocatalysts can be studied and similar results are expected from the metal photocatalysts. In this section the results obtained for the nine compounds are considered, compared and contrasted in order to suggest new directions for the improvement of the photocatalytic devices. In particular, the stability of the photosensitisers during irradiation was considered. The compounds studied are shown below in Figure 6.1.

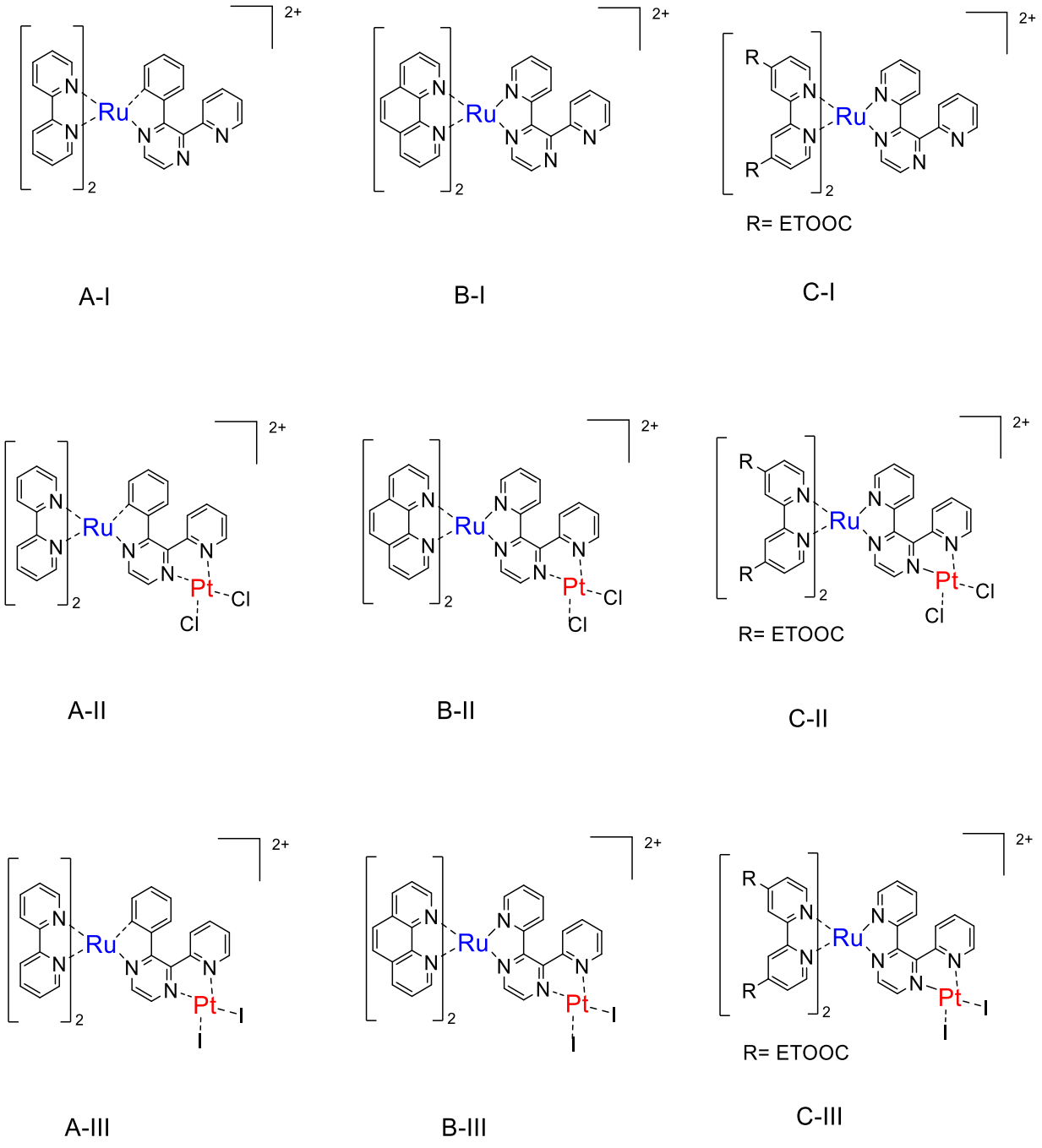

Figure 6-1:Photocatalytic compounds with 2,2'-bipyridyl,(bpy) 1.10-phenanthroline (phen) and 4,4'-diethoxycarbonyl-2,2'-bipyridine (dceb) .

Because of the fast decomposition of the compounds studied by the irradiation in the presence of TEA it is difficult to assess the structure of the HPLC compounds obtained. To give an example, the behaviour of compounds based on the 1,10-phenanthroline ligand is discussed. A problem with the compounds is the fact that over the years there has been very limited interest in the behaviour of l,10-phenanthroline type complexes. These type of compounds were studied in the 1980-1985 period, but as a result of the increased interest of 2,2'-bipyridyl compounds considerable less attention has been paid to ruthenium(II) phenanthroline compounds. During this period the synthesis of a number of mixed ligands, of the type $[Ru(phen)_2(L)]^{2+}$ were discussed. However, no photocatalytic studies were carried out and mostly the synthesis and characterisation of the compounds obtained was carried out. The only option to obtain information of the compounds is by the comparison between a number of the synthesised bis(phen)Ru type complexes prepared by by Durham *et al*. as shown in Figure 6-1 below and the UV/Vis spectra obtained by irradiation. [1]

Scheme 6-1: UV/Vis data from bis(phen) ruthenium complexes. [1]

Complex	UV/vis spectrum/ λ_{max} (nm)	
cis- $Ru(phen)_2(OH_2)_2^{2+}$	*469 (10.7)*	*264 (83)*
trans- $Ru(phen)_2(OH_2)_2^{2+}$	*500 (11.5)*	*266 (58)*
trans- $Ru(phen)_2(OH_2)(CH_3CN)^{2+}$	*467 (10.0)*	*264 (62)*
cis- $Ru(phen)_2(CH_3CN)_2^{2+}$	*420 (8.6)*	*383 (9.4)*
trans- $Ru(phen)_2(CH_3CN)_2^{2+}$	*442 (11.1)*	*263 (58)*
cis- $Ru(phen)_2(Py)_2^{2+}$	*445 (10.1*	*414 (11.0)*
trans- $Ru(phen)_2(Py)_2^{2+}$	*488 (12.0)*	*409 (6.4)*

The results obtained in the presence of TEA study indicate that a fast decomposition of **B-I** is taking place as shown in Chapter 4, Figure 4.16 a and b.

and Figure 4.17a shows the presence of a number of peaks with maxima of between 438 and 440 nm. This suggests that the monomeric **B-I** species is possibly in agreement with the excited states of the *trans* and *cis*- species of the ruthenium phenanthroline compounds shown in Scheme 6-1. As pointed out in the case for **B-I** and also for compound **B-II** a fast decay of the HPLC peak at about 4 min in the presence of TEA is observed, while a series of other features are observed. One unusual observation are the 3 sharp peaks that are formed fast during irradiation and it is possible that based these three peaks for the formation of the unusually shaped $[Ru(phen)_2(CH_3CN)_2]^{2+}$ compounds are obtained. At this stage, however, no direct assessment can be made concerning the nature of these observations. But as shown in Chapter 4, Figure 4.19 a number of wide range of components can be considered be related to compounds such as $[Ru(phen)_2(H_2O)_2]^{2+}$ a species that also has a λ_{max} value of about 500 nm. For other compound similar observations can be made. There are however a range of similar options in this case with a λ_{max} values of between 460 and 467 nm can be observed. This brief assessment shows that it is rather difficult to determine the composition of the compounds obtained used in Chapter 4, especially when irradiation techniques containing TEA are used.

In these studies, the irradiation of the compounds were divided into two species, without and with TEA. In addition, ^{1}H-NMR studies were also carried out. Irradiation without TEA for the **A** section compounds was carried out for 180 min and indicates that compounds **A-II** and **A-III** are stable under these conditions, but a small fraction of the **A-I** species shows a small reduction. For the **B** section similar results are obtained over a 180 min irradiation, but with a reduction of

about 20% for **B-I** and the formation of a small number of small peaks for both **A-I** and **B-I**. While, in the compounds of group **C**, the results obtained after 180 min irradiation are comparatively similar to compound group **A** and group **B**, it was found that the compound **C-I** is photo reactive and compound **C-II** photo stable. However, compound **C-III** is slightly photo reactive under these conditions. But there is a significantly reduction on by the area of the main peak in compound **C-I** by comparison with **A-I** and **B-I** and two different sharp peaks were appeared. The compound **C-II** is completely similar to **A-II** and **B-II**, as for the compound **C-III** higher frequency than **A-III** and **B-III** and only one sharp peak was appeared. These observations show that irradiation of the compounds irradiated without TEA are mostly stable.

When irradiation in the presence of TEA is carried out a very different behaviour is observed for the **A, B** and **C** group. Within 5 minutes the main peaks observed at 8.55 min and 6.30 min have almost disappeared in particular for **A-I** and **B-I,** some new peaks are observed for both compounds. These peaks are well defined and UV/Vis spectra (see Chapter 3and 4, Figures 3.19 and 4.16) and both compounds indicate that the peaks observed may be associated with products such as $[Ru(bpy)_2(CH_3CN)_2]^{2+}$and $[Ru(bpy)_2(CH_3CN)Cl]^{+}$. In the case of **C-I**, the amount of decomposition observed is large within 5 min but the degrading products were found to have broad poor-resolute peaks other than **A-I** and **B-I** (see Chapter 3 and 4 Figures 5.15). For compounds **A-II** and **B-II** again only irradiating for about 5 min is needed and only 1 min irradiating is needed for **C-II** (see Chapter 3 and 4 Figures 3.24, 4.18 and 5.16 respectively). During that period a large number of ill-defined peaks arise and it is not possible to identify

conclusively how the peaks observed can be determined. The irradiation for compounds **A-III**, **B-III** and **C-III** is very fast in the presence of TEA. The results show a great change of the almost completely degraded products after only 20 seconds, 30 seconds and 60 seconds respectively as shown in Chapters 3,4 and 5 and Figures 3.26, 3.20 and 5.19).

Apart from the HPLC studies ^{1}H-NMR experiments were also carried out. Spectra were obtained for the compounds **A-I** to **A-III**. Upon irradiation of compound **A-I** the spectrum obtained before irradiation, has been turned into a complex most likely $[Ru(bpy)_2(CH_3CN)_2]^{2+}$ as shown in Chapter 3, Figures 3.10 and 3.9. For spectra **A-II** and **A-III** small changes were observed for compound **A-III** only. For the phenanthroline based compounds the **B-I** spectrum degrades after 24 hours and again a spectrum obtained suggest the presence of $[Ru(phen)_2(CH_3CN)_2]^{2+}$. But compound **B-II** is found the be stable over the same time span. The last spectrum **B-III** again degrades and a phenanthroline type compound is most likely assigned to the formation of $[Ru(phen)_2(CH_3CN)_2]^{2+}$. This compound may be present, but alternative species such as $[Ru(phen)_2(CH_3CN)S]^{+}$ where S = solvent and their bpy analogues have also been observed. This observation will be discussed below.

There are surprises, during the ^{1}H-NMR irradiation, for example, during the irradiation of compound **A-I**, as shown in Chapter 3 Figure 3.12 in the ^{1}H-NMR spectra obtained the bridging ligand replaced with a non-deuteriated acetonitrile and compounds such as $[Ru(phen)_2(CH_3CN)_2]^{2+}$ are obtained. This is surprising since apart from deuterated acetonitrile no other non-deuterated acetonitrile has

been added. It is therefore unexpected that the compounds obtained are not deuterated. However, in general the presence of non-deuteriated acetonitrile has been ignored and Schemes such as shown below are generally used for the understanding of the behaviour of a typical RuPt photocatalyst.

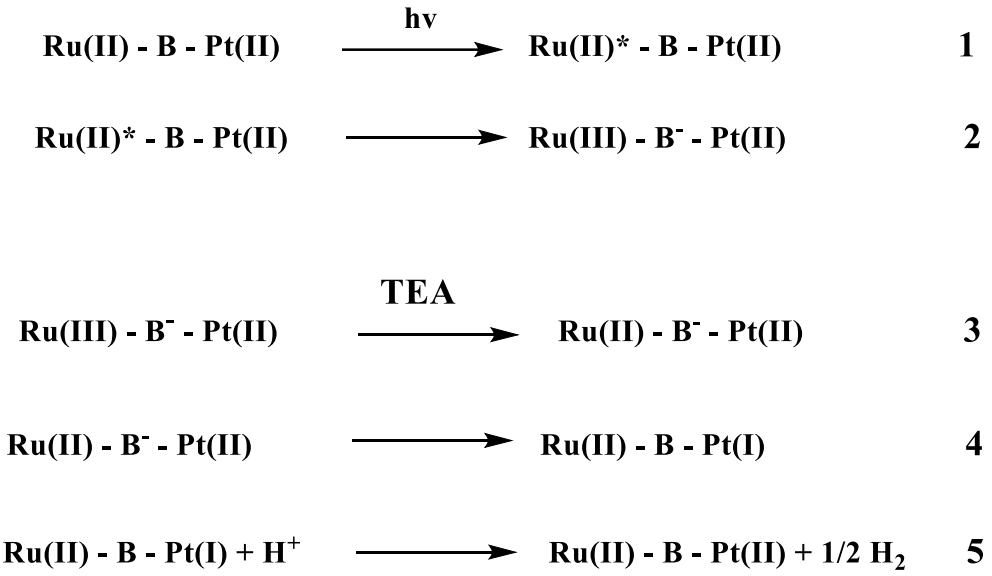

Scheme 6.2: Example of the reaction pathway for hydrogen generation by a RuPt photocatalyst. B = bridging ligand.

This Scheme is widely used, but it is incorrect, but it is generally used for simplicity but the presence of TEA is more or less ignored. However, for many years, interest in the study of such photoinduced transfer reactions or sacrificial agents in metal containing complexes have been carried out. A number of compounds have been studied in the 1970s. [2,3,4,5] From the 1973s on, many studies have been investigated, utilising organic compounds such as triphenylamines N,N'-dimethylaniline (DMA) and triethylamine in the investigation of light induced electron transfer reactions. The main reason for these studies is the investigation of transition metal compounds and the potential ability of

compounds such as TEA to act as sacrificial donor for the study of back-electron transfer agents. However, these studies clearly indicate that as a result of irradiation, the metal compounds studied, show strong back-electron transfer reactions and in that case reversible photo processes are not observed. [6] Scheme 6.3 outlined below gives an example of how the disproportion of radicals formed upon the decomposition of TEA radicals during photolysis.

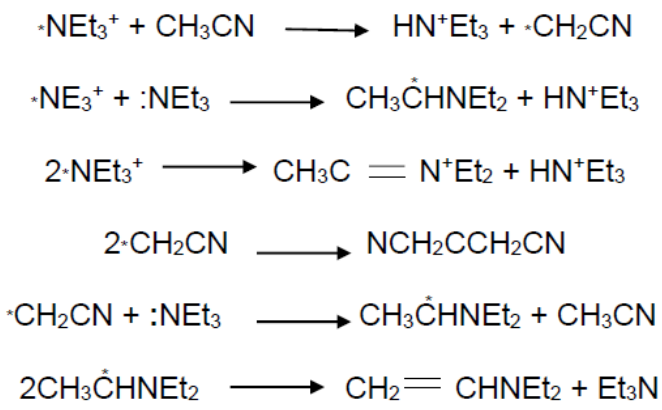

Scheme 6.3: A typical electron transfer arrangement after irradiation of Ruthenium polypyridyl complexes with triethylamine. TEA [7]

In these studies, it is also observed that the compound most formed during the catalytic process is acetaldehyde.[3,8] Nevertheless, rather high concentrations of TEA of 1. 3 M, were used in the photocatalytic studies carried out and TEA remains an of the most used quencher reductants in the investigation of ruthenium photocatalysts. However, differences between the concentrations used for photocatalysts and TEA tend to be applied. I typical example of an elegant detailed investigation of the quenching of photocatalytic compound by TEA is shown in Scheme 6.4.

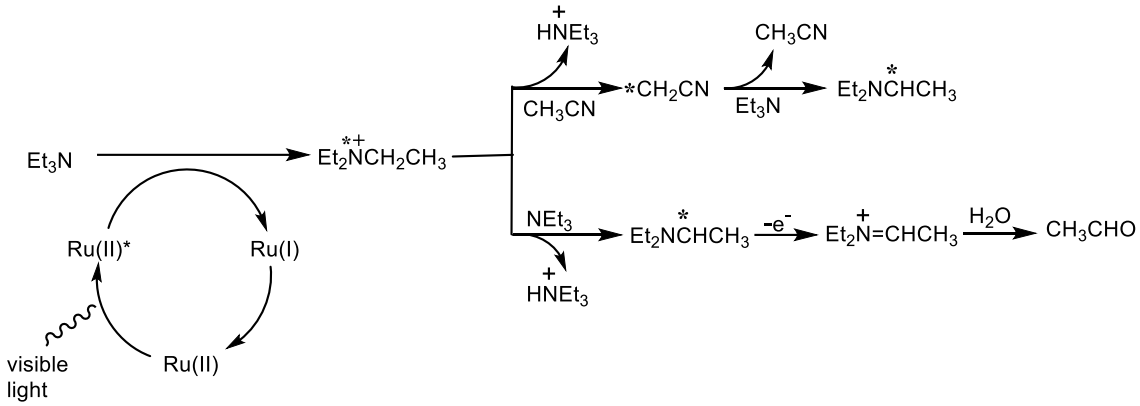

Scheme 6.4: An example of a reductive quenching of photoexcited Ru complexes in the presence of TEA. [9]

6.2 Future Work.

These observations clearly indicate that the use of TEA and other similar reductive quenching agents is not to be recommended. However, they are still applied extensively, regardless of the uses observed for TEA on its decomposition problems This problem has so far not been overcome and as a result the study of solar driven hydrogen generation using sacrificial agents needs to be reconsidered.

As outlined above when compounds such as **B-I** are irradiated in deuteriated acetonitrile the the ^{1}H-NMR spectrum indicates the presence of $[Ru(phen)_2(CH_3CN)_2]^{2+}$ but the ligand attached is not deuteriated as shown in the Scheme 6.4 and the solvent of irradiation is. One interesting observation has been that during the photocatalytic process compounds such as acetaldehyde, CH_3CN and other radical cations were observed as outlined in Scheme 6.4. This observation is explained by the fact that acetonitrile deuterons are exchanged by

protons from TEA in a radical reaction cascade with TEA radicals. The latter are formed upon reductive quenching of the excited photosensitizer. Interestingly deuterons, the nucleus of a deuterium atom consisting of a proton and a neutron. are exchanged by protons from acetonitrile and deuterons are exchanged by protons from TEA in a radical reaction cascade with TEA radicals.[9] An example of a such a reductive quenching of photoexcited Ru complexes is shown below in Scheme 6.4 where CH_3CN is also formed is this process.[9] This observation is important, since d_3-acetonitrile can be transformed into non deuteriated CH_3CN as is observed. As a result of these reactions, complications are considerable and alternative solutions need to be found.

In this thesis this change from deuterons to protons may yield the formation of useful targets for ^{1}H-NMR studies and a number of interesting novel compounds have been reported. A number of the compounds studied in this thesis have shown that upon irradiation deuteron ability to and create, most likely, their transformation into non deuteriated CH_3CN. It is clear, however, that in order to be able to use sacrificial agents in the efficient manner, different approaches, for example, by reducing the concentration of these agents that minimise the degradation of the photocatalysts studied. In addition, different solvents, bridging ligands and catalytic centres are needed. Without such an approach it is unlikely that stable solar cells well be developed unless the development of surface bound devices are developed.

6.3References

[1] P. Bonneson, J.I. Walsh, W.T Pennington, A. W. Cordes and B. Durham, Inorg. Six-Coordinate Complexes with 1, 10 -Phenanthroline Ligands in the Trans Configuration. Preparation of trans -Bis(l,10-phenanthroline)ruthenium(II) Complexes and Crystal Structure of trans-Bis(l,10-phenanthroline)bis(pyridine) Ruthenium (II) Hexafluorophosphate. Chem. 1983, 22, 1761-1765.

[2] A.A. Provatas, G.AS. Epling, J.D. Stuart, and A. Yeudaakimau. Selective Photoreduction of acetonitrile to acetaldehyde in dilute aqueous solutions. Toxicological and Environmental, Chemistry, 2014, 96, 3, 353-361

[3] Patricia J. DeLaive, B. P. Sullivan, T. J. Meyer, D. G. Whitten J. Am. Applications of light-induced electron-transfer reactions. Coupling of hydrogen generation with photoreduction of ruthenium (II) complexes by triethylamine. Chem. Soc.1979, 101, 14, 4007-4008.

[4] Pierre Boule J. Am, Dielectric measurements on triethylamine-iodine complex, Chem. Soc.1968, 90, 517-518.

[5] E. Anne Yerger, Gordon M. Barrow, J. Am. Acid-Base Reactions in Non-Dissociating Solvents. Acetic Acid and Diethylamine in Carbon Tetrachloride and Chloroform. Chem. Soc. 1955, 77, 4474-4481

[6] Patricia J. DeLaive, J. T. Lee, Hertha W. Sprintschnik, H. Abruña, T. J. Meyer, David G. Whitten, Photoinduced Redox Reactions of Hydrophobic Ruthenium(II) Complexes, J. Am. Chem. Soc 1977, 99,7094-7097.

[8] P. J. DeLaive, T. K. Foreman, C. Giannotti, D. G. Whitten J. Am, Photoinduced Electron Transfer Reactions of Transition-Metal Complexes with Amines. Mechanistic Studies of Alternate Pathways to Back Electron Transfer. Chem. Soc. 1980, 102, 5627-5631

[9] Tetrahedron Letters, The mechanism of anodic dealkylation of aliphatic amines in acetonitrile, S.D. Ross, 15, 1237-1973, 1973.

[10] J. Hu, J. Wang. H.Nguyen,N. Zheng, Beilstein J. The chemistry of amine cations produced by visible light photoredox catalysis. Org. Chem. 9, 1977-2001, 2013.

[11] J. Hu, J. Wang. H.Nguyen,N. Zheng, Beilstein J. The chemistry of amine cations produced by visible light photoredox catalysis. Org. Chem. 9, 1977-2001, 2013.